DELFT	Planning		Bosch Model																																					
Model	**Lpx**		**Lwl**		**Bpx**		**Dep**		**βχ**	**βτχ**	**Centroid**	**Lcg aft of Centroid**	**Lcg from Transom**		**Lcg/Lpx**	**Centerline angle**	**Ap**		**Twisted angle**	**Lpx/Bpx**	**Ap/Vol**	**Lpx/Ap**	**Lpx/Vol**	**Cv**	**Vcg**		**Shaft Angle**	**Lce**	
84	**4.922**	ft	**4.800**	ft	**1.476**	ft	**61.242**	Lb	**12.50**	**12.00**	**48.60**	**-4.3**	**2.180**	ft	**0.443**	**0.00**	**5.975**	ft^2	**0.50**	**3.33**	**6.115**	**4.054**	**4.979**	**0.292**	----------		**0.00**	**0.000**	ft
	1.500	m	1.463	m	0.450	m	27.340	kg					0.665	m			0.5550	m^2										0.0000	m
85	**4.922**	ft	**4.800**	ft	**1.476**	ft	**61.242**	Lb	**24.50**	**24.00**	**48.60**	**-4.3**	**2.180**	ft	**0.443**	**0.00**	**5.975**	ft^2	**0.50**	**3.33**	**6.115**	**4.054**	**4.979**	**0.292**	----------		**0.00**	**0.000**	ft
	1.500	m	1.463	m	0.450	m	27.340	kg					0.665	m			0.5550	m^2										0.0000	m
114	**7.087**	ft	**6.911**	ft	**1.772**	ft	**104.496**	Lb	**26.50**	**24.00**	**43.33**	**-6.7**	**2.599**	ft	**0.367**	**0.00**	*******	ft^2	**2.50**	**4.00**	**7.201**	**5.000**	**6.000**	**0.289**	**0.591**	ft	**0.00**	**0.000**	ft
	2.160	m	2.107	m	0.540	m	46.650	kg					0.792	m			0.9331	m^2							**0.180**	m		0.0000	m
	7.087	ft	**6.911**	ft	**1.772**	ft	**137.379**	Lb	**26.50**	**24.00**	**43.33**	**-6.7**	**2.599**	ft	**0.367**	**0.00**	*******	ft^2	**2.50**	**4.00**	**6.000**	**5.000**	**5.477**	**0.380**	**0.646**	ft	**0.00**	**0.000**	ft
	2.160	m	2.107	m	0.540	m	61.330	kg					0.792	m			0.9331	m^2							**0.197**	m		0.0000	m
115	**7.087**	ft	**6.911**	ft	**1.772**	ft	**104.496**	Lb	**27.00**	**24.00**	**43.33**	**-6.7**	**2.599**	ft	**0.367**	**0.00**	*******	ft^2	**3.00**	**4.00**	**7.201**	**5.000**	**6.000**	**0.289**	**0.591**	ft	**0.00**	**0.000**	ft
	2.160	m	2.107	m	0.540	m	46.650	kg					0.792	m			0.9331	m^2							**0.180**	m		0.0000	m
	7.087	ft	**6.911**	ft	**1.772**	ft	**137.379**	Lb	**27.00**	**24.00**	**43.33**	**-6.7**	**2.599**	ft	**0.367**	**0.00**	*******	ft^2	**3.00**	**4.00**	**6.000**	**5.000**	**5.477**	**0.380**	**0.646**	ft	**0.00**	**0.000**	ft
	2.160	m	2.107	m	0.540	m	61.330	kg					0.792	m			0.9331	m^2							**0.197**	m		0.0000	m
116	**7.087**	ft	**6.911**	ft	**1.877**	ft	**137.379**	Lb	**----?----**	**----?----**	**44.72**	**-6.5**	**2.707**	ft	**0.382**	**0.00**	*******	ft^2	**0.00**	**3.78**	**6.854**	**4.377**	**5.477**	**0.319**	**0.909**	ft	**0.00**	**0.000**	ft
	2.160	m	2.107	m	0.572	m	61.330	kg					0.825	m			1.0660	m^2							**0.277**	m		0.0000	m
	7.087	ft	**6.911**	ft	**1.877**	ft	**180.589**	Lb	**----?----**	**----?----**	**44.72**	**-6.5**	**2.707**	ft	**0.382**	**0.00**	*******	ft^2	**0.00**	**3.78**	**5.712**	**4.377**	**5.000**	**0.420**	**0.909**	ft	**0.00**	**0.000**	ft
	2.160	m	2.107	m	0.572	m	80.620	kg					0.825	m			1.0660	m^2							**0.277**	m		0.0000	m
Komer	**7.087**	ft	**6.911**	ft	**1.875**	ft	**137.379**	Lb	**----?----**	**----?----**	**44.72**	**-6.5**	**2.707**	ft	**0.382**	**0.00**	*******	ft^2	**0.00**	**3.78**	**6.854**	**4.377**	**5.477**	**0.320**	**0.461**	ft	**0.00**	**0.000**	ft
	2.160	m	2.107	m	0.571	m	61.330	kg					0.825	m			1.0660	m^2							**0.140**	m		0.0000	m
	7.087	ft	**6.911**	ft	**1.875**	ft	**137.379**	Lb	**----?----**	**----?----**	**44.72**	**-6.5**	**2.707**	ft	**0.382**	**0.00**	*******	ft^2	**0.00**	**3.78**	**6.854**	**4.377**	**5.477**	**0.320**	**0.461**	ft	**0.00**	**0.000**	ft
	2.160	m	2.107	m	0.571	m	61.330	kg					0.825	m			1.0660	m^2							**0.140**	m		0.0000	m
PolyCat	**8.662**	ft	**8.447**	ft	**2.426**	ft	**272.194**	Lb	**----?----**	**20.00**	**46.00**	**-6.5**	**3.421**	ft	**0.395**	**0.00**	*******	ft^2	******	**3.57**	**6.550**	**4.337**	**5.330**	**0.293**	**0.563**	ft	**0.00**	**0.000**	ft
	2.640	m	2.575	m	0.739	m	121.515	kg					1.043	m			1.6069	m^2							**0.172**	m		0.0000	m

DELFT	Planning	Bosch Model																						
Model	Flap Chord		Flap Angle	Lpx	Lwl	Bpx	Dep	βχ	βτχ	Centroid	Lcg aft of Centroid	Lcg from Transom	Lcg/Lpx	Centerline angle	Ap	Twisted angle	Lpx/Bpx	Ap/Vol	Lpx/Ap	Lpx/Vol	Cv	Vcg	Shaft Angle	Lce Transom
85	0.037	8.3 %	0	4.922 ft	4.800 ft	1.476 ft	61.242 Lb	24.50	24.00	48.60	-4.3	2.180 ft	0.443	0.00	5.975 ft^2	0.50	3.33	6.115	4.054	4.979	0.292	-------------	0.00	0.000 ft
				1.500 m	1.463 m	0.450 m	27.340 kg					0.665 m			0.5550 m^2									0.0000 m
	0.037	8.3 %	3	4.922 ft	4.800 ft	1.476 ft	61.242 Lb	24.50	24.00	48.60	-4.3	2.180 ft	0.443	0.00	5.975 ft^2	0.50	3.33	6.115	4.054	4.979	0.292	-------------	0.00	0.000 ft
				1.500 m	1.463 m	0.450 m	27.340 kg					0.665 m			0.5550 m^2									0.0000 m
	0.037	8.3 %	6	4.922 ft	4.800 ft	1.476 ft	61.242 Lb	24.50	24.00	48.60	-4.3	2.180 ft	0.443	0.00	5.975 ft^2	0.50	3.33	6.115	4.054	4.979	0.292	-------------	0.00	0.000 ft
				1.500 m	1.463 m	0.450 m	27.340 kg					0.665 m			0.5550 m^2									0.0000 m
	0.037	8.3 %	9	4.922 ft	4.800 ft	1.476 ft	61.242 Lb	24.50	24.00	48.60	-4.3	2.180 ft	0.443	0.00	5.975 ft^2	0.50	3.33	6.115	4.054	4.979	0.292	-------------	0.00	0.000 ft
				1.500 m	1.463 m	0.450 m	27.340 kg					0.665 m			0.5550 m^2									0.0000 m
	0.056	12.5 %	0	4.922 ft	4.800 ft	1.476 ft	61.242 Lb	24.50	24.00	48.60	-4.3	2.180 ft	0.443	0.00	5.975 ft^2	0.50	3.33	6.115	4.054	4.979	0.292	-------------	0.00	0.000 ft
				1.500 m	1.463 m	0.450 m	27.340 kg					0.665 m			0.5550 m^2									0.0000 m
	0.075	16.7 %	0	4.922 ft	4.800 ft	1.476 ft	61.242 Lb	24.50	24.00	48.60	-4.3	2.180 ft	0.443	0.00	5.975 ft^2	0.50	3.33	6.115	4.054	4.979	0.292	-------------	0.00	0.000 ft
				1.500 m	1.463 m	0.450 m	27.340 kg					0.665 m			0.5550 m^2									0.0000 m
	0.075	16.7 %	3	4.922 ft	4.800 ft	1.476 ft	61.242 Lb	24.50	24.00	48.60	-4.3	2.180 ft	0.443	0.00	5.975 ft^2	0.50	3.33	6.115	4.054	4.979	0.292	-------------	0.00	0.000 ft
				1.500 m	1.463 m	0.450 m	27.340 kg					0.665 m			0.5550 m^2									0.0000 m
	0.075	16.7 %	6	4.922 ft	4.800 ft	1.476 ft	61.242 Lb	24.50	24.00	48.60	-4.3	2.180 ft	0.443	0.00	5.975 ft^2	0.50	3.33	6.115	4.054	4.979	0.292	-------------	0.00	0.000 ft
				1.500 m	1.463 m	0.450 m	27.340 kg					0.665 m			0.5550 m^2									0.0000 m
	0.075	16.7 %	9	4.922 ft	4.800 ft	1.476 ft	61.242 Lb	24.50	24.00	48.60	-4.3	2.180 ft	0.443	0.00	5.975 ft^2	0.50	3.33	6.115	4.054	4.979	0.292	-------------	0.00	0.000 ft
	metre		derece	1.500 m	1.463 m	0.450 m	27.340 kg					0.665 m			0.5550 m^2									0.0000 m

REPORTS

Report No. 266

LABORATORIUM VOOR SCHEEPSBOUWKUNDE

TECHNISCHE HOGESCHOOL DELFT

TESTS WITH TWO PLANING BOAT MODELS IN WAVES

by

Ir. J.J. van den Bosch

February 1970

Contents

1. Nomenclature.

A_p	Area bounded by chines and transom, projected on a plane through the straight part of the keel.
a_f	Vertical acceleration forward at 0,1 L
$a_{0,4L}$	Vertical acceleration forward at 0,4 L
B_c	Breadth over chines, at any cross section.
$B_{cm}=\frac{A_p}{L}$	Mean breadth of area A_p.
$B_{c\ max}$	Maximum breadth over chines.
b	Span of planing surface, i.e. actual breadth of planing surface, measured at main spray point.
$F_{n\nabla}=\frac{V}{\sqrt{g\nabla^{1/3}}}$	Froude number based on volume of displacement at rest.
G	Center of gravity.
g	Acceleration due to gravity.
k_{yy}	Real radius of gyration for pitch.
L	Length of projected area A_p.
l_c	Wetted length of chine, measured from transom to main spray point.
l_k	Wetted length of keel, measured from transom.
$l_m=\frac{l_c+l_k}{2}$	Mean wetted length, used for the calculation of the Reynolds number.
R	Resistance.
$R_n=\frac{Vl_m}{\nu}$	Reynolds number.
S	Wetted surface, in contact with "solid" water.
V	Ship or model speed.
X_p	Center of the projected area A_p.
$Y_{\theta g(\omega)}$	Frequency response function for pitch.
$Y_{z\zeta(\omega)}$	Frequency responce function for heave.
z_a	Heave amplitude.
z_G	Rise of center of gravity.
α	Angle of incidence, i.e. angle between still water surface and
β	Deadrise angle.
Δ	Ship or model weight.
Θ_a	Pitch amplitude.
λ	Wave length.

ν	Kinematic viscosity
ω	Circular frequency.
ω_e	Circular frequency of encounter.
ρ	Mass density of water.
ζ_a	Wave amplitude.
$\tilde{\zeta}_{a1/3}$	Mean wave amplitude of highest third part.
∇	Volume of displacement at rest.

2. List of figures.

3. Introduction.

Although there exists a vast amount of literature on the forces and pressures on steady planing surfaces, there is surprisingly little to be found on the seakeeping behaviour of planing craft. For the use of planing boats on open water good seakeeping ability is one of the first requirements. The ability to reach high speeds in waves is largely limited by the occurrence of high vertical accelerations, which in turn are dependent on the speed, the motions of the ship and the hull from.

In an attempt to single out the influence of one geometrical parameter on the vertical accelerations, two models of which only the deadrise angles differed were tested in calm water and in headwaves.
The first model, denoted as model 84, was quite similar to the "Clement" form of the Series - 62 (1) *, the other, model 85, was derived from the first by doubling the angle of deadrise, keeping all other dimensions equal as far as possible.

* See list of references

4. Model data.

The form of both models is shown in figure 1.
The main particulars are given in the following table.

L	1,500	m	
$B_{c\ max}$	0,450	m	
B_{cm}	0,370	m	
∇	0,02734	m^3	
A_p	0,5550	m^2	
X_ρ forward of transom	0,729	m	= 48,6 percent of L
G forward of transom	0,665	m	= 44,3 percent of L
$\nabla^{1/3}$	0,301	m	
$\frac{L}{\nabla^{1/3}}$	4,98		
$\frac{A_p}{\nabla^{2/3}}$	6,11		
$\frac{L}{B_{cm}}$	4,05		
$\frac{L}{B_{c\ max}}$	3,33		

The deadrise angle of the prismatic part of the planing bottom of model 84 was 12 degrees, that of model 85 was 24 degrees.
The meaning of the used symbols is given in the relevant list .

5. Summary of the experiments.

5.1. Calm water tests.

The model was free to pitch and heave and restrained from other motions. The resistance dynomometer of the strain-gauge type was attached at an arbitrary height of 0,116 m above the keel. Previous experience has proved that the height of the point of attachment has only a very small influence on the equilibrium position of the model.

The following items were measured:

- the resistance with a strain gauge dynamometer
- the trim angle with a potentiometer
- the rise of the center of gravity with a potentiometer
- the form and extent of the wetted surface by underwater photographs

The results are summarized in figure 2.

5.2. Regular head waves.

These experiments were carried out for the speed range corresponding to $0,6 < F_{n\nabla} < 3.2$, and the wave lengths corresponding to.

$$\frac{\lambda}{L} = 0,8 - (1,0) - 1,2 - 1,6 - 2,0 - 2,5 \text{ and } 3,0$$

The wave length $\lambda = 0,8$ L was used for model 84, but the frequency of encounter was so close to the natural frequency of a part of the suspension system, that for the tests with the next model a somewhat larger wave length was used.

For the larger part of the program a standard wave height of 0,06 m or $\frac{L}{25}$ was used, but for a few speeds and wave lengths the tests were repeated for wave heights of 0,04 m and 0,08 m to get an impression of the linearity of the motions. The speeds corresponded to $F_{n\nabla} = 1,2 - 2,0 - 2,9$ or 3,2 and the wave lengths to $\frac{\lambda}{L} = 1,2 - 2,0 - 3,0$

The following items were determined:

- the mean resistance
- the mean angle of attack
- the mean rise of the center of gravity
- the pitch amplitude
- the heave amplitude
- the vertical acceleration forward at 0,1 L and at 0,4 L from the foreside of L.

An attempt to measure the phase-angle at high speed failed due to ventilation of the wave probe.
Some of the results of the measurements are presented in the figures 4 to 13. In the appendix the other results are summarized.

5.3. Irregular head seas.

The experiments were carried out at constant speed corresponding to $F_{n\nabla}=2,7$.
The model spectra are shown in figure 14, transformed for the frequency of encounter.

The following measurements were carried out:

- the wave height
- the pitch motion
- the heave motion
- the vertical accelerations at 0,1 L and 0,4 L

The form of the highest wave height spectrum corresponds rather roughly to a North Sea spectrum at the windspeed of a good Beaufort 4; for a ship with a displacement of about 45 ts, the length of the ship would be $L\sim 18$ m and the speed approximately 30 kn. The "significant" wave height would amount to 1,25 m.
From the wave height spectrum amd the motion spectra, shown in the figures 15 and 16, the moduliof the frequency-response-functions for pitch and heave were determined. There are presented in the figures 17 and 18. The frequency of occurrence of the vertical accelerations is shown in figure 19.

6. Discussion of the test results.

6.1. Calm water

As the hull form of model 84 closely resembled the "Clement" form, the trim and resistance should also fit in with the Series - 62. This happened not to be the case as is shown in figure 20. Close examination of the hull after the tests revealed that because of warping of the hull material a slight convexity had developed of the after part of the bottom. This can be the explanation of the discrepancy.

The resistance and angles of incidence calculated with the approximative method developed by Savitsky (2) from tests with planing prisms, are shown in the figures 20 and 21. For model 85 the agreement is reasonable; the slightly different angle of incidence can be explained by the fact that the breadth of the planing hull at the transom is considerably smaller for the model than for the prismatic forms. For low speeds the method fails, because the actual model can not be considered any longer as a prism, when the convex forward bottom parts enter the water.

It is remarkable that the resistance of the deep - V model is only slightly more than that of its flatter counterpart. When extrapolating the resistances to ship values, these differences become even smaller because of the larger wetted surface of the deep - V model, and the decrease of the frictional resistance coefficient with the increase of Reynolds number.
Probably the trim angles of the model 84 are too large for least resistance.

6.2. Regular head waves.

The question of linearity is important, or rather it is important to know if tests in irregular waves will give results which will predict the true order of quality of two models, that is to say, when model A appears to be better than model B in regular waves, the same should follow from tests in irregular waves with a sufficiently wide frequency range. This follows automatically when the motions can be described by a set of lineer differential equations. It seems even probable that quite a lot of non-linearity can be introduced before this will invalidate the comparison.

The first impression of the linearity can be had from the recordings of the motions and the accelerations, as shown in the figures 4 and 5. When looking

at the recorded accelerations of model 84, with the steep rise when the bow hits the water surface, it is seen that this evident non-linearity appears to have a relatively small influence on the sine-character of the pitch motion.

In the figures 12 and 13 the ratios between the motion amplitudes and the wave height are given for different wave heights. Obviously the only non-linearities of some importance occur at the highest speed and the largest wave length. This concerns the amplitudes; nothing is known about the phases. The reduced pitch amplitudes of model 84 tend to increase with the wave height, while the reverse is true for model 85.

The mean angle of attack and the mean rise of the center of gravity which together determine the mean attitude of the model, are presented in the figures 7 and 8. Evidently especially model 84 comes much higher out of the water in waves than in smooth water. This indicates that the motion is not strictly linear.

The results of the resistance measurements were remarkable in the case of model 84. For a number of wave lengths the mean resistance appeared to be smaller than the smooth water resistance in a speed range around $F_{n\nabla}=3$. This could not be explained, but the impression existed that the phase relations between the motions and the wave were responsible for the phenomenon

The reduced amplitudes of pitch and heave are presented in the figures 9 and 10. The motions of model 85 appear to be less than those of model 84 for all wave lengths in the high speed range above $F_{n\nabla} = 2$

The vertical accelerations forward, presented in figure 11 differ markedly for both models, as was allready apparent from the recordings shown in figure 5. The superiority of model 85 holds for all speeds and wave lengths tested.

6.3. Irregular head seas.

The measurements of the wave height and the motions, and the subsequent analyses of the wave height spectrum and the motion spectra, yealded the frequency-amplitude-responses of pitch and heave. This has been done on the assumption that the motions would be sufficiently linear to justify this procedure. The results for two different wave spectra are shown in the figures 17 and 18. The spectra are shown in the figures 14 to 16. Unfortunately the recording of the pitch motion of model 84 in the lower wave spectrum appeared to have been spoiled by an instrumental failure. This is the reason why these results have been omitted from the figure.

The comparison of the responses for regular and irregular waves reveals that for the high frequency flank of the curves the agreement is reasonable. The tendency of the curves for regular waves to rise at the top above those for irregular waves, has not been explained. The general order has not been affected by this.
The analyses of the irregular motions shows very consistent results for the two different wave height spectra and the relative qualities of the models, as have been found from the tests in regular waves, are truly reproduced. The accelerations experienced by the flat model are not as striking as those which have been observed in regular waves, but the difference between the two models is still considerable, as is shown in the frequency of occurrence distributions in figure 19.

7. General conclusions.

The increase of the deadrise angle results in a considerable gain in seakeeping ability at the cost of some power The decrease of the vertical accelerations is partly a direct outcome of the larger deadrise, partly an indirect consequence of the influence of the hull form on the mean attitude of the boat and on the motions. Model 85 sits lower in the water than model 84, its trimangle is less, and its motions, in particular pitch are less, features which tend to soften the impact in waves. Visual observations gave the impression that also the phase of the motions with respect to the waves was different and this also could have contributed to the evidently better performance of the deep - V model. This rather complex relation between deadrise angle and seakindliness cautions one against generalization.

The tests in irregular waves showed that a certain degree of non-linearity does not appear to invalidate the qualitative conclusions which can be drawn when comparing the behaviour of one model with that of the other, under the same conditions. Of course more evidence should be provided before such a statement can be generalized.

It seems advisable to repeat the experiments in irregular waves at a higher speed but up till now this is not within the reach of the facilities of the model tank in Delft.

8. References.

(1) Clement, E.P. and Blount, D.L.,
"Resistance Tests of a Systematic Series of Planing Hull Forms".
Transactions of The Society of Naval Architects and Marine Engineers.
Vol.71 1963 p. 491

(2) Savitsky,D.
"Hydrodynamic Design of Planing Hulls".
Marine Technology Vol.1 no.1 October 1964.

9. Appendix:

Summary of test results, including those which have been left out of the figures.

9.1. Calm water

Model 84 $\nu = 1{,}052 \times 10^{-6}$ m^2/sec.					
V m/sec	R kg.	α degr.	z_G cm	l_m m	S m^2
1,43	1,10	0,14	-0,78	1,46	0,637
1,72	2,01	1,15	-1,30	1,43	0,637
2,03	3,10	3,53	-1,39	1,40	0,631
2,22	3,30	4,26	-1,03	1,38	0,627
2,47	3,40	4,42	-0,45	1,35	0,615
2,61	3,50	4,51	-0,24	1,33	0,604
2,85	3,60	4,74	0,00	1,29	0,580
3,03	3,80	5,01	+0,24	1,24	0,552
3,33	4,10	6,11	+0,93	1,14	0,473
3,76	4,30	7,00	+2,23	1,04	0,411
3,91	4,37	6,88	+2,52	1,01	0,398
3,47	4,21	6,31	+1,28	1,10	0,446
4,48	4,44	6,47	+3,70	0,92	0,359
5,13	4,35	5,93	+4,30	0,89	0,345
5,62	4,47	5,48	+4,73	0,84	0,327
5,88	4,64	5,25	+4,89	0,80	0,315
3,24	4,05	5,55	+0,62	1,17	0,496
1,89	2,66	2,32	-1,48	1,41	0,635
0,99	0,31	-0,15	-0,42	1,50	0,610

Model 85 $\nu = 1{,}052 \times 10^{-6}$ $m^2/sec.$					
V m/sec	R kg	α degr.	z_G cm	l_m m	S m^2
1,00	0,36	-0,22	-0,38	1,50	0,628
1,49	1,32	-0,50	-0,82	1,47	0,641
3,09	4,27	3,44	0,00	1,31	0,622
4,01	4,50	5,18	+1,66	1,16	0,498
5,10	4,84	5,22	+3,22	1,03	0,453
2,52	3,69	3,58	-0,68	1,38	0,624
5,60	5,14	5,10	+3,60	1,00	0,432
3,52	4,59	4,32	+0,72	1,25	0,612
5,56	5,11	5,10	+3,60	1,00	0,433
2,09	3,14	2,72	-1,40	1,43	0,640
4,48	4,62	5,36	+2,54	1,10	0,488
6,01	5,34	4,80	+4,00	0,98	0,419

9.2. Regular waves $\nu = 1{,}052 \times 10^{-6}$ m^2/sec.

Model 84

V m/sec	R kg	α degr.	z_G cm.	ζ_a cm.	z_a cm.	Θ_a degr.	a_f g	$a_{0,4L}$ g
		λ = 1,20 m.		λ/L = 0,8				
3,03	4,19	5,06	+0,20	2,25	0,31	0,45	0,64	0,33
3,53	4,73	6,76	+1,76	2,36	0,46	0,75	1,53	0,86
1,00	0,63	-0,20	-0,40	2,45	0,26	0,71	0,16	0,07
1,98	3,17	2,40	-1,50	2,42	0,32	0,39	0,22	0,14
4,58	4,78	6,60	+4,32	2,61	0,50	0,60	3,64	1,63
5,03	4,93	6,32	+4,92	2,08	0,40	0,48	3,97	1,77
5,59	4,96	5,78	+5,36	2,34	0,48	0,40	4,32	2,19
		λ = 1,80 m.		λ/L = 1,2				
1,03	1,02	0,80	0,00	3,09	1,92	3,86	0,42	0,17
2,00	3,31	3,44	-1,40	3,29	0,41	1,14	0,19	0,11
2,96	4,50	5,38	0,00	2,76	0,57	1,24	0,67	0,33
4,12	5,40	7,44	+3,60	2,65	1,03	1,40	3,36	1,55
5,07	3,51	6,82	+4,90	3,10	1,02	1,16	6,92	3,92
1,50	1,51	0,58	-0,78	3,15	1,12	1,99	0,29	0,12
2,49	3,72	4,88	-0,42	3,30	0,42	1,00	0,47	0,19
3,56	5,21	7,38	+2,00	2,76	0,98	1,47	1,70	0,95
4,58	5,24	7,18	+4,42	2,79	1,01	1,23	4,60	1,98
5,56	4,02	6,30	+5,18	2,45	0,99	1,10	5,95	2,94
2,01	3,21	3,04	-1,54	2,00	0,21	0,69	0,14	0,00
3,59	4,75	6,78	+2,06	2,09	0,75	1,05	1,08	0,51
5,04	-	6,20	+4,56	1,80	0,75	0,88	2,48	1,13
2,06	3,67	4,00	-1,56	3,74	0,45	1,34	0,28	0,11
3,52	5,16	6,96	+1,88	3,30	1,20	1,93	3,74	1,43
5,05	5,50	6,42	+4,68	3,33	1,25	1,36	7,41	3,77

Model 84

V m/sec.	R kg.	α degr.	z_G cm	ζ_a cm	z_a cm	Θ_a degr.	a_f g	$a_{0,4L}$ g
λ = 2,40 m.				λ/L = 1,6				
1,00	0,81	0,26	-0,22	3,00	2,48	4,90	0,36	0,23
1,98	3,19	3,26	-1,40	2,95	2,05	2,70	0,30	0,20
3,00	4,45	5,20	+0,24	3,10	1,17	2,14	0,64	0,28
4,00	5,16	7,56	+3,60	2,92	1,76	2,11	2,21	1,21
5,07	3,66	6,68	+5,18	3,05	1,68	1,81	6,80	2,81
5,63	4,21	5,80	+5,48	3,08	1,57	1,59	8,99	4,03
4,54	4,89	7,16	+4,60	3,00	1,70	1,90	4,53	1,82
2,55	3,89	5,78	-0,48	3,00	1,14	2,04	0,44	0,20
1,50	1,56	0,60	-0,72	3,00	3,22	4,20	0,44	0,31
3,47	5,03	7,22	+1,72	2,60	1,46	2,00	1,25	0,63
λ = 3,00 m.				λ/L = 2,0				
1,02	0,62	0,18	-0,30	3,06	2,60	4,20	-	-
1,99	3,18	3,20	-1,40	2,96	3,13	3,35	0,38	0,27
2,99	4,24	4,80.	+0,12	3,01	1,91	2,79	0,58	0,26
4,01	4,42	6,86	+3,20	2,70	2,36	2,86	1,66	0,94
5,07	4,94	6,20	+4,62	2,80	2,24	2,46	6,37	2,31
5,55	5,08	5,86	+5,14	2,99	2,15	2,29	7,31	2,93
4,58	4,71	6,62	+4,28	3,00	2,35	2,71	3,89	1,60
2,56	3,98	4,62	-0,38	3,00	2,24	3,00	0,37	0,23
1,46	1,42	0,42	-0,66	2,95	2,91	4,30	0,38	0,22
3,48	4,31	6,24	+1,50	2,65	2,07	2,68	0,96	0,49
2,03	3,24	3,18	-1,40	2,21	2,50	2,52	0,27	0,18
3,55	4,74	6,60	+1,00	2,50	1,80	2,14	0,71	0,36
5,00	4,85	6,00	+4,82	2,18	1,90	2,00	2,72	1,20
2,00	3,51	3,02	-1,16	4,00	4,41	4,52	0,51	0,32
3,54	5,14	5,78	+1,82	3,89	2,79	3,56	1,71	0,91
5,12	5,75	6,22	+3,16	3,80	2,90	3,11	9,38	3,96

Model 84

V m/sec.	R kg	α degr.	z_G cm.	ζ_a cm	z_a cm	Θ_a degr.	a_f g	$a_{0,4L}$ g
			λ = 3,75 m.		λ/L = 2,5			
1,04	0,47	0	-0,30	3,00	2,75	3,30	0,15	0,11
2,00	2,99	3,12	-1,36	2,95	3,60	2,91	0,26	0,23
3,96	4,59	6,72	+2,70	2,58	3,30	3,40	1,23	0,67
5,54	4,22	5,50	+5,40	2,75	3,23	3,05	5,96	2,65
5,04	3,88	6,02	+4,80	2,59	3,38	3,33	5,12	2,22
3,07	4,21	5,98	+0,42	2,62	3,06	3,15	0,40	0,28
4,57	4,77	6,36	+4,44	3,00	3,33	3,26	2,57	1,30
5,07	3,92	5,98	+4,92	2,60	3,35	3,28	4,73	1,95
4,66	4,74	6,30	+4,56	2,80	3,43	3,28	2,98	1,47
2,55	3,65	4,48	-0,30	3,00	3,21	2,94	0,23	0,25
1,50	1,37	0,06	-0,94	2,91	2,86	3,23	0,15	0,17
4,89	4,78	6,10	+4,86	2,40	3,53	3,25	3,50	1,71
			λ = 4,50 m.		λ/L = 3,0			
1,02	0,39	-0,08	-0,36	3,06	2,82	2,80	0,10	0,09
1,98	2,97	3,10	-1,44	3,00	3,40	2,62	0,19	0,17
2,98	4,01	5,00	+0,28	2,76	3,52	2,80	0,26	0,22
4,03	4,61	6,80	+3,30	2,65	4,00	3,44	0,79	0,43
4,58	4,62	6,20	+4,40	2,98	4,32	3,80	1,53	0,80
5,07	4,88	5,74	+4,80	2,60	4,53	3,96	3,00	1,52
5,62	5,12	4,90	+5,32	2,85	4,54	3,97	6,72	3,11
3,54	4,47	6,60	+1,68	2,70	3,70	3,24	0,45	0,32
1,53	1,45	0,16	-0,94	3,10	2,96	2,76	0,13	0,14
2,54	3,64	4,56	-0,26	3,15	3,55	2,52	0,20	0,23
2,02	3,18	3,24	-1,38	3,99	4,42	3,39	0,29	0,19
3,56	4,84	6,20	+1,96	3,80	4,99	4,26	1,00	0,32
5,02	5,44	4,74	+5,20	3,61	5,90	4,74	5,30	2,48
2,02	3,11	3,00	-1,48	2,29	2,60	1,90	0,15	0,19
3,51	4,57	6,46	+1,60	2,11	2,75	2,39	0,32	0,20
5,01	4,74	5,80	+4,66	2,11	3,60	3,28	1,67	0,78

Model 85

V m/sec.	R kg.	α degr.	z_G cm.	ζ_a cm.	z_a cm.	Θ_a degr.	a_f g	$a_{0,4L}$ g
		λ = 1,50 m.			λ/L = 1,0			
1,56	1,60	-0,20	-0,59	3,35	0,41	0,74	0,13	0,07
3,02	5,01	4,16	-0,44	2,83	0,38	0,49	0,42	0,24
4,04	5,14	6,08	+1,90	2,88	0,45	0,63	0,87	0,48
4,99	5,14	6,06	+3,40	2,65	0,47	0,69	1,19	0,62
5,47	5,29	5,74	+4,08	2,85	0,45	0,55	1,49	0,78
3,50	5,04	4,76	+0,34	2,69	0,34	0,48	0,56	0,29
4,52	5,11	5,90	+2,80	2,82	0,40	0,60	0,96	0,40
2,07	3,37	2,66	-1,78	3,00	0,13	0,40	0,18	0,07
2,51	3,74	3,50	-0,92	3,21	0,24	0,40	0,38	0,18
		λ = 1,80 m.			λ/L = 1,2			
1,02	0,96	0,30	-0,06	3,12	1,83	3,73	0,39	0,20
2,17	3,73	2,96	-1,38	3,10	0,22	0,89	0,17	0,10
3,13	4,50	3,70	-0,42	2,66	0,39	0,64	0,39	0,24
3,53	4,67	4,50	+0,38	3,00	0,45	0,73	0,52	0,32
4,43	5,87	5,80	+2,50	2,56	0,66	0,90	1,02	0,58
5,21	5,78	5,68	+3,32	2,37	0,55	0,77	1,08	0,61
2,48	3,90	3,50	-1,06	2,65	0,20	0,70	0,27	0,14
4,00	5,48	5,68	+1,78	2,85	0,60	0,95	0,81	0,45
5,57	5,75	5,64	+3,80	2,52	0,60	0,78	1,35	0,80
2,31	3,90	3,42	-0,98	3,82	0,21	1,07	0,32	0,19
3,48	4,63	4,68	+0,28	3,44	0,64	0,96	0,72	0,40
5,49	5,99	5,60	+3,84	3,50	0,81	1,00	1,95	1,05
2,04	3,23	2,50	-1,68	2,00	0,15	0,54	0,06	0,00
3,47	4,91	4,48	+0,44	2,09	0,31	0,52	0,38	0,17
5,50	5,38	5,76	+3,82	1,95	0,44	0,55	0,86	0,46

Model 85

V m/sec.	R kg.	α degr.	z_G cm.	ζ_a cm.	z_a cm	Θ_a degr.	a_f g	$a_{0,4L}$ g
		λ = 2,40 m.			λ/L = 1,6			
1,02	0,85	-0,06	-0,42	2,85	2,12	4,68	0,38	0,18
2,03	3,55	3,12	-1,60	3,00	1,92	2,59	0,43	0,24
2,49	4,14	3,92	-0,98	3,16	1,10	1,94	0,48	0,19
3,04	4,74	4,00	-0,50	2,98	0,88	1,60	0,56	0,23
3,53	5,03	4,84	+0,20	3,05	0,96	1,35	0,65	0,32
4,08	5,00	6,00	+1,86	2,80	1,15	1,43	0,96	0,45
4,46	4,91	5,60	+2,54	2,63	1,20	1,39	0,99	0,51
5,48	5,13	5,50	+3,82	2,80	1,72	1,32	1,49	0,77
5,01	4,97	5,68	+3,22	2,77	1,24	1,33	1,29	0,69
		λ = 3,00 m.			λ/L = 2,0			
1,02	0,63	-0,18	-0,22	3,00	2,44	3,97	0,27	0,14
2,00	3,26	2,42	-1,16	3,07	3,33	3,45	0,42	0,32
2,94	4,53	3,10	-0,32	2,92	1,90	2,61	0,48	0,26
4,05	5,34	5,00	+1,56	2,70	1,71	1,99	0,54	0,39
5,07	5,01	5,14	+3,22	2,60	1,84	1,91	1,13	0,33
5,62	5,26	4,98	+3,78	2,70	1,74	1,77	1,34	-
5,52	5,14	4,96	+3,62	2,39	1,77	1,77	1,29	0,79
4,55	5,05	5,40	+2,60	2,60	1,85	1,95	1,12	0,54
3,48	5,15	3,84	+0,04	2,86	1,64	2,07	0,69	0,27
2,44	3,99	3,48	-1,00	2,96	2,60	3,01	0,50	0,19
2,03	3,53	2,52	-1,22	3,76	4,21	4,30	0,48	0,34
3,52	5,49	3,28	+0,10	3,52	1,82	2,51	0,65	0,32
5,03	5,31	5,00	+3,26	3,23	2,18	2,24	1,51	0,85
2,03	3,35	2,56	-1,54	2,38	2,69	2,79	0,28	0,26
3,54	5,15	4,00	+0,24	2,09	1,19	1,65	0,38	0,23
5,00	5,11	5,36	+3,12	2,07	1,50	1,55	0,80	0,46

Model 85

V m/sec	R kg.	α degr.	z_G cm.	ζ_a cm.	z_a cm.	Θ_a degr.	a_f g	$a_{0,4L}$ g
		λ = 3,75 m.			λ/L = 2,5			
1,03	0,48	-0,30	-0,26	2,96	2,90	3,35	0,16	0,11
2,03	3,21	2,40	-1,30	2,98	3,60	3,21	0,32	0,24
2,52	3,98	3,44	-0,64	3,00	3,52	3,06	0,32	0,27
3,00	4,61	3,38	-0,08	3,08	3,20	3,08	0,41	0,28
3,50	5,35	3,66	+0,13	2,65	2,66	2,82	0,46	0,28
4,05	5,63	4,52	+1,56	2,72	2,53	2,57	0,60	0,36
4,54	5,47	5,54	+2,64	2,60	2,86	2,61	0,82	0,44
5,05	5,43	5,60	+3,36	2,80	2,82	2,55	1,08	0,60
5,56	5,74	5,44	+3,76	2,68	2,84	2,53	1,31	0,75
		λ = 4,50 m.			λ/L = 3,0			
1,05	0,47	-0,32	-0,40	2,95	2,79	2,60	0,00	0,10
2,02	3,20	2,34	-1,60	3,00	3,26	2,70	0,16	0,15
2,46	3,89	3,64	-0,56	3,00	3,60	2,52	0,20	0,18
2,99	4,51	3,24	-0,40	2,82	3,56	2,70	0,27	0,21
4,01	5,41	4,80	+1,50	3,00	3,54	2,90	0,43	0,28
3,48	5,28	3,52	+0,12	3,00	3,41	2,90	0,33	0,24
4,43	5,38	5,32	+2,52	2,67	3,69	2,95	0,58	0,36
5,02	5,63	5,56	+3,28	2,60	3,78	3,00	0,83	0,45
5,53	6,03	5,30	+3,74	2,75	3,90	3,12	1,08	0,54
2,00	3,11	1,50	-1,60	4,20	4,40	3,75	0,25	0,18
3,52	5,47	3,36	+0,18	3,98	4,55	3,73	0,44	0,29
5,53	6,74	4,92	+3,68	3,87	4,63	3,65	1,57	0,75
5,56	5,87	5,20	+3,96	2,20	3,10	2,48	0,78	0,46
2,01	3,14	2,24	-1,64	2,40	2,50	2,10	0,11	0,08
3,55	5,25	3,70	+0,36	2,21	2,63	2,26	0,23	0,19

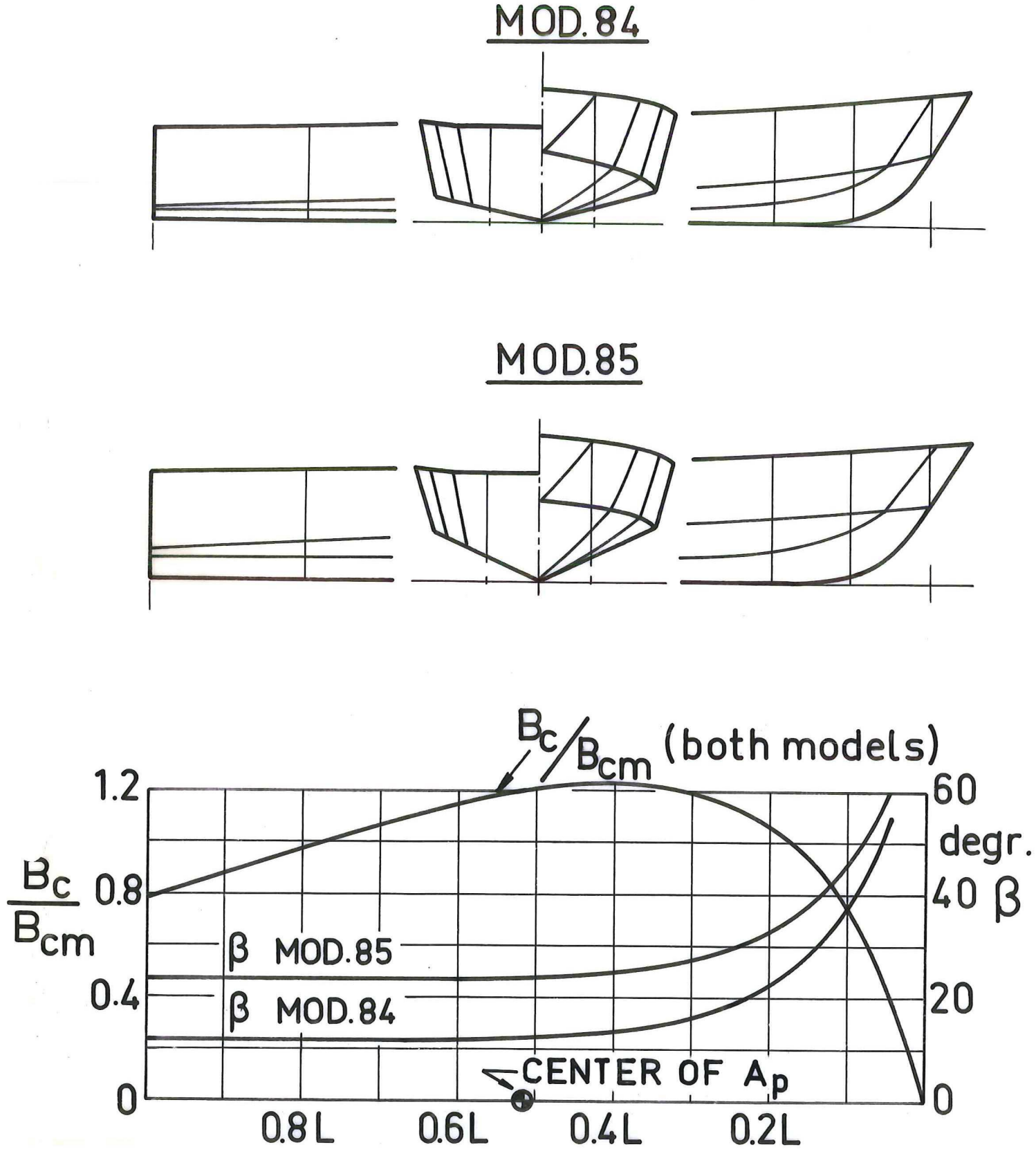

Fig. 1: Formcharacteristics of both models

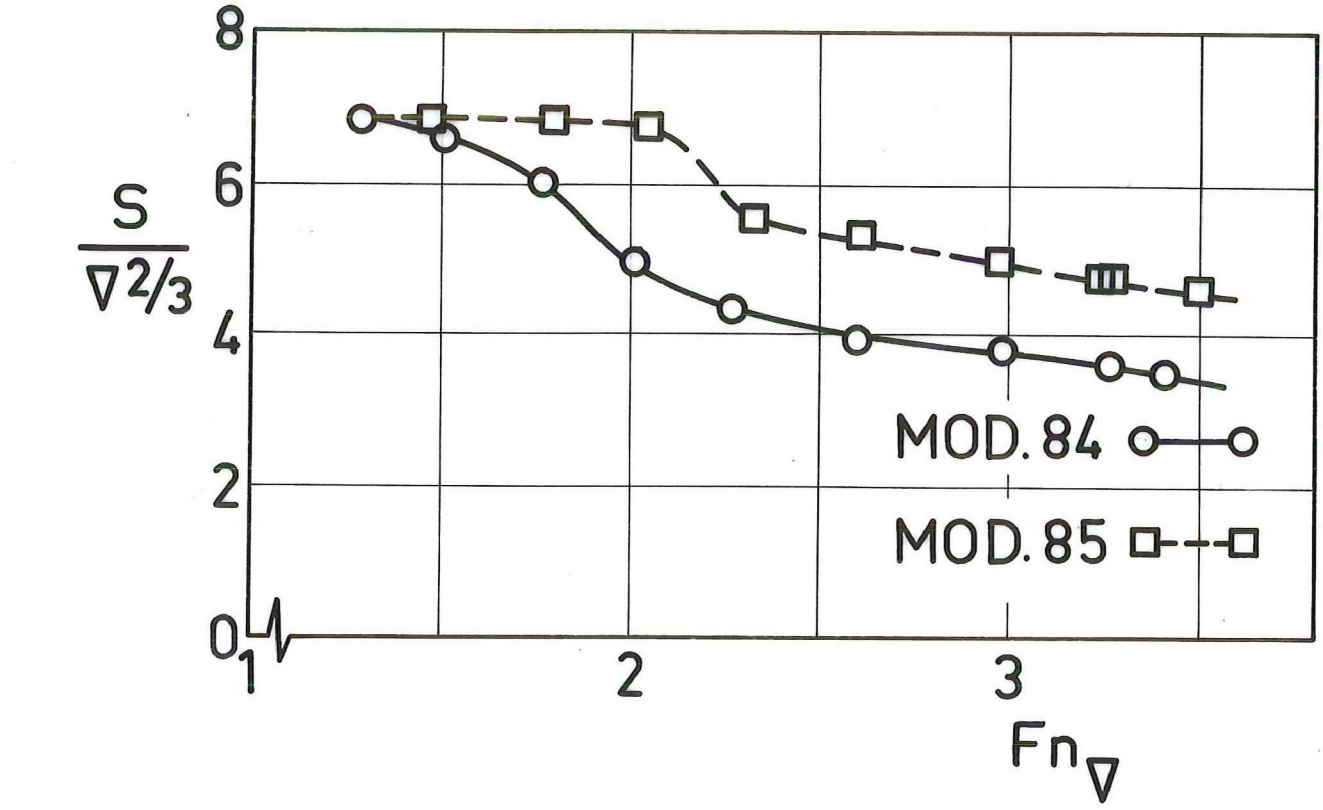

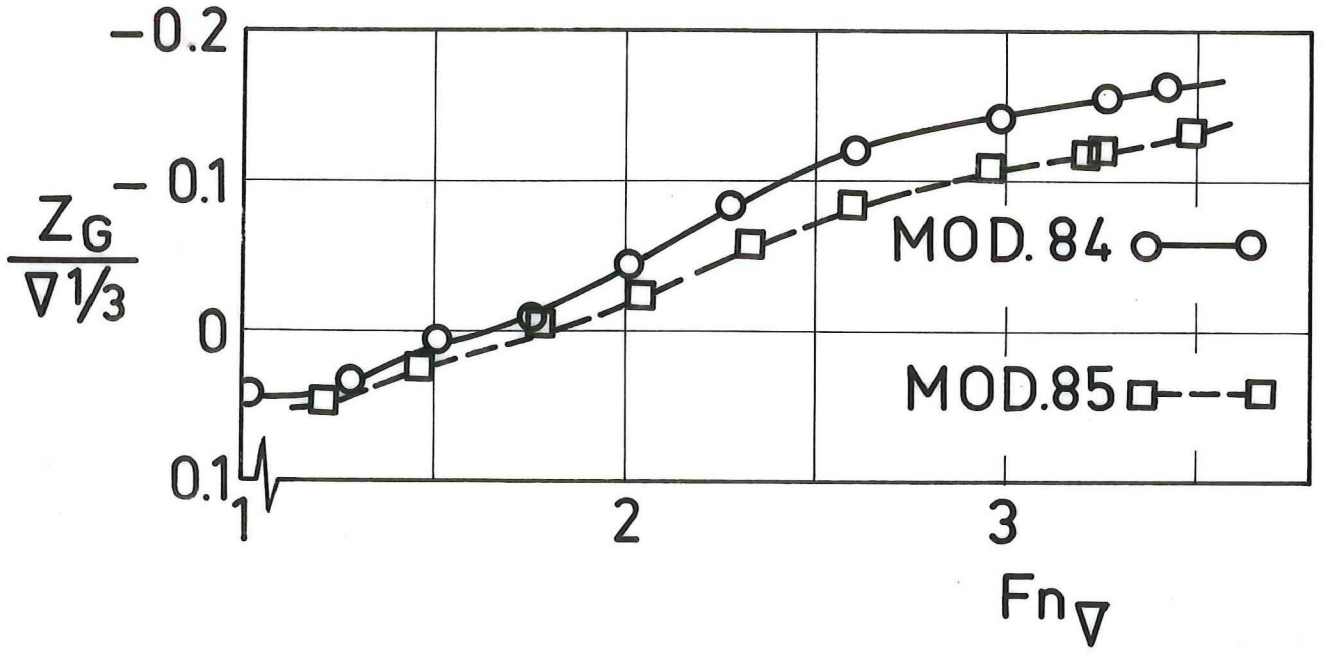

Fig. 2: Wetted surface and center of gravity rise in calm water

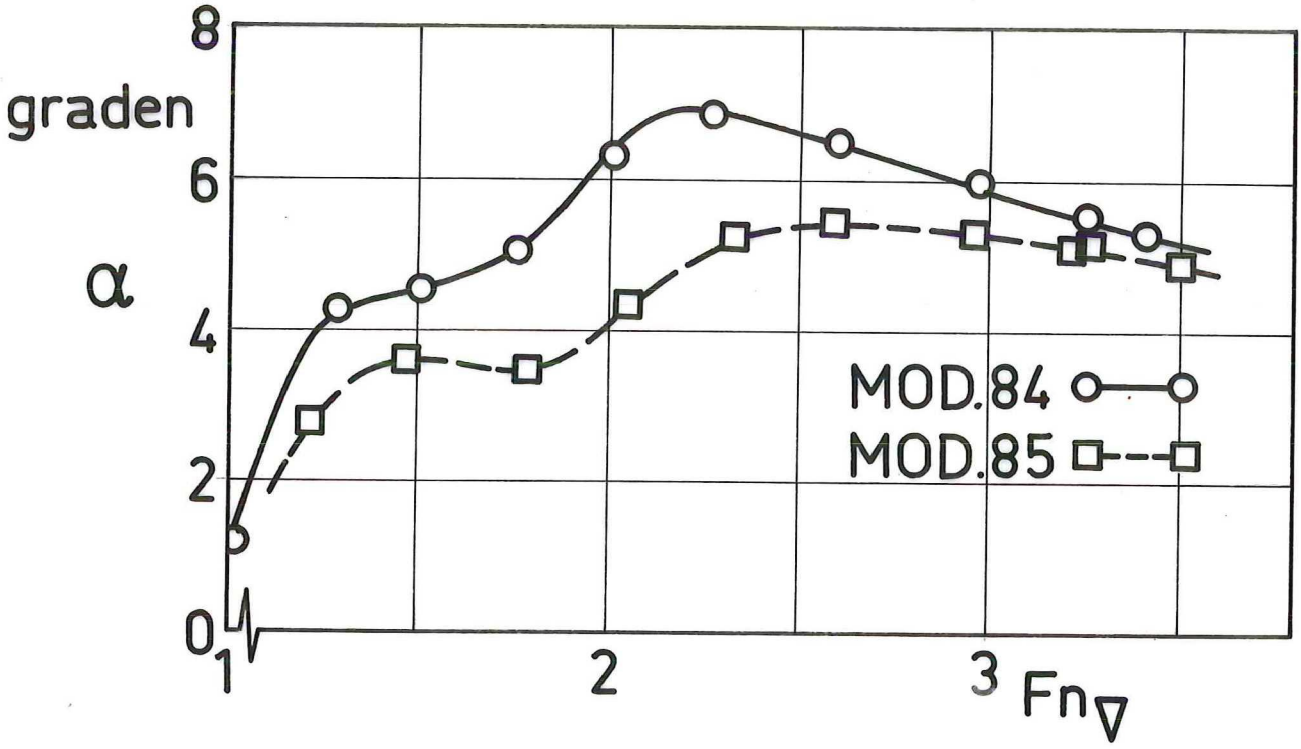

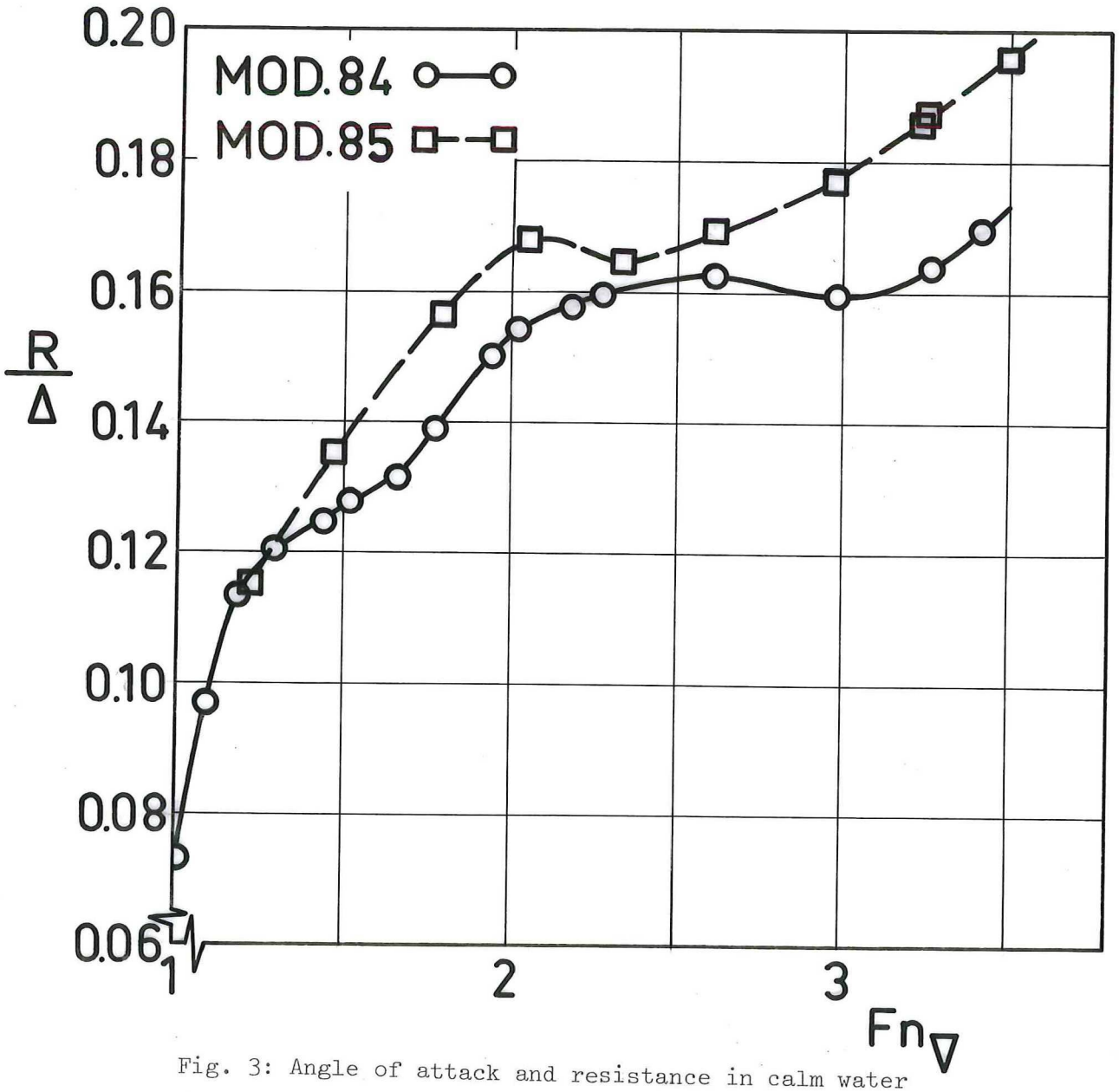

Fig. 3: Angle of attack and resistance in calm water

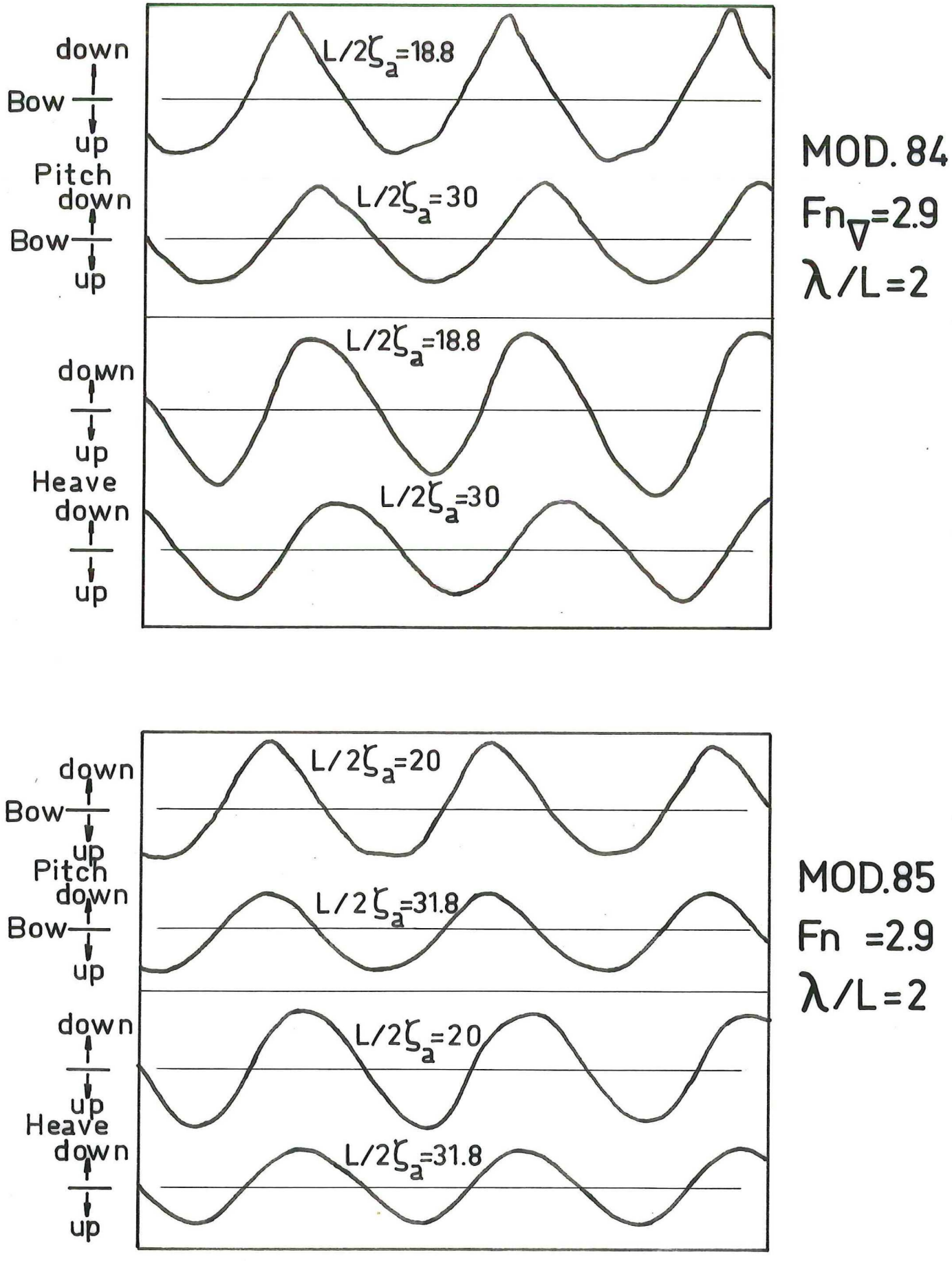

Fig. 4: Sample of motion recordings for different wave heights

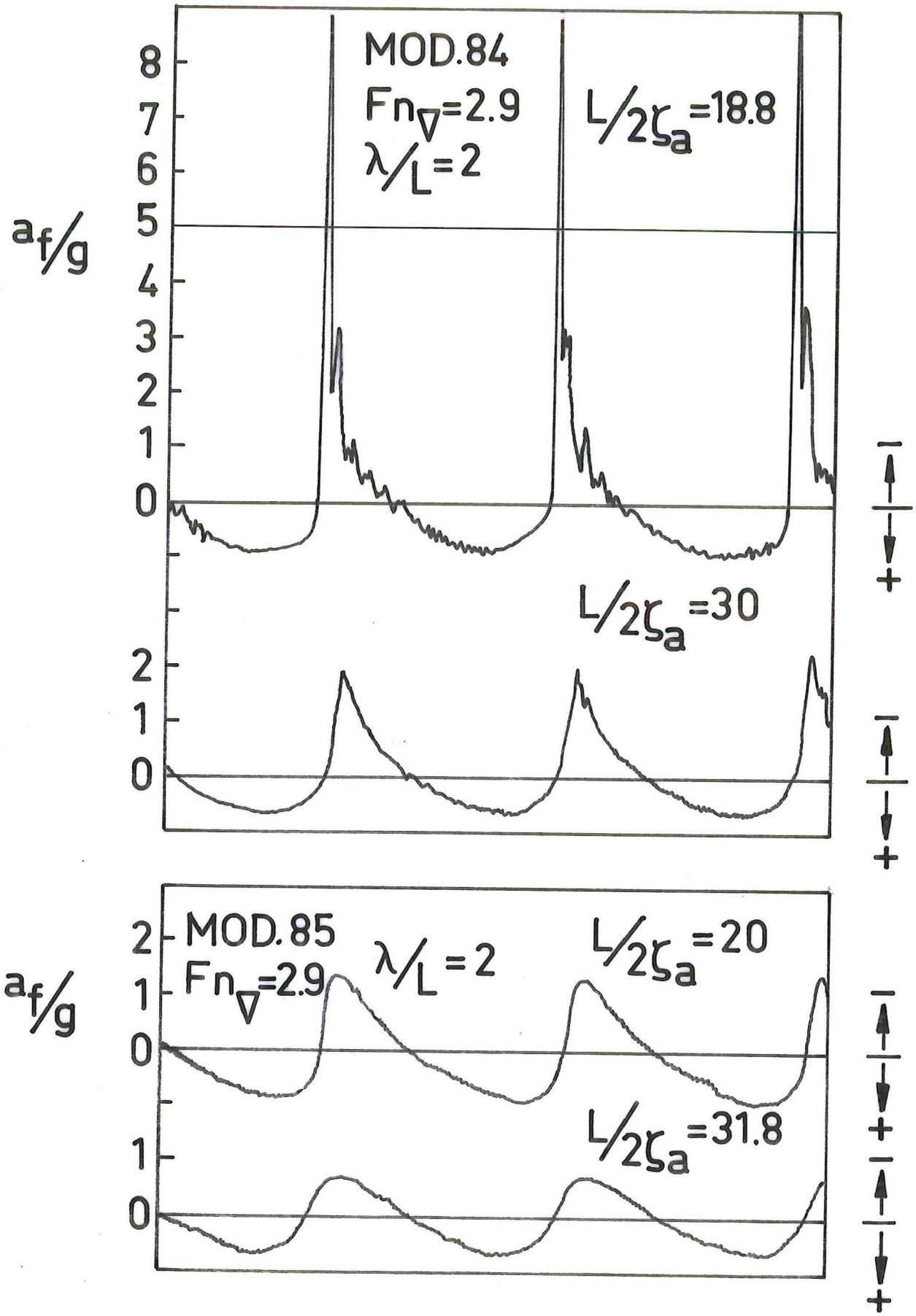

Fig. 5: Some recordings of the vertical accelerations at 0.1 L

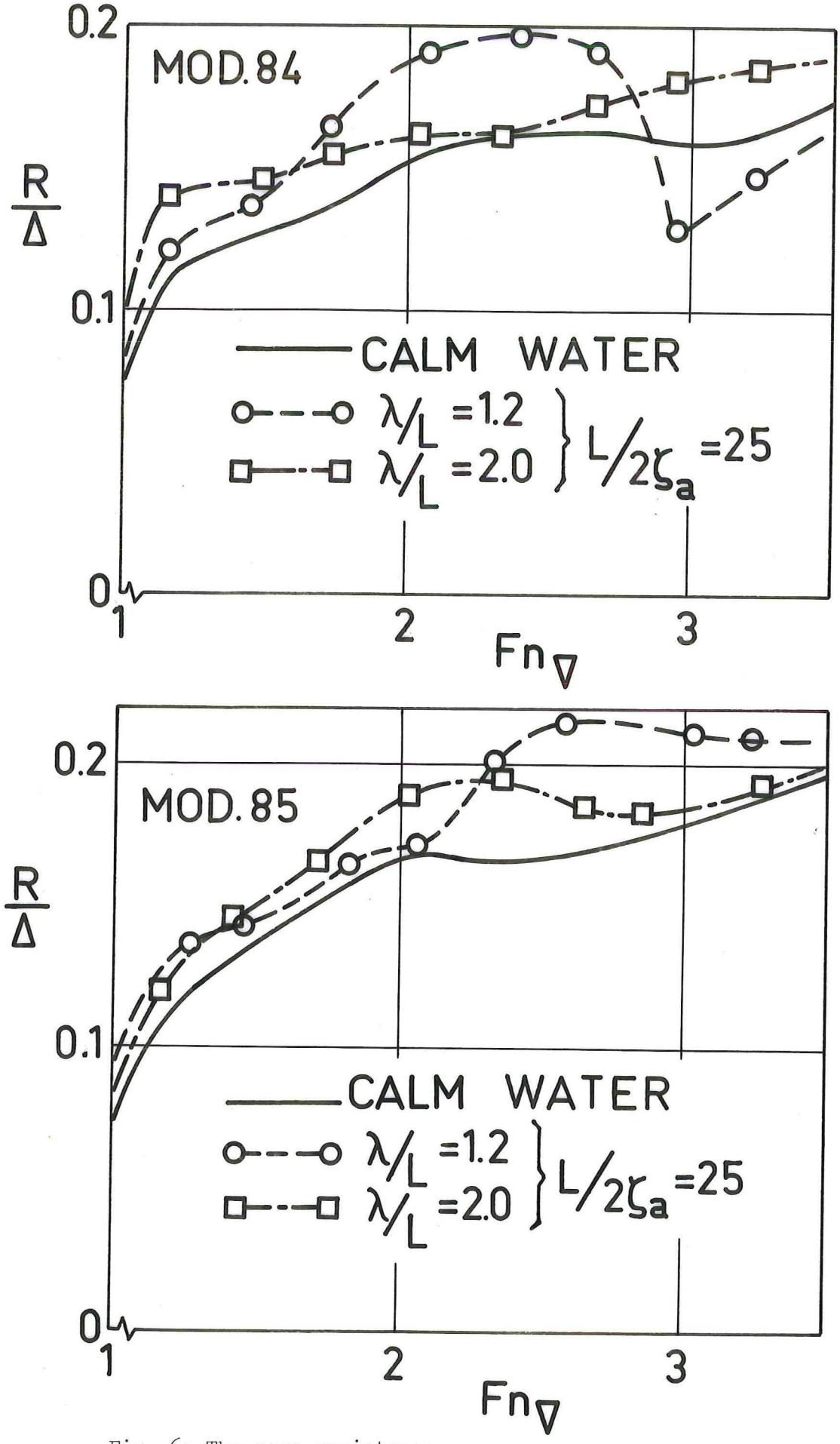

Fig. 6: The mean resistance

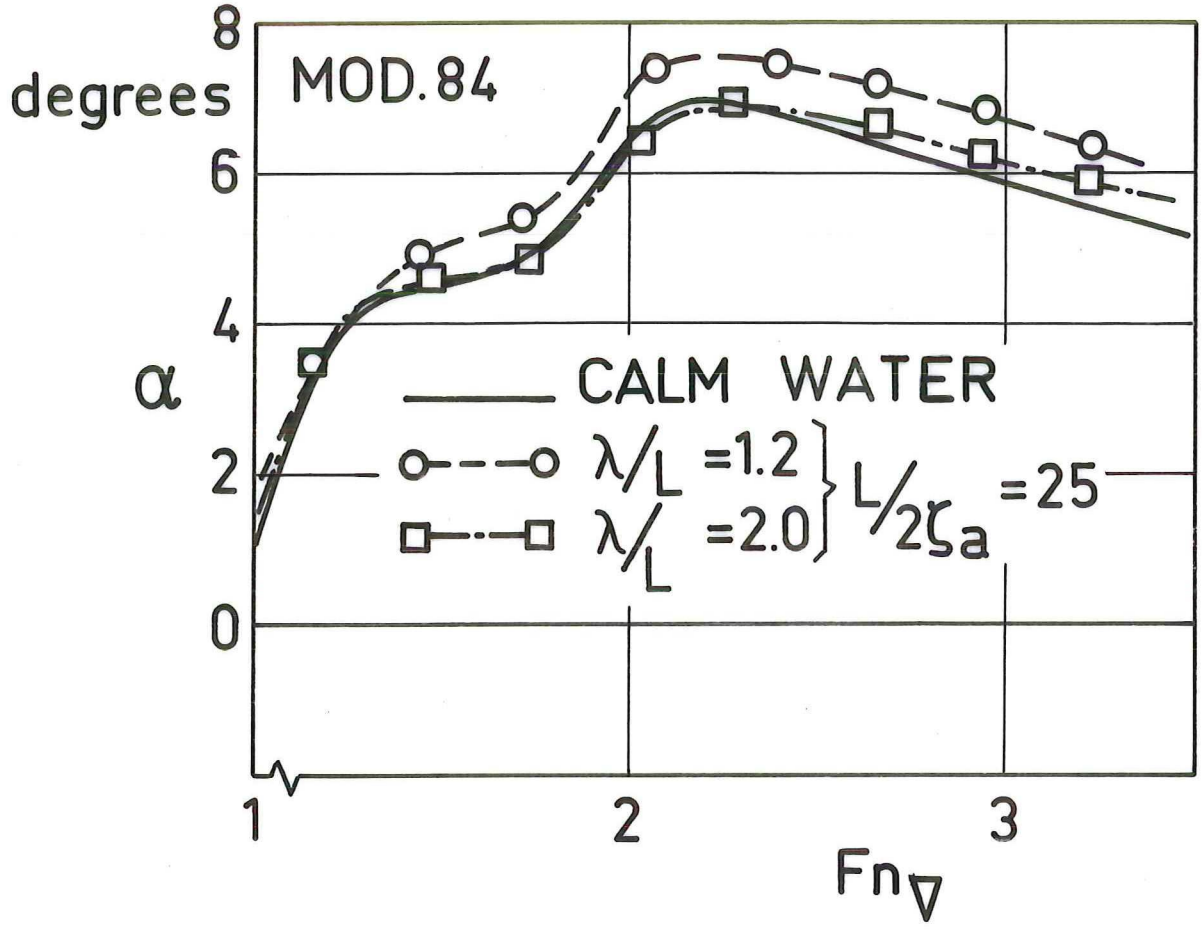

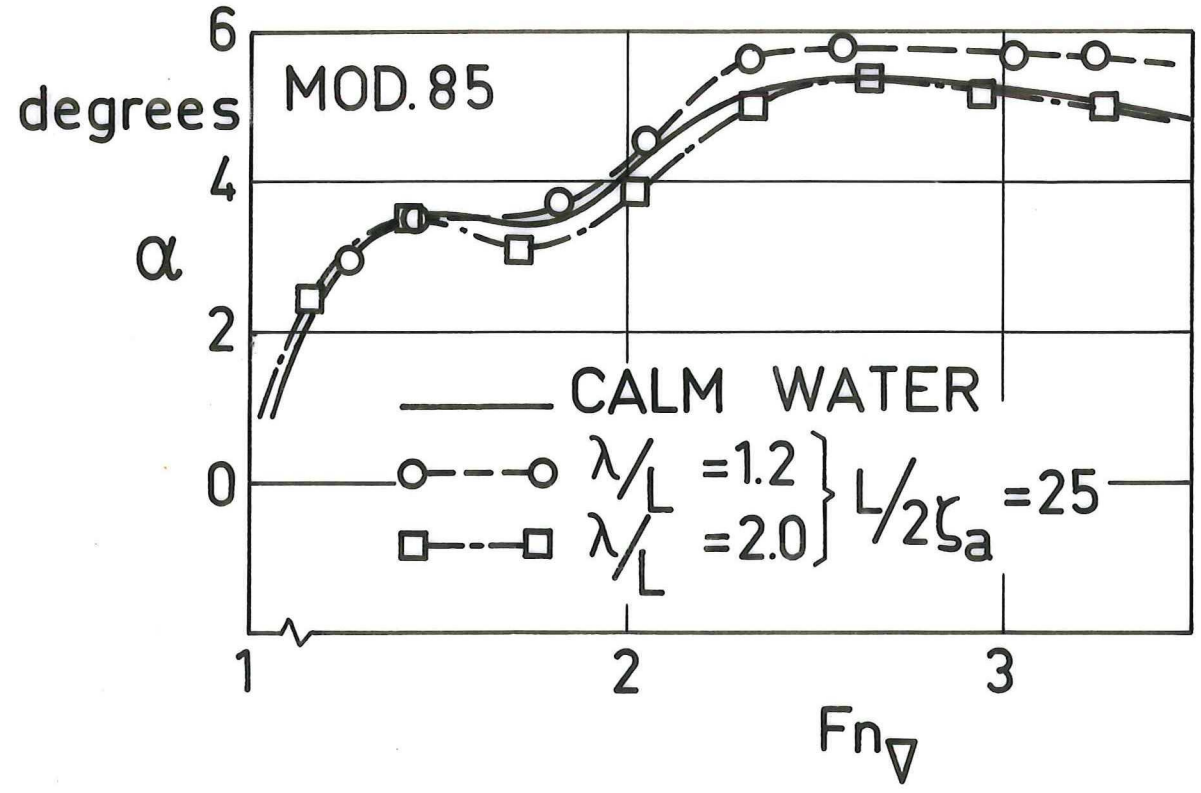

Fig. 7: The mean angle of attack

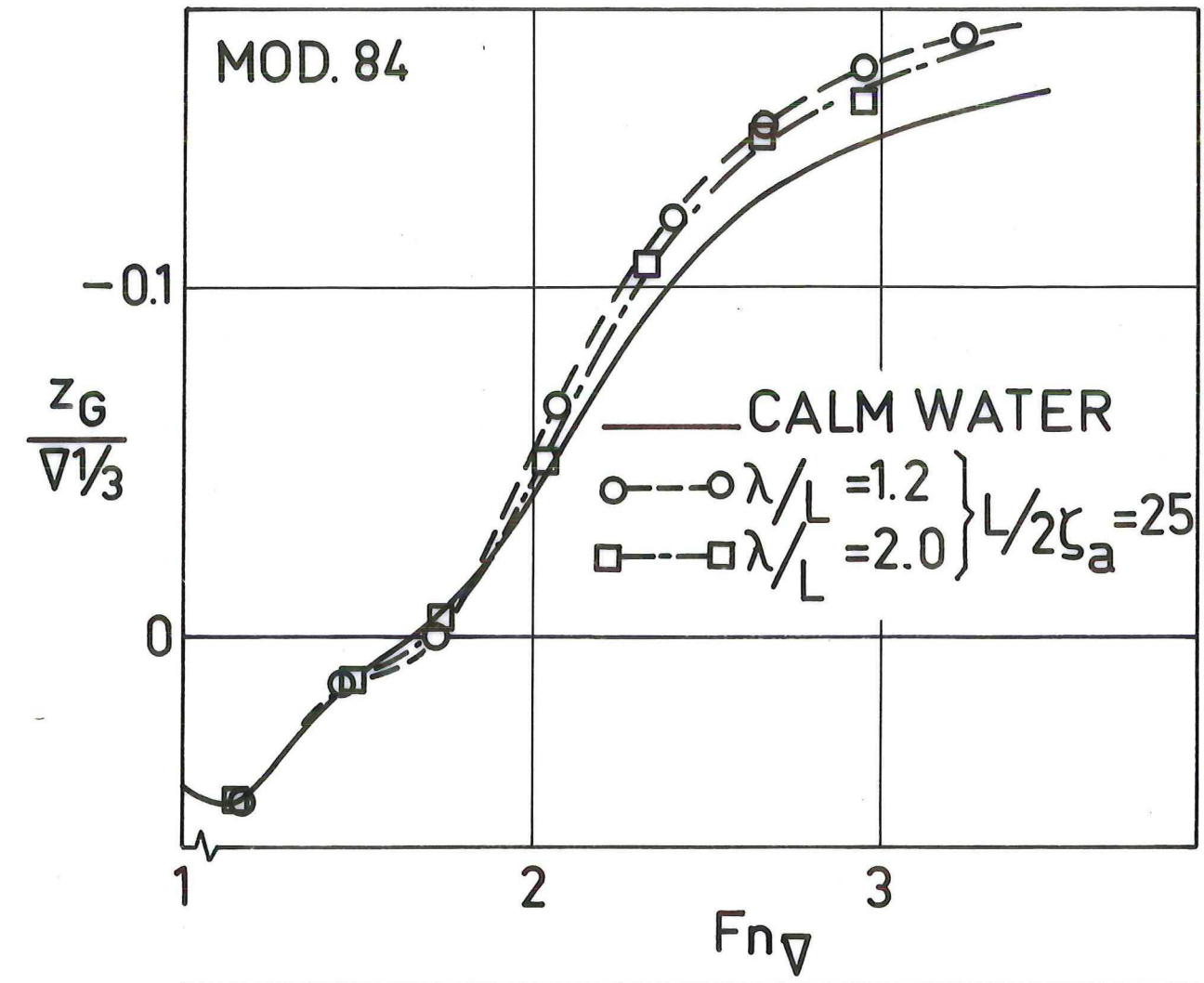

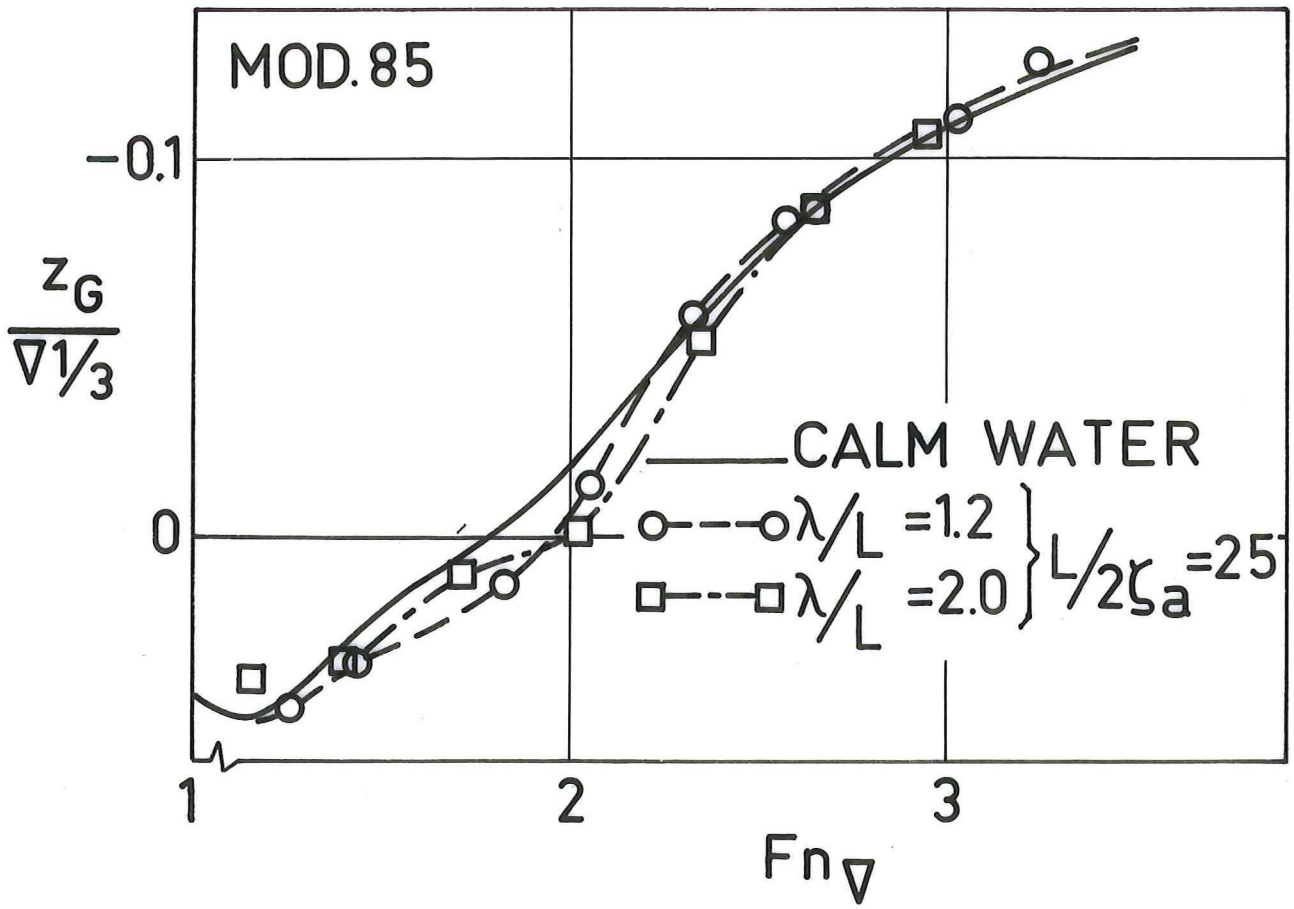

Fig. 8: The mean rise of the center of gravity

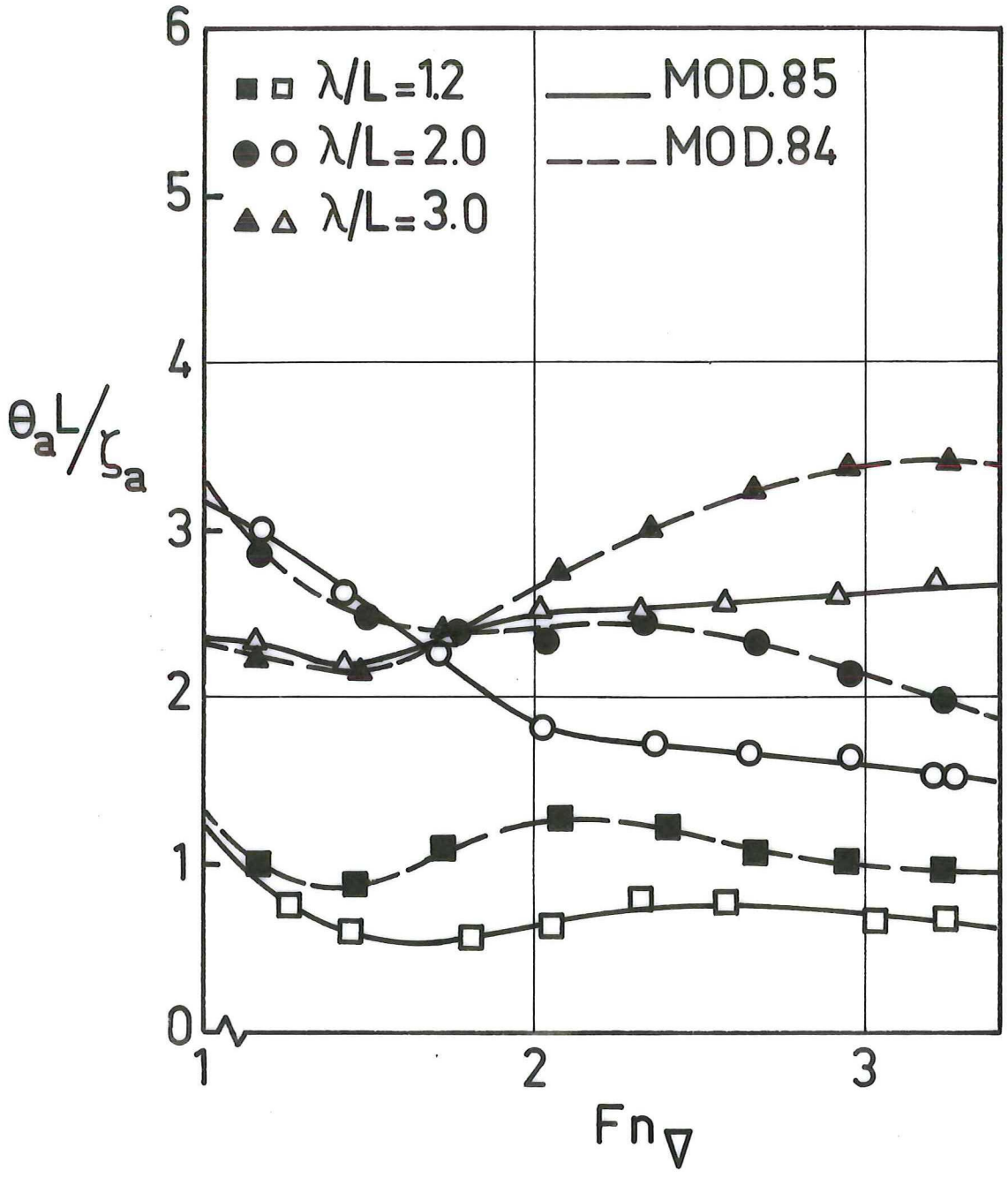

Fig. 9: The reduced pitch amplitudes

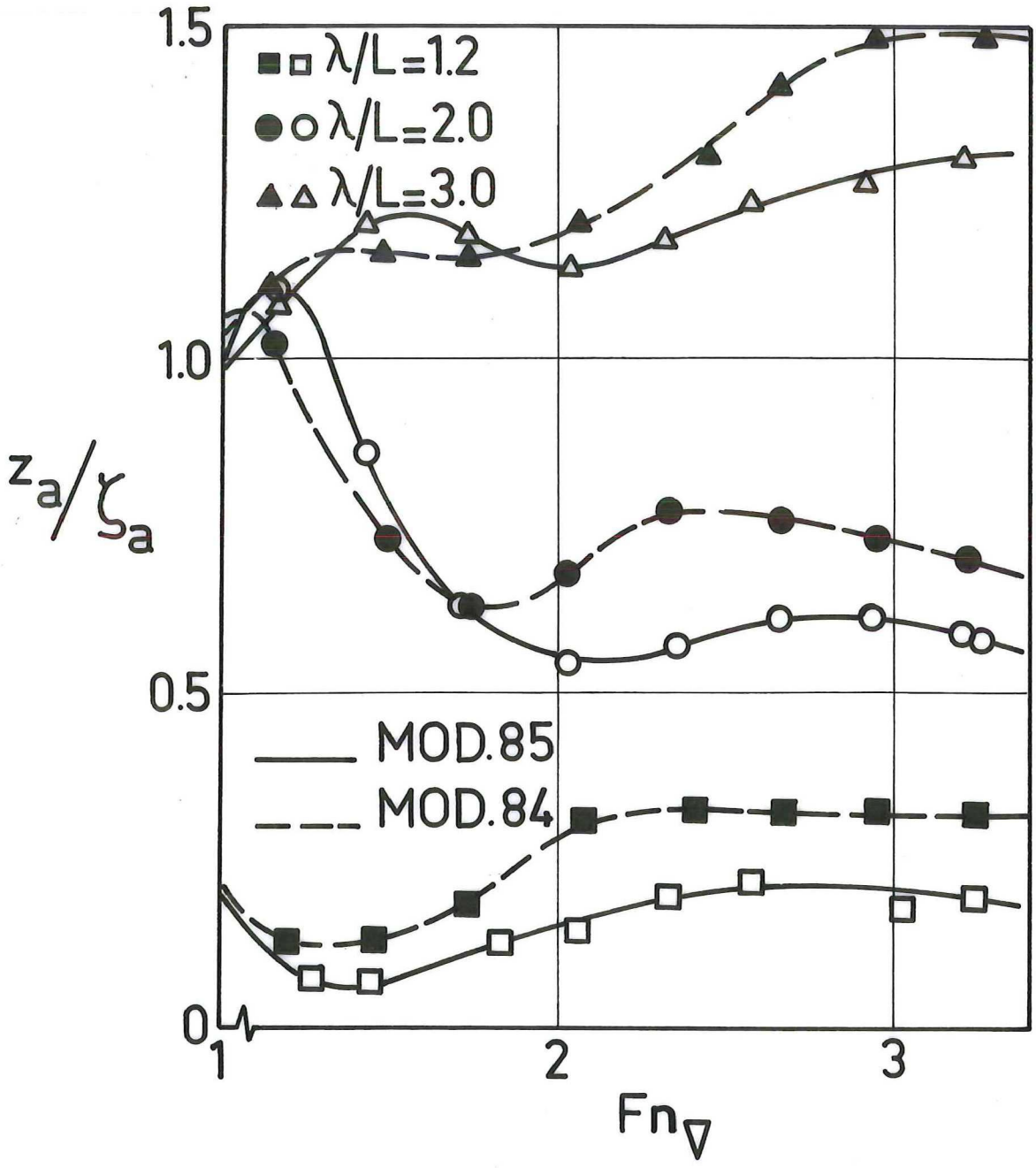

Fig. 10: The reduced heave amplitudes

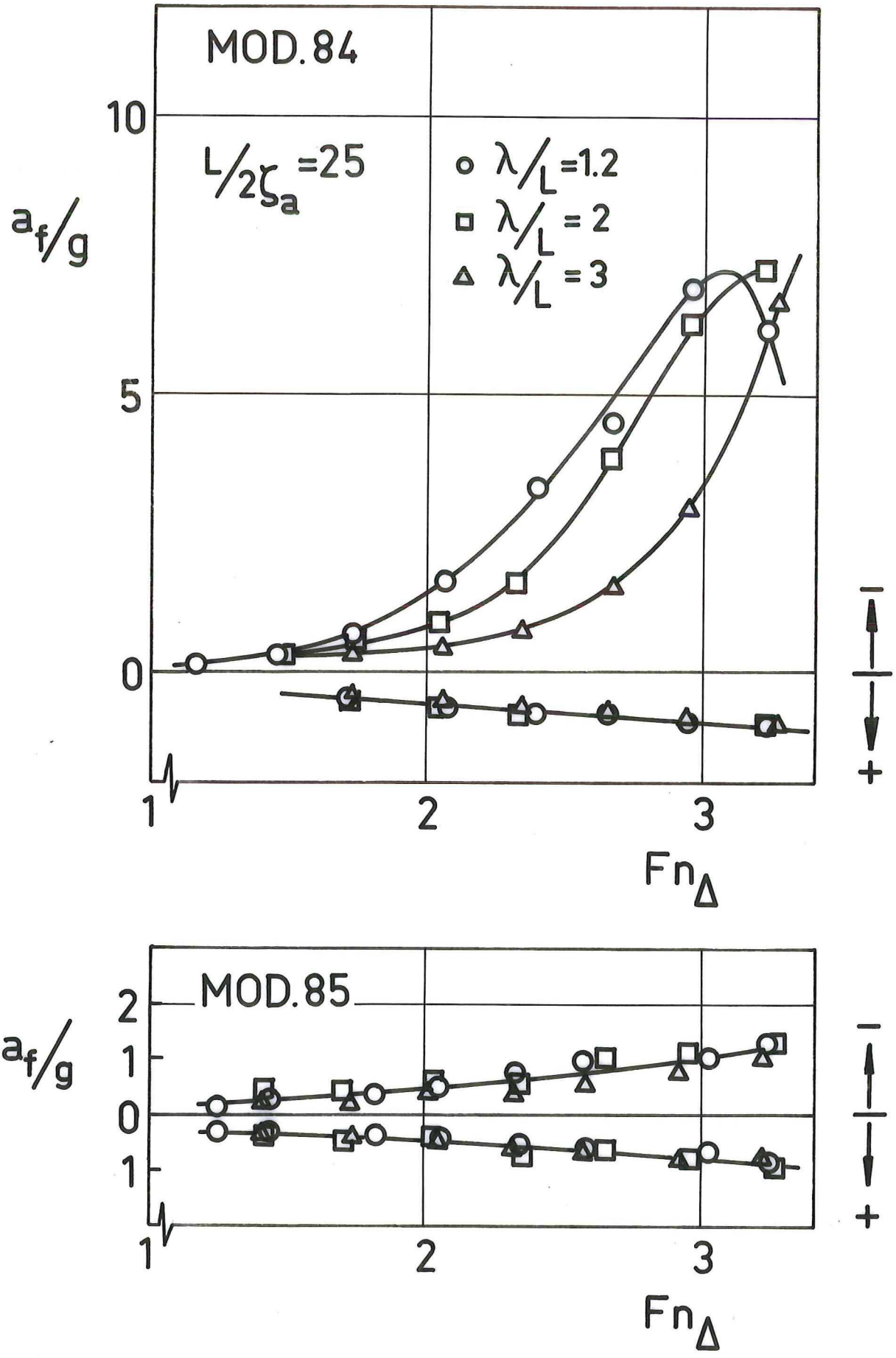

Fig. 11: The vertical accelerations forward at 0.1 L

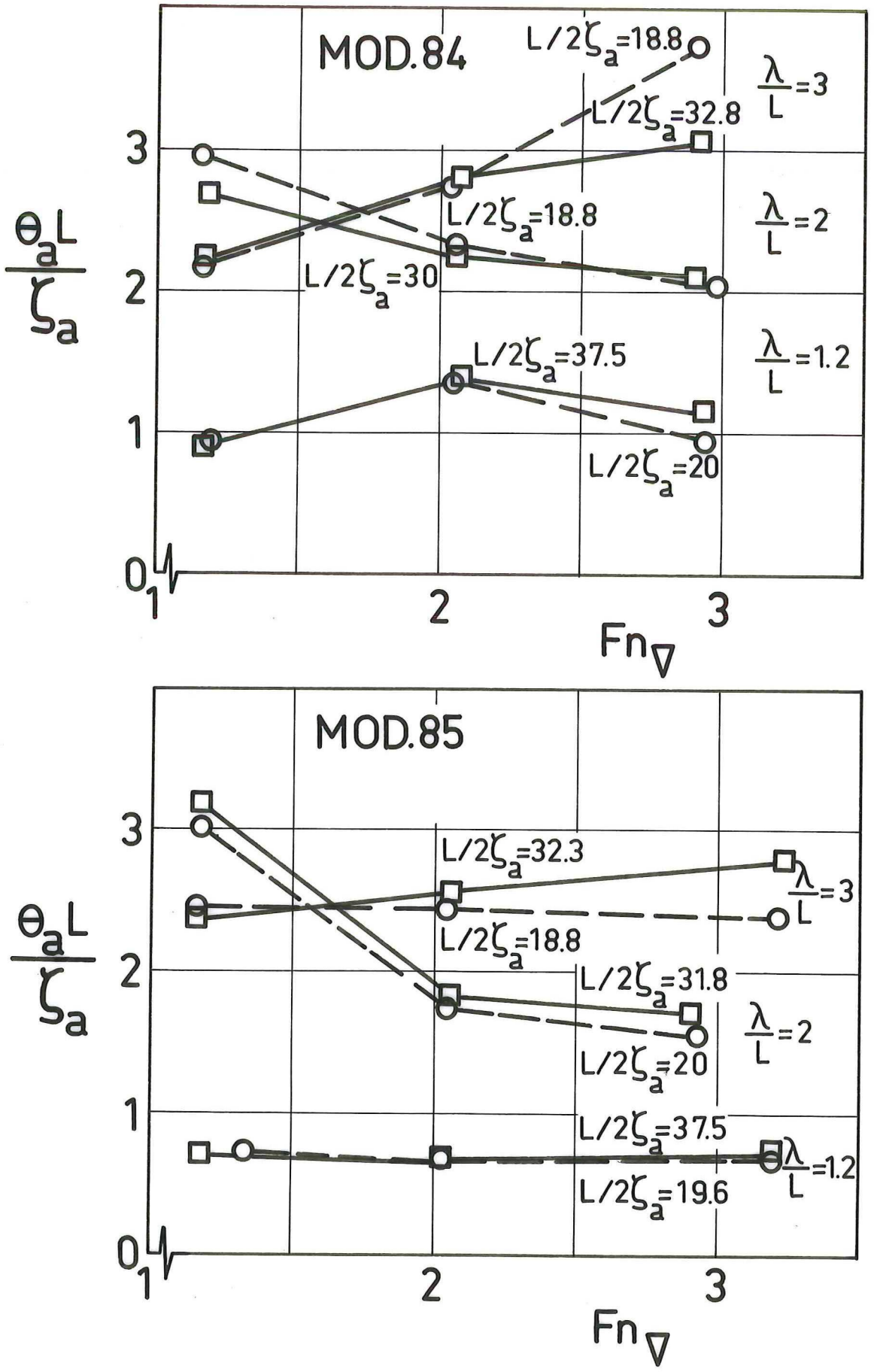

Fig. 12: Check of the linearity of the pitch amplitudes

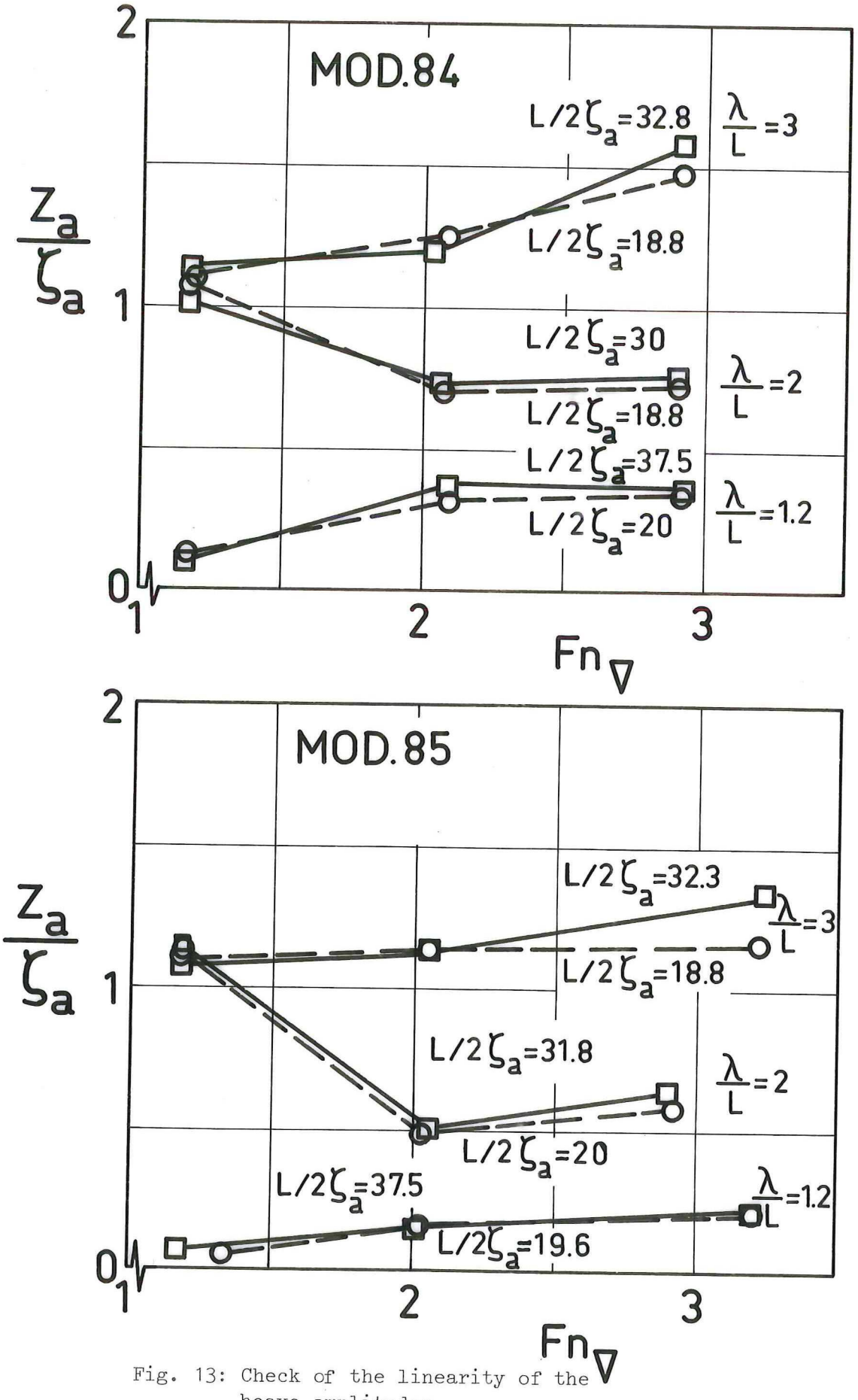

Fig. 13: Check of the linearity of the heave amplitudes

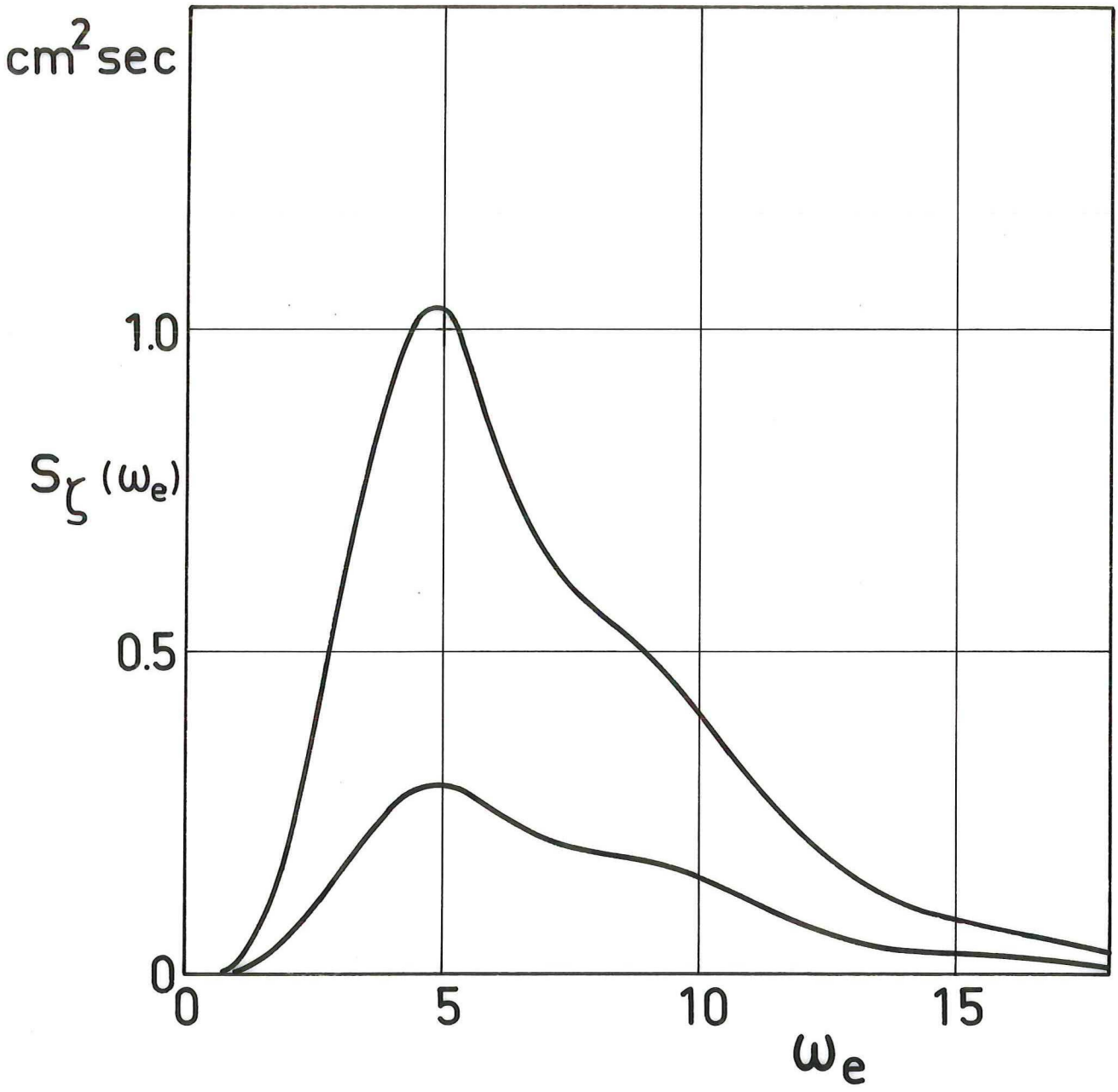

Fig. 14: Wave spectra

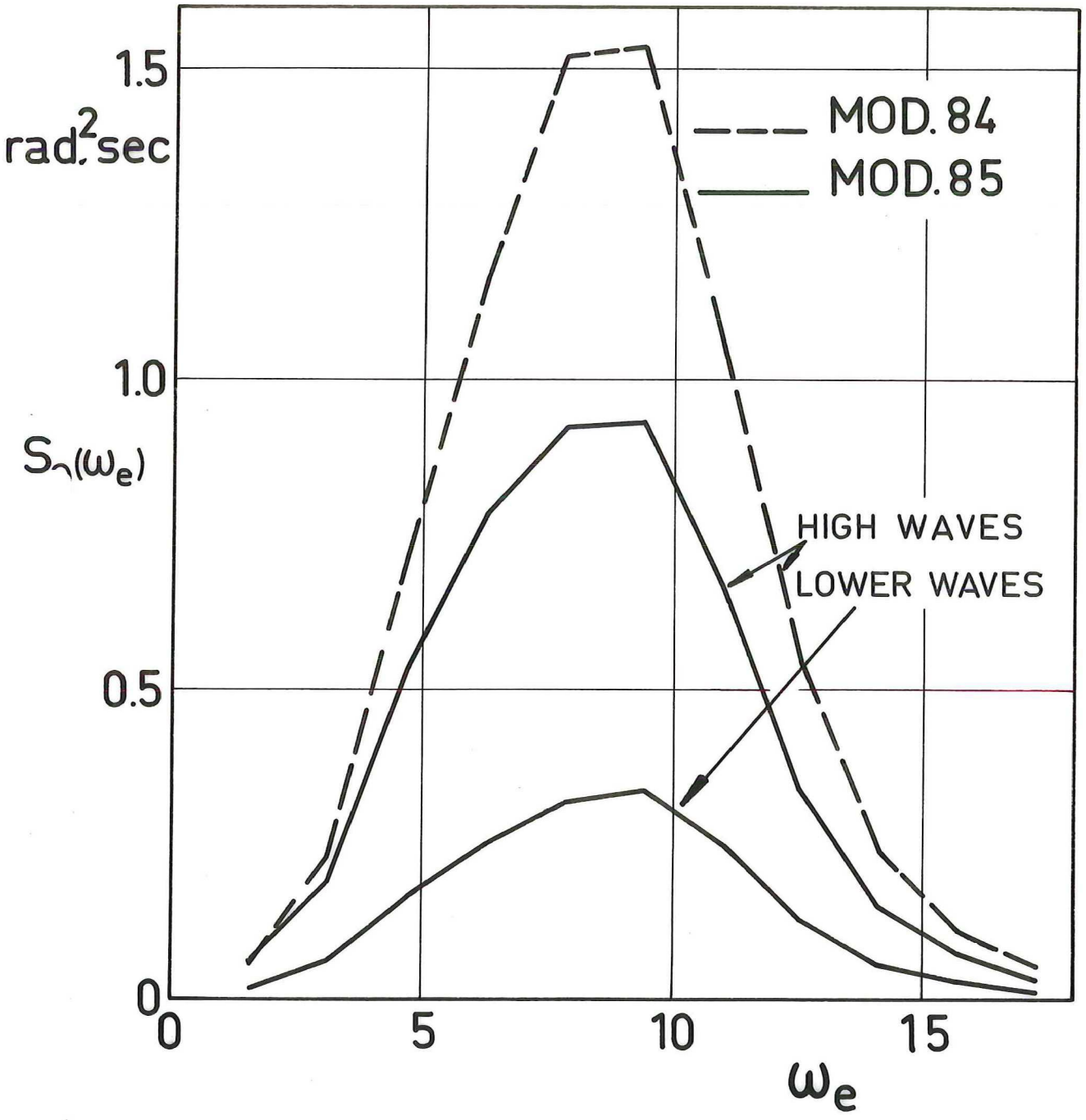

Fig. 15: Pitch spectra

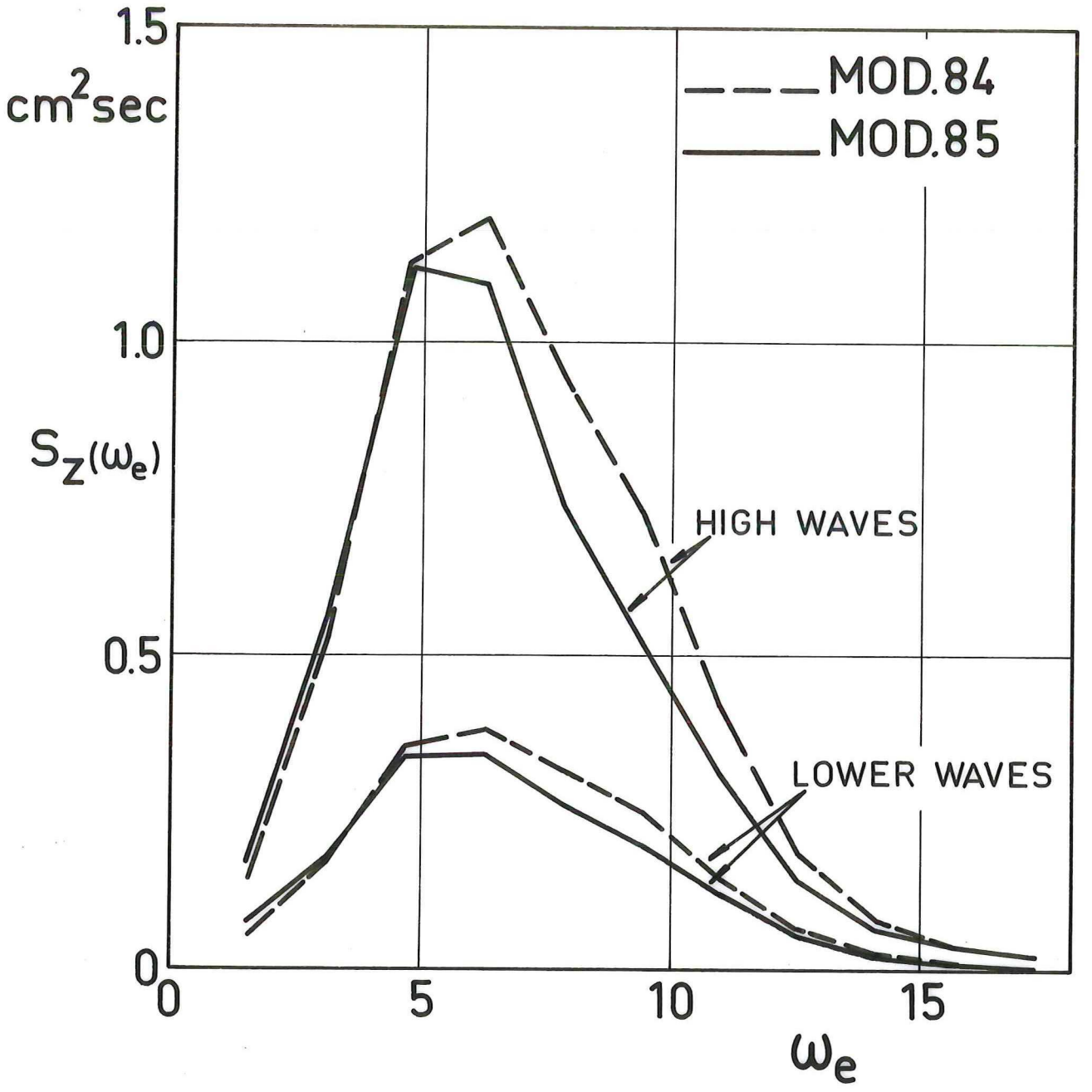

Fig. 16: Heave spectra

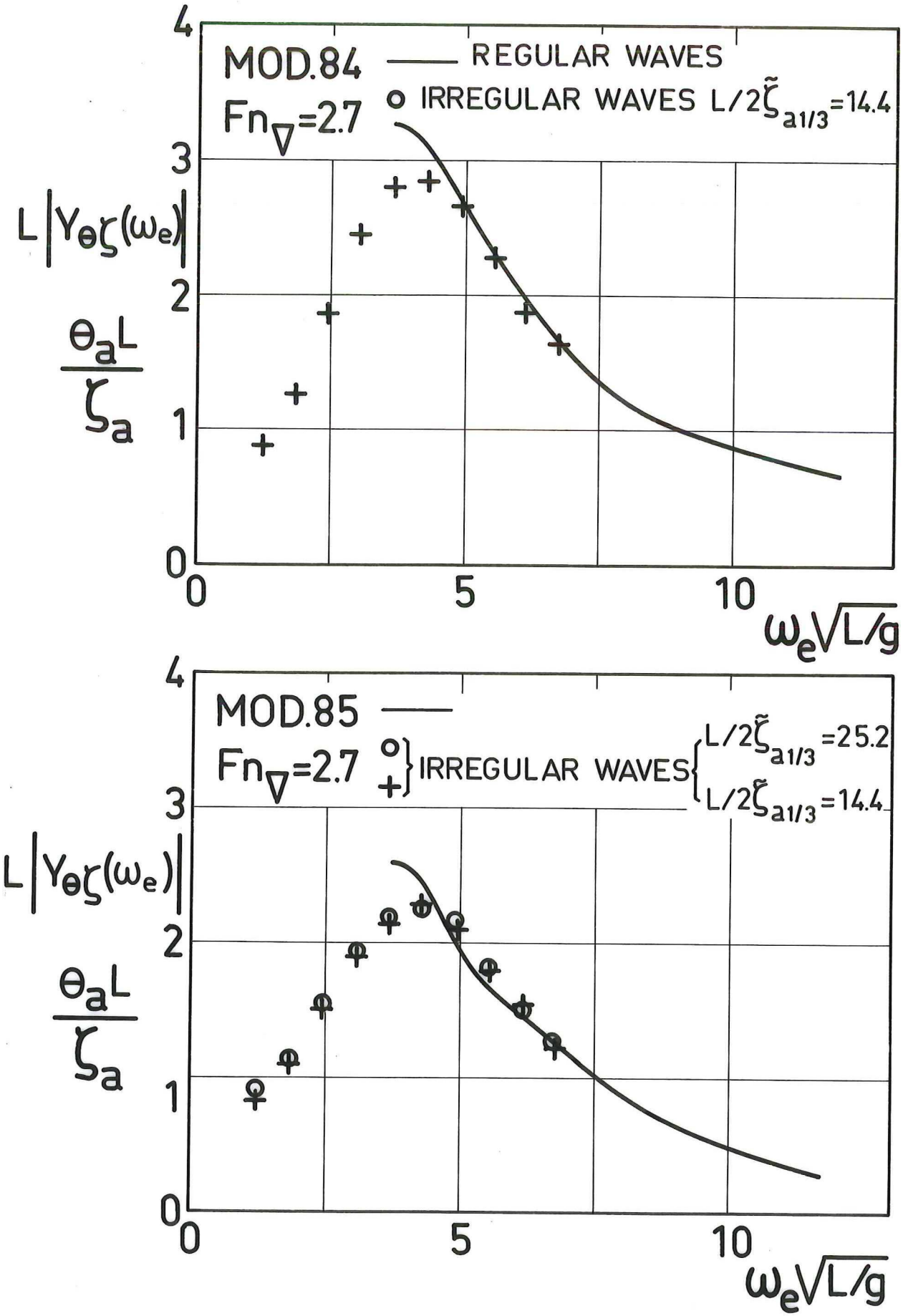

Fig. 17: Comparison of the pitch response in regular and irregular waves

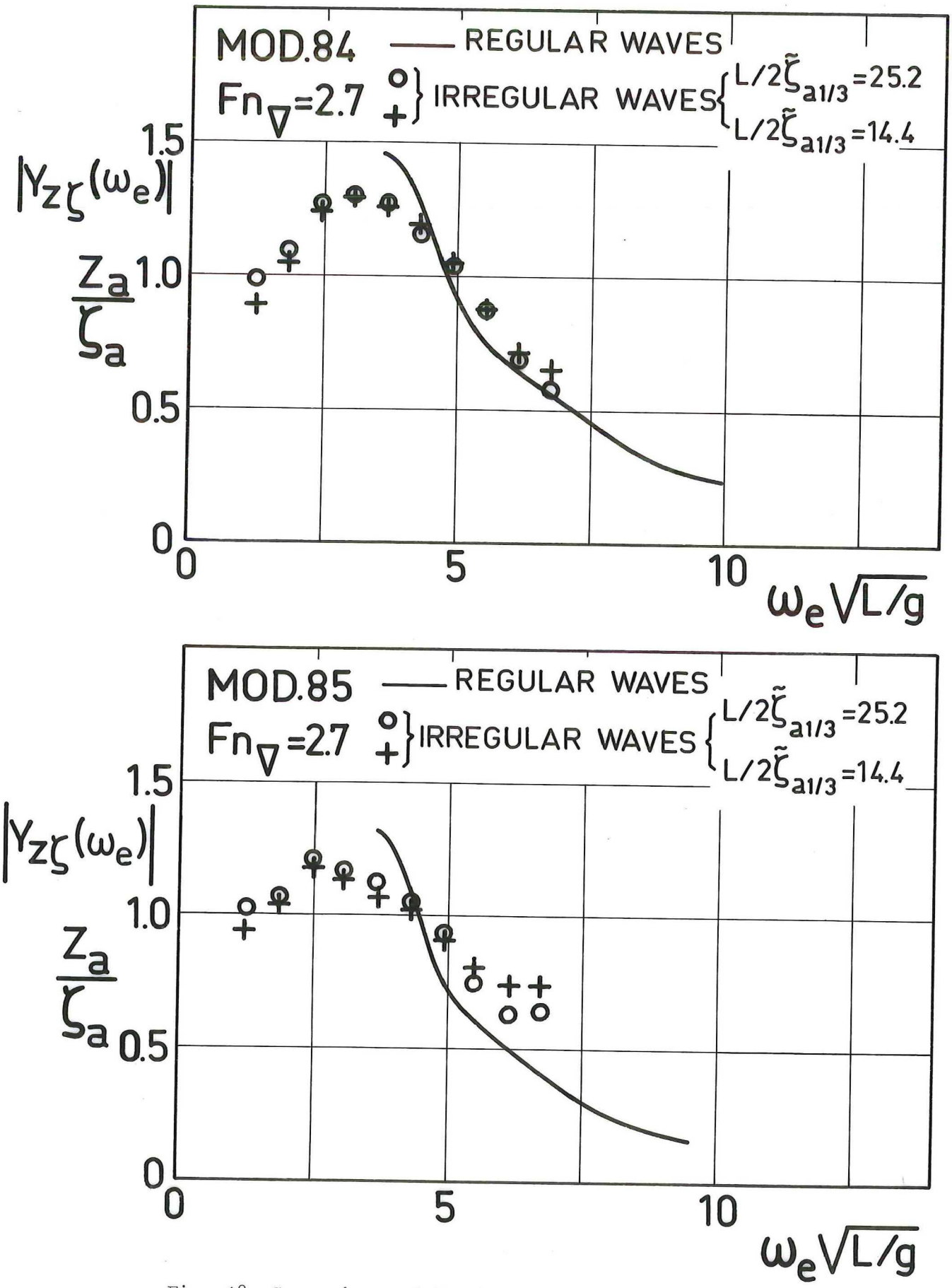

Fig. 18: Comparison of the heave response in regular and irregular waves

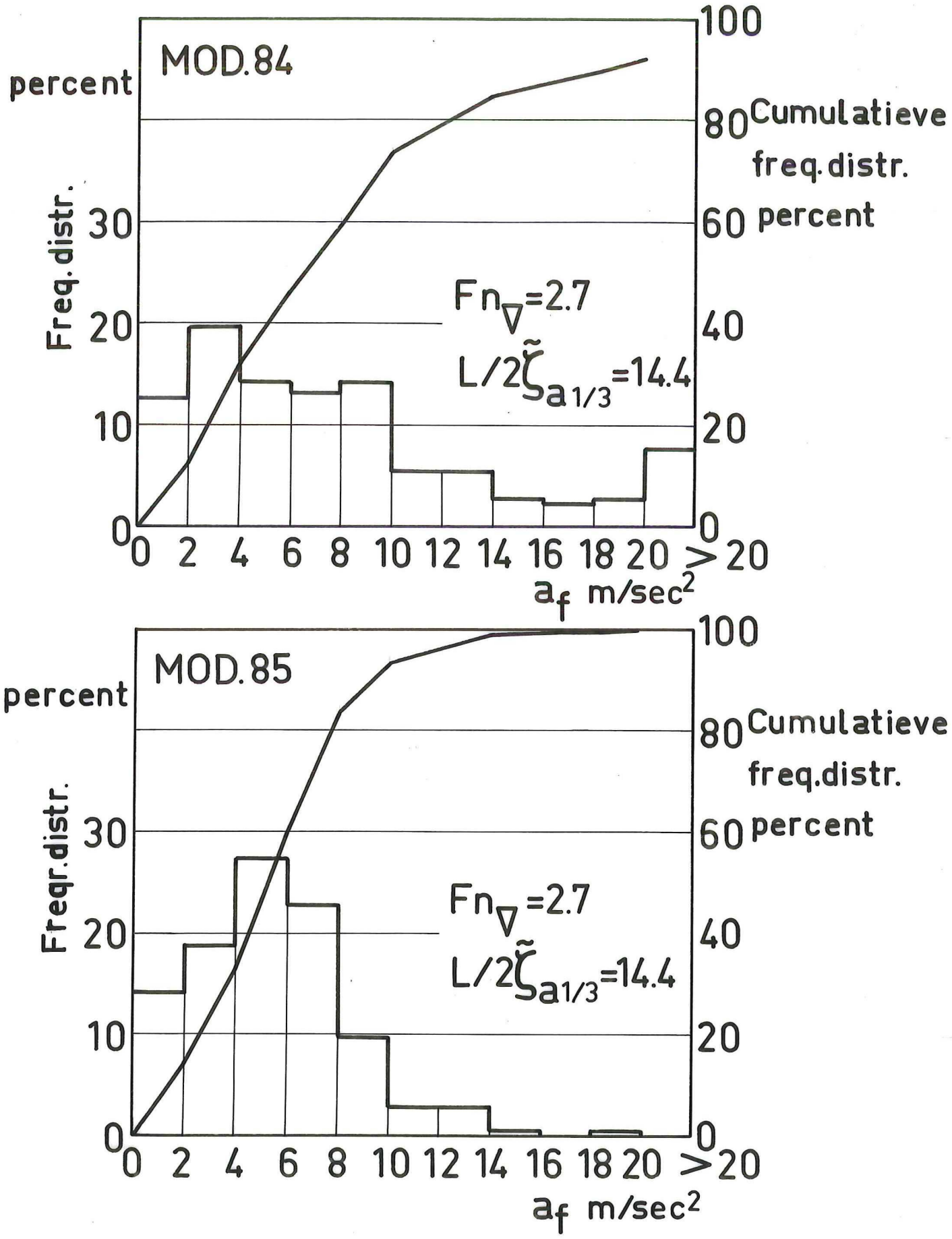

Fig. 19: Frequency of occurence of the peak accelerations at 0.1 L

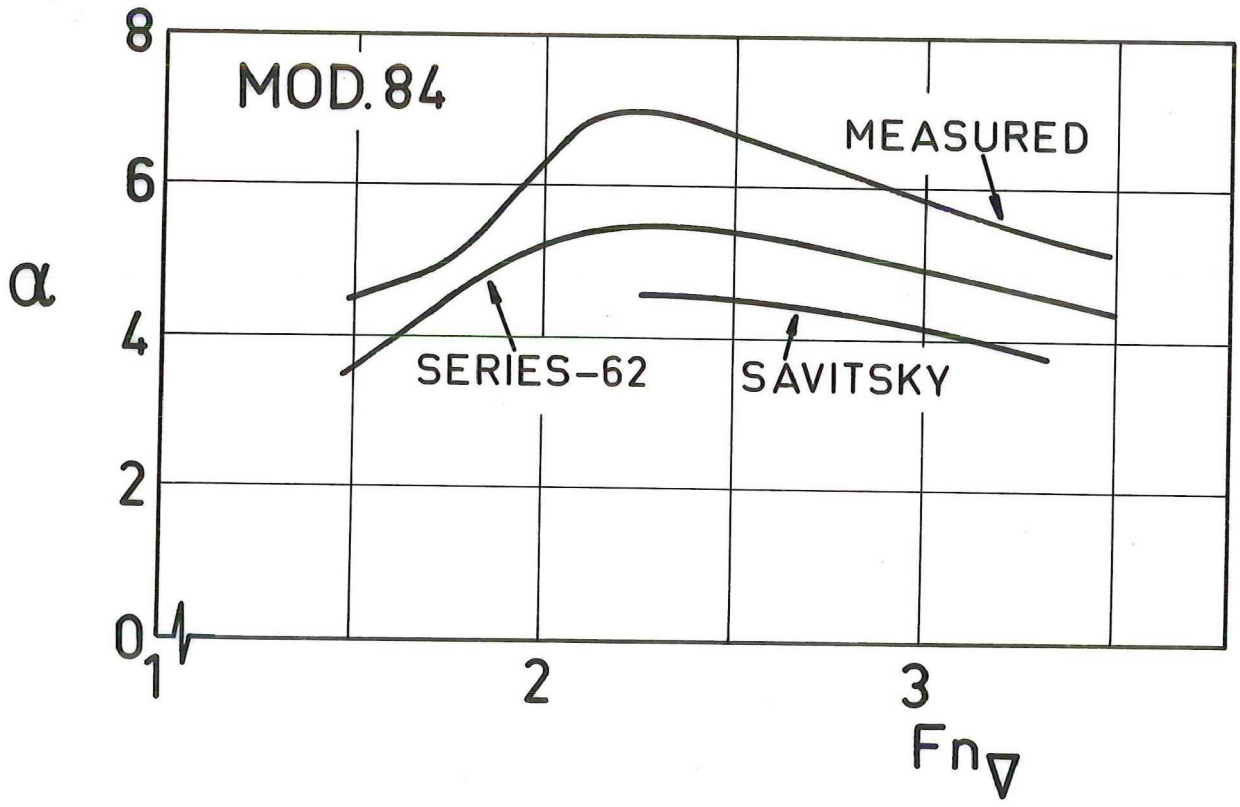

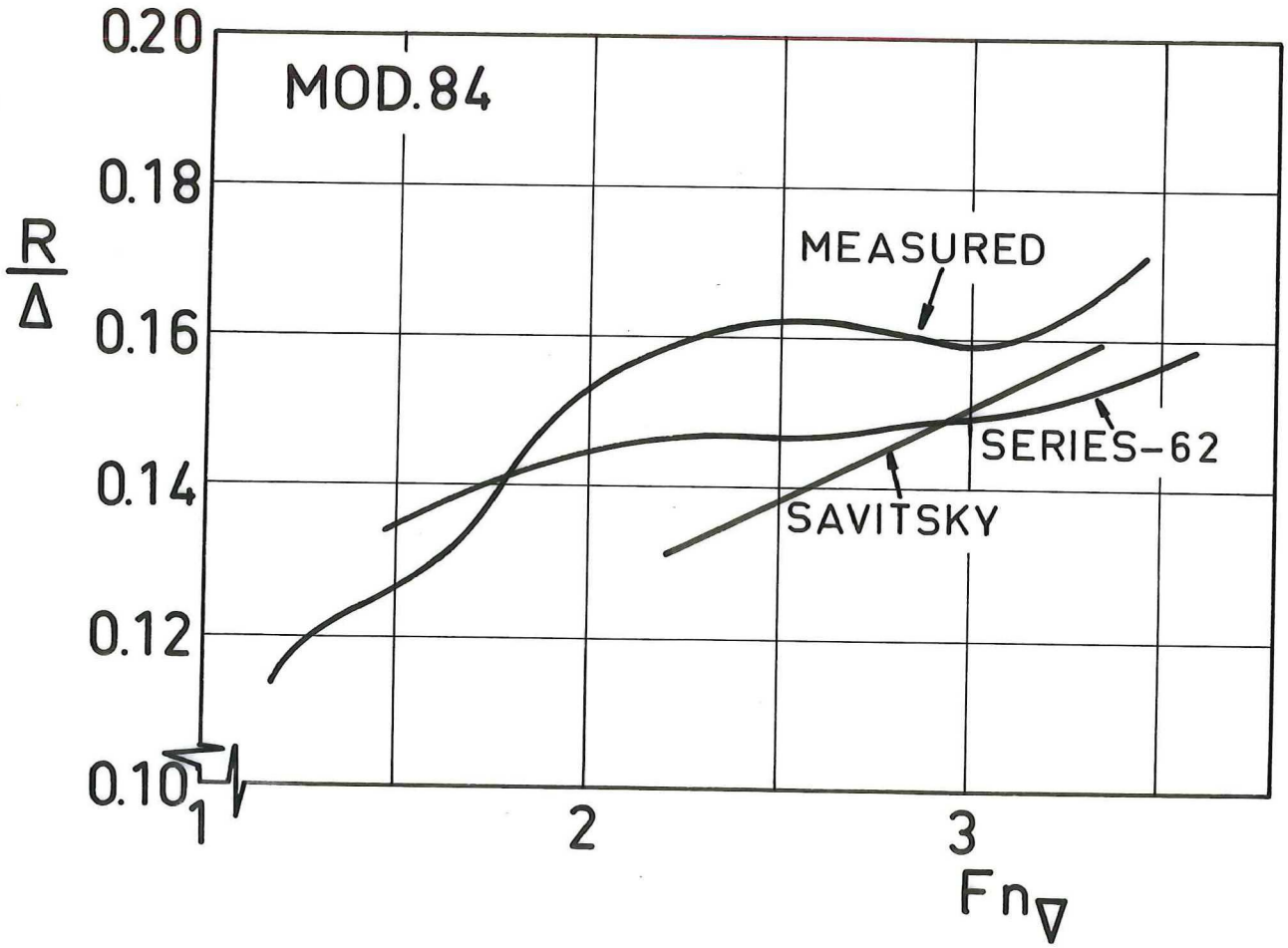

Fig. 20: Comparison of measured values of resistance and angle of attack with published data. Model 84

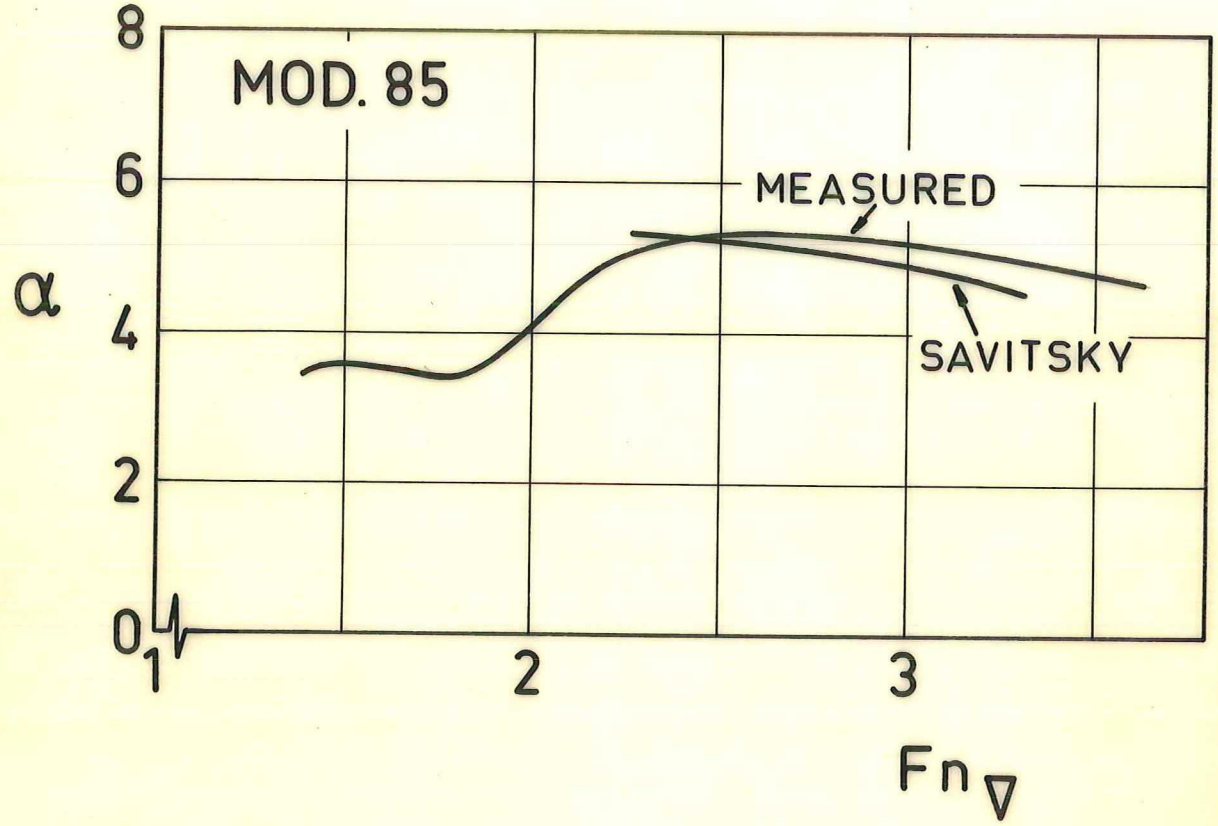

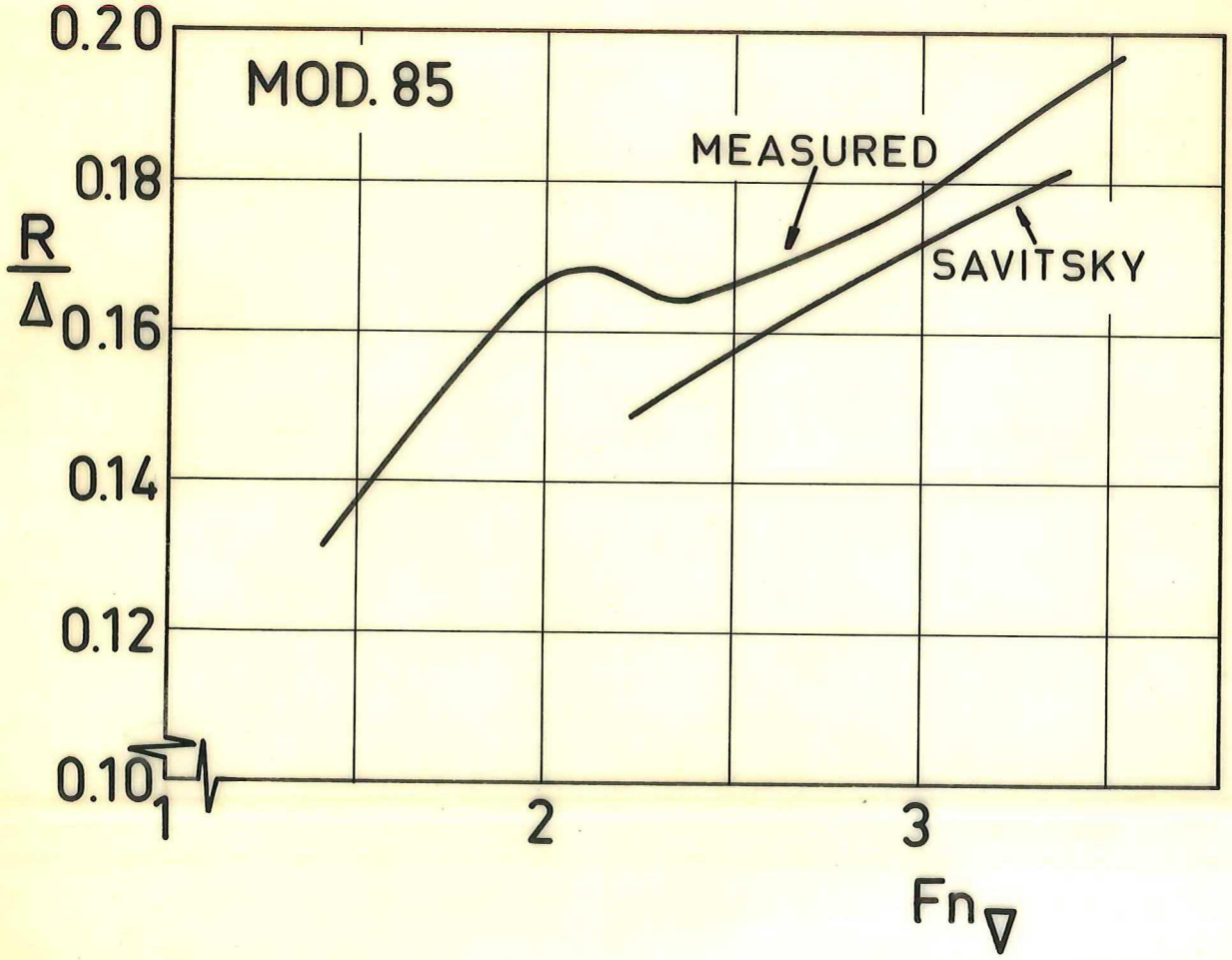

Fig. 21: Comparison of measured values of resistance and angle of attack with published data. Model 85

Report No. 355

LABORATORIUM VOOR SCHEEPSBOUWKUNDE

TECHNISCHE HOGESCHOOL DELFT

RESISTANCE DATA OF HULLFORM 114

by

Ir. J.J. v.d. Bosch

September 1972

Contents

1. Nomenclature

A_p	Horizontal projection of the area bounded by chines and transom, excluding external spray strips
$[A] = \frac{A_p}{\nabla^{2/3}}$	
B_c	Breadth over chines at any cross section
$B_{cm} = \frac{A_p}{L_p}$	Average breadth of area A_p
B_{cmax}	Maximum breadth over chines
b	Span of planing surface, i.e. actual breadth of planing surface measured at main spray point
C_A	Incremental resistance coefficient
$F_{n\nabla} = \frac{V}{\sqrt{g\nabla^{1/3}}}$	Speed-displacement coefficient based on volume of displacement at rest
G	Centre of gravity
g	Acceleration due to gravity
L_p	Length of A_p
l_c	Wetted length of chine, measured parallel to the keel from transom to main spray point
l_k	Wetted length of keel measured from transom
$l_m = \frac{l_c + l_k}{2}$	Mean wetted length
$[M] = \frac{L_p}{\nabla^{1/3}}$	
R	Resistance
R_A	Incremental resistance
S	Wetted surface
$[S] = \frac{S}{\nabla^{2/3}}$	
W	Weight density of water
V	Ship or model speed
X_p	Centre of area A_p
Z_G	Rise of centre of gravity
α	Angle of incidence, i.e. angle between still water surface and keel

α_o	initial trim angle between still water surface and keel
β	Deadrise angle
Δ	Ship or model weight
ν	Kinematic viscosity
ρ	Mass density of water
$\overline{AX}_p$	Distance of X_p from transom at keel
$\overline{AC}$	Distance of G from transom at keel
$\overline{KG}$	Height of G above base line
$\nabla = \frac{\Delta}{w}$	Volume of the displacement of the ship at rest

2. List of figures

3. Introduction

The tested model was one of a series of three :
the numbers 114, 115 and 116.
The aim of the test series was to compare the three hull forms with regard to the resistance in smooth water and the behaviour in irregular head seas in the speed range betwee $F_{nV} = 2$ and $F_{nV} = 4$. This was done in order to develop a hull form with a good overall performance at sea which could function as a parent for a systematic series.
In this report the resistance data of hull form 114 in sea water are given for displacements of up to 800 metric tons. For the information about the other test results the reader is referred to the references [1] , [2] and [3] .

The tests, although being a part of the research program of the Shipbuilding Laboratory of the University of Technology, were carried out at the Netherlands Ship Model Basin under the responsibility of the Netherlands Ship Research Centre, TNO.

4. Modeldata

The hull form is shown in figure 1.

The main particulars of the model 114 are given in the following table :

A_p	0.93312 m^2
B_{cmax}	0.54 m
B_{cm}	0.432 m
L_p	2.16 m
$L_{p/B_{cmax}}$	4
$L_{p/B_{cm}}$	5

	Test 1	Test 2
∇	0.04665 m^3	0.06133 m^3
$\overline{AX}_p$	0.936 m	0.936 m
$\overline{AG}$	0.792 m	0.792 m
$\overline{KG}$	0.18 m	0.197 m
[A]	7.2	6
[M]	6	5.477

5. Test procedure

The model was tested at the loading conditions stated in the preceding section, over a speed range which corresponded to the range of Froude numbers from $F_{nV} = 1.6$ to $F_{nV} = 4.0$.

The model was attached to the towing carriage in its centre of gravity by an air lubricated support, which allowed the model to pitch, heave and roll freely.

The following parameters were measured :

- the modelspeed, which equalled the carriage speed
- the resistance, measured by a strain-gauge dynamometer
- the rise of the centre of gravity, measured by a potentiometer
- the trim angle, measured by a gyroscope
- the form and magnitude of the area wetted by solid water were determined from visual observation.

6. Test results

The actual results are given in the appendix 1. The faired results are given in the figures 2 to 5. In figure 3 the resistance/weight ratio $\frac{R}{\Delta}$ is given for a standard displacement of $\Delta = 16000$ kg in seawater with a weight density of 1025 kg/m^3 and a temperature of 15°C, using the I.T.T.C. 1957 extrapolator without roughness allowance. When it is desired to take into account this additional resistance, use can be made of the curve in the lower part of the figure where the additional resistance/weight ratio $\frac{R_A}{\Delta}$ is given for an incremental resistance coefficient $C_A = 0.0002$.
This curve holds for any value of the ship's displacement; for

$$\frac{R_A}{\Delta} = \frac{C_A \cdot \frac{1}{2}\rho V^2 S}{\rho g \nabla} = 0.0001 . F_{n\nabla}^2 . \quad S$$

The angle of incidence is given in the same figure.

In figure 3 the wetted surface and the mean length of the wetted surface are given, reduced to nondimensional coefficients.

In figure 4 the wetted length at the keel and at the chine are given and the rise of the centre of gravity, also reduced to nondimensional coefficients.

In figure 5 the resistance/weight ratio is given for displacements of 1 to 250 metric tons. The resistance has been computed for seawater with $w = 1025$ kg/m^3 and $t = 15^\circ$ C. Use has been made of the I.T.T.C. 1957 extrapolator without roughness allowance.

7. Discussion of test results

There are no exceptional things to report.
The resistance and trim curves are smooth without accessive humps.
The resistance characteristics are good, considering the high deadrise of the hull.

8. References

[1] "Resistance data of hull form 115"
Shipbuilding Laboratory of the University of Technology, Delft.
Report no. 356.

[2] "Resistance data of hull form 116"
Shipbuilding Laboratory of the University of Technology, Delft.
Report no. 357

[3] "Comparative model tests of three planing hulls in calm water and irregular head waves"
Shipbuilding Laboratory of the University of Technology, Delft.
Report no. 358.

Appendix I

Results of resistance test with model 114 in still water

Test 1

Displacement 46.65 dm^3

Temperature 21.0 centigrade

model speed	rise of centre of gravity	trim angle	model resistance	wetted length of keel	wetted length of chine	wetted surface
m/sec	cm	degrees	kg	cm	cm	m^2
3.08	.52	2.84	5.33	196.5	176.0	1.040
3.86	1.67	3.27	6.13	-	-	.995
4.48	2.47	3.42	6.65	187.0	151.5	.960
5.17	2.93	3.08	7.30	-	-	-
5.98	3.34	3.02	8.11	179.0	129.0	-
6.64	3.84	2.84	9.21	-	-	-
7.46	4.54	2.60	10.31	179.0	118.0	-
6.00	-	-	-	-	-	.890
7.50	-	-	-	-	-	.870

Results of resistance test with model 114 in still water

Test 2

Displacement 61.33 dm^3

Temperature 21.9 centigrade

model speed	rise of centre of gravity	trim angle	model resistance	wetted length of keel	wetted length of chine	wetted surface
m/sec	cm	degrees	kg	cm	cm	m^2
3.28	.84	3.70	7.80	-	-	-
3.88	2.19	4.27	8.45	189.5	161.5	1.055
4.67	3.34	4.36	8.85	-	-	-
5.60	4.31	3.94	9.64	-	-	-
6.16	4.72	3.75	10.32	-	-	-
6.94	5.60	3.37	11.09	-	-	-
7.86	6.21	2.75	12.10	-	-	-
3.20	-	-	-	194.5	176.0	1.095
4.80	-	-	-	183.0	143.5	.905
5.61	-	-	-	178.5	131.0	.865
7.00	-	-	-	173.0	118.0	.840
7.84	-	-	-	172.0	114.0	.835

Appendix II

Table of offsets of model 114

wl	ord 0 mm	ord 2 mm	ord 4 mm	ord 6 mm	ord 7 mm	ord 8 mm	ord 9 mm	ord 10 mm
0	2.7	2.7	2.7	2.7	-	-	-	-
4	102.8	102.8	102.8	96.8	81.4	50.5	-	-
8	190.5	190.5	188.6	165.4	137.3	92.8	25.5	-
12	241.3	260.7	258.3	219.4	181.9	128.0	52.7	-
16	261.2	285.2	290.4	259.4	220.0	159.4	78.3	-
20	273.4	299.9	307.1	280.5	245.2	186.5	103.2	-
24	281.0	309.2	320.4	298.0	264.9	210.2	129.4	17.3
28	284.9	316.4	332.3	314.6	284.7	235.2	157.5	43.8

Deckline

ord	beam mm	height
0	285	300.0
2	319	315.6
4	341	331.2
6	333.5	346.8
7	315.4	354.6
8	281.5	362.4
9	223.6	370.2
10	130.2	378.0

Chine

ord	beam mm	height mm
0	225.0	97.0
2	254.0	112.2
4	269.9	127.4
6	250.5	146.7
7	209.7	159.4
8	170.4	174.9
9	99.1	193.6
10	2.7	216.0

Keel and Stem

ord	beam	height
6	2.7	0
7	2.7	0.2
8	2.7	5.7
9	2.7	49.0
10	2.7	216.0

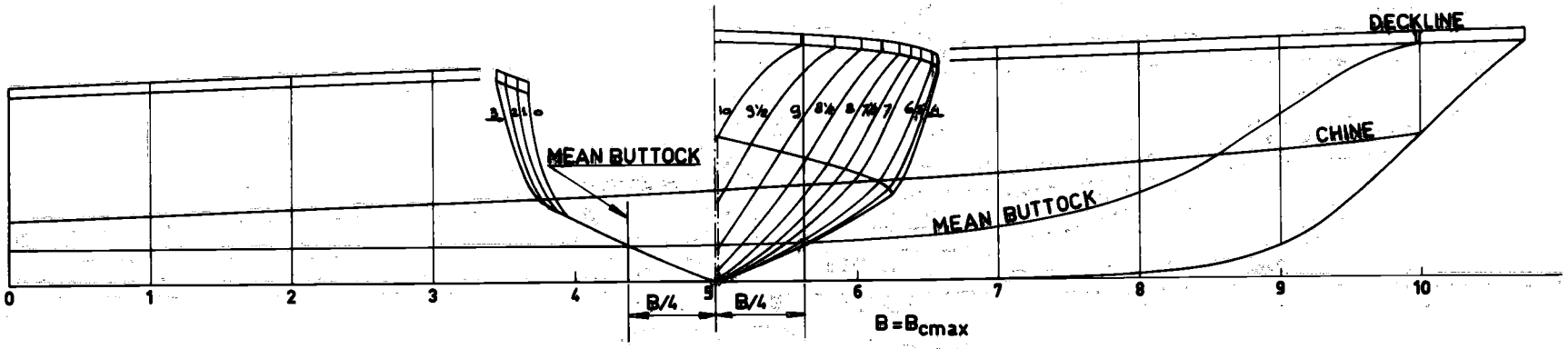

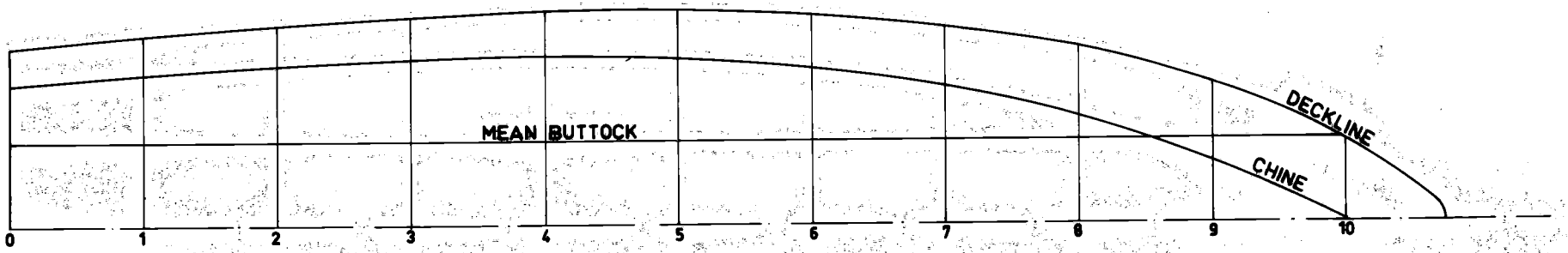

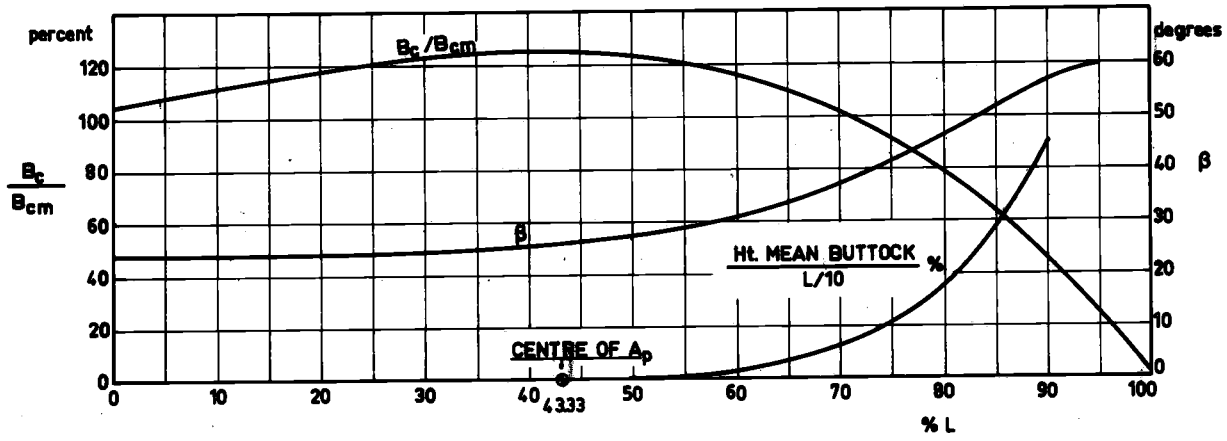

DETAIL SPRAYSTRIPS
SCALE 1:5 FOR Δ = 16 TON

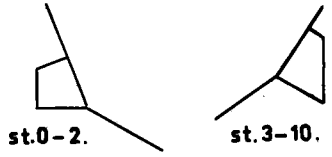

Fig.1. Lines and formcharacteristics of the hull of model 114.

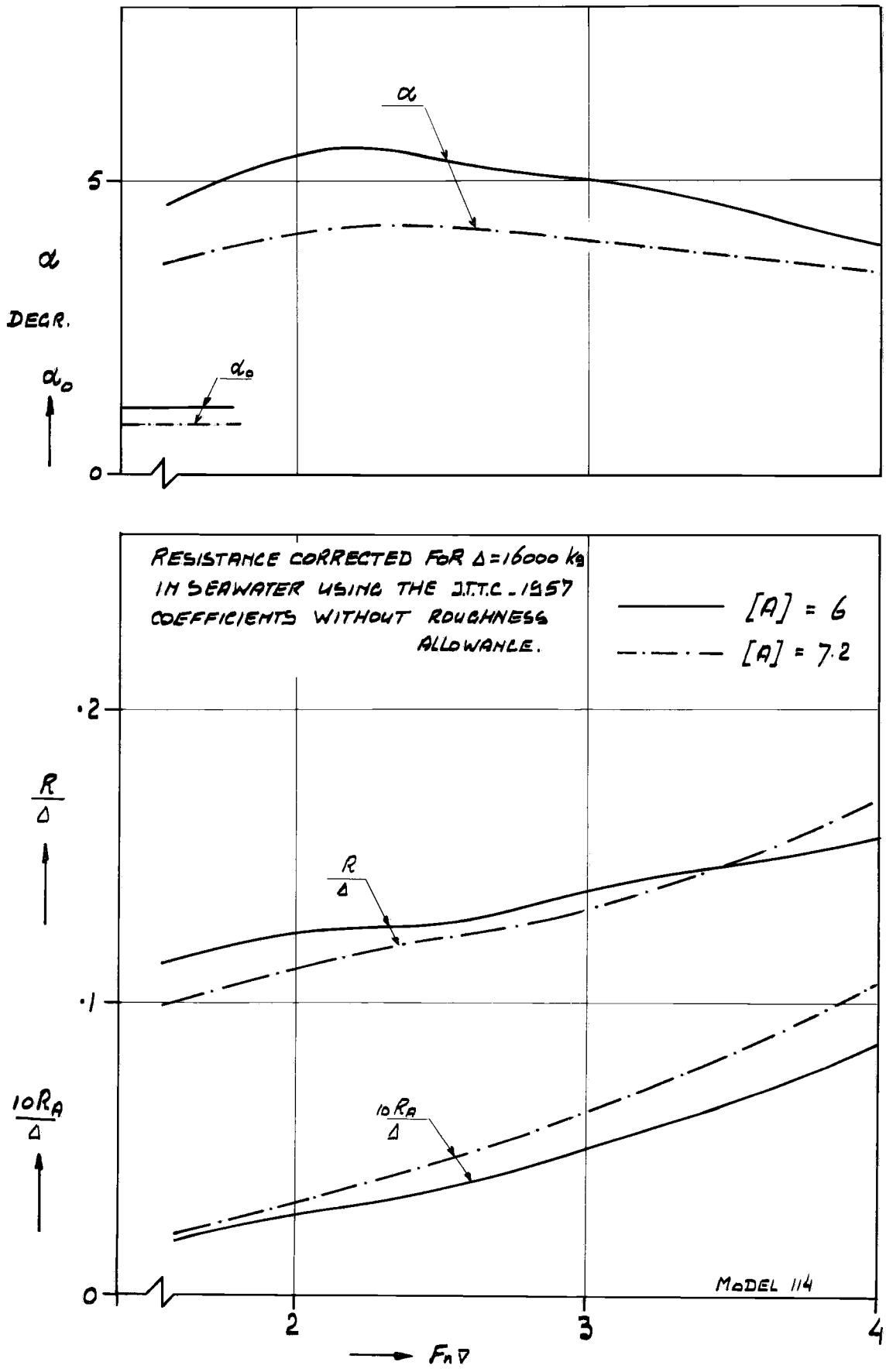

fig. 9 Resistance-weight ratio of the standard ship and angle of attack

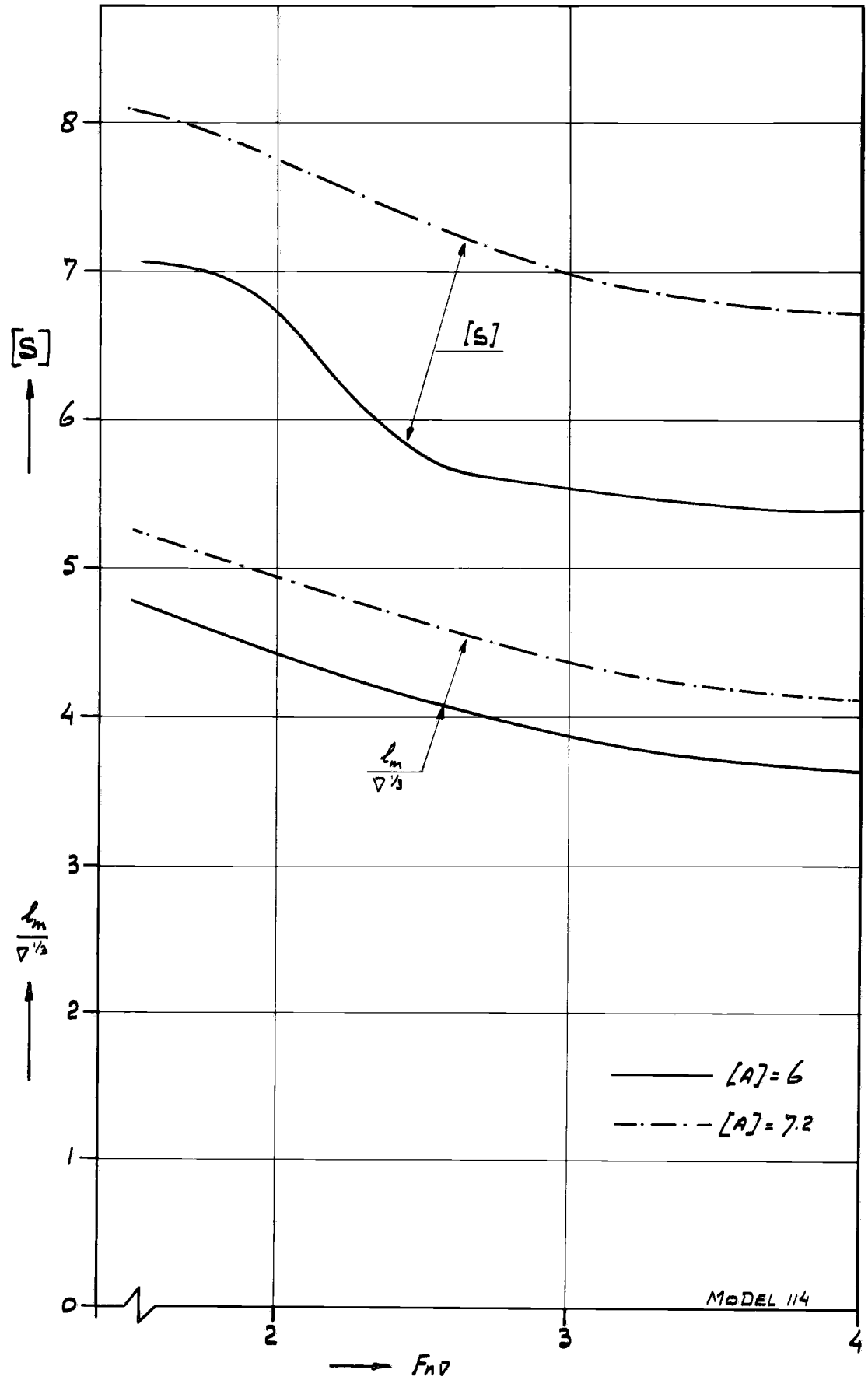

fig. 3 Wetted surface and mean wetted length ratio's

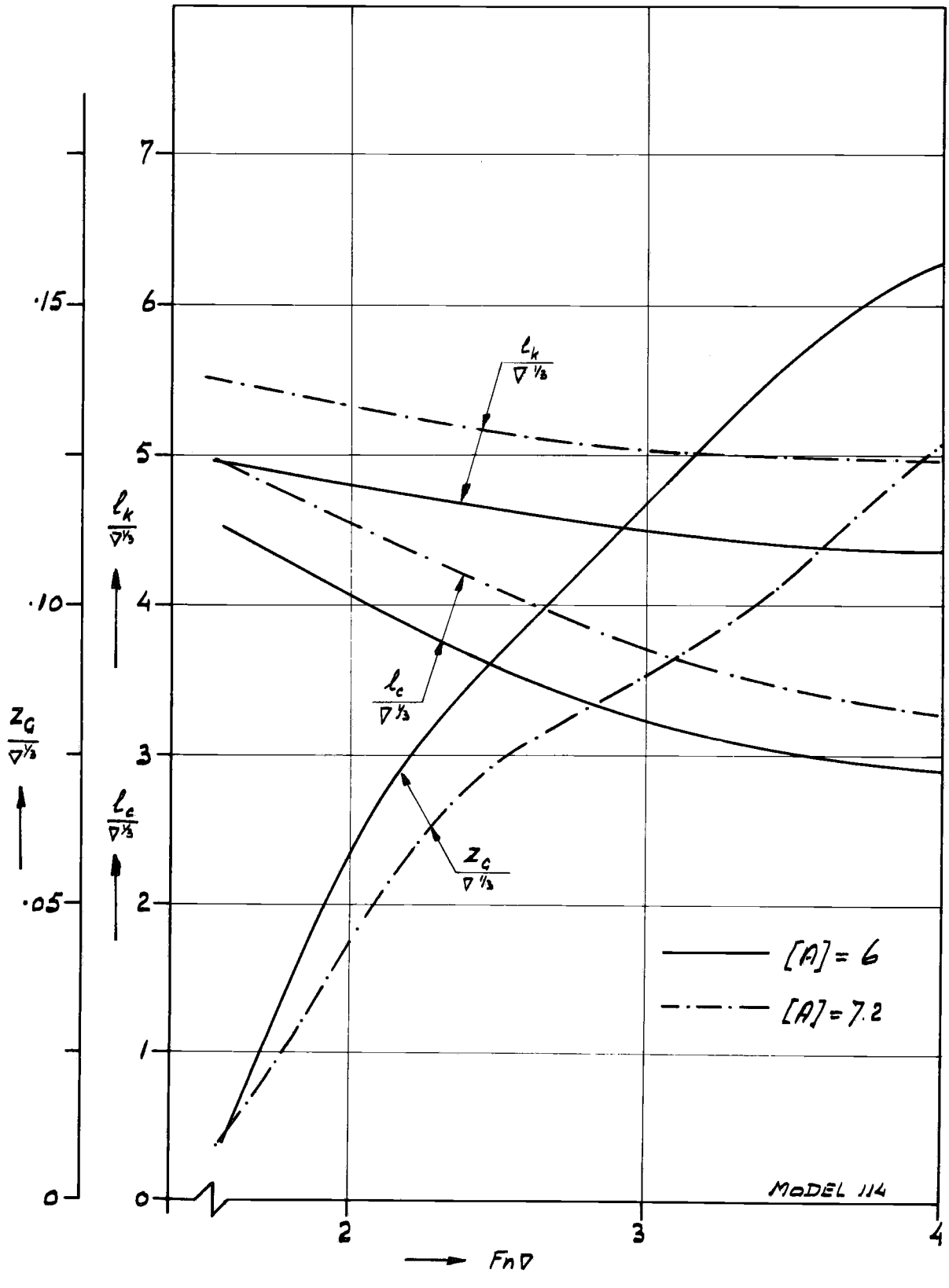

fig. 4 Wetted length ratio's and rise of centre of gravity

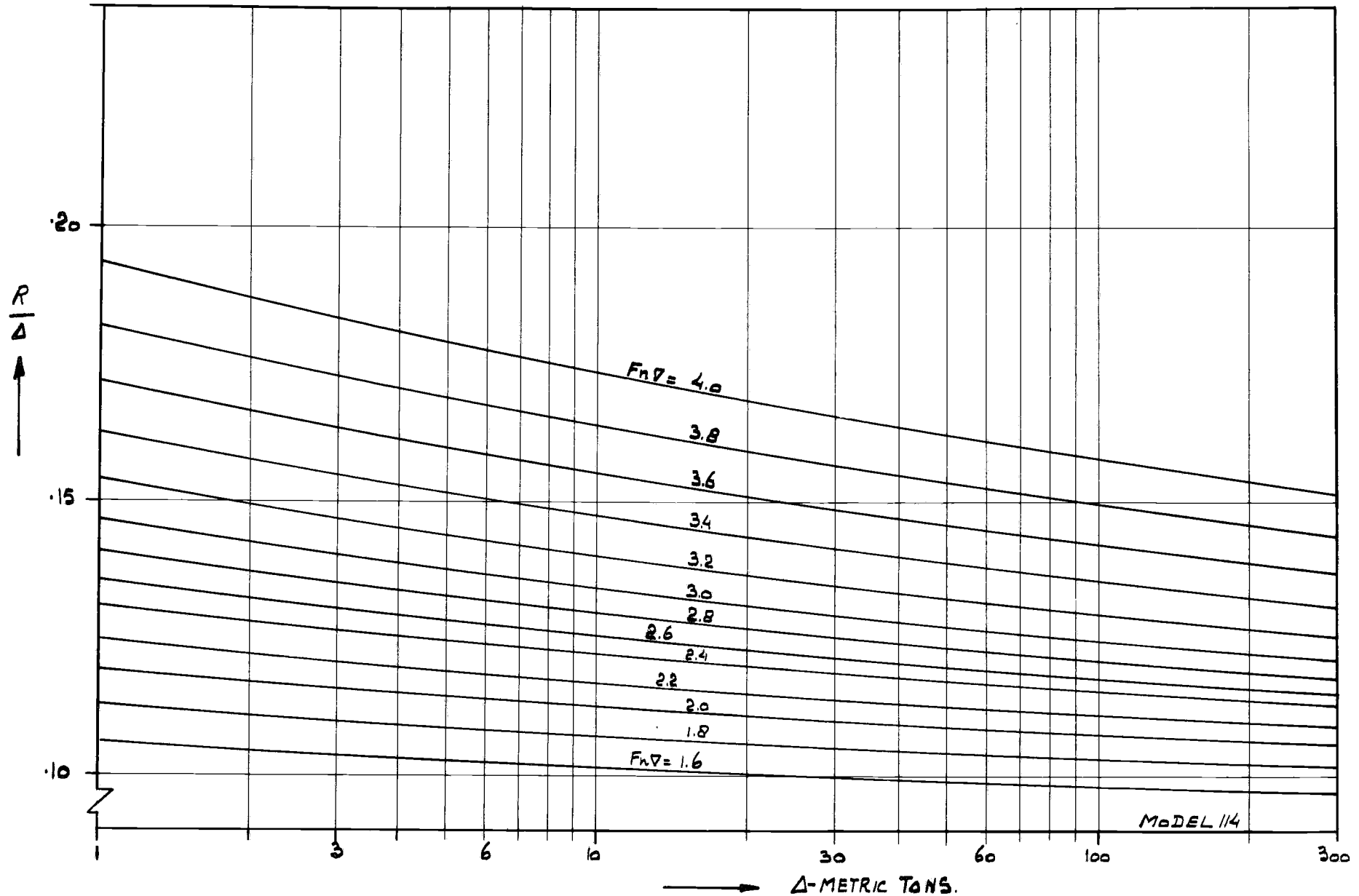

fig. 5 A Resistance-weight ratio as a function of Δ and $F_{n\nabla}$ [A] = 7.2

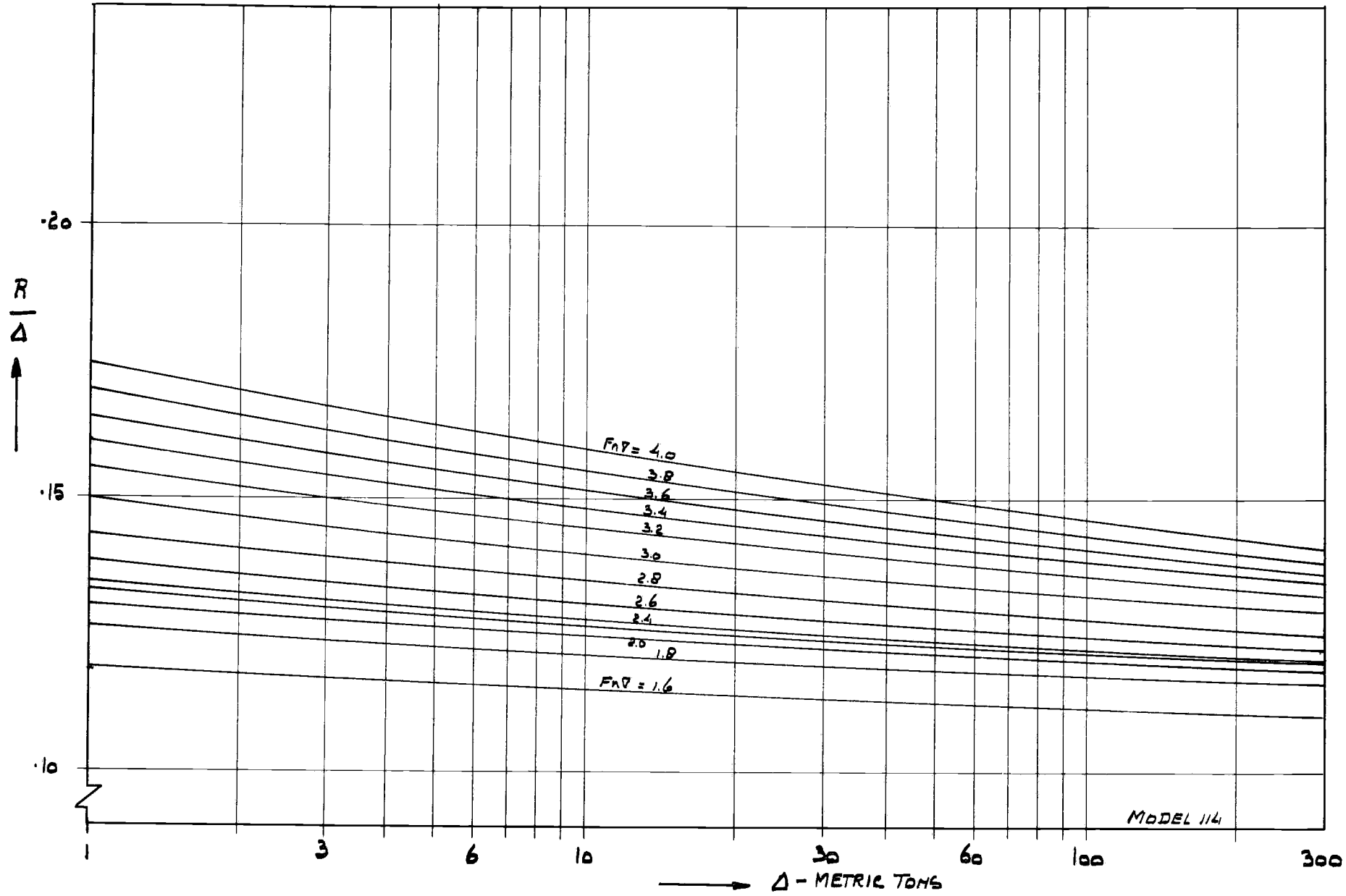

fig. 5 B Resistance-weight ratio as a function of Δ and $F_{n\nabla}$ [A] = 6

Report No. 356

LABORATORIUM VOOR SCHEEPSBOUWKUNDE

TECHNISCHE HOGESCHOOL DELFT

RESISTANCE DATA OF HULL FORM 115

by

Ir. J.J. v.d. Bosch

September 1972

Contents

1. Nomenclature

A_p	Horizontal projection of the area bounded by chines and transom, excluding external spray strips
$[A] = \frac{A_p}{\nabla^{2/3}}$	
B_c	Breadth over chines at any cross section
$B_{cm} = \frac{A_p}{L_p}$	Average breadth of area A_p
B_{cmax}	Maximum breadth over chines
b	Span of planing surface, i.e. actual breadth of planing surface measured at main spray point
C_A	Incremental resistance coefficient
$F_{n\nabla} = \frac{V}{\sqrt{g\nabla^{1/3}}}$	Speed-displacement coefficient based on volume of displacement at rest
G	Centre of gravity
g	Acceleration due to gravity
L_p	Length of A_p
l_c	Wetted length of chine, measured parallel to the keel from transom to main spray point
l_k	Wetted length of keel measured from transom
$l_m = \frac{l_c + l_k}{2}$	Mean wetted length
$[M] = \frac{L_p}{\nabla^{1/3}}$	
R	Resistance
R_A	Incremental resistance
S	Wetted surface
$[S] = \frac{S}{\nabla^{2/3}}$	
W	Weight density of water
V	Ship or model speed
X_p	Centre of area A_p
Z_G	Rise of centre of gravity
α	Angle of incidence, i.e. angle between still water surface and keel

α_o	initial trim angle between still water surface and keel
β	Deadrise angle
Δ	Ship or model weight
ν	Kinematic viscosity
ρ	Mass density of water
$\overline{AX}_p$	Distance of X_p from transom at keel
$\overline{AG}$	Distance of G from transom at keel
$\overline{KG}$	Height of G above base line
$\nabla = \frac{\Delta}{w}$	Volume of the displacement of the ship at rest

2. List of figures

3. Introduction

The tested model was one of a series of three : the numbers 114, 115 and 116.
The aim of the test series was to compare the three hull forms with regard to the resistance in smooth water and the behaviour in irregular head seas in the speed range betwee $F_{n\nabla} = 2$ and $F_{n\nabla} = 4$. This was done in order to develop a hull form with a good overall performance at sea which could function as a parent for a systematic series.
In this report the resistance data of hull form 1'5 in sea water are given for displacements of up to 300 metric tons. For the information about the other test results the reader is referred to the references [1] , [2] and [3] .

The tests, although being a part of the research program of the Shipbuilding Laboratory of the University of Technology, were carried out at the Netherlands Ship Model Basin under the responsibility of the Netherlands Ship Research Centre, TNO.

4. Modeldata

The hullform is shown in figure 1.

The main particulars of the model 115 are given in the following table :

A_p	.93312	m^2
B_{cmax}	0.54	m
B_{cm}	0.432	m
L_p	2.16	m
$L_{/Bcmax}$	4	
$L_{/Bcm}$	5	

	Test 1		Test 2	
∇	.04665	m^3	.06133	m^3
$\overline{AX}_p$	1.008	m	1.008	m
$\overline{AG}$	0.864	m	0.864	m
$\overline{KG}$	.18	m	.197	m
[A]	7.2		6	
[M]	6		5.477	

5. Test procedure

The model was tested at the loading conditions stated in the preceding section, over a speed range which corresponded to the range of Froude numbers from $F_{n\nabla} = 1.6$ to $F_{n\nabla} = 4.0$.

The model was attached to the towing carriage in its centre of gravity by an air lubricated support, which allowed the model to pitch, heave and roll freely.

The following parameters were measured :

- the modelspeed, which equalled the carriage speed
- the resistance, measured by a strain-gauge dynamometer
- the rise of the centre of gravity, measured by a potentiometer
- the trim angle, measured by a gyroscope
- the form and magnitude of the area wetted by solid water were determined from visual observation.

6. Test results

The actual results are given in the appendix 1. The faired results are given in the figures 2 to 5. In figure 2 the resistance/weight ratio $\frac{R}{\Delta}$ is given for a standard displacement of $\Delta = 16000$ kg in seawater with a weight density of 1025 kg/m^3 and a temperature of 15°C, using the I.T.T.C. 1957 extrapolator without roughness allowance. When it is desired to take into account this additional resistance, use can be made of the curve in the lower part of the figure where the additional resistance/weight ratio $\frac{R_A}{\Delta}$ is given for an incremental resistance coefficient $C_A = 0.0002$.
This curve holds for any value of the ship's displacement; for

$$\frac{R_A}{\Delta} = \frac{C_A \cdot \frac{1}{2}\rho V^2 S}{\rho g \nabla} = 0.0001 . F_{n\nabla}^2 . \quad S$$

The angle of incidence is given in the same figure.

In figure 3 the wetted surface and the mean length of the wetted surface are given, reduced to nondimensional coefficients.

In figure 4 the wetted length at the keel and at the chine are given and the rise of the centre of gravity, also reduced to nondimensional coefficients.

In figure 5 the resistance/weight ratio is given for displacements of 1 to 250 metric tons. The resistance has been computed for seawater with w = 1025 kg/m^3 and t = 15° C. Use has been made of the I.T.T.C. 1957 extrapolator without roughness allowance.

7. Discussion of test results

There are no exceptional things to report.
The resistance and trim curves are smooth without accessive humps.
The resistance characteristics are good, considering the high deadrise of the hull.

8. References

[1] "Resistance data of hull form 114"
Shipbuilding Laboratory of the University of Technology, Delft.
Report no. 355.

[2] "Resistance data of hull form 116"
Shipbuilding Laboratory of the University of Technology, Delft.
Report no. 357

[3] "Comparative model tests of three planing hulls in calm water and irregular head waves"
Shipbuilding Laboratory of the University of Technology, Delft.
Report no. 358.

Appendix I

Results of resistance test with model 115 in still water

Test 1

Displacement 46.65 dm^3

Temperature 21.8 centigrade

model speed	rise of centre of gravity	trim angle	model resistance	wetted length of keel	wetted length of chine	wetted surface
m/sec	cm	degrees	kg	cm	cm	m^2
3.04	-	2.77	5.15	202	194	1.070
3.73	1.21	3.27	6.04	-	-	-
4.48	2.24	3.47	6.75	-	-	-
4.41	2.19	3.45	6.76	-	-	-
5.17	2.40	3.47	7.47	-	-	-
5.21	2.60	3.43	7.50	-	-	-
5.94	2.88	3.35	8.57	-	-	-
5.84	2.88	3.23	8.44	-	-	-
6.69	3.39	3.10	9.57	-	-	-
7.52	4.14	2.78	11.00	-	-	-
4.50	-	-	-	194.0	170.0	.995
5.20	-	-	-	191.5	172.0	.970
7.54	-	-	-	186.0	157.5	.940

Results of resistance test with model 115 in still water

Test 2

Displacement 61.33 dm^3

Temperature 21.8 centigrade

model speed	rise of centre of gravity	trim angle	model resistance	wetted length of keel	wetted length of chine	wetted surface
m/sec	cm	degrees	kg	cm	cm	m^2
3.11	.34	3.62	7.60	-	-	-
3.98	1.80	4.28	8.76	-	-	-
4.67	3.20	4.17	9.17	-	-	-
5.58	3.91	3.42	9.71	-	-	-
6.22	4.43	3.30	10.29	190.5	143.0	.905
6.97	5.18	3.50	11.06	-	-	-
7.82	5.35	2.82	12.02	-	-	-
3.08	-	-	-	204.5	198.5	1.125
3.92	-	-	-	199.5	177.5	2.085
4.64	-	-	-	195.0	163.0	.960
7.85	-	-	-	187.5	139.0	.900

Appendix II

Table of offsets of model 115

wl	ord 0 mm	ord 2 mm	ord 4 mm	ord 6 mm	ord 7 mm	ord 8 mm	ord 9 mm	ord 10 mm
0	2.7	2.7	2.7	2.7	-	-	-	-
4	102.8	102.8	102.8	99.3	88.4	61.9	-	-
8	183.0	190.5	189.0	174.4	153.1	112.7	37.1	-
12	199.9	236.9	261.0	236.5	206.7	156.1	71.0	-
16	212.0	252.3	280.5	276.8	251.6	195.2	103.7	-
20	221.9	264.1	295.1	295.7	274.9	225.9	135.0	-
24	231.1	275.2	307.8	311.8	294.6	251.3	164.8	21.3
28	239.6	285.2	319.9	326.1	311.6	273.8	194.4	54.3

Deckline

ord	Beam	Height
0	240	300.0
2	289	315.6
4	328.4	331.2
6	341.4	346.8
7	331.4	354.6
8	304.6	362.4
9	249.7	370.2
10	147.9	378.0

Chine

ord	Beam	Height
0	180	75.0
2	225.1	97.1
4	260.3	119.0
6	267.3	142.3
7	249.0	155.8
8	206.3	171.8
9	128.7	191.4
10	2.7	216.0

Keel and Stem

ord	Beam	Height
6	2.7	0
7	2.7	.1
8	2.7	3.7
9	2.7	41.6
10	2.7	216.0

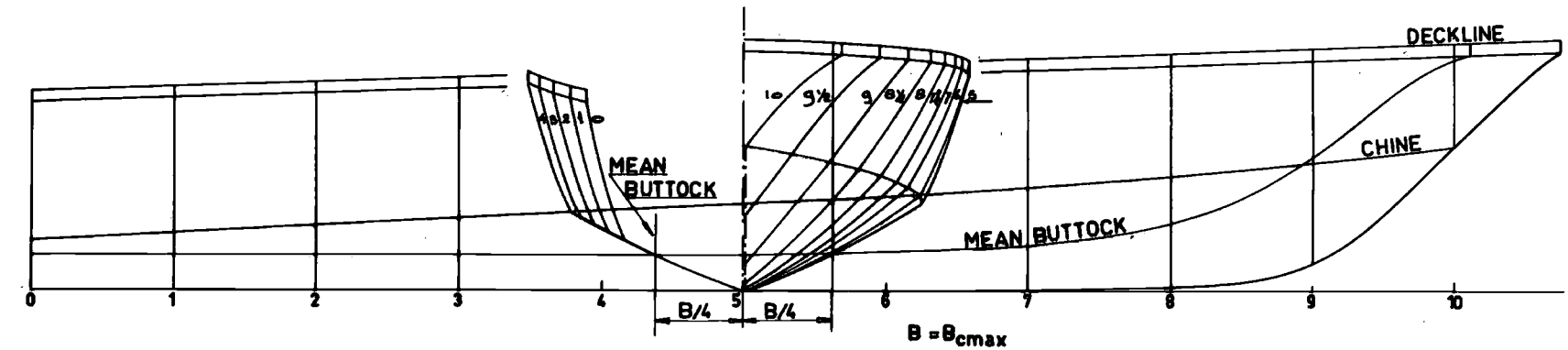

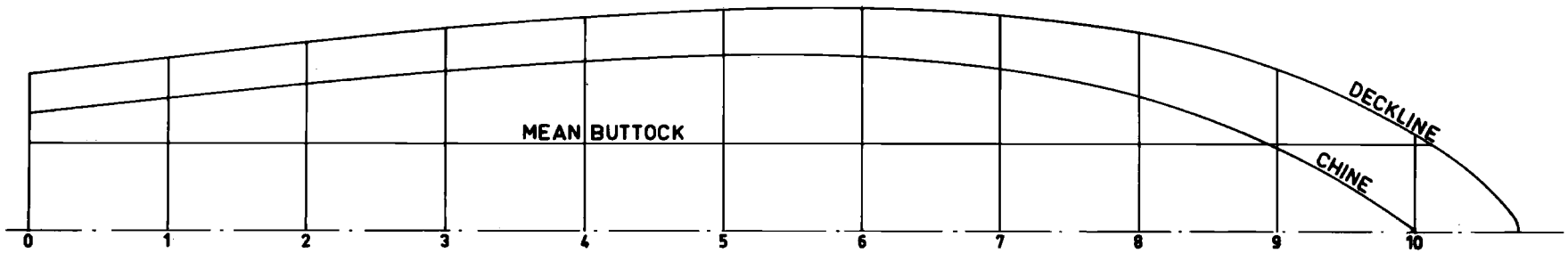

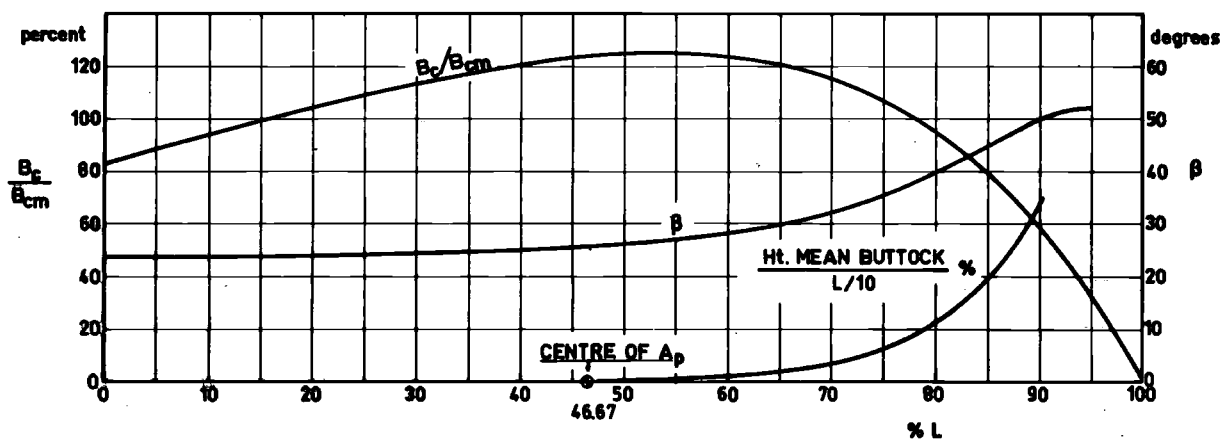

DETAIL SPRAYSTRIPS
SCALE 1:5 FOR Δ = 16 TON

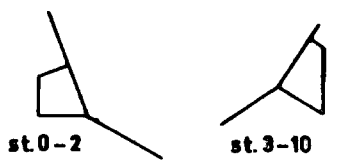

Fig. 1 Lines and formcharacteristics of the hull of model 115.

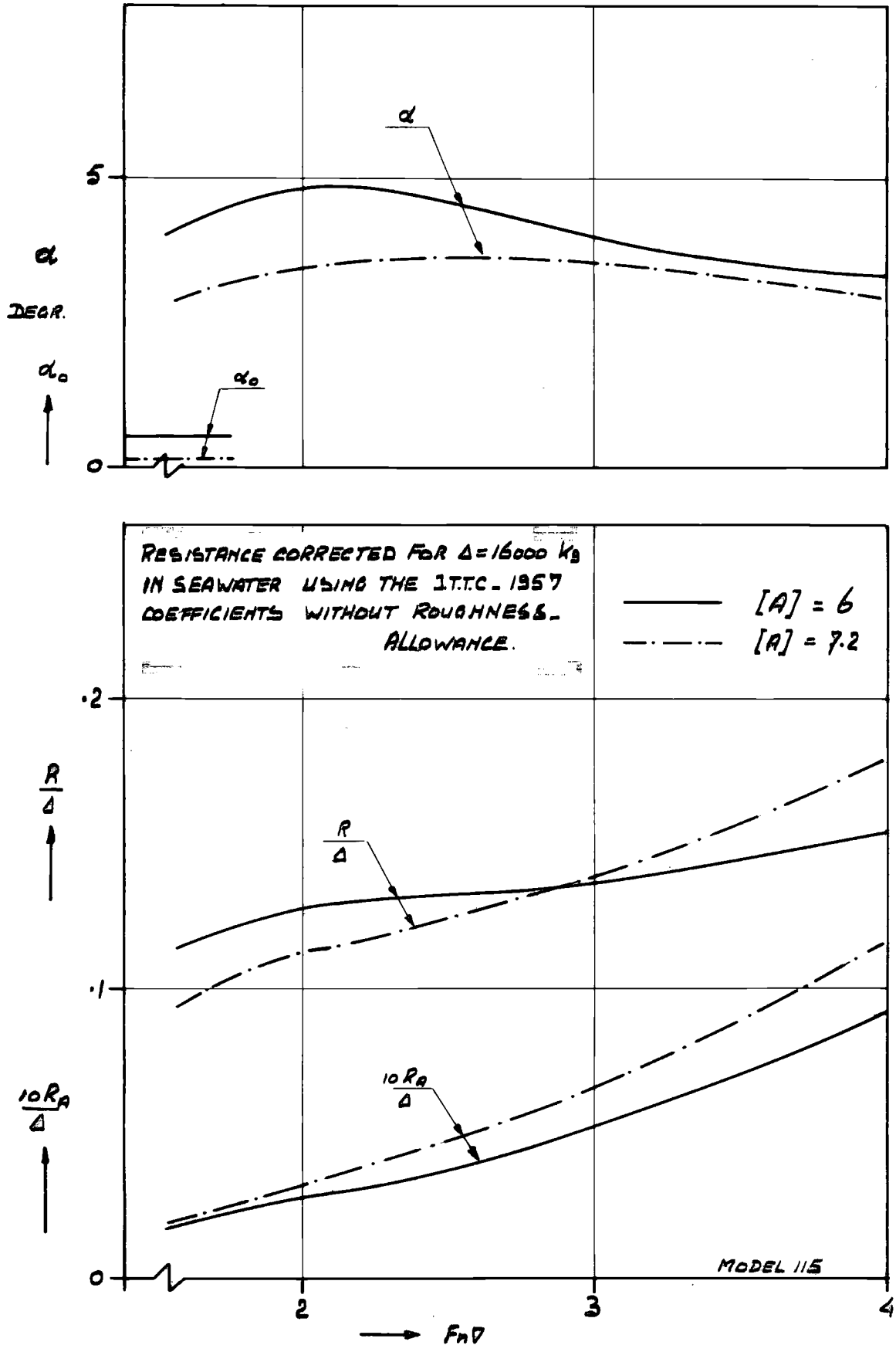

fig. 2 Resistance-weight ratio of the standard ship and angle of attack

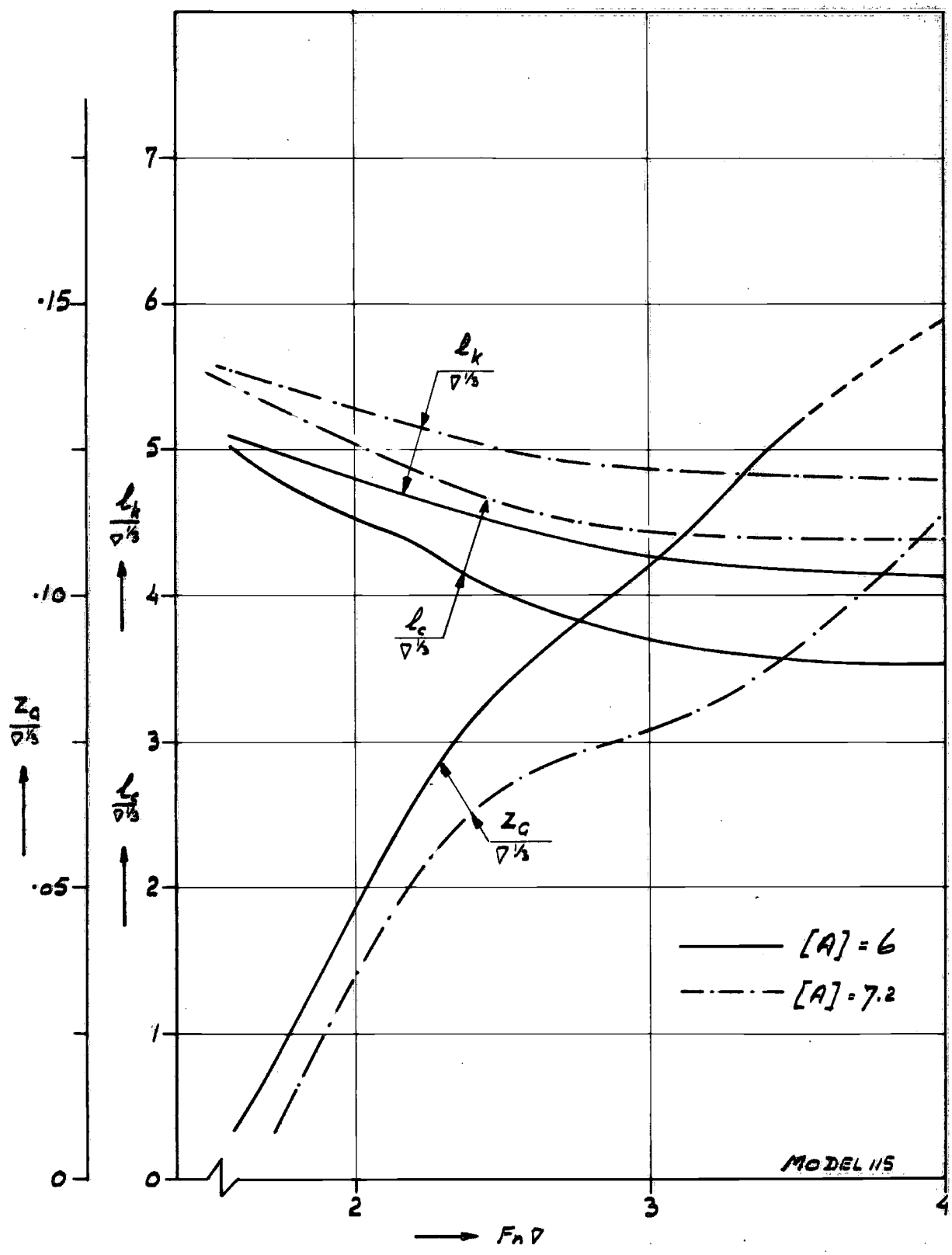

fig. 4 Wetted length ratio's and rise of centre of gravity

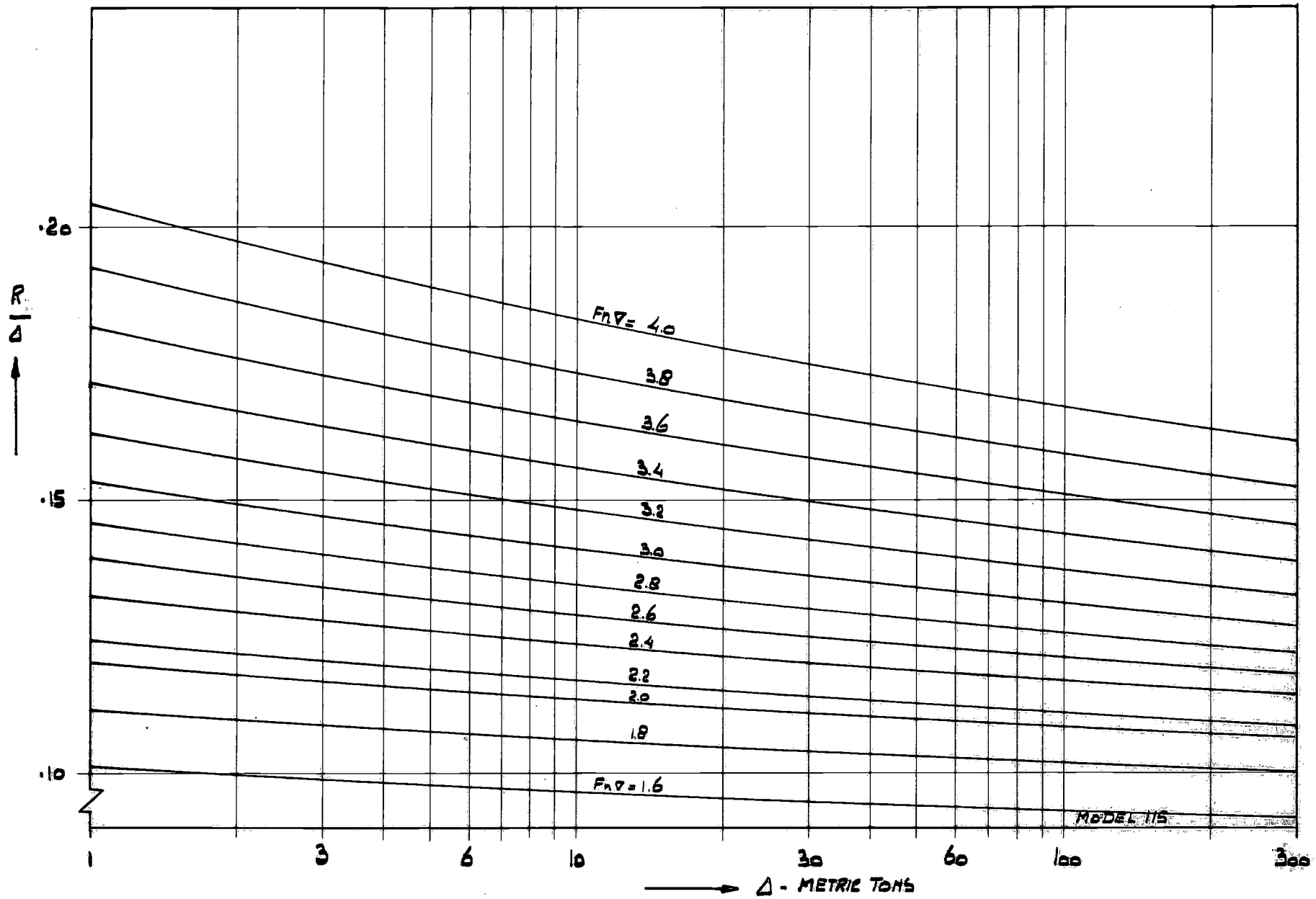

fig. 5 A Resistance-weight ratio as a function of Δ and $F_{n\nabla}$ [A] = 7.2

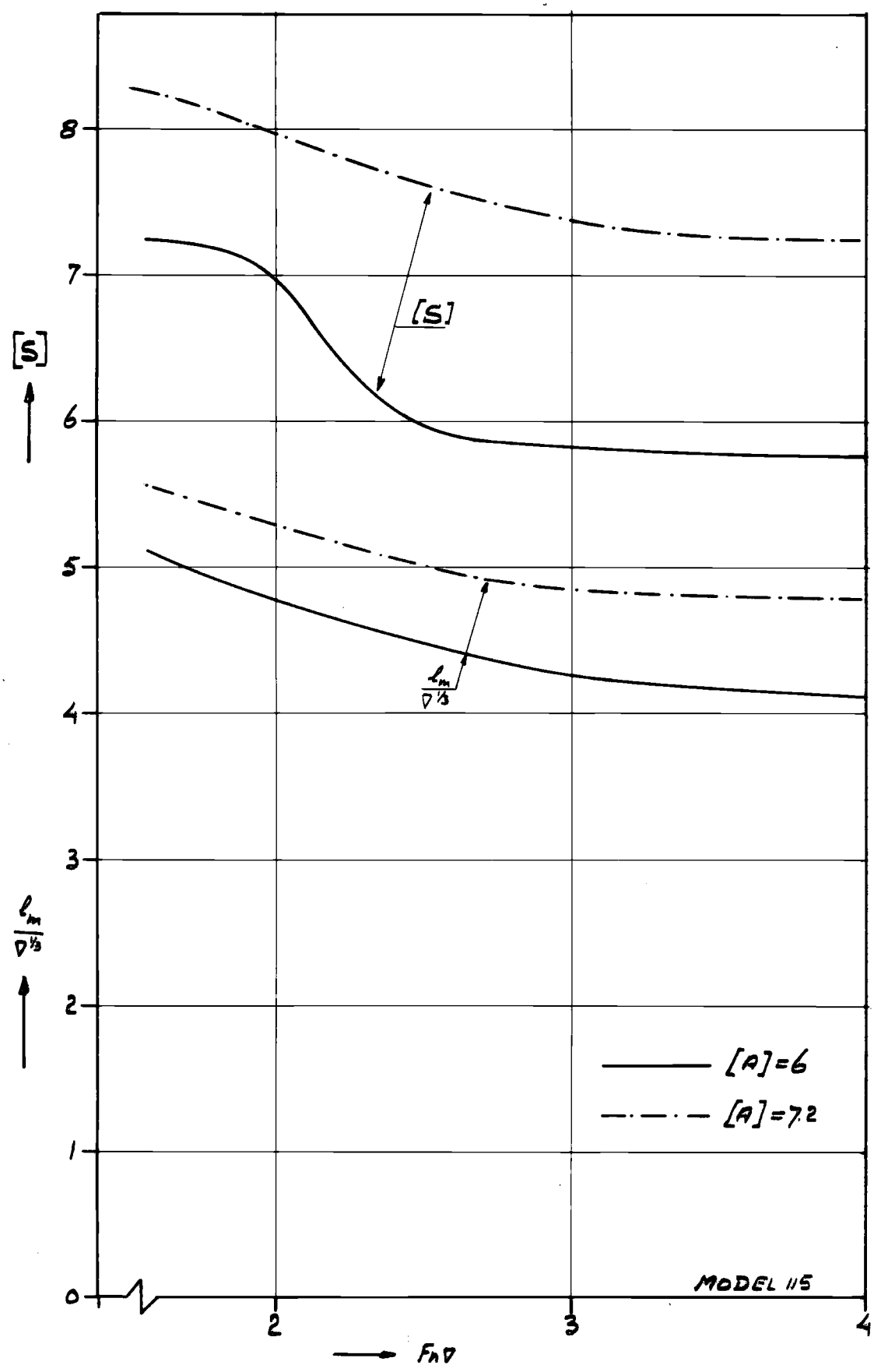

fig. 3 Wetted surface and mean wetted length ratio's

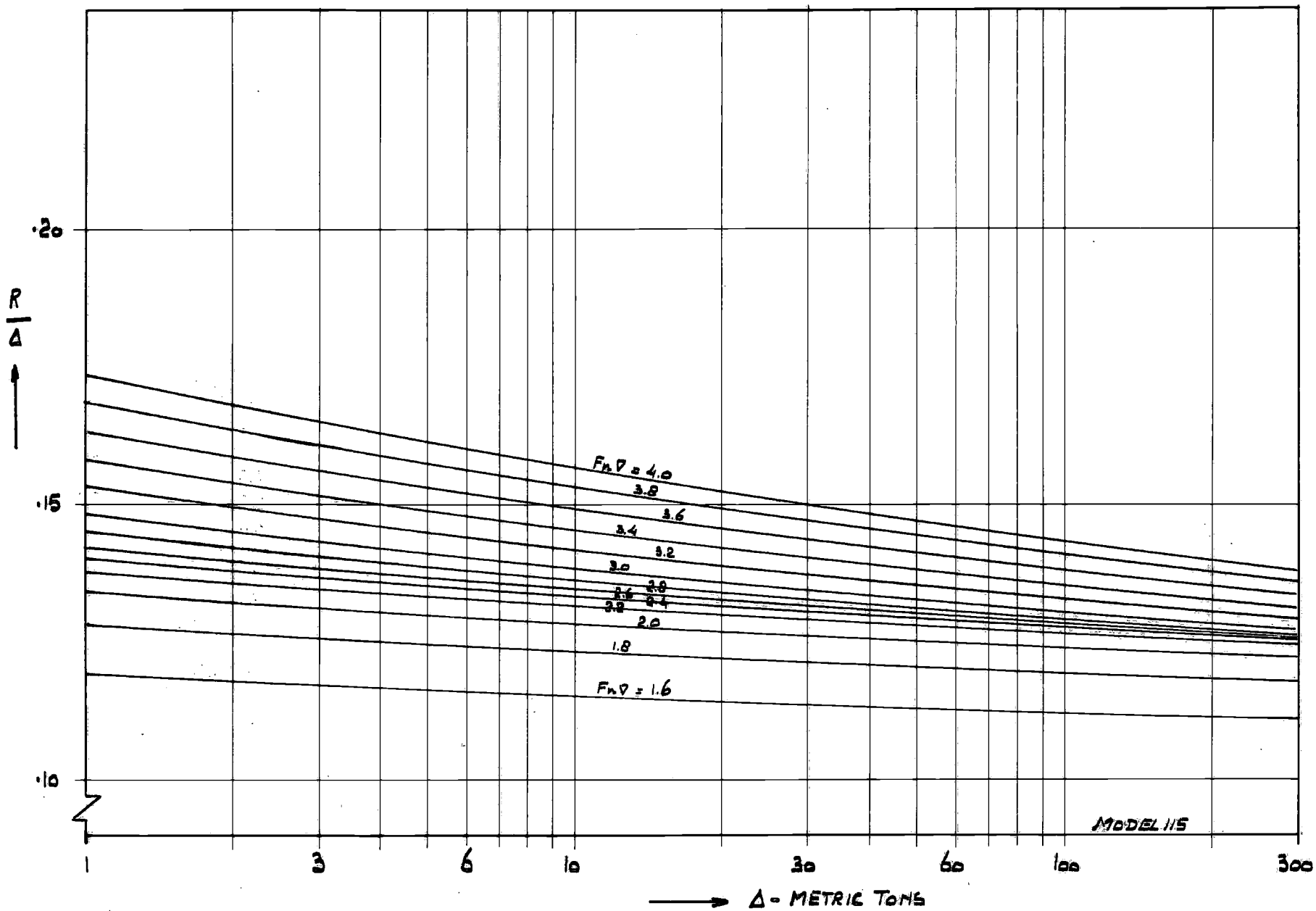

fig. 5 B Resistance-weight ratio as a function of Δ and $F_{n\nabla}$ [A] = 6

Report No. 357

LABORATORIUM VOOR SCHEEPSBOUWKUNDE

TECHNISCHE HOGESCHOOL DELFT

RESISTANCE DATA OF HULL FORM 116

by

Ir. J.J. v.d. Bosch

September 1972

Contents

1. Nomenclature

A_p	Horizontal projection of the area bounded by chines and transom, excluding external spray strips
$[A] = \frac{A_p}{\nabla^{2/3}}$	
B_c	Breadth over chines at any cross section
$B_{cm} = \frac{A_p}{L_p}$	Average breadth of area A_p
B_{cmax}	Maximum breadth over chines
b	Span of planing surface, i.e. actual breadth of planing surface measured at main spray point
C_A	Incremental resistance coefficient
$F_{n\nabla} = \frac{V}{\sqrt{g\nabla^{1/3}}}$	Speed-displacement coefficient based on volume of displacement at rest
G	Centre of gravity
g	Acceleration due to gravity
L_p	Length of A_p
l_c	Wetted length of chine, measured parallel to the keel from transom to main spray point
l_k	Wetted length of keel measured from transom
$l_m = \frac{l_c + l_k}{2}$	Mean wetted length
$[M] = \frac{L_p}{\nabla^{1/3}}$	
R	Resistance
R_A	Incremental resistance
S	Wetted surface
$[S] = \frac{S}{\nabla^{2/3}}$	
W	Weight density of water
V	Ship or model speed
X_p	Centre of area A_p
Z_G	Rise of centre of gravity
α	Angle of incidence, i.e. angle between still water surface and keel

α_o	initial trim angle between still water surface and keel
β	Deadrise angle
Δ	Ship or model weight
ν	Kinematic viscosity
ρ	Mass density of water
$\overline{AX}_p$	Distance of X_p from transom at keel
$\overline{AG}$	Distance of G from transom at keel
$\overline{KG}$	Height of G above base line
$\nabla = \frac{\Delta}{w}$	Volume of the displacement of the ship at rest

2. List of figures

3. Introduction

The tested model was one of a series of three :
the numbers 114, 115 and 116.
The aim of the test series was to compare the three hull forms with regard to the resistance in smooth water and the behaviour in irregular head seas in the speed range betwee $F_{n\nabla} = 2$ and $F_{n\nabla} = 4$. This was done in order to develop a hull form with a good overall performance at sea which could function as a parent for a systematic series.
In this report the resistance data of hull form 116 in sea water are given for displacements of up to 300 metric tons. For the information about the other test results the reader is referred to the references [1] , [2] and [3] .

The tests, although being a part of the research program of the Shipbuilding Laboratory of the University of Technology, were carried out at the Netherlands Ship Model Basin under the responsibility of the Netherlands Ship Research Centre, TNO.

4. Modeldata

The hullform is shown in figure 1.

The main particulars of the model 116 are given in the following table :

A_p	1.066 m^2
B_{cmax}	.572 m
B_{cm}	.494 m
L_p	2.16 m
L/B_{cmax}	.378
L/B_{cm}	.437

	Test 1	Test 2
∇	0.06133 m^3	0.08062 m^3
$\overline{AX}_p$	.966 m	.966 m
$\overline{AG}$	0.825	0.825
$\overline{KG}$	.277 m	.277 m
[A]	6	5
[M]	5.477	5

5. Test procedure

The model was tested at the loading conditions stated in the preceding section, over a speed range which corresponded to the range of Froude numbers from $F_{n\nabla} = 1.6$ to $F_{n\nabla} = 4.0$.

The model was attached to the towing carriage in its centre of gravity by an air-lubricated support, which allowed the model to pitch, heave and roll freely.

The following parameters were measured :

- the modelspeed, which equalled the carriage speed
- the resistance, measured by a strain-gauge dynamometer
- the rise of the centre of gravity, measured by a potentiometer
- the trim angle, measured by a gyroscope
- the form and magnitude of the area wetted by solid water were determined from visual observation.

6. Test results

The actual results are given in the appendix 1. The faired results are given in the figures 2 to 5. In figure 2 the resistance/weight ratio $\frac{R}{\Delta}$ is given for a standard displacement of $\Delta = 16000$ kg in seawater with a weight density of 1025 kg/m^3 and a temperature of 15°C, using the I.T.T.C. 1957 extrapolator without roughness allowance. When it is desired to take into account this additional resistance, use can be made of the curve in the lower part of the figure where the additional resistance/weight ratio $\frac{R_A}{\Delta}$ is given for an incremental resistance coefficient $C_A = 0.0002$.
This curve holds for any value of the ship's displacement; for

$$\frac{R_A}{\Delta} = \frac{C_A \cdot \frac{1}{2}\rho V^2 S}{\rho g \nabla} = 0.0001 . F_{n\nabla}^2 . S$$

The angle of incidence is given in the same figure.

In figure 3 the wetted surface and the mean length of the wetted surface are given, reduced to nondimensional coefficients.

In figure 4 the wetted length at the keel and at the chine are given and the rise of the centre of gravity, also reduced to nondimensional coefficients.

In figure 5 the resistance/weight ratio is given for displacements of 1 to 250 metric tons. The resistance has been computed for seawater with $w = 1025$ kg/m^3 and $t = 15^{\circ}$ C. Use has been made of the I.T.T.C. 1957 extrapolator without roughness allowance.

7. Discussion of test results

The trim- and resistance curves show the typical squatting of round bottom craft at relatively high speeds. The resistance is above say $F_{n\nabla} \approx 2$ higher than the resistance of comparable hard-chine boats.

8. References

[1] "Resistance data of hull form 114"
Shipbuilding Laboratory of the University of Technology, Delft.
Report no. 355

[2] "Resistance data of hull form 115
Shipbuilding Laboratory of the University of Technology, Delft.
Report no. 356

[3] "Comparative model tests of three planing hulls in calm water and irregular head waves"
Shipbuilding Laboratory of the University of Technology, Delft.
Report no. 358.

Appendix I

Results of resistance test with model 116 in still water.

Test 1

Displacement 61.33 dm^3

Temperature 20.5° centigrade.

model speed	rise of centre of gravity	trim angle	model resistance	wetted length of keel	wetted length of chine	wetted surface
m/sec	cm	degrees	kg	cm	cm	m^2
3.04	-	3.41	7.32	210	128	1.295
3.98	1.21	3.21	8.31	208.5	116	1.255
4.65	2.05	3.67	10.20	-	-	-
5.44	2.63	4.62	12.71	180.0	88.5	.999
6.70	4.62	5.30	13.96	162.5	66.5	.925
6.94	5.07	5.33	14.43	-	-	-
7.90	6.04	5.11	15.33	-	-	-
6.18	3.78	5.11	13.54	-	-	-
3.12	-	3.53	7.33	-	-	-
4.62	-	-	-	202.5	105.5	1.175
6.20	-	-	-	164.5	75.0	.940
6.96	-	-	-	160.0	63.0	.890
7.82	-	-	-	159.0	53.0	.840

Results of resistance test with model 116 in still water.

Test 2

Displacement 80.62 dm^3

Temperature 20.5° centigrade

model speed	rise of centre of gravity	trim angle	model resistance	wetted length of keel	wetted length of chine	wetted surface
m/sec	cm	degrees	kg	cm	cm	m^2
3.29	.18	4.26	10.84	-	-	-
4.06	1.72	4.26	12.41	-	-	-
4.94	2.96	5.30	14.42	-	-	-
5.82	5.36	7.40	17.97	-	-	-
6.63	6.58	6.64	18.79	-	-	-
7.41	7.25	6.11	19.26	-	-	-
3.25	-	-	-	208.5	134	1.310
4.08	-	-	-	203.5	125.5	1.275
4.88	-	-	-	186.0	110.0	1.160
5.74	-	-	-	159.5	90.0	.960
6.62	-	-	-	153.0	74.0	.890
7.43	-	-	-	153.0	67.0	.870

Appendix II

Table of offsets of model 116

wl	ord 0	ord 2	ord4	ord 6	ord 7	ord 8	ord 9	ord 10
9	-	-	-	63.0	56.6	37.5	14.0	-
12		135.3	163.6	140.0	110.7	73.4	31.0	-
15	215.3	228.3	229.8	193.2	157.2	109.0	49.8	-
18	243.0	255.2	257.8	230.3	195.7	143.6	72.6	
21	256.5	268.2	273.7	256.3	227.0	176.3	97.5	-
24	264.2	277.0	284.7	275.5	253.0	207.0	123.0	-
30	270.6	288.5	300.2	295.3	279.7	240.7	161.7	8.8
33	-	-	-	302.5	288.2	252.2	176.0	20.8

Deckline

ord	Beam	Height
0	272.7	330.0
2	292.0	321.2
4	304.3	319.1
6	302.6	330.5
7	290.0	342.0
8	260.6	358.4
9	197.8	381.5
10	60.0	416.6

Chine

ord	Beam	Height
0	266.9	257.6
2	278.5	248.7
4	286.7	244.7
6	280.2	248.7
7	263.6	252.6
8	224.2	258.1
9	145.2	266.0
10	0	276.5

Skeg

ord	Height
4	15.0
6	34.4
8	54.0
9	63.5

Keel

ord	Height
0	129.6
2	113.4
4	92.3
6	71.3
8	64.7
9	69.0

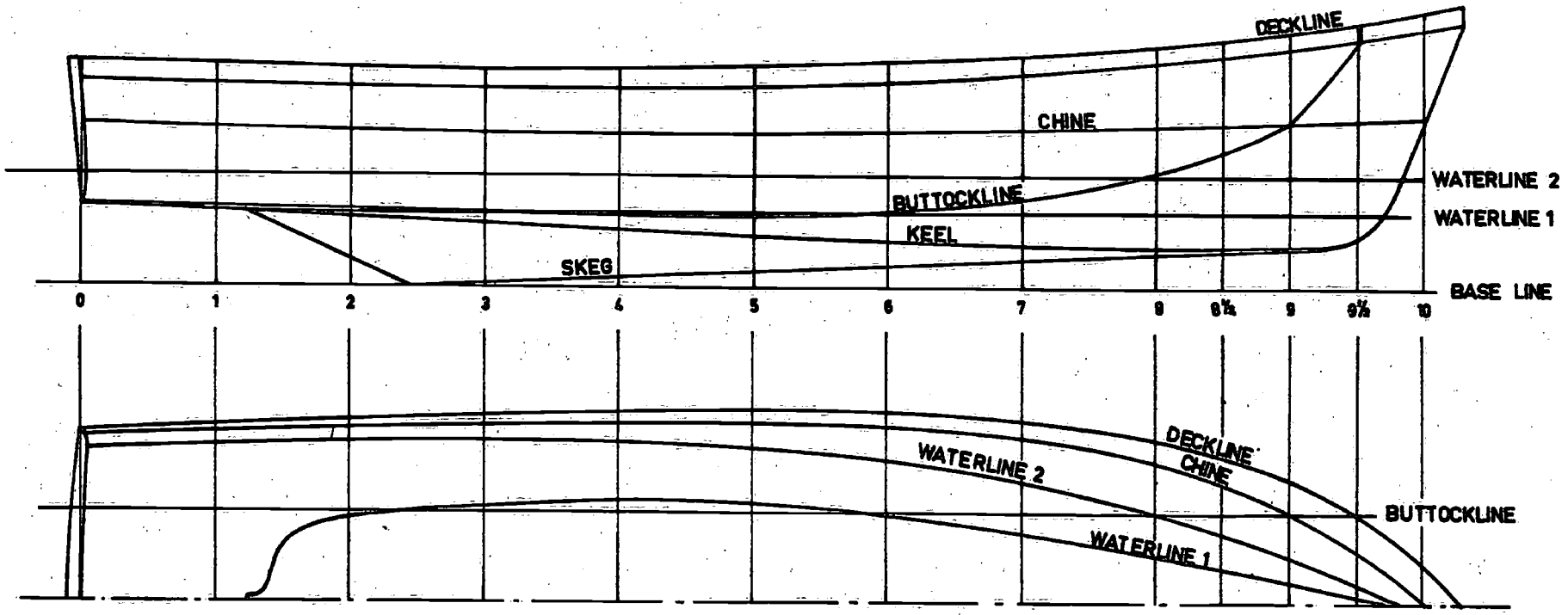

DETAIL FENDER
SCALE 1:5 FOR Δ =16 TON

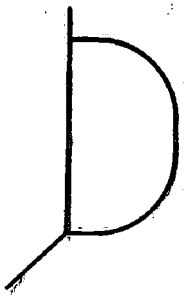

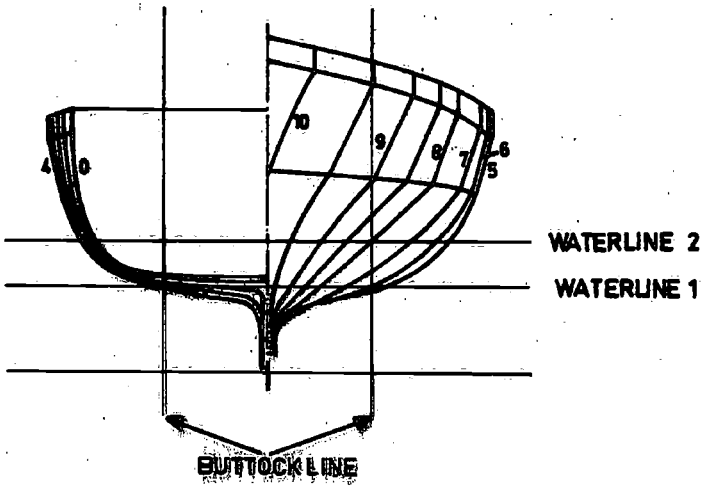

Fig. 1. Lines and formcharacteristics of the hull of model 116.

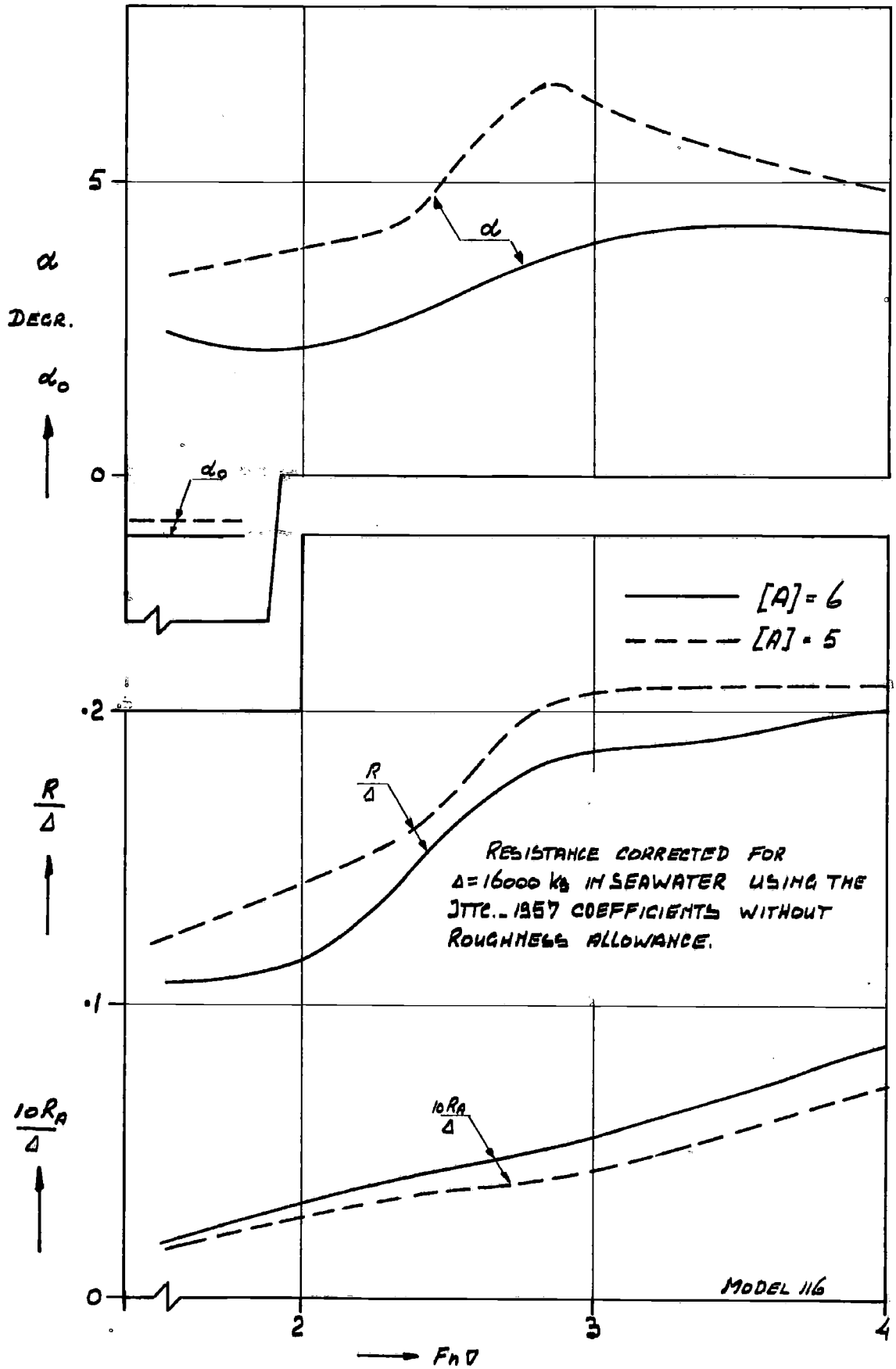

fig. 2 Resistance-weight ratio of the standard ship and angle of attack

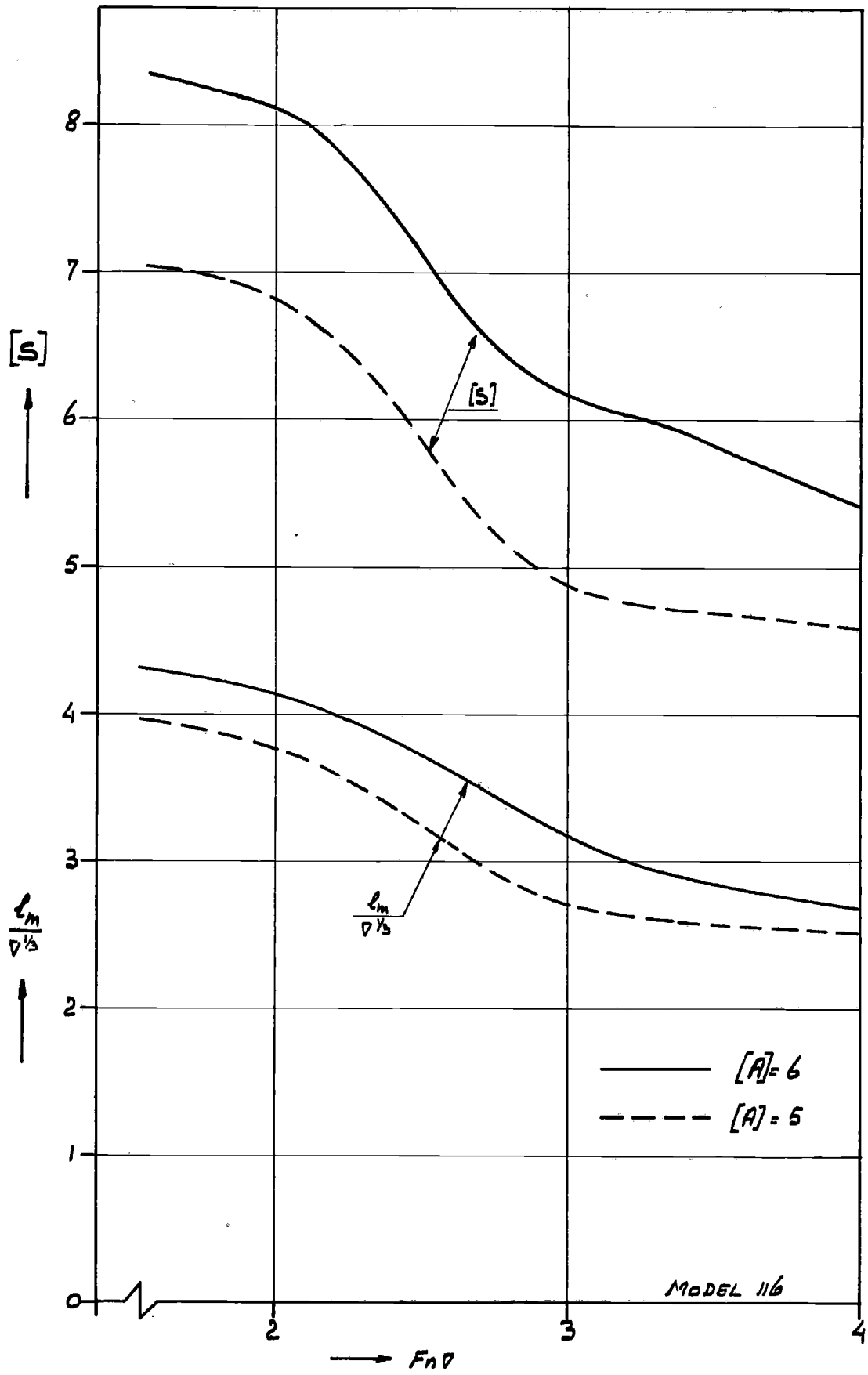

fig. 3 Wetted surface and mean wetted length ratio's

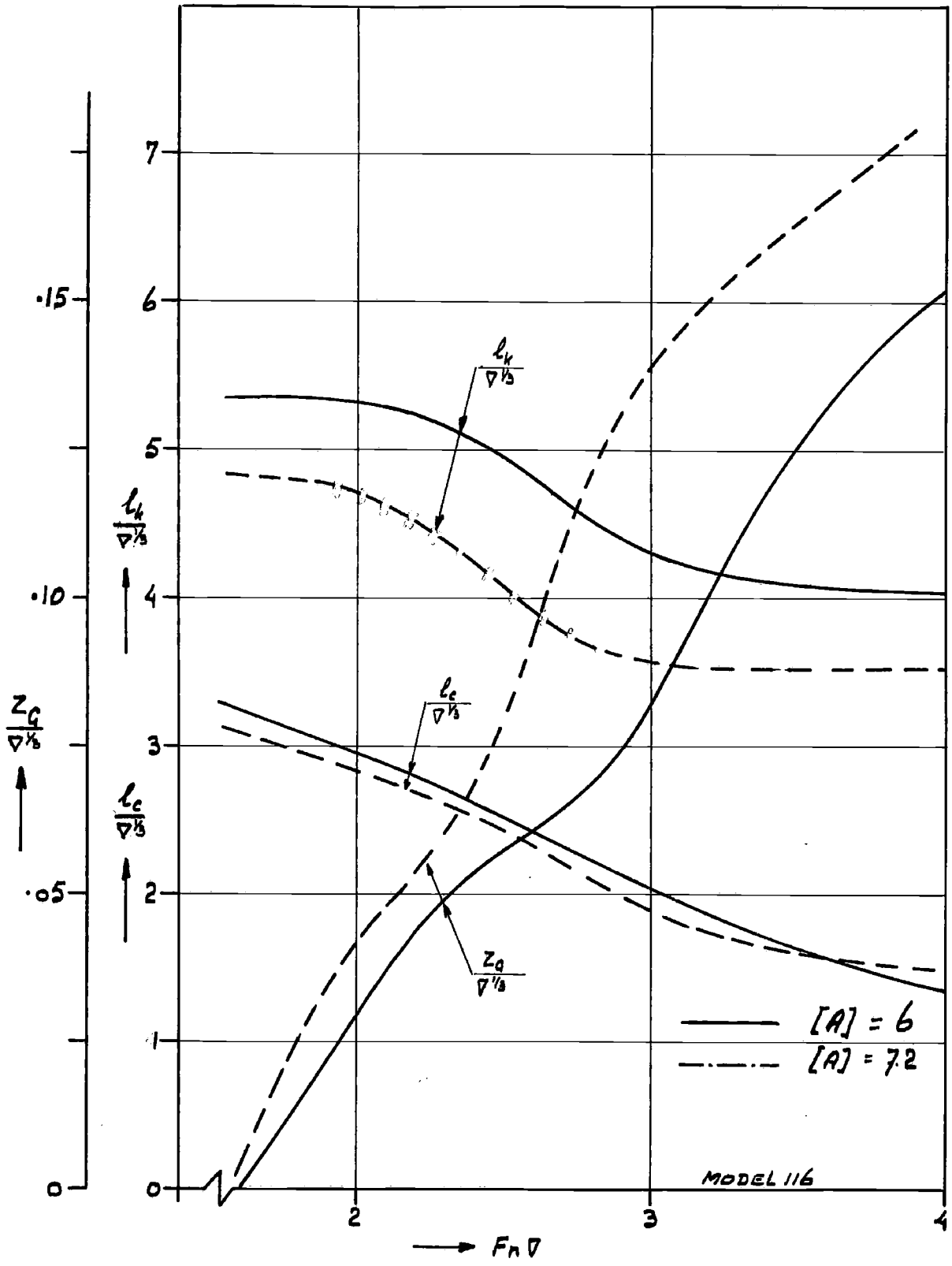

fig. 4 Wetted length ratio's and rise of centre of gravity

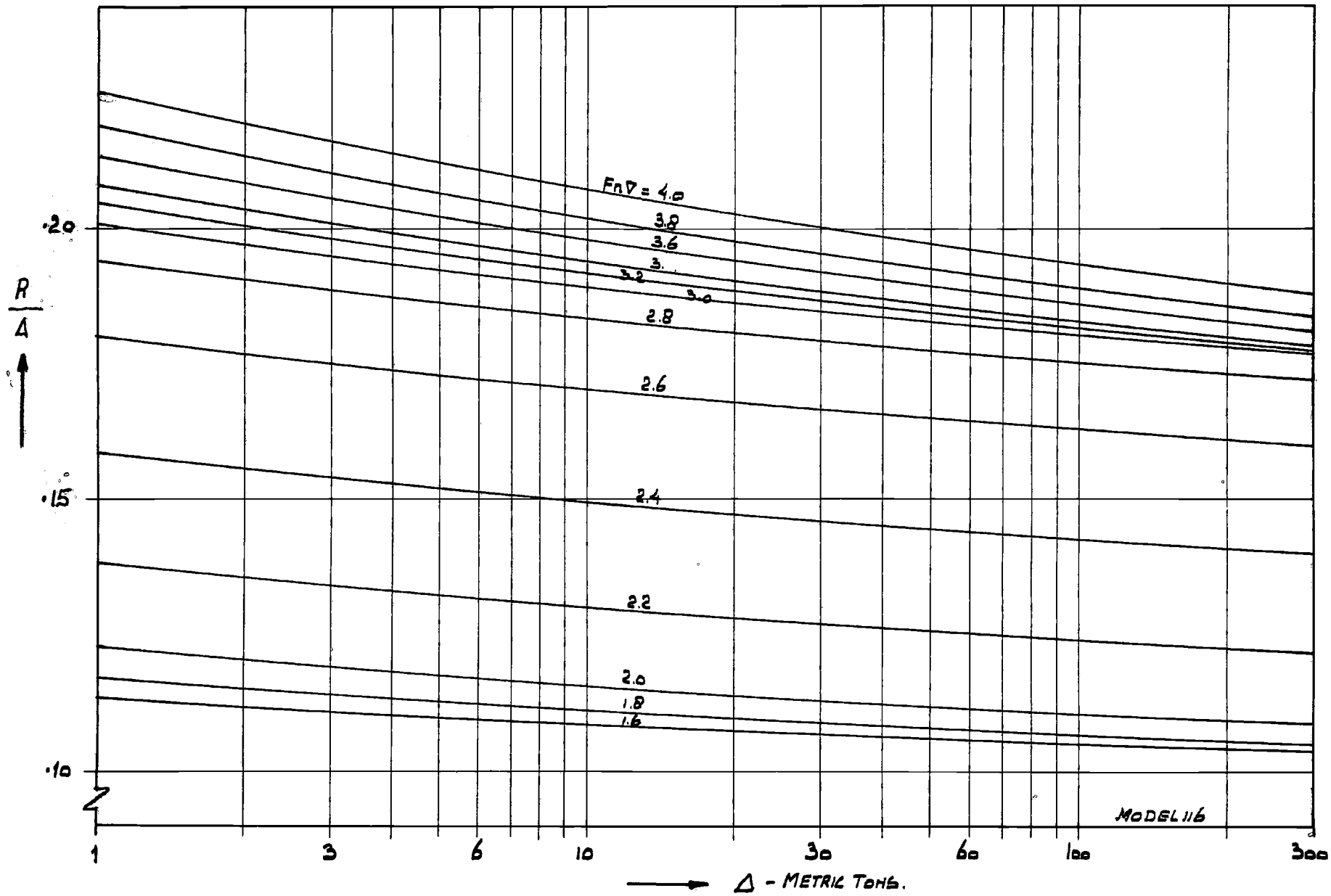

fig. 5 A Resistance-weight ratio as a function of Δ and $F_{n\nabla}$ [A] = 6

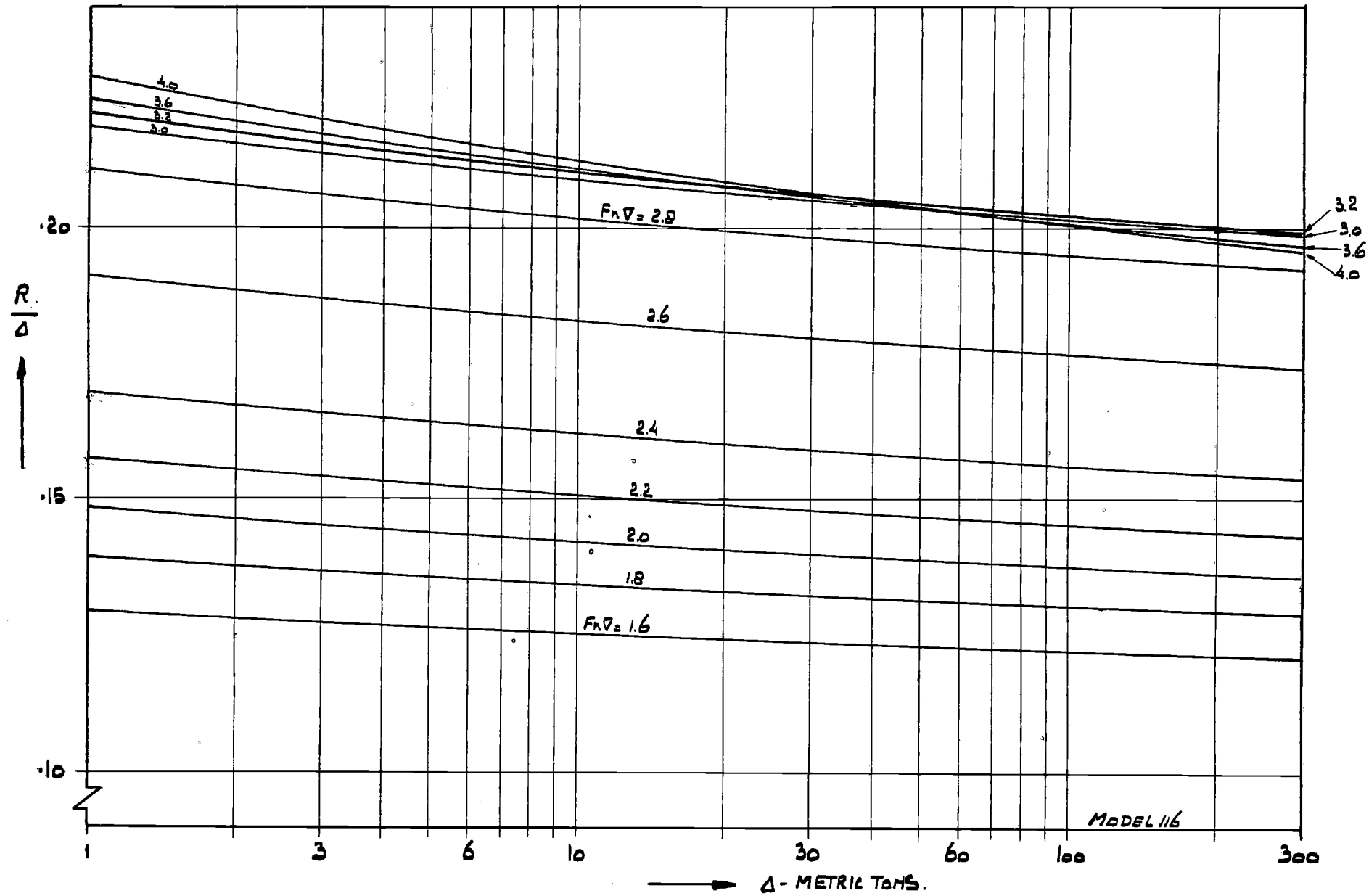

fig. 5 B Resistance-weight ratio as a function of Δ and $F_{n\nabla}$ [A] = 5

REPORT No. 196 S
(Sgo H/259, 259a, 259b,
S H/283, 376)
REPORT 358

December 1974

NEDERLANDS SCHEEPSSTUDIECENTRUM TNO
NETHERLANDS SHIP RESEARCH CENTRE TNO
SHIPBUILDING DEPARTMENT LEEGHWATERSTRAAT 5, DELFT

★

COMPARATIVE TESTS OF FOUR FAST MOTOR BOAT MODELS IN CALM WATER AND IN IRREGULAR HEAD WAVES AND AN ATTEMPT TO OBTAIN FULL-SCALE CONFIRMATION

(VERGELIJKENDE PROEVEN MET MODELLEN VAN VIER SNELLE MOTORBOTEN IN VLAK WATER EN IN ONREGELMATIGE VOORINKOMENDE GOLVEN, ALSMEDE EEN POGING TOT VERIFIKATIE OP WARE GROOTTE)

by

IR. J. J. VAN DEN BOSCH

Issued by the Council

VOORWOORD

In de loop der jaren zijn zeer nuttige gegevens gepubliceerd die betrekking hebben op het ontwerpen van planerende vaartuigen voor het gebruik in vlak, of bijna vlak, water. Nauwelijks enig gegeven echter, is beschikbaar voor het ontwerpen van planerende vaartuigen geschikt voor het gebruik op zee.

Om deze reden heeft het Laboratorium voor Scheepsbouwkunde van de Technische Hogeschool Delft het initiatief genomen tot een aantal onderzoekingen die zijn gericht op de ontwikkeling van een type planerend motorvaartuig, met een knikspantvorm, dat in staat zou zijn een hoge snelheid te behouden bij algemeen voorkomende golfkondities, bijvoorbeeld op de Noordzee.

Daar er geen theoretische oplossing bestaat voor het bepalen van het hydrodynamisch gedrag van planerende vlakken in golven en er, zoals reeds gesteld, in het algemeen zeer weinig over dit onderwerp is gepubliceerd, rees de overtuiging dat een systematisch opgezette reeks modelproeven van groot nut zou zijn.

In de sleeptank van het Laboratorium voor Scheepsbouwkunde werd een reeks voorbereidende proeven uitgevoerd die het uitgangspunt leverden voor het onderzoekprogramma dat in deze publikatie wordt beschreven.

Dit programma omvatte proeven in vlak water en in onregelmatige vóórinkomende golven met twee knikspantmodellen en een model van een bestaande rondspant-boot, later werden hieraan nog proeven met een ander knikspantmodel toegevoegd.

Financiële steun werd verkregen van de werven Amerglass B.V., B.V. Scheepswerf Damen, Le Comte-Holland B.V. en Schottel-Nederland B.V., van de twee reddingmaaatschappijen de Koninklijke Noord- en Zuid-Hollandsche Redding-Maatschappij en de Koninklijke Zuid-Hollandsche Maatschappij tot Redding van Schipbreukelingen, van de Rijkspolitie te water, alsmede van de Nijverheidsorganisatie TNO.

De proeven werden uitgevoerd door het Nederlands Scheepsbouwkundig Proefstation.

Later werden door het Laboratorium voor Scheepsbouwkunde op de Noordzee proeven op ware grootte uitgevoerd met twee vaartuigen waarvan de modellen in de sleeptank waren beproefd. Deze proeven werden uitgevoerd in nauwe samenwerking met de KNZHRM en Scheepswerf Damen, de eigenaars van de twee betreffende schepen en met Rijkswaterstaat.

Zoals vermeld, heeft een aanzienlijk aantal bedrijven en instellingen direkt bijgedragen aan deze onderzoekingen, hun enthousiaste en waardevolle medewerking wordt in hoge mate gewaardeerd.

Met de hier gepresenteerde resultaten is een solide basis verkregen voor een verzameling ontwerpgegevens, geschikt voor het bovenomschreven doel. Een verdere uitbreiding van de systematische gegevens, o.a. omvattende de invloed van variatie in L/B is echter zeer wenselijk.

HET NEDERLANDS SCHEEPSSTUDIECENTRUM TNO

PREFACE

In the course of years very useful data have been published concerning the design of planing boats for use in still, or nearly still, water. Hardly any data, however, are available for the design of planing boats suitable for operation at sea.

For this reason the Shipbuilding Laboratory of the Delft University of Technology took the initiative in a number of investigations which were aimed at the development of a type of planing motorboat, having a V-shaped bottom, that would be able to maintain high speeds at sea under generally occurring wave conditions, for instance, on the North Sea.

As the theoretical solution for the hydrodynamic behaviour of planing surfaces in waves does not exist and, as mentioned, generally very little is published on this subject, it was felt that a methodically set up series of model tests could be very useful.

A series of preliminary tests was carried out in the towing tank of the Shipbuilding Laboratory, it provided the starting point for the test programme described in this publication.

This programme included experiments in still water and in irregular head waves with two V-bottom models and a model of an existing round-bottom craft, later on experiments in waves with another V-bottom model were added.

Financial support was obtained from the shipyards Amerglass B.V., B.V. Scheepswerf Damen, Le Comte-Holland B.V. and Schottel-Nederland B.V., the two lifeboat institutes Koninklijke Noord- en Zuid-Hollandsche Redding-Maatschappij and Koninklijke Zuid-Hollandsche Maatschappij tot Redding van Schipbreukelingen and the Rijkspolitie te water (Dutch Government Water Police) as well as from the Organization for Industrial Research TNO.

The experiments were carried out by the Netherlands Ship Model Basin.

Later the Shipbuilding Laboratory carried out full scale tests on the North Sea with two vessels of which the models had been tested in the towing tank. These tests were carried out in close collaboration with the lifeboat institute KNZHRM and Damen's Shipyard, owners of the two vessels concerned and with Rijkswaterstaat (Ministry of Public Works).

It will be noticed that a considerable number of companies and institutions has contributed directly to these investigations, their enthusiastic and valuable cooperation is highly appreciated.

With the results presented, a sound base has been obtained for a collection of design data suitable for the purpose mentioned above. A further extension of the systematic data, i.a. comprising the influence of L/B variation, however, is highly desirable.

THE NETHERLANDS SHIP RESEARCH CENTRE TNO

CONTENTS

LIST OF SYMBOLS

A_p	Horizontal projection of the area bounded by the chines and transom, excluding external spray strips
$[A] = \frac{A_p}{\nabla^{\frac{2}{3}}}$	
a_f	Vertical acceleration at forward measuring point
a_{fa}	Vertical acceleration amplitude at forward measuring point
$\tilde{a}_{fa\frac{1}{3}}$	Average of one third highest values of a_{fa}
a_m	Vertical acceleration at midship measuring point
a_{ma}	Vertical acceleration amplitude at midship measuring point
$\tilde{a}_{ma\frac{1}{3}}$	Average of one third highest values of a_{ma}
B_c	Breadth over chines at any cross section
$B_{cm} = \frac{A_p}{L_p}$	Average breadth of area A_p
$B_{c_{max}}$	Maximum breadth over chines
C_A	Incremental resistance coefficient
$F_{n\nabla} = \frac{V}{\sqrt{g \cdot \nabla^{\frac{1}{3}}}}$	Froude number based on volume of displacement at rest
G	Centre of gravity of vessel
g	Acceleration of gravity
k_{yy}	Radius of inertia for pitch
L_p	Length of A_p
$[M] = \frac{L_p}{\nabla^{\frac{1}{3}}}$	Slenderness coefficient
R	Resistance
R_A	Incremental resistance
R_{Aw}	Resistance increase due to waves
S	Wetted surface in contact with "solid" water
$[S] = \frac{S}{\nabla^{\frac{2}{3}}}$	Non-dimensional wetted surface
$S_\zeta(\omega)$	Wave height spectrum
w	Weight density of water
V	Ship or model speed
X_p	Centre of gravity of area A_p
z	Heave motion
z_a	Heave amplitude
$\tilde{z}_{a\frac{1}{3}}$	Average of one third highest values of z_a
z_G	Rise of centre of gravity
α	Angle of incidence, i.e. angle between still water surface and keel
α_0	Initial trim angle between still water surface and keel
$\alpha_p = \frac{A_p}{L_p \cdot B_{c_{max}}} = \frac{B_{cm}}{B_{c_{max}}}$	Area coefficient of A_p
β	Deadrise angle
θ	Pitch angle
θ_a	Pitch amplitude
$\tilde{\theta}_{a\frac{1}{3}}$	Average of one third highest values of θ_a
Δ	Ship or model weight
λ	Model scale
ν	Kinematic viscosity

ω	Circular frequency
ϱ	Mass density of water
ζ_a	Wave amplitude
$\bar{\zeta}_{a\frac{1}{3}}$	Average of one third highest values of ζ_a
$\bar{\zeta}_{w\frac{1}{3}}$	Average height of one third highest waves
$\overline{AX_p}$	Distance of X_p from transom at keel
$\overline{AG}$	Distance of G from transom at keel
$\overline{KG}$	Height of G above base line
$\nabla = \frac{\Delta}{w}$	Volume of the displacement of the ship at rest

COMPARATIVE TESTS OF FOUR FAST MOTOR BOAT MODELS
IN CALM WATER AND IN IRREGULAR HEAD WAVES AND AN ATTEMPT TO OBTAIN FULL-SCALE CONFIRMATION *

by

Ir. J. J. VAN DEN BOSCH

Summary

Results of resistance tests with four fast motor boat models are given. Also the tests with these models in irregular head waves are described and the results are shown in the form of cumulative frequency distributions of the motions and accelerations. The influence of different values of the slenderness is investigated.
Full scale tests with two of the boats were carried out on the North Sea. The results of these tests are compared with the model results. The differences could be made more or less plausible, when a non-linear relation is assumed between the wave height and the vertical slamming accelerations.

1 Introduction

In this report the results from a series of model- and full-scale tests with fast planing craft, which were carried out during the years 1971 and 1972, are summarized.

Because of the ever returning demand for high speed vessels for coastal services, a research programme was set up with the purpose to develop a hull form with a good seakeeping behaviour combined with a reasonable power demand over a wide range of speeds. This hull could eventually act as a parent for a systematically varied series, somewhat like the well-known Series 62 [1] but with a different idea in mind. The Series 62 form a comprehensive and very valuable source on the resistance of planing craft, but in the author's opinion the basic form is not suited for high speeds in waves, because of its low deadrise angle and its full forebody. The present trend to increase the deadrise angle of the offshore raceboats is not without reason. That the angle of deadrise has a tremendous influence on the vertical accelerations in head seas was confirmed by the results of some tests carried out at the shipbuilding Laboratory. Two models derived from the Series 62, with the same plan form but with a different angle of deadrise were tested at high speed in regular and irregular head waves. The influence of the deadrise on the vertical accelerations proved to be of paramount importance [2, 3].

A model of the parenthull would have to be tested on smooth water and in waves. The experiments would offer no insurmountable technical difficulties, but it was realized that the interpretation, that is the evaluation of the results expressed in terms of good, reasonable or bad, could offer problems.

As regards the resistance, the Series 62 which is recognized as very good in the planing range could be taken as a yardstick. The larger deadrise would certainly result in a larger resistance, but this would have to be accepted as the price for the better behaviour in waves.

The judgement of the latter qualities would offer more problems. A yardstick like the Series 62 was, and is still unavailable when it concerns the seakeeping qualities. To overcome this difficulty in a certain way it was decided to test also a model of the "Komer", a Nelson 40′ rescue craft [4] built by Vosper-Thornycroft at Portsmouth and used by the Koninklijke Noord- en Zuid-Hollandsche Redding Maatschappij (K.N.Z.H.R.M.) a Netherlands lifeboat Institute. This boat is generally recognized as a good seaboat, and she is able to maintain a relatively high speed. The behaviour of this vessel offers of course no absolute criterion, but it seemed very useful to be able to check the performance of the newly designed hull against the known performance of an existing ship. Moreover, the KNZHRM promised all cooperation for the modeltests, and for full-scale tests also if that was wanted.

One difficulty remained, viz. the "Komer" differed quite appreciably from the design considered, being a typical round-sectioned boat, whereas the new design was meant to be a hard-chine hull. It was feared that the round bottom might introduce scale effects.

Luckily the Damen shipyard at Hardinxveld also offered to collaborate. This yard planned at that moment the serial production of their high speed launch "Polycat". They promised to join the modeltests in waves and the full-scale tests, while resistance tests with the model had already been carried out and the results were available.

Now the programme looked as follows:

1. Resistance tests with four models i.e. two newly designed hull forms designated 114 and 115, which are discussed in a paragraph below
   the Nelson 40′ "Komer"
   the "Polycat".

* Report no. 358 of the Shipbuilding Laboratory, Delft University of Technology.

Purpose: measurement of the smooth water resistance and comparison of the four models.

2. Modeltests in irregular head waves with the above four models at two speeds.
   Purpose: determination of the motions and vertical accelerations in waves with a realistic spectrum. Comparison of the models among themselves and the possibility to compare model and full-scale behaviour of the "Komer" and "Polycat".
3. Full-scale tests with the ships "Komer" and "Polycat", to confirm the model results.

2 Observations about the hull form

The design contemplated was meant to be of a simple form. A hard-chine hull was chosen because of its planing ability with the accompanying low resistance at high speeds.

The main parameters which seem to influence the behaviour of a planing boat are:

1. the length-breadth ratio here defined as $L_p/B_{c_{max}}$
2. the deadrise angle β
3. the longitudinal position of the centre of gravity of the "planing" area A_p
4. the load parameter $[A] = A_p/\nabla^{\frac{2}{3}}$
5. the slenderness defined here as $[M] = L_p/\nabla^{\frac{1}{3}}$
6. the longitudinal position of the centre of gravity of the ship's weight
7. the radius of inertia in pitch k_{yy}.

The first three items refer to the ship's geometry alone, the other four are also related to the ship's load. Apart from these, some characteristics of form also contribute to the performance of the ship, e.g. the chine should be defined very clearly, preferably with a rather sharp sprayrail, the buttocks should be

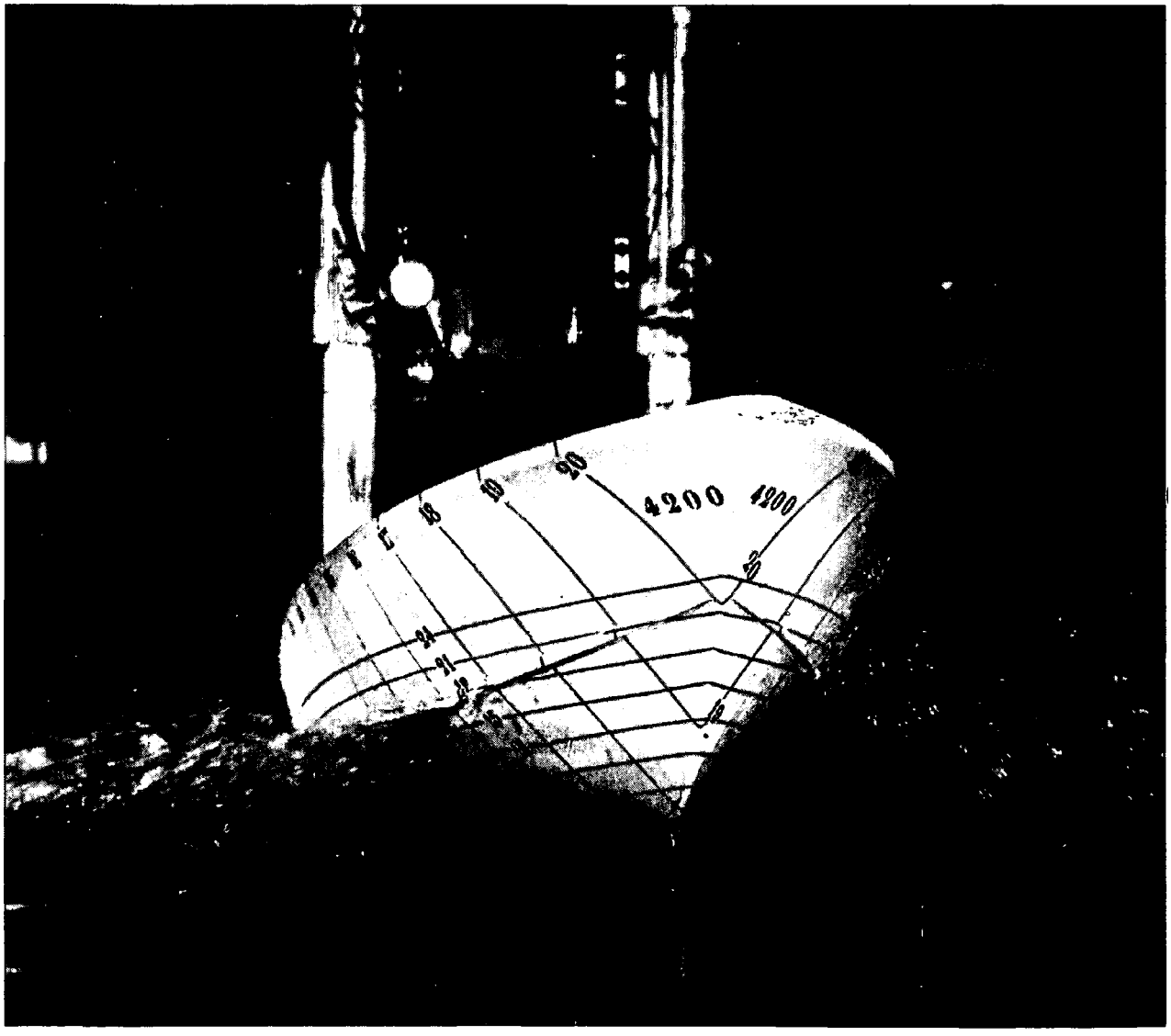

Hull 115 during resistance test ($[M] = 5.48$)

straight in the afterpart of the bottom area, and there should be no or only a slight warp in this part.

The coefficient [A] was taken from the work of Clement and is assumed to be a measure of the planing area supporting the weight of the ship.

A high value of [A] correlates generally with a large resistance at high speeds. The slenderness [M] is of old related to the wave resistance. Its importance is felt at lower speeds at which the ship is not fully planing. In this range large resistance humps can occur. The detrimental effect of the resistance hump on the performance of the ship in waves is discussed at some length by Noordenbos and Van den Bosch in a paper before the Symposium Yacht Architecture 1973 in Amsterdam [3]. It was thought useful to use the slenderness in addition to the load parameter [A].

The parameters [A] and [M] are of course linked to each other by the $L_p/B_{c_{max}}$ ratio and the area coefficient $\alpha_p = A_p/L_p \cdot B_{c_{max}}$ which generally does not differ much from 0.8 for this type of ship.

For the methodical series the following items were selected as variables: the $L_p/B_{c_{max}}$ and the loading, i.e. the ships' weight and the position of the centre of gravity.

The other parameters had to be determined at the beginning.

The deadrise angle of the aftership was arbitrarily fixed at 24 degrees. This angle is about two times that of the Series 62. A larger deadrise would probably give lower vertical accelerations, a higher resistance and less stability especially for the small displacements.

A parameter of which the influence was unknown was the position of the centre of gravity of A_p, which controls the relative fullness of the fore- and after body. In the series 62 this point lies very far forward which results in a full forebody and a slender afterbody.

Table 1. Hull form data of models

	hull 114		hull 115		"Komer"		"Polycat"
item	test 1	test 2	test 1	test 2	test 1	test 2	
$L_p/B_{c\max}$	4	4	4	4	3.78	3.78	3.57
L_p/B_{cm}	5	5	5	5	4.37	4.37	4.42
[M]	6	5.48	6	5.48	5.48	5	5.33
[A]	7.2	6	7.2	6	6.85	5.71	6.55
α_p	0.8	0.8	0.8	0.8	0.865	0.865	0.808
$\overline{AX_p}/L_p$	0.433	0.433	0.467	0.467	0.447	0.447	0.460
$\overline{AG}/L_p$	0.367	0.367	0.400	0.400	0.382	0.382	0.395
$\overline{X_pG}/L_p$	0.067	0.067	0.067	0.067	0.065	0.065	0.065
β aft in degrees	24		24		not defined		20
L_p of model in metres	2.16		2.16		2.16		2.64

For the design under consideration two alternatives were drawn, one with a full forebody, but not extremely full, and the other with a slender forebody. For both designs the area coefficient was fixed at $\alpha_p = 0.8$.

It was anticipated that the radius of inertia would certainly influence the pitch motion and the vertical accelerations, but it was not well possible to include the variation of the radius of inertia in this programme. This quantity, therefore, was fixed at $k_{yy} = 0.25L_p$ a value which has been confirmed by calculations for some designs. Also it was felt that the practical possibilities to alter the value of k_{yy} significantly for a given ship are so small that it did not seem justified to include the radius of inertia as a variable in these preliminary test series.

Following Clement and Blount the value of $L_p/B_{c_{max}} = 4$ was chosen for the new design.

3 Hull form particulars

In table 1 the most important proportions of the four hulls under consideration are summarized. Three of the models were tested at two different displacements, in the first place to investigate the influence of the slenderness and in the second place to make the comparison possible with the full scale tests with the "Komer".

For the meaning of the symbols used the reader is referred to the list of symbols on page 5.

For the comparison of the model results in the following paragraphs, the model displacements are all reduced to the same standard displacement of 16 metric tons (tf) in seawater. This figure is arbitrarily chosen but well suited for its purpose, as it does not differ much from the actual displacements of the "Komer" and "Polycat" and it is a handy value for the calculation ($\nabla^{\frac{1}{3}} \approx 2.5$ and speed in m/sec is about 5 times $F_{n\nabla}$).

In table 2 the lengths and breadths of the ships are given for this standard displacement.

Table 2. Lengths and breadths of ships at displacement of 16 tf

		hull 114		hull 115		"Komer"		"Polycat"
		test 1	test 2	test 1	test 2	test 1	test 2	
L_p	m	15.00	13.69	15.00	13.69	13.69	12.50	13.33
$B_{c\max}$	m	3.75	3.42	3.75	3.42	3.63	3.31	3.73

The figures 1 to 3 show the models 114, 115 and "Komer". The hulls 114 and 115 look very similar. The difference of these two lies only in the position of the centre of gravity X_p of the area A_p.

The hull form of the "Komer" is entirely different from these two, being a typical round sectioned launch.

The lines of the "Polycat" are not available.

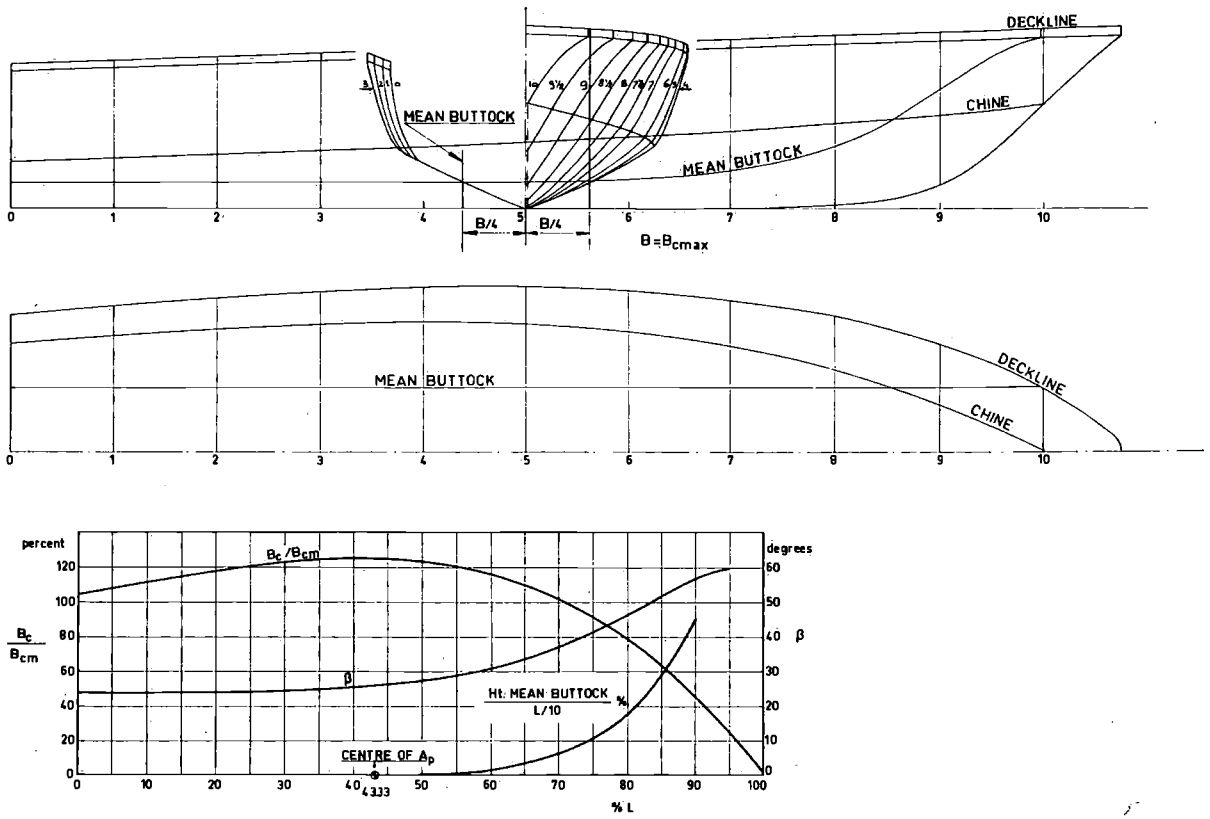

Fig. 1. Lines and form characteristics of the hull form 114.

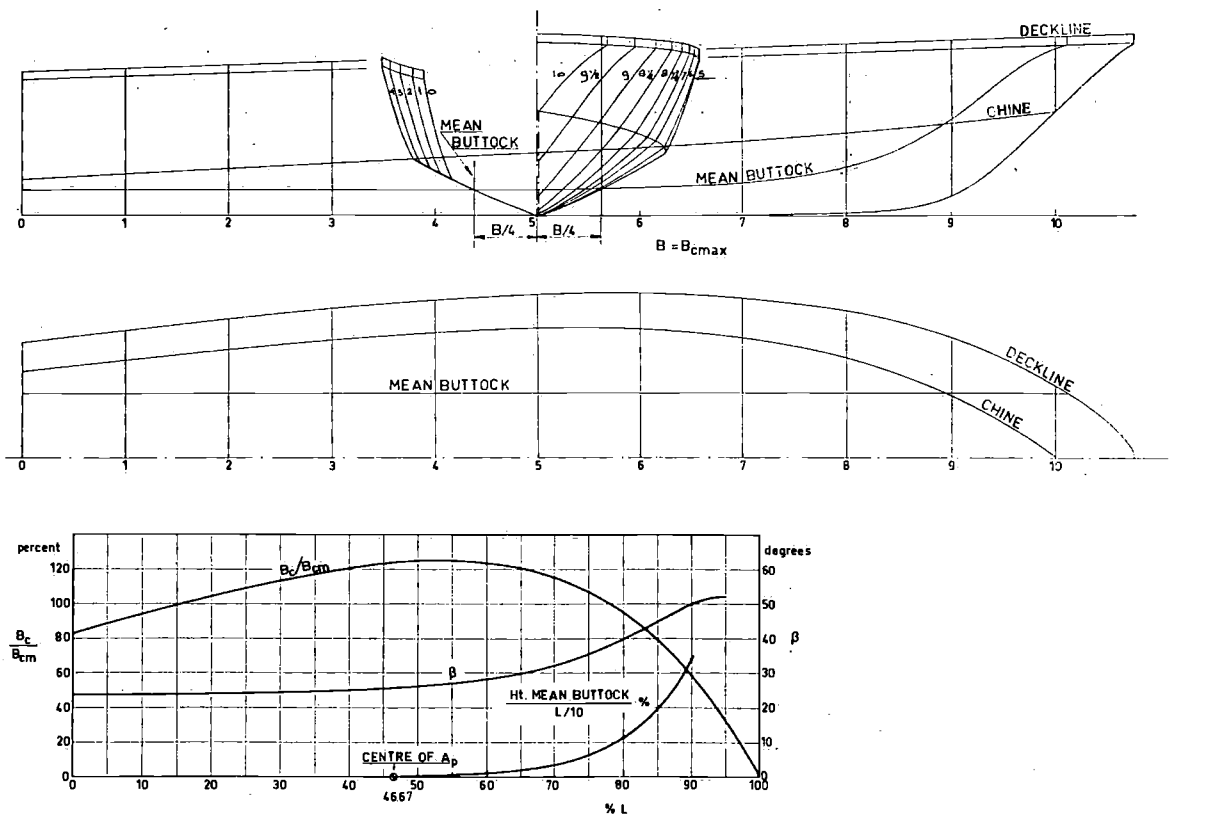

Fig. 2. Lines and form characteristics of the hull form 115.

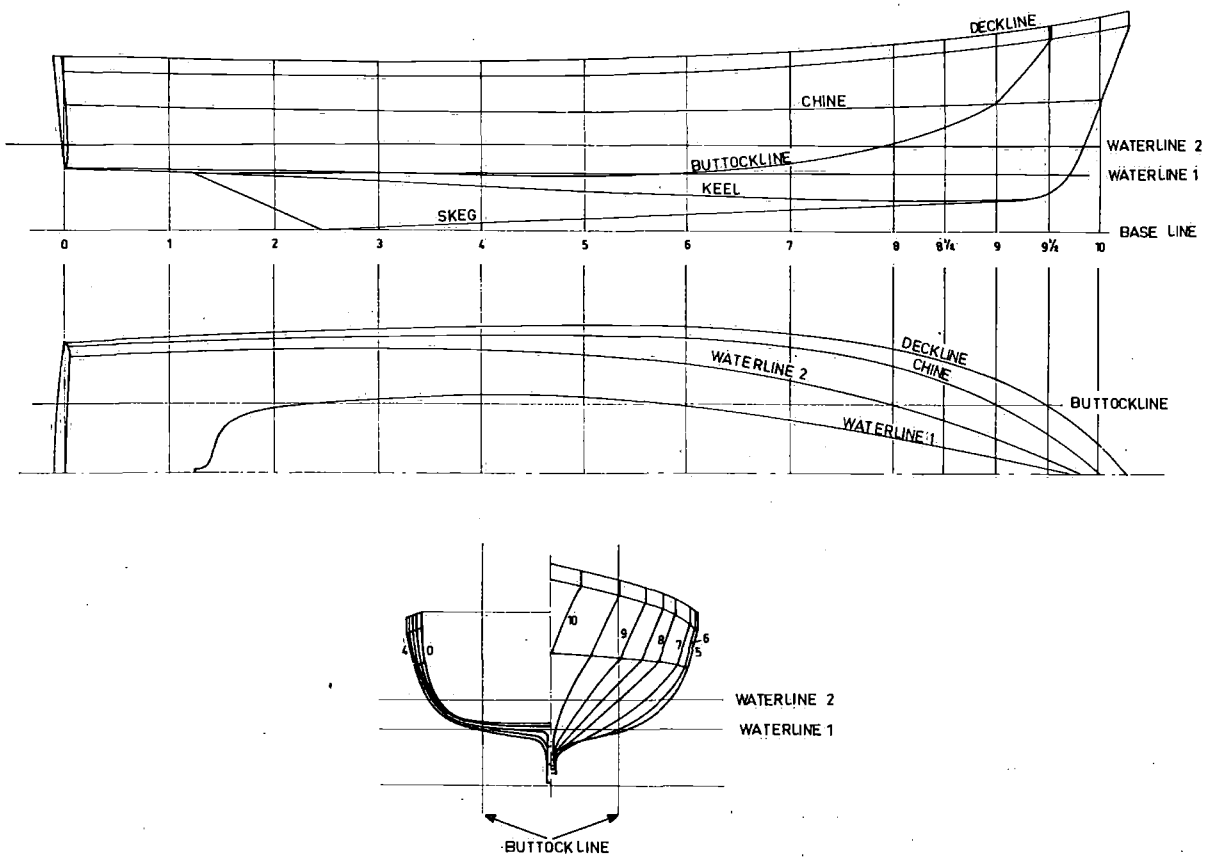

Fig. 3. Lines of "Komer".

4 Smooth water modeltests

4.1 *Measurements*

The models were attached in the centre of gravity, and free to trim and move vertically. The following quantities were measured:

1. the speed,
2. the resistance,
3. the rise of the centre of gravity,
4. the trim angle,
5. the form and area of the wetted surface from visual observation and underwater photographs.

The speed ranged from $F_{n\nabla} = 1.6$ to $F_{n\nabla} = 4.0$ for the models 114, 115 and "Komer" and from $F_{n\nabla} = 1.0$ to $F_{n\nabla} = 3.7$ for "Polycat".

4.2 *Most important results*

The figures 4 to 7 show the resistance/weight ratio and the trim angle for the ships of standard displacement in seawater with a density of 1025 kgf/m^3, a temperature of 15°C and a kinematic viscosity $\nu = 1.191.10^{-6}$ m^{2}sec^{-1}. The extrapolation is carried out with the use of the I.T.T.C. 1957 extrapolator without any allowance. When it is desired to take an additional frictional resistance into account, use can be made of the curve in the lower part of the figure, which was calculated using the measured wetted surface and an incremental resistance coefficient $C_A = 0.0002$. The additional resistance/weight ratio holds for any value of the displacement.

In the figures 8 to 14 the resistance/weight ratio is presented as a function of Froude number and displacement, again in seawater and without allowance.

4.3 *Discussion of the results*

The main purpose of the tests was to investigate the performance of the two newly designed hulls and to judge the results. The best way to do this seems to compare them with the Series 62, keeping in mind that it can be expected that the resistance will be higher, because of the larger deadrise and the generally recognized high quality of the Series 62 hullform. This indeed appears to be the case as is shown in figure 15, in which the resistance is given for all ships and for the corresponding Series 62 hull, obtained by interpolation from the data published. All ships had the same or nearly the same slenderness. It is seen that the resistance penalty for the high deadrise hard-chine hulls is not so serious up to $F_{n\nabla} = 3$, but beyond this the designed forms become progressively worse. It should be kept in

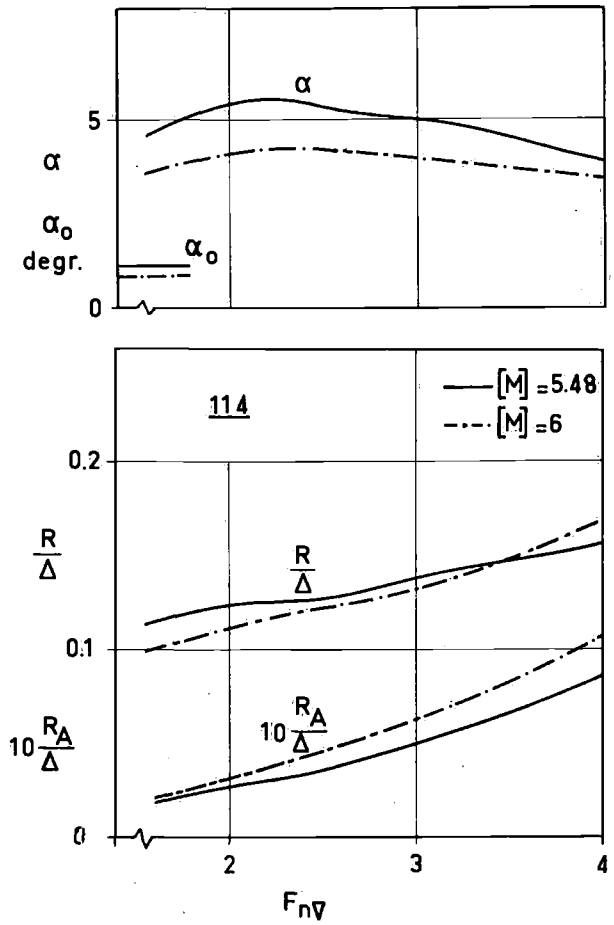

Fig. 4. Resistance and trim of hull 114 at standard displacement of 16 tons in seawater.

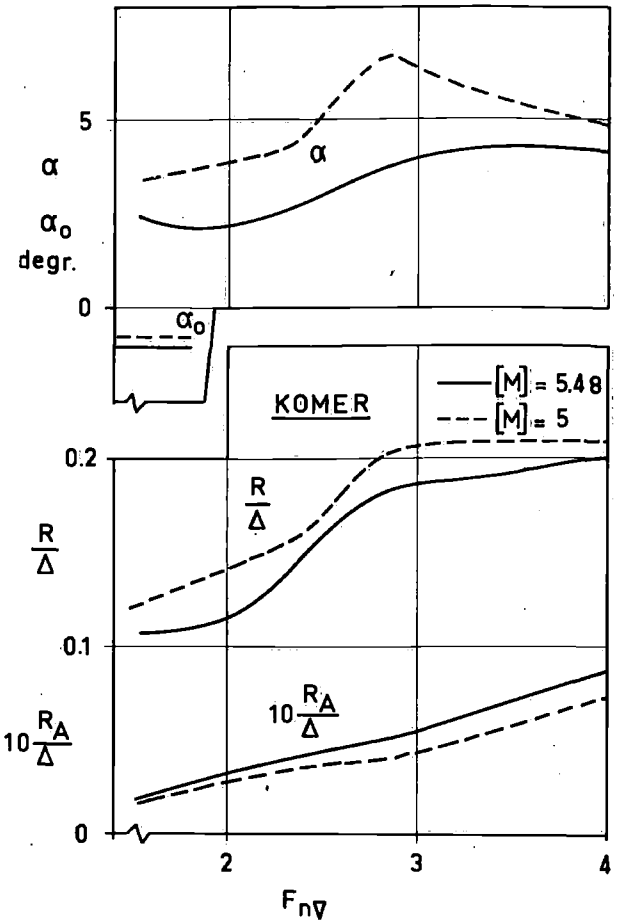

Fig. 6. Resistance and trim of "Komer" at standard displacement of 16 tons in seawater.

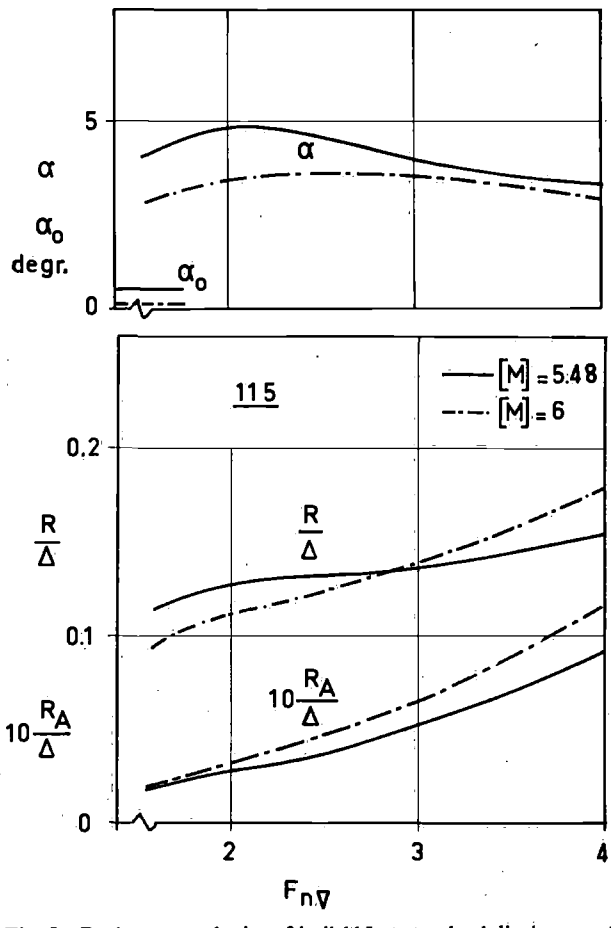

Fig. 5. Resistance and trim of hull 115 at standard displacement of 16 tons in seawater.

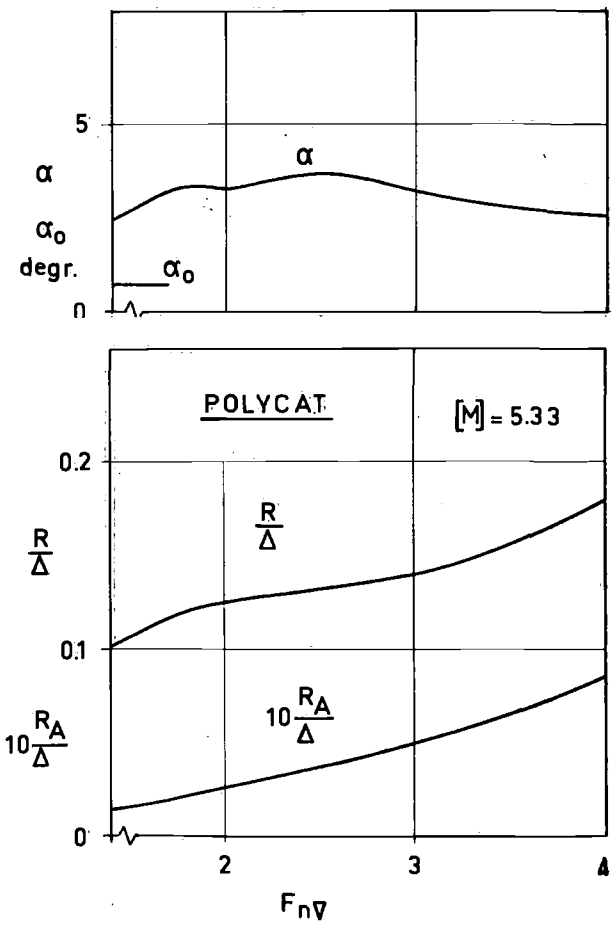

Fig. 7. Resistance and trim of "Polycat" at standard displacement of 16 tons in seawater.

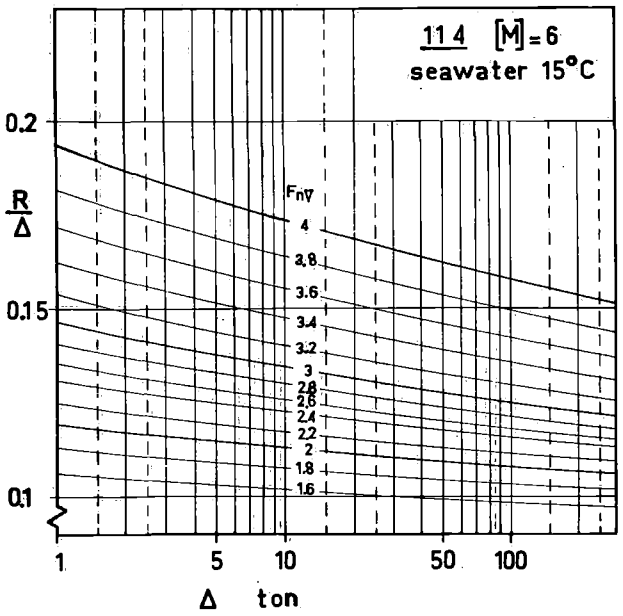

Fig. 8. Resistance of hull 114 at $[M]=6$ in seawater, as a function of the displacement.

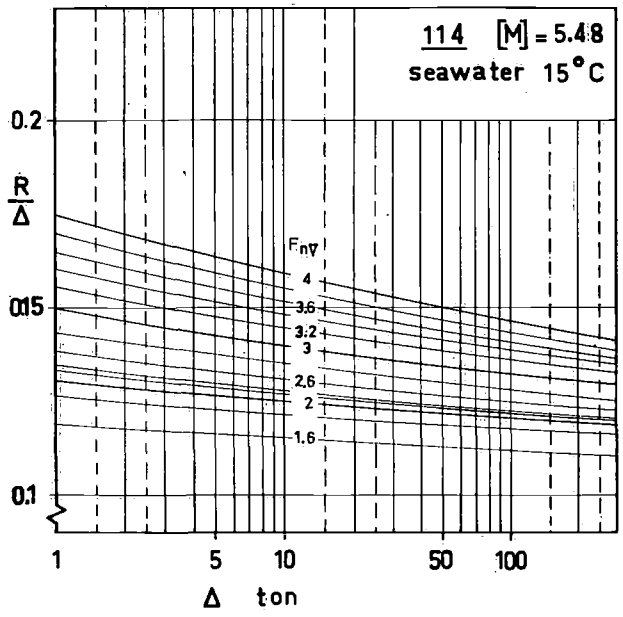

Fig. 9. Resistance of hull 114 at $[M]=5{,}48$ in seawater, as a function of the displacement.

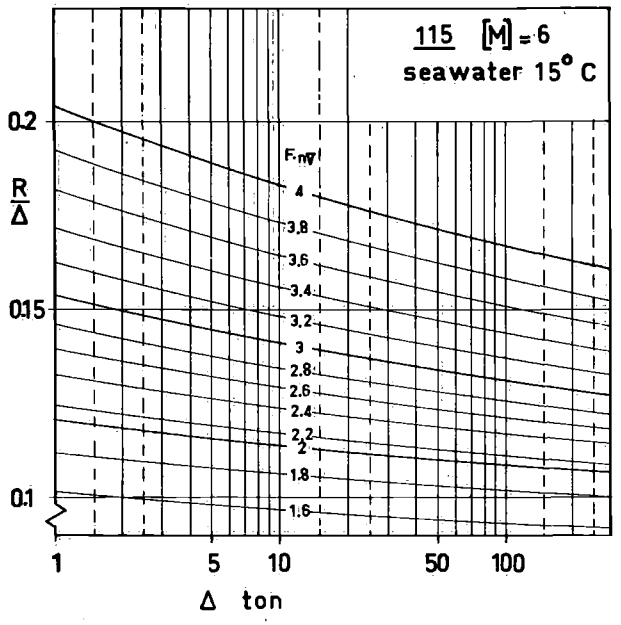

Fig. 10. Resistance of hull 115 at $[M]=6$ in seawater, as a function of the displacement.

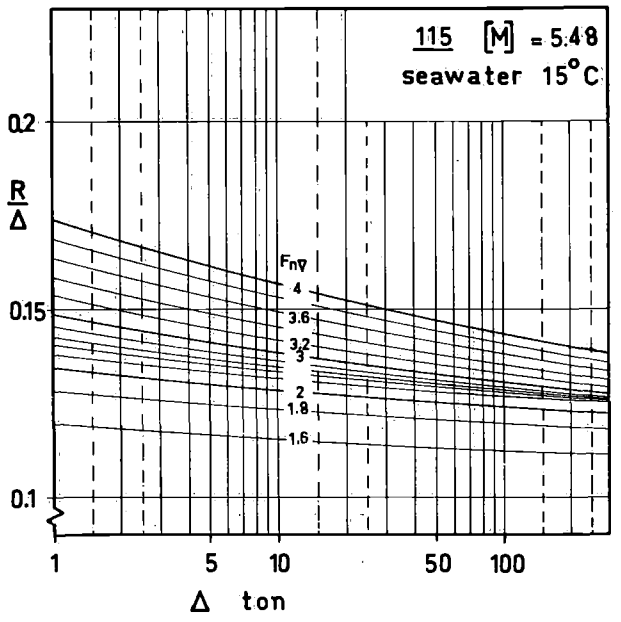

Fig. 11. Resistance of hull 115 at $[M]=5{,}48$ in seawater as a function of the displacement.

mind, however, that for the given position of the centre of gravity the Series 62 hull runs practically at its optimal trim, while for the other ships, and this holds especially for the Polycat, a shift of the centre of gravity backwards will increase the running trim and thereby decrease the resistance. Moreover, it should be realized that for ships of this size the Froude number $F_{n\nabla}=3.2$ already corresponds to a speed of more than 30 knots which in most cases is sufficiently high.

The resistance of the "Komer" is much higher in the speed range around $F_{n\nabla}=3$, which results in the need of more powerful engines, a greater fuel consumption larger weight, and therefore less deadweight. Here the "raison d'être" of the planing hull is clearly demonstrated.

It can be concluded that there's not much difference between the hull forms 114 and 115 and that both of them have a reasonable low resistance. Hull form 114 seems to be slightly preferable, if the backwards position of the centre of gravity can be obtained in practice.

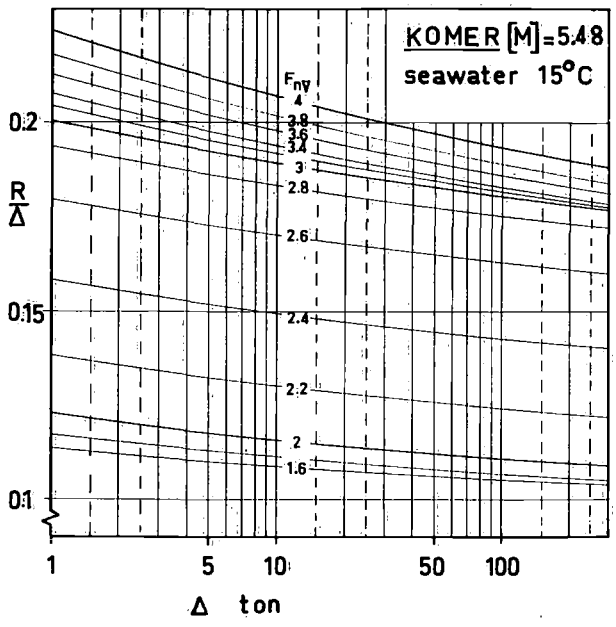

Fig. 12. Resistance of "Komer" at $[M] = 5.48$ in seawater, as a function of the displacement.

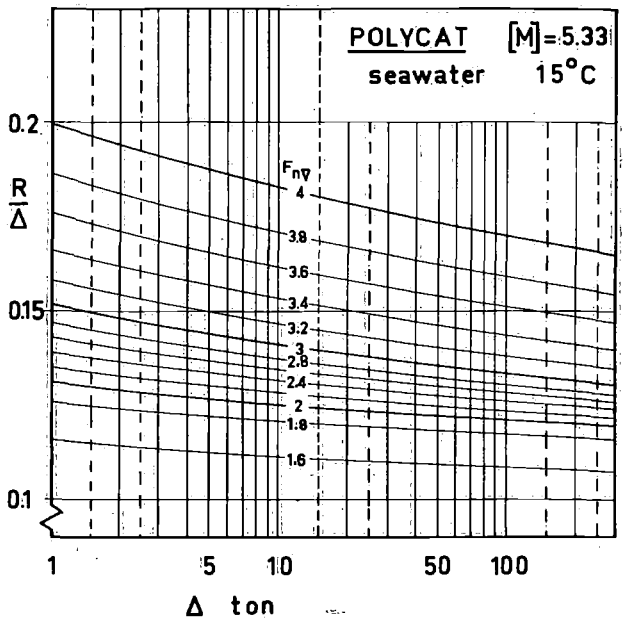

Fig. 14. Resistance of "Polycat" at $[M] = 5.33$ in seawater, as a function of the displacement.

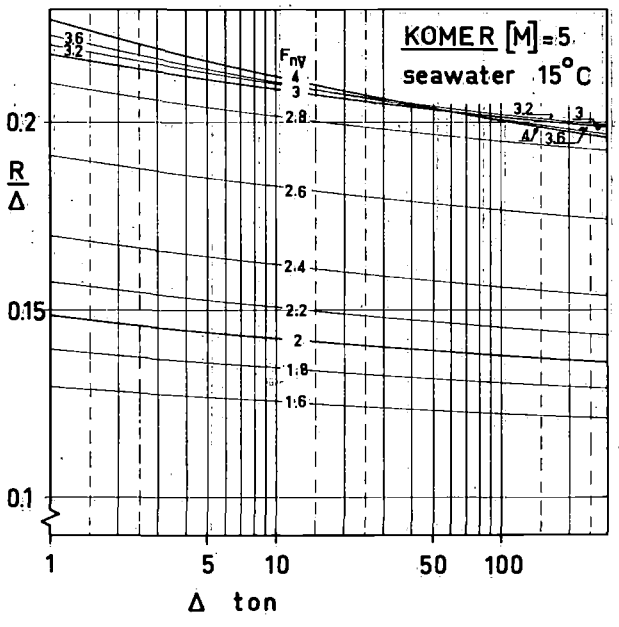

Fig. 13. Resistance of "Komer" at $[M] = 5$ in seawater, as a function of the displacement.

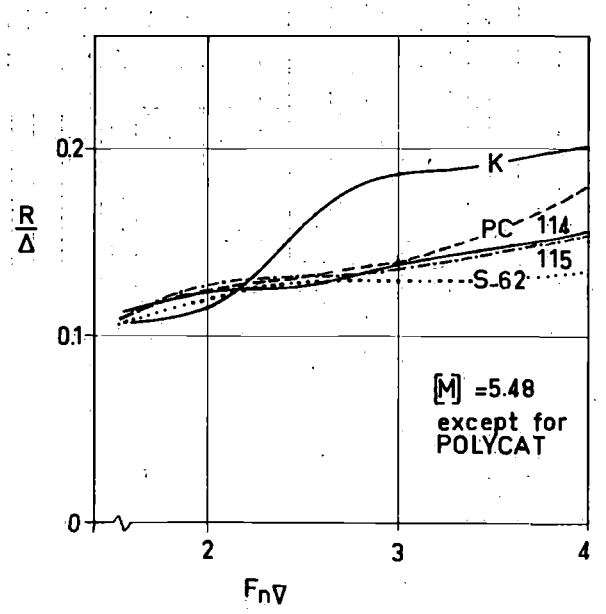

Fig. 15. Comparison of the resistance of the different ships with a corresponding hull form of the Series 62 at the same slenderness.

5 Modeltests in irregular head waves

5.1 *Review of the tests*

Their purpose was threefold, viz.:

1. to compare the qualities of the models 114 and 115 and "Komer" at the same conditions, i.e. the same slenderness.
2. to investigate the influence of the slenderness on the motions and accelerations.
3. to compare the "Komer" and "Polycat" with displacements corresponding to their actual full scale displacements.

These three points had some implications with regard to the model scale, which will be discussed later.

The models were attached in their centre of gravity and free to move in pitch and heave, while the other motions were restrained.

The following quantities were measured:

1. the heave motion including the rise of the centre of gravity,
2. the pitch motion including the trim,
3. the vertical accelerations at three positions, viz. at the fore end, at the middle and at the after end of L_p.
4. the resistance.

The tests were carried out at two speeds corresponding to $F_{n\nabla} = 2.4$ and $F_{n\nabla} = 3.2$, in irregular head waves with a spectrum of which more is said in the next paragraph.

The length and the number of the runs were chosen in such a way that more than 300 oscillations were experienced. In the report on these tests prepared by the NSMB the motions and accelerations were presented in the form of frequency of occurrence diagrams. In this publication only the most important will be shown, which suffice for the purpose of the explanation.

5.2 *The wave-height spectrum*

From the beginning it has been the aim to correlate the model results with full-scale measurements. It was realized that preferably the full scale sea conditions should be reproduced in the towing tank. It was not possible, however, to carry out the full scale tests first as the "Polycat" had yet to be built. Therefore a wave spectrum was sought which could be held as a reasonable presentation of a sea state frequently occurring on the North Sea, and which would also offer a realistic set of conditions to judge the seagoing abilities of the vessels from. Several North Sea spectra which were measured in the past were analyzed. From these a selection was made of wave conditions for westerly winds of force B 4. It appeared that the spectra could be represented reasonably well by the Pierson-Moskowitz formulation.

It was recognized that the motions and especially the vertical accelerations of a planing craft travelling in waves are non-linear phenomena. Therefore the usual methods of the spectral analyses are not applicable.

In order to compare different hulls in the future, the spectrum had to be standarized and a fixed relation between the spectrum and the size of the ship had to be established.

As the displacement is considered to be the main quantity determining the ship's size, the spectrum should be related to ∇ or $\nabla^{\frac{1}{3}}$. For the standard ship's displacement of 16 metric tons in seawater, $\nabla^{\frac{1}{3}} = 2.5$. It occurs that for a wind velocity of 7.65 m/sec, well into the Beaufort 4 range, the significant wave height amounts to 1.25 m. This has been chosen as a standard, so that

$$\tilde{\zeta}_{w\frac{1}{3}}/\nabla^{\frac{1}{3}} = 0.5$$

With this condition the Pierson-Moskowitz formulation reduces to the following model spectrum:

$$S_\zeta(\omega) = \frac{0.78}{\omega^5} e^{-\frac{2\lambda}{\omega^4}} \qquad \text{m}^2\text{sec}$$

in which λ stands for the model scale. This spectrum was chosen as a standard for the model comparison, but this implied that for every value of the model displacement the programme of the wave maker in the towing tank had to be changed. This was considered too expensive, and it was decided to set the wave programme for the average model displacement $\nabla = 0.06133$ m^3 or $\nabla^{\frac{1}{3}} = 0.394$ m. This programme was used for the models 114, 115 and "Komer" for all displacements. The model of the "Polycat" which had a different size was tested at a different wave height, but in accordance with the ratio:

$$\tilde{\zeta}_{w\frac{1}{3}}/\nabla^{\frac{1}{3}} = 0.5$$

5.3 *Corrections for the wave height*

As the models 114 and 115 were also tested at a smaller displacement, the wave height was too high relatively, while for the higher displacement of the "Komer" the waves were too low. In figure 16 the three modelspectra as they should have been, are shown. As it occurred only the middle one was used.

From the measurement of the motions it appeared that the damping was large, which also means that the motions will not be very sensitive for slight variations of the frequency range of the wave spectrum. From figure 16 it will be evident that the frequency shift of the spectra is very small, so that it seems justified to correct the motions only for the amplitude divergences and not for the frequency shift.

The motions are corrected in direct proportion to the wave height, although it was realized that the motions of planing craft are not strictly linear. This will be clear from figure 17 which shows the frequency of occurrence diagram of heave for model 114, slenderness $[M] = 6$ and $F_{n\nabla} = 2.4$ as an example. The upper part of the diagram shows the frequency of occurrence and the cumulative frequency distribution of the upwards amplitudes of heave, the lower part the downwards amplitudes. Both were measured from the position of the centre of gravity at rest. If the heave motion were linear, the upper and lower part would

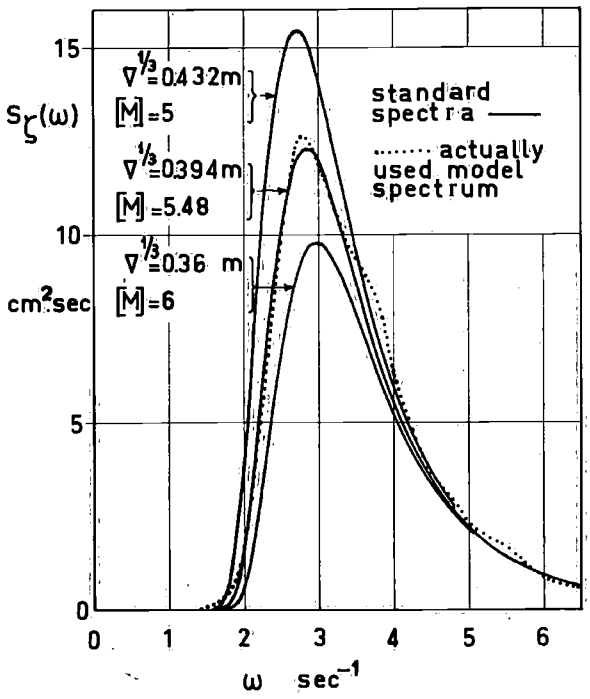

Fig. 16. The standard spectra for the different model displacements and the actually used spectrum.

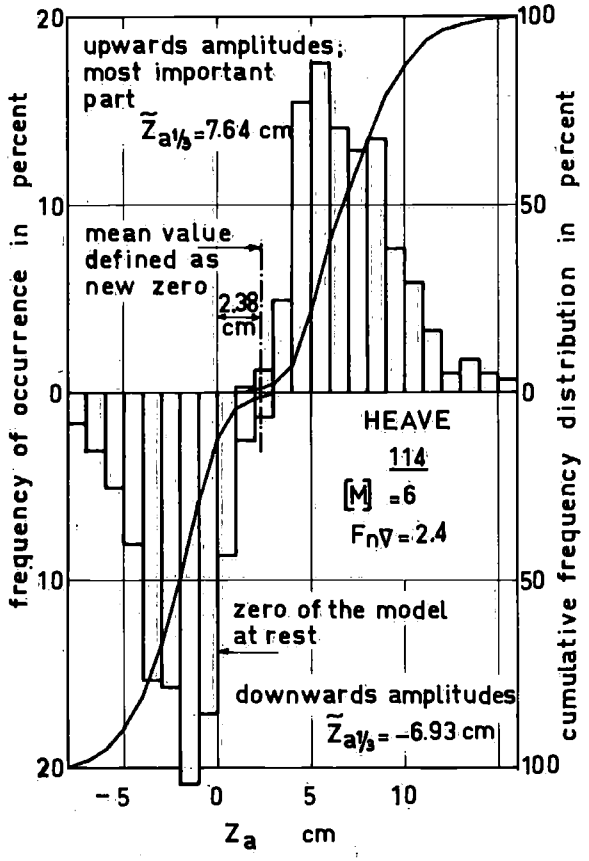

Fig. 17. Example of frequency of occurrence diagram.

be identical, and the mean value would equal the rise of the centre of gravity on smooth water at the considered speed. As it is, the mean heave is 5% larger than the rise of the centre of gravity in smooth water and the difference between the upper significant amplitude and the lower one is about 10%. Nevertheless it is considered right to correct the motions linearly with the wave height for this will bring the results closer to the truth, without overcorrecting if it concerns the upwards amplitudes, which will be used for the comparison.

The accelerations are also corrected linearly. This is disputable. If the accelerations were entirely caused by slamming they would vary as the square of the relative velocity between the ship's bottom and the water surface, and other things being linear the relative velocity would vary in direct proportion to the wave height. But, not every peak of the accelerations is due to slamming and the accelerations will not be determined entirely by the extant slamming peaks. So if the accelerations are corrected in proportion to the wave height the correction will not be overdone, but will probably be far too low.

In fact the motions and accelerations are presented as non-dimensional figures, but the way in which these parameters are made non-dimensional corresponds to a linear relation between the motions and the wave height.

5.4 *Presentation and discussion of the results*

5.4.1 Comparison of 114, 115 and Komer at the same slenderness

In the figures 18 and 19 the cumulative frequency distributions for heave are shown for the speed coefficients $F_{n\nabla} = 2.4$ and $F_{n\nabla} = 3.2$. In the figures 20 and 21 the cumulative frequency distributions for the pitch motion are shown. And in the figures 22 to 25 the vertical accelerations both at the fore end and at the middle of L_p are presented.

As regards the motion amplitudes it is striking that they appear to be nearly unaffected by the speed. The model 114 shows somewhat smaller heave motions than the other two models. As regards the pitch motion there is not much difference between the three models.

The accelerations at the lowest speed are nearly identical at the stem, while on midlength the "Komer" shows remarkably lower accelerations. The opposite is the case at the highest speed. Here the accelerations of the "Komer" both at the fore end and at the middle of L_p are evidently higher.

In table 3 the significant values reduced to non-dimensional quantities are summarized.

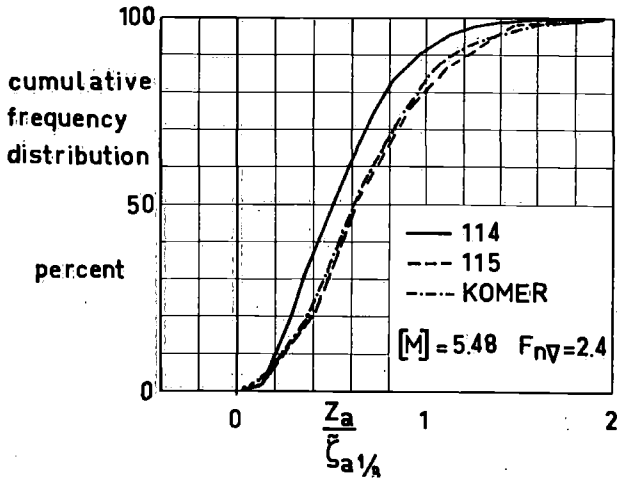

Fig. 18. Heave amplitudes of 114, 115 and "Komer" at $[M]=5.48$ and $F_{n\nabla}=2.4$.

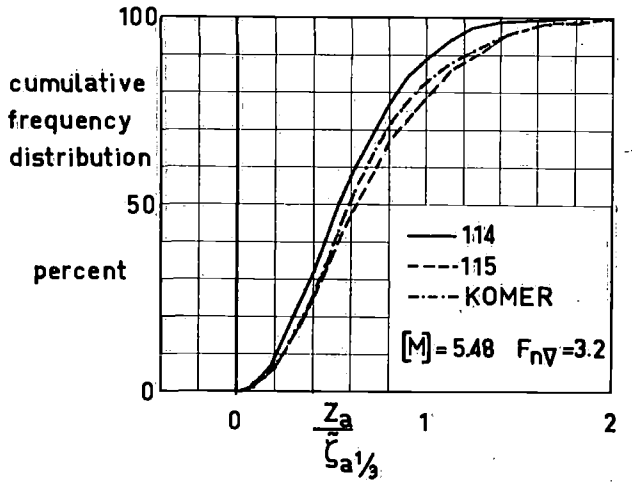

Fig. 19. Heave amplitudes of 114, 115 and "Komer" at $[M]=5.48$ and $F_{n\nabla}=3.2$.

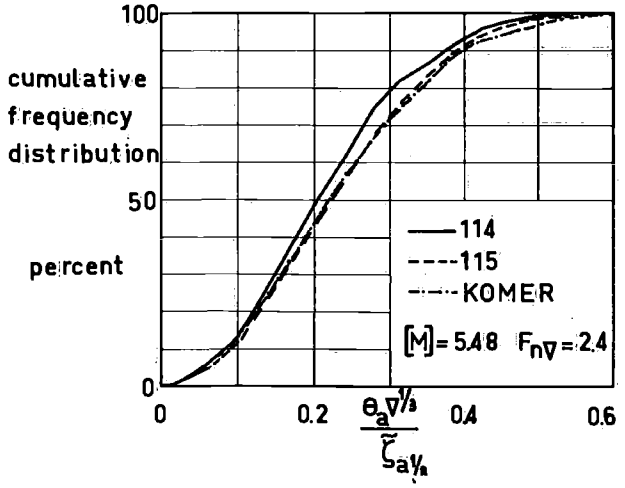

Fig. 20. Pitch amplitudes of 114, 115 and "Komer" at $[M]=5.48$ and $F_{n\nabla}=2.4$.

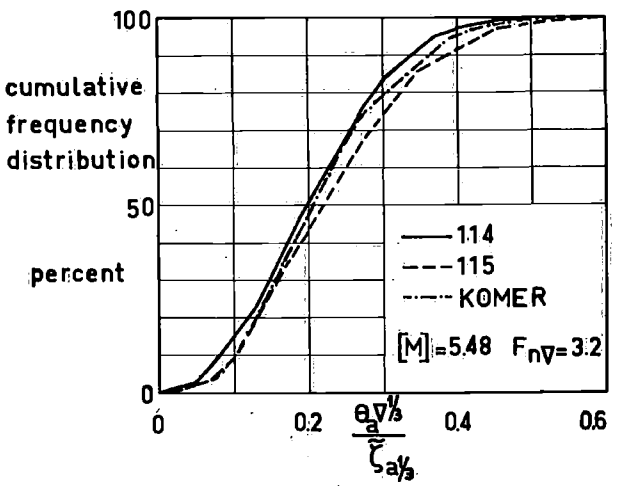

Fig. 21. Pitch amplitudes of 114, 115 and "Komer" at $[M]=5.48$ and $F_{n\nabla}=3.2$.

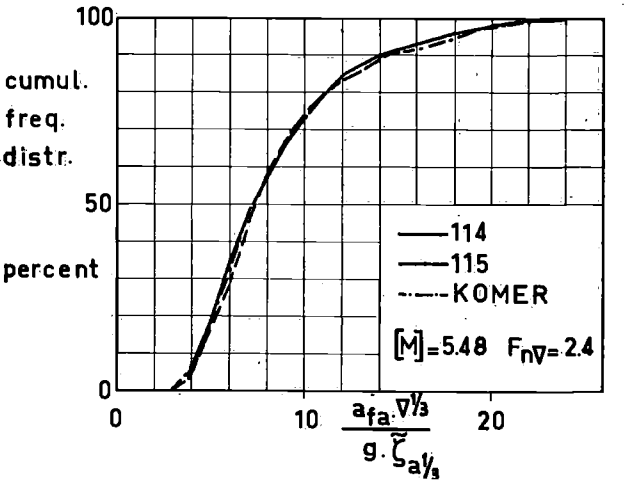

Fig. 22. Forward accelerations of 114, 115 and "Komer" at $[M]=5.48$ and $F_{n\nabla}=2.4$.

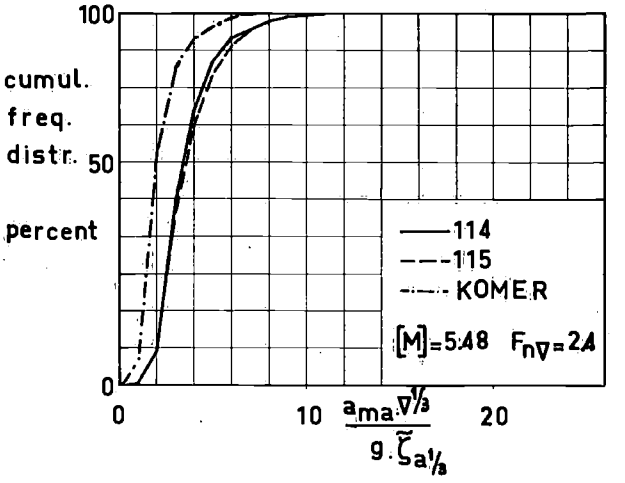

Fig. 23. Midship accelerations of 114, 115 and "Komer" at $[M]=5.48$ and $F_{n\nabla}=2.4$.

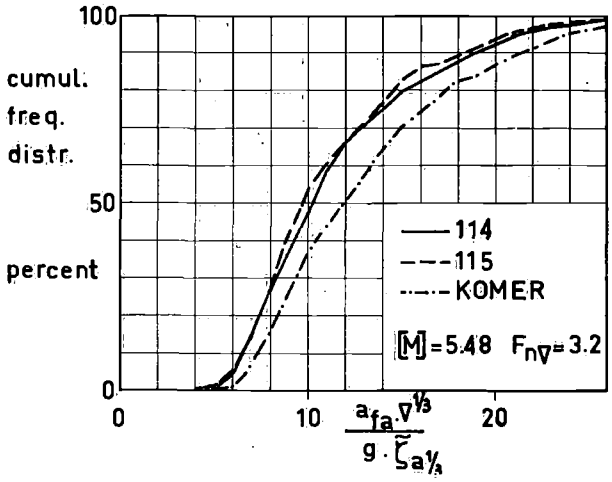

Fig. 24. Forward accelerations of 114, 115 and "Komer" at $[M] = 5.48$ and $F_{n\nabla} = 3.2$.

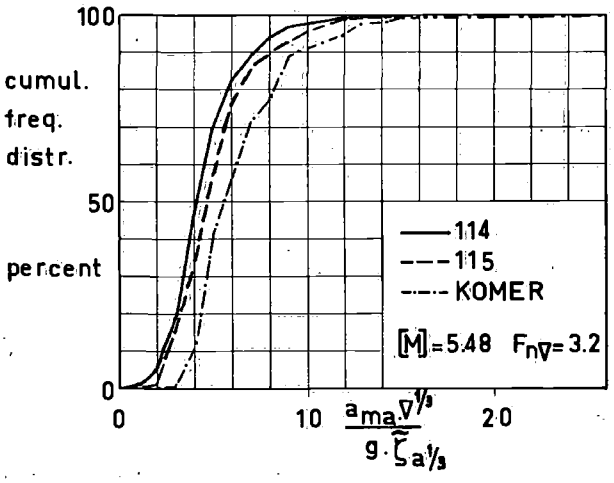

Fig. 25. Midship accelerations of 114, 115 and "Komer" at $[M] = 5.48$ and $F_{n\nabla} = 3.2$.

Table 3. Significant values of motions of three models for $[M] = 5.48$

	model 114		model 115		"Komer"	
$F_{n\nabla} \rightarrow$	2.4	3.2	2.4	3.2	2.4	3.2
$\frac{\tilde{z}_{a\frac{1}{3}}}{\tilde{\zeta}_{a\frac{1}{3}}}$	0.893	0.966	1.092	1.174	1.091	1.091
$\frac{\tilde{\theta}_{a\frac{1}{3}} \cdot \nabla^{\frac{1}{3}}}{\tilde{\zeta}_{a\frac{1}{3}}}$	0.340	0.316	0.366	0.354	0.373	0.334
$\frac{\tilde{a}_{fa\frac{1}{3}} \cdot \nabla^{\frac{1}{3}}}{g\tilde{\zeta}_{a\frac{1}{3}}}$	13.08	17.46	13.45	17.02	13.57	19.99
$\frac{\tilde{a}_{ma\frac{1}{3}} \cdot \nabla^{\frac{1}{3}}}{g\tilde{\zeta}_{a\frac{1}{3}}}$	5.18	6.94	5.38	7.63	3.13	9.91

From the results it appears that model 114 is slightly superior when the motions are considereal, but this superiority is not as evident in view of the vertical accelerations, except over "Komer" at the highest speed.

5.4.2 Influence of the slenderness

The same type of figures as in the preceding paragraph is used here to show the influence of the slenderness for each model individually. For these figures the original curves had to be corrected as set forth in paragraph 5.3.

The figures 26 and 27 concern model 114: the vertical accelerations forward and at mid length are shown for the Froude numbers 2.4 and 3.2 for the slenderness ratios 5.48 and 6.

The figures 28 and 29 concern model 115 and the figures 30 and 31 concern "Komer".

In nearly all cases an increase of the slenderness results in an appreciable reduction of the vertical accelerations, only for "Komer" these reductions are not so large, especially not for the highest speed and measured at mid length.

The significant values, again reduced to non-dimensional quantities, for other slenderness ratios than $[M] = 5.48$, are summarized in table 4.

Table 4. Significant values of motions of three models for $[M] = 6$ resp. 5

$[M] \rightarrow$	model 114 6		model 115 6		"Komer" 5	
$F_{n\nabla} \rightarrow$	2.4	3.2	2.4	3.2	2.4	3.2
$\frac{\tilde{z}_{a\frac{1}{3}}}{\tilde{\zeta}_{a\frac{1}{3}}}$	0.778	0.870	0.978	1.039	1.020	1.212
$\frac{\tilde{\theta}_{a\frac{1}{3}} \cdot \nabla^{\frac{1}{3}}}{\tilde{\zeta}_{a\frac{1}{3}}}$	0.263	0.260	0.298	0.281	0.403	0.415
$\frac{\tilde{a}_{fa\frac{1}{3}} \cdot \nabla^{\frac{1}{3}}}{g \cdot \tilde{\zeta}_{a\frac{1}{3}}}$	9.60	14.69	10.48	15.13	14.51	20.93
$\frac{\tilde{a}_{ma\frac{1}{3}} \cdot \nabla^{\frac{1}{3}}}{g \cdot \tilde{\zeta}_{a\frac{1}{3}}}$	3.63	6.05	3.37	5.53	5.63	9.50

5.4.3 The "Komer" and "Polycat" compared

In this paragraph these two vessels are compared on the basis of the non-dimensional presentation. The resultant figures give no realistic prediction of the motions and accelerations during the full scale tests, but rather compare the hull forms at the same displacement and at the same wave height.

In the figures 32 to 35 it is shown that the heave amplitudes of the two hull forms are essentially the

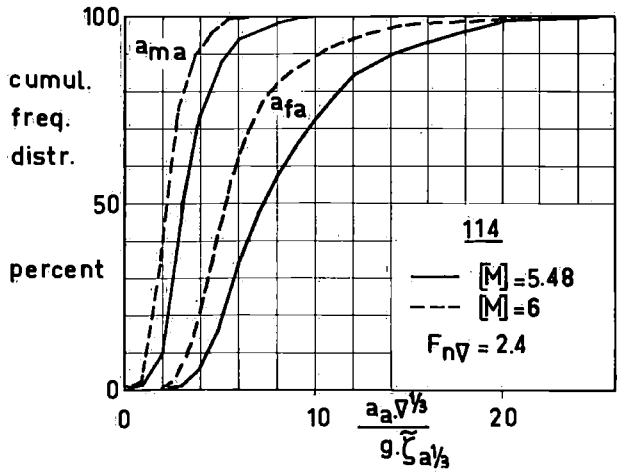

Fig. 26. Influence of the slenderness on the accelerations of 114 at $F_{n\nabla} = 2.4$.

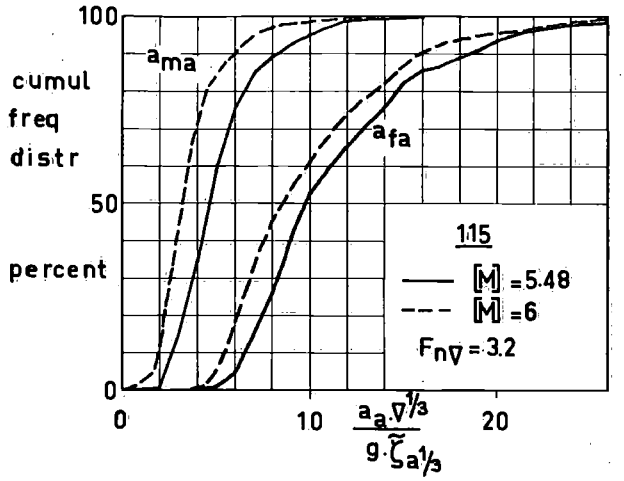

Fig. 29. Influence of the slenderness on the accelerations of 115 at $F_{n\nabla} = 3.2$.

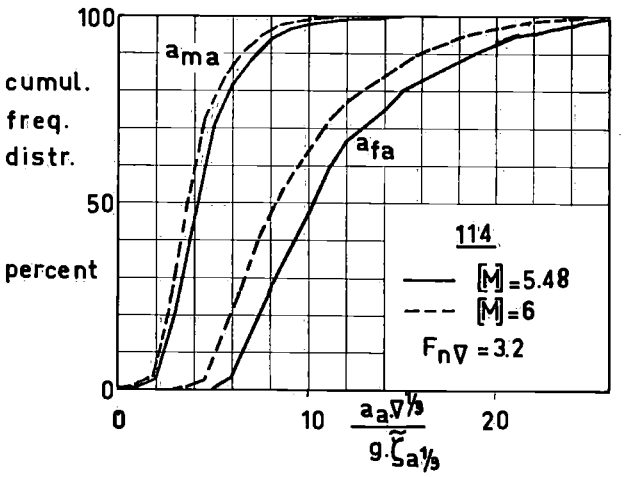

Fig. 27. Influence of the slenderness on the accelerations of 114 at $F_{n\nabla} = 3.2$.

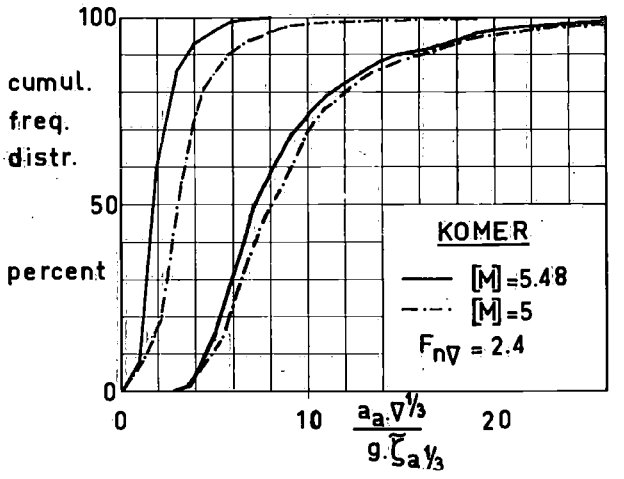

Fig. 30. Influence of the slenderness on the accelerations of "Komer" at $F_{n\nabla} = 2.4$.

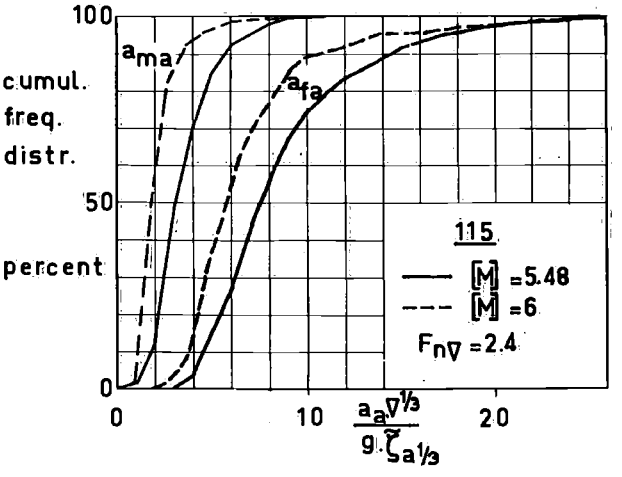

Fig. 28. Influence of the slenderness on the accelerations of 115 at $F_{n\nabla} = 2.4$.

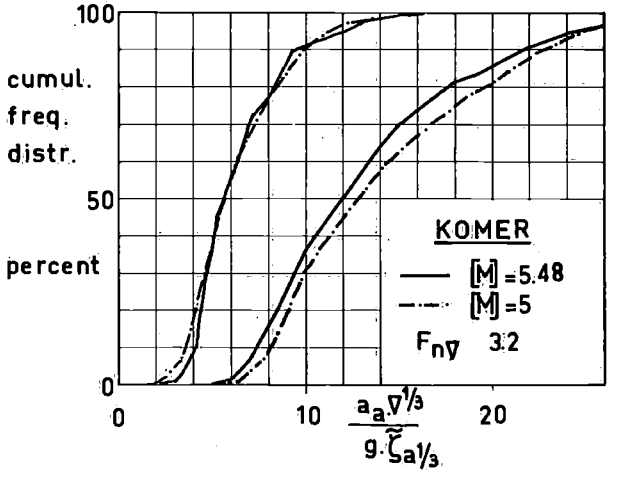

Fig. 31. Influence of the slenderness on the accelerations of "Komer" at $F_{n\nabla} = 3.2$.

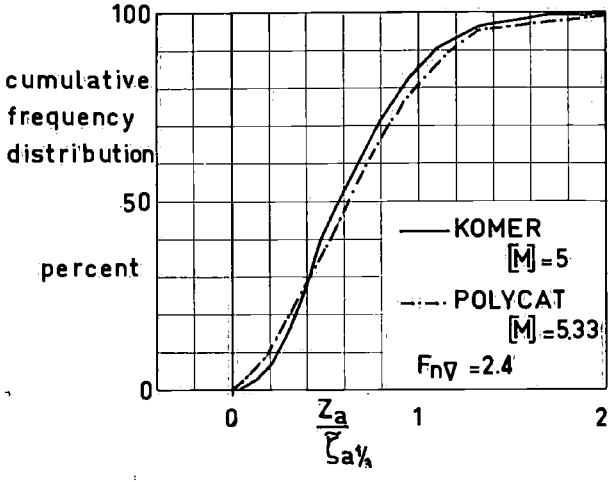

Fig. 32. Comparison of the heave amplitudes of "Komer" and "Polycat" at $F_{n\nabla} = 2.4$.

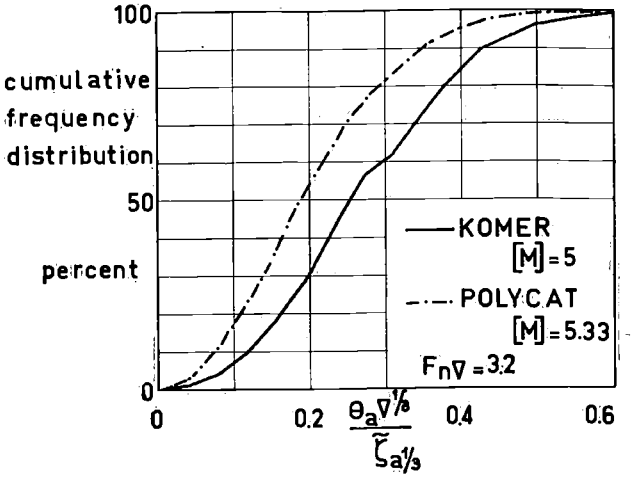

Fig. 35. Comparison of the pitch amplitudes of "Komer" and "Polycat" at $F_{n\nabla} = 3.2$.

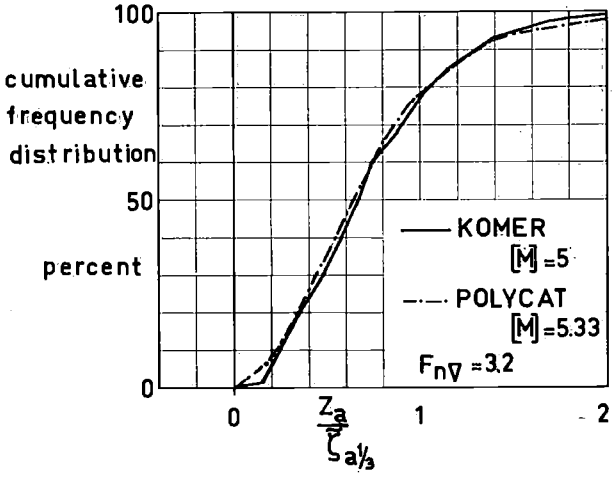

Fig. 33. Comparison of the heave amplitudes of "Komer" and "Polycat" at $F_{n\nabla} = 3.2$.

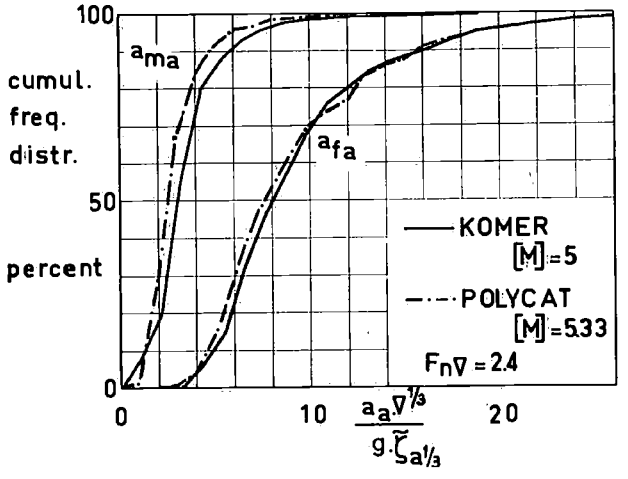

Fig. 36. Comparison of the accelerations of "Komer" and "Polycat" at $F_{n\nabla} = 2.4$.

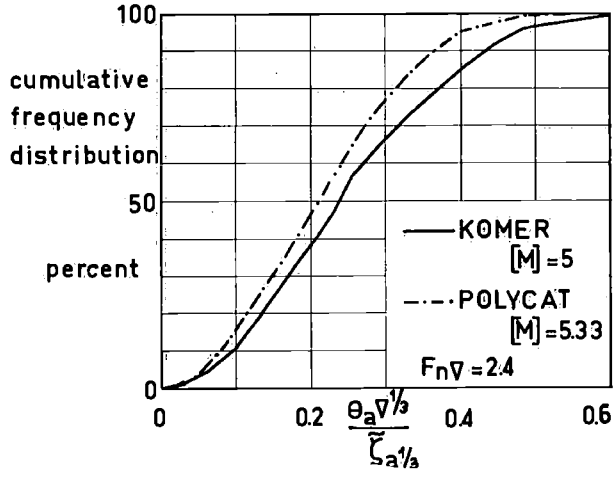

Fig. 34. Comparison of the pitch amplitudes of "Komer" and "Polycat" at $F_{n\nabla} = 2.4$.

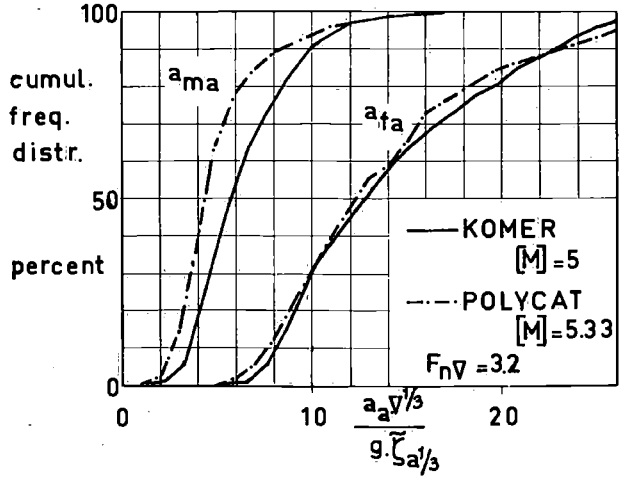

Fig. 37. Comparison of the accelerations of "Komer" and "Polycat" at $F_{n\nabla} = 3.2$.

same, but that the pitch amplitudes of "Polycat" are clearly smaller.

The vertical accelerations, as shown in the figures 36 and 37 do not differ very much except at mid-length at the highest speed, where "Polycat" is slightly superior.

The significant values of the heave and pitch motions and of the accelerations of the two hulls are put together in table 5.

Table 5. Significant values of motions of "Polycat" and "Komer"

	"Polycat"		"Komer"	
$[M] \rightarrow$	5.33		5	
$F_{n\nabla} \rightarrow$	2.4	3.2	2.4	3.2
$\frac{\tilde{z}_{a\frac{1}{3}}}{\tilde{\zeta}_{a\frac{1}{3}}}$	1.081	1.194	1.020	1.212
$\frac{\tilde{\vartheta}_{a\frac{1}{3}} \cdot \nabla^{\frac{1}{3}}}{\tilde{\zeta}_{a\frac{1}{3}}}$	0.345	0.320	0.403	0.415
$\frac{\tilde{a}_{fa\frac{1}{3}} \cdot \nabla^{\frac{1}{3}}}{g \cdot \tilde{\zeta}_{a\frac{1}{3}}}$	14.50	21.00	14.51	20.93
$\frac{\tilde{a}_{ma\frac{1}{3}} \cdot \nabla^{\frac{1}{3}}}{g \cdot \tilde{\zeta}_{a\frac{1}{3}}}$	4.60	7.84	5.63	9.50

5.4.4 Added resistance in waves

The average resistance of the models were measured during the tests in waves. The differences between the resistance in waves, and the smooth water resistance was calculated and was corrected for the wave height with the assumption that the added resistance varies as the square of the significant wave height.

The results are summarized in table 6.

There does not appear to be, as far as can be judged from these tests, any systematic relation between the hull form parameters and the added resistance, except for the remarkably low added resistance of the "Komer" at the highest Froude number. This phenomenon is accompanied by a large increase in the centre of gravity rise, without a significant alteration of the trim angle. This indicates that the unstationary character of the flow decreases the squating tendency and thereby diminishes the wetted surface. Part of the higher smooth water resistance of this model is compensated by the lower added resistance in waves.

Table 6. Added resistance in waves

hullform	$[M]$	$F_{n\nabla}$	R_{Aw}/Δ
114	6	2.4	0.0222
	6	3.2	0.0333
	5.48	2.4	0.0306
	5.48	3.2	0.0293
115	6	2.4	0.0258
	6	3.2	0.0308
	5.48	2.4	0.0323
	5.48	3.2	0.0381
Komer	5.48	2.4	0.0192
	5.48	3.2	0.0135
	5	2.4	0.0310
	5	3.2	0.0050
Polycat	5.33	2.4	0.0341
	5.33	3.2	0.0340

6 Summarized conclusions from the modeltests

The following conclusions can be drawn:

1. As regards resistance in smooth water the three hard-chine craft are clearly superior over the round-bottom boat "Komer". In waves this superiority still exists but to a smaller degree.
2. The high deadrise hard-chine hulls show a somewhat greater resistance than the corresponding hull of the Series 62, due to the higher deadrise angle.
3. As regards motions and accelerations in waves the models 114 and 115 are slightly superior to "Komer". Model 114 is generally the best of the three.
4. The slenderness has a large influence on the motions and accelerations, on the assumption that with the alteration of the displacement the radius of inertia in pitch is kept constant. Then a reduction of the displacement is accompanied by a reduction of the accelerations.
5. The comparison of the behaviour in waves of the "Komer" and "Polycat" models reveals that the heave amplitudes do not differ much, but that the pitch amplitudes of "Polycat" are less, especially at the highest speed. Generally there is not much difference in the vertical accelerations except at the highest speed in the midship region. Here the accelerations of the "Polycat" model are lower.
6. Generally the models 114 and 115 perform somewhat better than the models of the existing ships "Polycat" and "Komer". Probably these differencies can be attributial to the different length/breadth ratios.

7 Full-scale tests

7.1 *General information*

The purpose of the tests was to compare the model results with full-scale results, especially the vertical accelerations occurring. Because of the anticipated non-linearity of these, the idea was to carry out the measurements at different sea states so that an insight could be gained in the influence of the wave-height on the magnitude of the accelerations.

The first series of measurements proceeded satisfactorily but in waves of which the significant height was appreciably lower than the standard chosen earlier, viz. $\zeta_{w\frac{1}{3}} = 0.5\nabla^{\frac{1}{3}}$. For "Polycat" this value would have been $\zeta_{w\frac{1}{3}} = 1.24$ m and for "Komer" $\zeta_{w\frac{1}{3}} = 1.19$ m. As it was, the measured significant wave height merely reached $\zeta_{w\frac{1}{3}} = 0.84$ m.

Two days after the first tests the wave conditions seemed to be right and the second series of measurements was started. These did not succeed for during the first run one of the tape recorders left off and shortly afterwards a short circuit aboard the "Polycat" prevented the manoeuvring of the electro-magnetically activated gear of one of the engines. Although both these failures were not really serious, they could not easily be repaired under the prevailing conditions.

Polycat came home comfortably on one engine but time was up.

An analysis of the wave measurements revealed that the significant height was about 10% higher than the "standard" and that the form of the spectrum showed a good likeness. Unfortunately there was no further opportunity to carry out the measurements wanted.

The tests were carried out on the North Sea, about 30 miles from the shore, west of IJmuiden in the neighbourhood of a stationary wave-buoy of Rijkswaterstaat (Ministry of Public Works).

Three ships took part in the tests the "Komer" and the "Polycat" of course, and the "Prins Hendrik" another lifeboat of the K.N.Z.H.R.M. which was kept anchored in the centre of the test area and was equipped with wave height measuring instruments developed by the Shipbuilding Laboratory.

The measurements from this party were used in this report. The data from the wave-buoy of Rijkswaterstaat were available if desired, but were not used here.

7.2 *Measurements*

The following items were measured:

1. The wave-height by a drifting wave buoy, equipped with a accelerometer and a transmitter. The frequency modulated signal was received and recorded by the instruments stationed on the "Prins Hendrik".
2. The vertical accelerations on two positions on both the "Komer" and the "Polycat". On the "Komer" the positions of the forward and midships accelerometers corresponded reasonably well with those used during the modeltests.
   On the "Polycat" the forward accelerometer had to be placed more backward. As a consequence the data had to be corrected. This was done on the assumptions that the ship moved as a rigid body and so the accelerations are distributed linearly along the length, and that the point at which the vertical acceleration equals zero, lies at a quarter of the length L_p from the transom. This was observed during the model tests. The correction amounts to 35%.
3. The speed. For the runs which passed closely to the "Prins Hendrik", the speed was determined by the time which elapsed between the moment that the two running ships crossed the three-mile circle on the radar display of the "Prins Hendrik" and the moment that this ship was passed. The radar had been checked against the large shore-based radar installation at IJmuiden. The distance in question proved to be 3.15 miles. The speeds were not corrected for possible currents.
   For the other runs the log of the "Komer" was used. This was a small log of the rotating type. Its reading was 5% too high compared with the former method.

The measurements were carried out at two engine speeds. It appeared impossible to adjust the desired speed at the indication of the log which was not sufficiently steady. Instead the r.p.m. of the engines were set at a rate which corresponded, according to the commander of the "Komer" to the desired speed: r.p.m. 1950 corresponding to 22.5 kts (i.e. $F_{n\nabla} = 2.4$). This agreed indeed for the distance covered recorded by the log, taken over two runs, one against the waves and one with the waves. The possibility exists that the log indication of the distance covered through the water is more reliable than the speed calculated with the aid of the radar.

As this remains uncertain the "radar" speed is considered as the right one. The speed according to the log is about 5% higher.

Six runs were made on the first day, two against the waves, two with the waves from behind, one run with the waves on the bow at 45 degrees with the wave direction, and one run with the waves abeam.

Some data of the runs are given in table 7.

Table 7. Data of measuring runs

run	relative course degrees	speed (radar) kts	$F_{n\nabla}$ "Komer"	engine setting "Komer" r.p.m.
1	180	20.4	2.17	1950
2	0	22.3	2.37	1950
3	180	24.7	2.63	2150
4	0	28.1	3.00	2150
5	135	24.8	2.64	2150
6	90	26.7	2.85	2150

The engine setting of 2150 r.p.m. of the "Komer" was the highest attainable.

7.3 *Presentation and discussion of the test results*

The wave-height spectrum, measured on the first day is shown in figure 38 together with the standarized spectrum desired for the "Komer". It will be clear that they are rather far apart.

The cumulative frequency distribution of the accelerations are given in the figures 39 to 42. The runs with the following waves are not shown. On these runs the accelerations at the forward and at the midship positions never exceeded $1g$ and $\frac{1}{2}g$ respectively.

The given accelerations at the forward position aboard the "Polycat" are corrected.

For the two runs in head waves the forward accelerations are reduced to the non-dimensional quantities

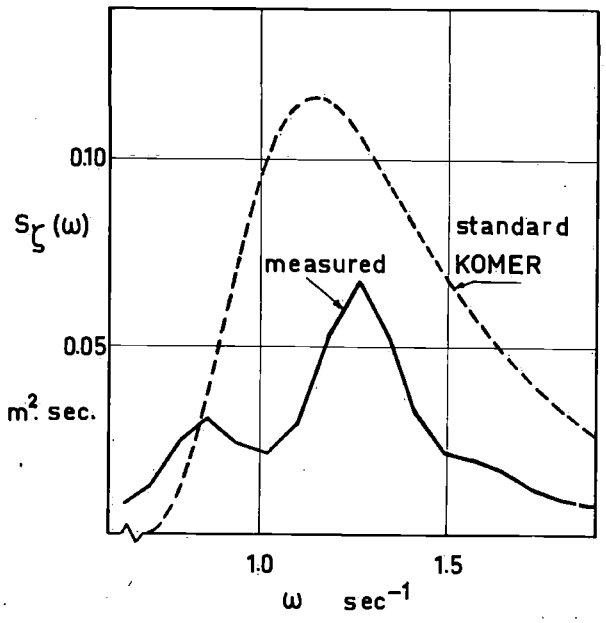

Fig. 38. Comparison of the measured full-scale spectrum and the spectrum wanted.

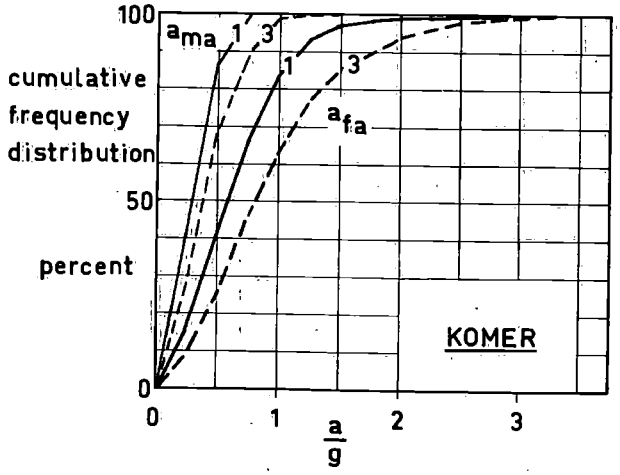

Fig. 39. Accelerations of full-scale "Komer" in head waves, runs 1 and 3.

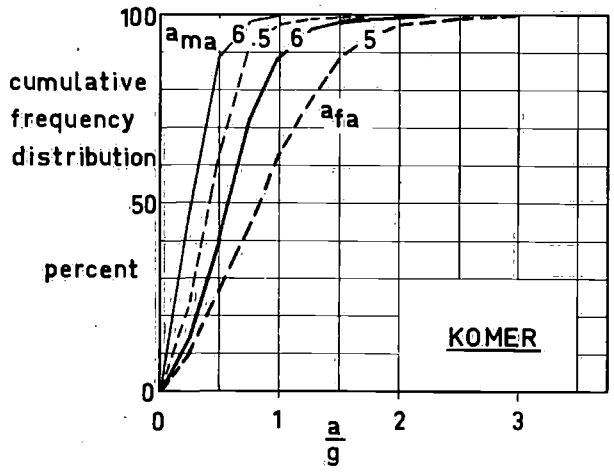

Fig. 40. Accelerations aboard "Komer" on different courses with respect to the waves, runs 5 and 6.

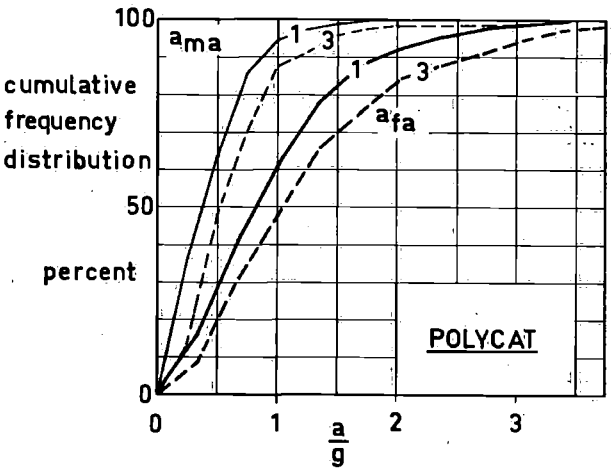

Fig. 41. Accelerations of full-scale "Polycat" in head waves, runs 1 and 3.

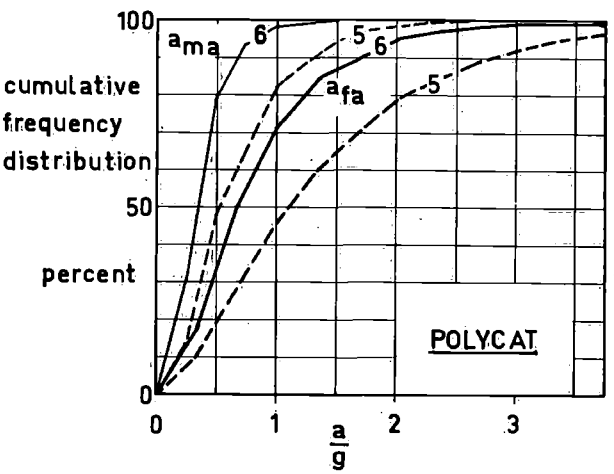

Fig. 42. Accelerations aboard "Polycat" on different courses with respect to the waves, runs 5 and 6.

in the same way as the model results, a linear relation being assumed between the accelerations and the wave-height.

The results are shown in the figures 43 and 44 together with the model results for the Froude number $F_{n\nabla} = 2.4$.

The agreement between the full-scale and the model results is plainly bad, which suggests that for the large difference between the wave heights wanted and measured the assumed linear relationship is too far beside the truth. In the following it is attempted to make the difference plausible.

It is generally assumed that the dynamic pressure peaks which cause the slamming accelerations have only a very short duration and therefore contain only little energy. For that reason the motion of the craft in waves will only be influenced very slightly by the slamming pressures and remain roughly proportional to the wave-height. The vertical velocity between the water surface and any part of the ship's bottom will also be roughly proportional to the wave height, but the slamming pressures will vary as the square of the vertical velocities and therefore as the square of the wave height, provided that the appropriate parts of the bottom emerge from the water. If not, no slam will occur. When the waves are low a large percentage of the encounters will not result in a slam and the corresponding accelerations will be low. When the wave height increases the motions increase also and the moment will come when the bottom emerges so far that slamming is started. Vertical accelerations will then increase stepwise, which will result in a shift of the frequency of occurrence distribution in the lower ranges. In the range of the higher accelerations it can

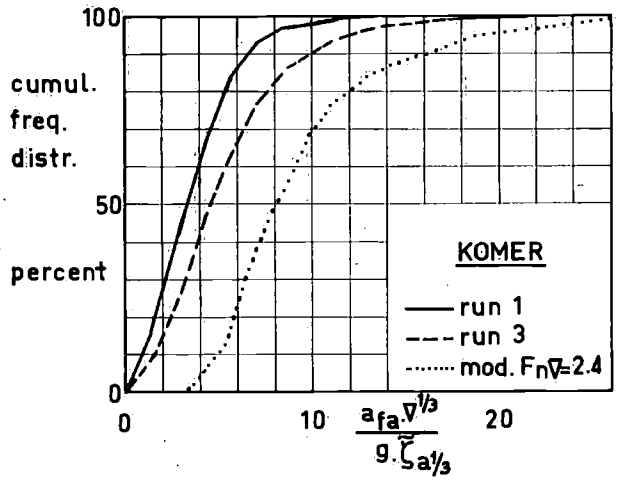

Fig. 43. Comparison of forward accelerations aboard "Komer", with model results, based on an assumed linear relation with the wave height.

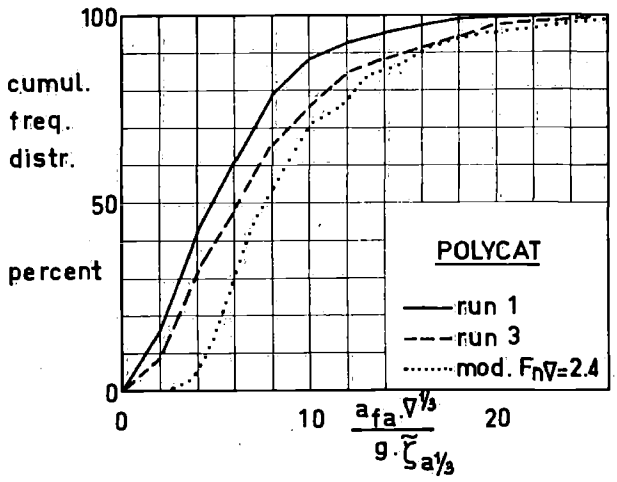

Fig. 44. Comparison of forward accelerations aboard "Polycat", with model results, based on an assumed linear relation with the wave height.

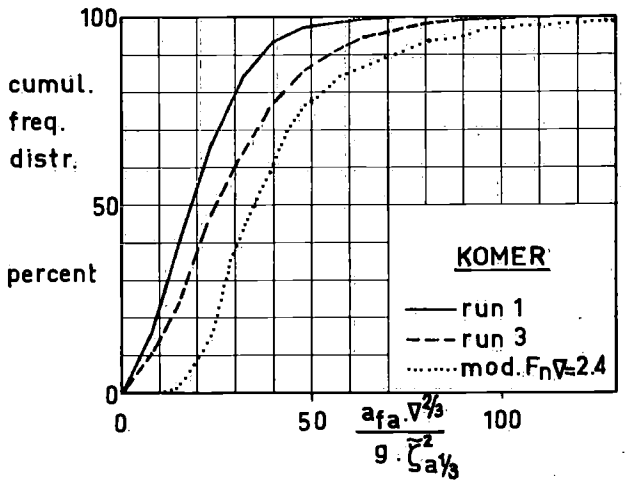

Fig. 45. Comparison of forward accelerations aboard "Komer" with model results, based on a quadratic relation with the wave height.

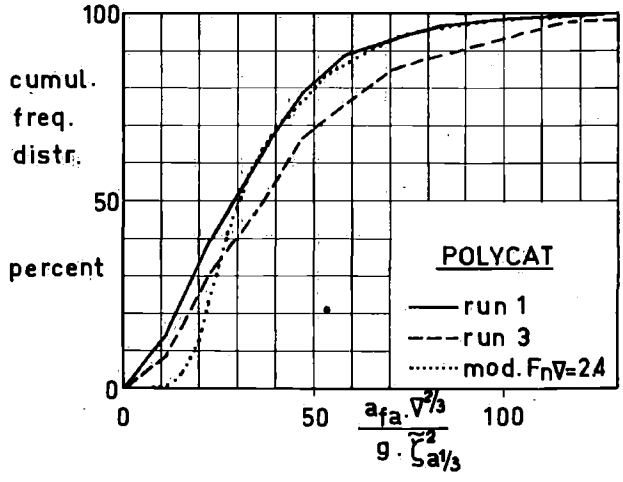

Fig. 46. Comparison of forward accelerations aboard "Polycat", with model results, based on a quadratic relation with the wave height.

be anticipated that a quadratic relation with the wave height is approximately true.

With the above considerations in mind the figures 45 and 46 have been drawn. In these the accelerations are made non-dimensional, based on the assumption that they vary as the square of the wave height. The result of this comparison is more acceptable, at least for the "Polycat". The shift of the cumulative frequency curve in the lower ranges is still there. This is understandable as the threshold will not be affected by this calculation. In the range of the higher accelerations the uncertainty about the speed remains. If the "logspeed" had been used instead of the "radar speed" the agreement would have been perfect.

It seems that for the "Komer" the threshold effect is much more important. This was also evident during the tests, when the running ships and their behaviour were considered. The "Polycat" dances on the surface of the water, while the "Komer" does not emerge easily and seems to be held in the water. That seems the reason why the "Komer" experiences lower accelerations than the "Polycat" as long as the waves are low.

The measurements at other directions relative to the waves are included here because they show some interesting aspects. When run 3 and run 5 are compared is it clear that with the waves on the bow at 45 degrees the accelerations are as high as, or may be somewhat higher than, in headwaves. At 90 degrees there is clearly a considerable reduction of the accelerations.

7.4 *Conclusions from the full-scale tests*

No really good correlation between the full-scale and model results could be obtained. This is attributed to the complicated non-linear relation between the vertical accelerations and the wave height. The wave height at sea was considerably lower than the scaled up model waves, which was the cause why the non-linear effects proved to be of such importance.

The equality of the "Polycat" and "Komer" regarding their behaviour in waves as appeared from the modeltests, was not confirmed by these measurements at sea, which again is attributed to the non-linearity of the accelerations, and to the different ways in which both ships are affected.

References

1. CLEMENT, E. P. and D. L. BLOUNT, Resistance Tests of a Systematic Series of Planing Hull Forms. Trans. SNAME Vol. 71, 1963.
2. VAN DEN BOSCH, J. J., Tests with two planing boat models in waves. Shipbuilding Laboratory Delft University of Technology, Report no. 266, 1970.
3. VAN DEN BOSCH, J. J., Over de vaareigenschappen van planerende motorboten. Symposium Yacht Architecture 1969, H.I.S.W.A. Amsterdam.
4. THORNYCROFT, P., Nelson 40, Yachting World, August 1972.
5. VAN DEN BOSCH, J. J. and P. H. NOORDENBOS, Design Considerations for a High Speed Seagoing Launch. Symposium Yacht Architecture 1973, H.I.S.W.A. Amsterdam.

PUBLICATIONS OF THE NETHERLANDS SHIP RESEARCH CENTRE TNO

LIST OF EARLIER PUBLICATIONS AVAILABLE ON REQUEST
PRICE PER COPY DFL. 10.— (POSTAGE NOT INCLUDED)

M = engineering department S = shipbuilding department C = corrosion and antifouling department

Reports

114 S The steering of a ship during the stopping manoeuvre. J. P. Hooft, 1969.
115 S Cylinder motions in beam waves. J. H. Vugts, 1968.
116 M Torsional-axial vibrations of a ship's propulsion system. Part I. Comparative investigation of calculated and measured torsional-axial vibrations in the shafting of a dry cargo motorship. C. A. M. van der Linden, H. H. 't Hart and E. R. Dolfin, 1968.
117 S A comparative study on four different passive roll damping tanks. Part II. J. H. Vugts, 1969.
118 M Stern gear arrangement and electric power generation in ships propelled by controllable pitch propellers. C. Kapsenberg, 1968.
119 M Marine diesel engine exhaust noise. Part IV. Transferdamping data of 40 modelvariants of a compound resonator silencer. J. Buiten, M. J. A. M. de Regt and W. P. Hanen, 1968.
120 C Durability tests with prefabrication primers in use for steel plates. A. M. van Londen and W. Mulder, 1970.
121 S Proposal for the testing of weld metal from the viewpoint of brittle fracture initiation. W. P. van den Blink and J. J. W. Nibbering, 1968.
122 M The corrosion behaviour of cunifer 10 alloys in seawaterpiping-systems on board ship. Part I. W. J. J. Goetzee and F. J. Kievits, 1968.
123 M Marine refrigeration engineering. Part III. Proposal for a specification of a marine refrigerating unit and test procedures. J. A. Knobbout and R. W. J. Kouffeld, 1968.
124 S The design of U-tanks for roll damping of ships. J. D. van den Bunt, 1969.
125 S A proposal on noise criteria for sea-going ships. J. Buiten, 1969.
126 S A proposal for standardized measurements and annoyance rating of simultaneous noise and vibration in ships. J. H. Janssen, 1969.
127 S The braking of large vessels II. H. E. Jaeger in collaboration with M. Jourdain, 1969.
128 M Guide for the calculation of heating capacity and heating coils for double bottom fuel oil tanks in dry cargo ships. D. J. van der Heeden, 1969.
129 M Residual fuel treatment on board ship. Part III. A. de Mooy, P. J. Brandenburg and G. G. van der Meulen, 1969.
130 M Marine diesel engine exhaust noise. Part V. Investigation of a double resonatorsilencer. J. Buiten, 1969.
131 S Model and full scale motions of a twin-hull vessel. M. F. van Sluijs, 1969.
132 M Torsional-axial vibrations of a ship's propulsion system. Part II. W. van Gent and S. Hylarides, 1969.
133 S A model study on the noise reduction effect of damping layers aboard ships. F. H. van Tol, 1970.
134 M The corrosion behaviour of cunifer-10 alloys in seawaterpiping-systems on board ship. Part II. P. J. Berg and R. G. de Lange. 1969.
135 S Boundary layer control on a ship's rudder. J. H. G. Verhagen, 1970.
136 S Observations on waves and ship's behaviour made on board of Dutch ships. M. F. van Sluijs and J. J. Stijnman, 1971.
137 M Torsional-axial vibrations of a ship's propulsion system. Part III. C. A. M. van der Linden, 1969.
138 S The manoeuvrability of ships at low speed. J. P. Hooft and M. W. C. Oosterveld, 1970.
139 S Prevention of noise and vibration annoyance aboard a sea-going passenger and carferry equipped with diesel engines. Part I. Line of thoughts and predictions. J. Buiten, J. H. Janssen, H. F. Steenhoek and L. A. S. Hageman, 1971.
140 S Prevention of noise and vibration annoyance aboard a sea-going passenger and carferry equipped with diesel engines. Part II. Measures applied and comparison of computed values with measurements. J. Buiten, 1971.
141 S Resistance and propulsion of a high-speed single-screw cargo liner design. J. J. Muntjewerf, 1970.
142 S Optimal meteorological ship routeing. C. de Wit, 1970.
143 S Hull vibrations of the cargo-liner "Koudekerk". H. H. 't Hart, 1970.
144 S Critical consideration of present hull vibration analysis. S. Hylarides, 1970.
145 S Computation of the hydrodynamic coefficients of oscillating cylinders. B. de Jong, 1973.
146 M Marine refrigeration engineering. Part IV. A Comparative stuyd on single and two stage compression. A. H. van der Tak, 1970.
147 M Fire detection in machinery spaces. P. J. Brandenburg, 1971.
148 S A reduced method for the calculation of the shear stiffness of a ship hull. W. van Horssen, 1971.
149 M Maritime transportation of containerized cargo. Part II. Experimental investigation concerning the carriage of green coffee from Colombia to Europe in sealed containers. J. A. Knobbout, 1971.
150 S The hydrodynamic forces and ship motions in oblique waves. J. H. Vugts, 1971.
151 M Maritime transportation of containerized cargo. Part I. Theoretical and experimental evaluation of the condensation risk when transporting containers loaded with tins in cardboard boxes. J. A. Knobbout, 1971.
152 S Acoustical investigations of asphaltic floating floors applie a steel deck. J. Buiten, 1971.
153 S Ship vibration analysis by finite element technique. Part II. Vibration analysis. S. Hylarides, 1971.
154 S Canceled.
155 M Marine diesel engine exhaust noise. Part VI. Model experiments on the influence of the shape of funnel and superstructure on the radiated exhaust sound. J. Buiten and M. J. A. M. de Regt, 1971.
156 S The behaviour of a five-column floating drilling unit in waves. J. P. Hooft, 1971.
157 S Computer programs for the design and analysis of general cargo ships. J. Holtrop, 1971.
158 S Prediction of ship manoeuvrability. G. van Leeuwen and J. M. J. Journée, 1972.
159 S DASH computer program for Dynamic Analysis of Ship Hulls. S. Hylarides, 1971.
160 M Marine refrigeration engineering. Part VII. Predicting the control properties of water valves in marine refrigerating installations A. H. van der Tak, 1971.
161 S Full-scale measurements of stresses in the bulkcarrier m.v. 'Ossendrecht'. 1st Progress Report: General introduction and information. Verification of the gaussian law for stress-response to waves. F. X. P. Soejadi, 1971.
162 S Motions and mooring forces of twin-hulled ship configurations. M. F. van Sluijs, 1971.
163 S Performance and propeller load fluctuations of a ship in waves. M. F. van Sluijs, 1972.
164 S The efficiency of rope sheaves. F. L. Noordegraaf and C. S s, 1972.
165 S Stress-analysis of a plane bulkhead subjected to a lateral load. P. Meijers, 1972.
166 M Contrarotating propeller propulsion, Part I, Stern gear, line shaft system and engine room arrangement for driving contra-rotating propellers. A. de Vos, 1972.
167 M Contrarotating propeller propulsion. Part II. Theory of the dynamic behaviour of a line shaft system for driving contra-rotating propellers. A. W. van Beek, 1972.
169 S Analysis of the resistance increase in waves of a fast cargo ship. J. Gerritsma and W. Beukelman, 1972.
170 S Simulation of the steering- and manoeuvring characteristics of a second generation container ship. G. M. A. Brummer, C. B. van de Voorde, W. R. van Wijk and C. C. Glansdorp, 1972.
172 M Reliability analysis of piston rings of slow speed two-stroke marine diesel engines from field data. P. J. Brandenburg, 1972.
173 S Wave load measurements on a model of a large container ship. Tan Seng Gie, 1972.
174 M Guide for the calculation of heating capacity and heating coils for deep tanks. D. J. van der Heeden and A. D. Koppenol, 1972.
175 S Some aspects of ship motions in irregular beam and following waves. B. de Jong, 1973.
176 S Bow flare induced springing. F. F. van Gunsteren, 1973.
177 M Maritime transportation of containerized cargo. Part III. Fire tests in closed containers. H. J. Souer, 1973.
178 S Fracture mechanics and fracture control for ships. J. J. W. Nibbering, 1973.

179 S Effect of forward draught variation on performance of full ships. M. F. van Sluijs and C. Flokstra, 1973.
180 S Roll damping by free surface tanks with partially raised bottom. J. J. van den Bosch and A. P. de Zwaan, 1974.
182 S Finite element analysis of a third generation containership. A. W. van Beek, 1973.
183 M Marine diesel engine exhaust noise. Part VII. Calculation of the acoustical performance of diesel engine exhaust systems. J. Buiten, E. Gerretsen and J. C. Vellekoop, 1974.
184 S Numerical and experimental vibration analysis of a deckhouse. P. Meijers, W. ten Cate, L. J. Wevers and J. H. Vink, 1973.
185 S Full scale measurements and predicted seakeeping performance of the containership "Atlantic Crown". W. Beukelman and M. Buitenhek, 1973.
186 S Waves induced motions and drift forces on a floating structure. R. Wahab, 1973.
187 M Economical and technical aspects of shipboard reliquefaction of cargo "Boil-off" for LNG carriers. J. A. Knobbout, 1974.
188 S The behaviour of a ship in head waves at restricted water depths. J. P. Hooft, 1974
189 M Marine diesel engine exhaust noise. Part VIII. A revised mathematical model for calculating the acoustical source strength of the combination diesel engine – exhaust turbine. P. J. Brandenburg, 1974.
190 M Condition monitoring, trend analysis and maintenance prediction for ship's machinery (literature survey). W. de Jong, 1974.
1 Further analysis of wave-induced vibratory ship hull bending moments. F. F. van Gunsteren, 1974.
192 S Hull resonance no explanation of excessive vibrations. S. Hylarides, 1974.
193 S Wave induced motions and loads on ships in oblique waves. R. Wahab and J. H. Vink, 1974.
194 M On the potentialities of polyphenylene oxide (PPO) as a wet-insulation material for cargo tanks of LNG-carriers. G. Opschoor, 1974.
195 S Numerical hull vibration analysis of a Far East container ship. P. Meijers, 1974.
196 S Comparative tests of four fast motor boat models – in calm water and in irregular head waves and an attempt to obtain full-scale confirmation. J. J. van den Bosch, 1974.
197 M Transverse vibrations of ship's propulsion systems. Part I. Theoretical analysis. S. Hylarides, 1974.
198 M Maritime transportation of containerized cargo. Part IV. Evaluation of the quality loss of tropical products due to moisture during seatransport. P. J. Verhoef, 1974.
199 S Acoustical effects of mechanical short-circuits between a floating floor and a steel deck. J. Buiten and J. W. Verheij, 1974.
200 M Corrosivity monitoring of crankcase lubricating oils for marine diesel engines. L. M. Rientsma and H. Zeilmaker, 1974.
201 S Progress and developments of ocean weather routeing. C. de Wit, 1974.
202 M Maritime transportation of containerized cargo. Part V. Fire tests in a closed aluminium container. H. J. Souer, 1974.
2 Transverse vibrations of ship's propulsion systems. Part II. Experimental analysis. L. J. Wevers, 1974.
206 S Synthesis of cooperative fatigue investigations with notched plates and welded ship structures of St 42 and St 52. J. J. W. Nibbering, H. G. Scholte and J. van Lint, 1974.

Communications (Mededelingen)

18 S An experimental simulator for the manoeuvring of surface ships. J. B. van den Brug and W. A. Wagenaar, 1969.
19 S The computer programmes system and the NALS language for numerical control for shipbuilding. H. le Grand, 1969.
20 S A case study on networkplanning in shipbuilding (Dutch). J. S. Folkers, H. J. de Ruiter, A. W. Ruys, 1970.
21 S The effect of a contracted time-scale on the learning ability for manoeuvring of large ships (Dutch). C. L. Truijens, W. A. Wagenaar, W. R. van Wijk, 1970.
22 M An improved stern gear arrangement. C. Kapsenberg, 1970.
23 M Marine refrigeration engineering. Part V (Dutch). A. H. van der Tak, 1970.
24 M Marine refrigeration engineering. Part VI (Dutch). P. J. G. Goris and A. H. van der Tak, 1970.
25 S A second case study on the application of networks for productionplanning in shipbuilding (Dutch). H. J. de Ruiter, H. Aartsen, W. G. Stapper and W. F. V. Vrisou van Eck, 1971.
26 S On optimum propellers with a duct of finite length. Part II. C. A. Slijper and J. A. Sparenberg, 1971.
27 S Finite element and experimental stress analysis of models of shipdecks, provided with large openings (Dutch). A. W. van Beek and J. Stapel, 1972.
28 S Auxiliary equipment as a compensation for the effect of course instability on the performance of helmsmen. W. A. Wagenaar, P. J. Paymans, G. M. A. Brummer, W. R. van Wijk and C. C. Glansdorp, 1972.
29 S The equilibrium drift and rudder angles of a hopper dredger with a single suction pipe. C. B. van de Voorde, 1972.
30 S A third case study on the application of networks for productionplanning in shipbuilding (Dutch). H. J. de Ruiter and C. F. Heijnen, 1973.
31 S Some experiments on one-side welding with various backing materials. Part I. Manual metal arc welding with coated electrodes and semi-automatic gas shielded arc welding (Dutch). J. M. Vink, 1973.
32 S The application of computers aboard ships. Review of the state of the art and possible future developments (Dutch). G. J. Hogewind and R. Wahab, 1973.
33 S FRODO, a computerprogram for resource allocation in networkplanning (Dutch). H. E. I. Bodewes, 1973.
34 S Bridge design on dutch merchant vessels; an ergonomic study. Part I: A summary of ergonomic points of view (Dutch). A. Lazet, H. Schuffel, J. Moraal, H. J. Leebeek and H. van Dam, 1973.
35 S Bridge design on dutch merchant vessels; an ergonomic study. Part II: First results of a questionnaire completed by captains, navigating officers and pilots. J. Moraal, H. Schuffel and A. Lazet, 1973.
36 S Bridge design on dutch merchant vessels; an ergonomic study. Part III: Observations and preliminary recommendations. A. Lazet, H. Schuffel, J. Moraal, H. J. Leebeek and H. van Dam, 1973.
37 S Application of finite element method for the detailed analysis of hatch corner stresses (Dutch), J. H. Vink, 1973.
38 S A computerprogram for displacement and stress analysis with membrane elements on constructions consisting of plates and trusses. User's manual (Dutch). G. Hommel and J. H. Vink, 1974.
39 S Some experiments on one-side welding with various backing materials. Part II. Mechanised gas-shielded arc welding in the flat and horizontal position (Dutch). J. M. Vink, 1974.

International SHIPBUILDING Progress

MARINE TECHNOLOGY MONTHLY

CONTENTS

VOLUME 32 - JANUARY 1985 - No. 365

A STUDY ON MOTIONS OF HIGH SPEED PLANING BOATS WITH CONTROLLABLE FLAPS IN REGULAR WAVES

by

Wang Long-Wen*

Summary

A controllable transom flap in planing boats not only may reduce the resistance at cruising speeds in still water, but also could be designed to make a boat run at or near optimum attitude in various environments, which results in a reduction in both resistance and vertical motion in waves.

In the present study, considering the controllable flap as an exciting force and moment, the motion equations of high speed planing boats with controllable flaps in regular waves have been based on a modified strip theory. An attempt is made to evaluate the feasibility and effectiveness of the controllable flap as a means of controlling the running trim to optimize the overall performance.

The theoretical calculation pointed out that when the force and moment excited by flaps were in phase with wave disturbances considerable vertical motions would be set up, but once a suitable phase could be established between flap exciting forces and wave disturbances, the controlled flaps would reduce the motion amplitudes effectively.

Model tests carried out in the Ship Hydromechanics Laboratory of the Delft University of Technology have also shown that controllable flaps may be used not only for minimizing resistances in various conditions, but also for reducing heave and pitch motions, especially at or near the resonant frequency. The tests also proved that in automatic systems of controlling flaps, a pitch velocity feedback to the flap is effective.

1. Introduction

In recent years, planing boats have been used in more exposed areas, for instance as pilot boats, coast guard vessels, workboats and small naval vessels. Such a small boat operating in a rough-water environment frequently experiences violent motions. Even on calm water, porpoising motion may occur and may be severe as the speed is increased.

There are several ways to improve the behaviour of a planing boat in a seaway. The experiment of two models with different deadrise angles carried out by Bosch [1] showed that increase in deadrise angle would result in a considerable gain in seakeeping ability at cost of some power.

In his study [2], [3], Fridsma concluded that like deadrise, trim is an equally important parameter to planing boat behaviour in a seaway. A two degrees increase in running trim from 4° to 6° accounts for a 17% increase in motion at $V/\sqrt{L} = 2$ and a 33% increase at $V/\sqrt{L} = 4$.

Accelerations are built up in direct proportion to the trim over the range of 3° to 7°. From the porpoising limits for prismatic planing hulls given by Day and Haag [4], it is seen that increase in running trim may lead to porpoising. Savitsky [15] pointed out that in any case if a boat is porpoising at a given speed and load, the rule is to lower the trim angle to avoid porpoising. Therefore, adjusting the running trim not only may reduce motions of planing boats in waves, but also may improve its porpoising instability on calm water.

The simplest way to lower the running trim is to use a flap. This flap may be constructed as a small transverse wedge or plate across the bottom added to the transom, if the longitudinal center of gravity can not be moved because the boat dimensions are fixed.

In a study of flap effectiveness [6] Brown conducted a series of experiments with flaps and described their results as some simple expressions for the increase in lift, drag, and moment caused by flaps.

Later, A. Millward [7] analyzed the effect of flaps on resistance of high speed planing hulls according to his experiments with flaps, drawing the same conclusion as Savitsky and Brown did earlier [8] that flaps may be used to reduce the resistance over a range of speeds and loading conditions.

A major reason for reduction in resistance is that the use of flaps makes it possible that boats could run at or near optimum trim angle. which results in a minimum drag-lift ratio. It is obvious that the running trim will change when boat speed changes.

The works mentioned previously are based on the experiments with fixed flaps on calm water which only fit to a specified condition. In order to make it suitable to various environments, especially in waves for overall performance it is necessary to use a flap with a controllable angle.

A theoretical analysis has been made in an attempt to evaluate the function of a controllable flap as a kind

*) Report no. 615 of the Ship Hydromechanics Laboratory of the Delft University of Technology, Delft, The Netherlands.

of heave and pitch amplitude-reducing device. In the present study, the controllable flap is considered to deliver an exciting force or moment. The motion equations of planing boats with controlled flaps in calm water and in regular waves were based on a modified strip theory. A great impetus to the research was provided by the publication of Martin's paper [9] and Zarnick's work [10] thanks to which the motion equations used in this paper could be solved conveniently.

At the same time, further experiments with controllable flaps were carried out in the Ship Hydromechanics Laboratory of the Delft University of Technology to investigate its feasibility and effectiveness; these tests include:

1. effect of flaps on resistance, rise and running trim of models;
2. added forces and moments caused by flaps;
3. motions of models excited by oscillating flaps;
4. choice of feedback control systems;
5. responses of the models with and without controllable flaps in waves.

2. Influence of flaps on the performance of planing boats

2.1. Exciting forces and moments due to flaps

A controllable flap is a portion of the planing surface hinged to the transom of a boat, so that it can be deflected up and down, changing the normal force and moment to obtain and to control the desired attitude of a boat. In the present situation, the flap is a V-shaped planing surface having a constant angle of deadrise equal to that of the boat. Therefore, its hydrodynamic characters may be calculated by means of existing planing theories. Among them the theory proposed by Shuford [11] has a reasonable foundation and has been shown to agree with data covering the widest range of conditions. A lift coefficient for prismatic surfaces in pure planing is:

$$C_L = \frac{0.5\pi S\tau}{1+S}\cos^2\tau(1-\sin\beta) + \frac{4}{3}\sin^2\tau\cos^3\tau\cos\beta$$

where:

S = aspect ratio $2b/lm$
$2b$ = beam of planing surface
lm = mean wetted length of planing surface
β = angle of dead rise
τ = trim angle

It is convenient for calculation to use experimental results. Brown [6] made a systematic investigation for planing surfaces with fixed flaps, and expressed the increase in lift and moment due to flaps in following forms.

Lift increment:

$$\Delta F = 0.046[\tfrac{1}{2}\rho(2b)^2U^2]\lambda_F\sigma\delta$$

$$\Delta C_{L_{\text{FLAP}}} = 0.046\lambda_F\sigma\delta$$

Moment increment about the trailing edge of flaps:

$$\Delta M = 0.6(2b)\Delta F$$

$$\Delta C_{M_{\text{FLAP}}} = 0.6\,\Delta C_{L_{\text{FLAP}}}$$

where:

$\Delta C_{L_{\text{FLAP}}}$ = flap lift increment coefficient
$\Delta C_{M_{\text{FLAP}}}$ = flap moment increment about the trailing edge of flaps
σ = flap span-beam ratio
δ = flap deflection
b = half-beam of planing surface
λ_F = flap chord-beam ratio $L_F/2b$
L_F = flap chord

In the present study to determine forces and moments excited by flaps, Model 85 with fixed flaps (see appendix 1. and figure 1) having different chords (L_F = 0.083 to 0.167 · $2b$) and deflections (δ = 0 to 9°) was tested at $V/\sqrt{L}$ = 3.6 to 4.5 corresponding to the planing condition, at which the flow separates from the chine.

The experimental results were plotted in figures 2 and 3, and summarized in the following expressions:

$$\Delta C_{L_{\text{FLAP}}} = 0.042\lambda_F\sigma\delta$$

$$\Delta C_{M_{\text{FLAP}}} = 0.55\Delta C_{L_{\text{FLAP}}}$$

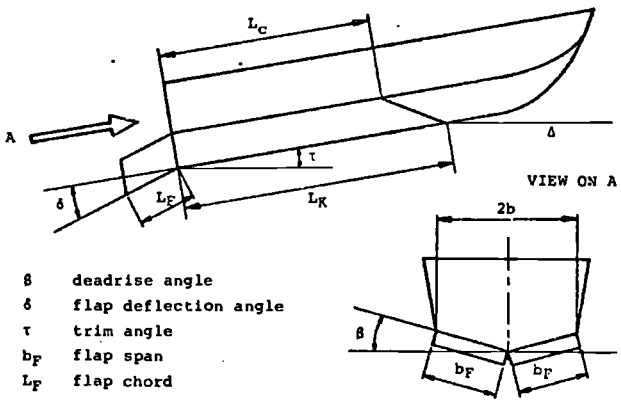

Figure 1. Model 85 with transom flaps.

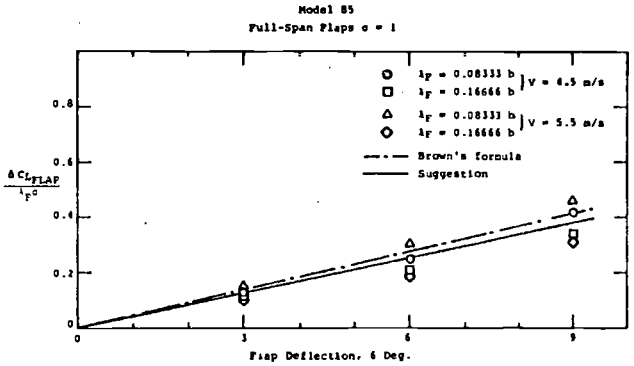

Figure 2. Added lift due to flap.

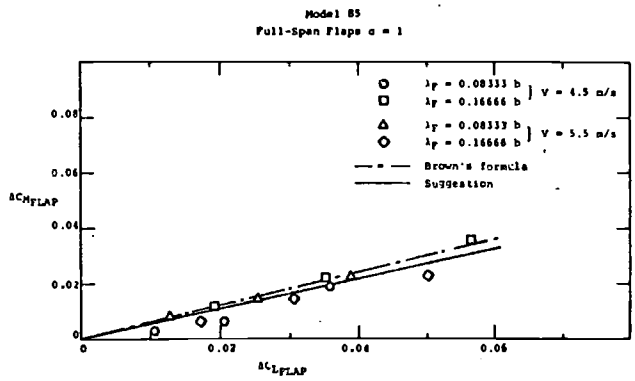

Figure 3. Added moment due to flap.

These results are in agreement with those obtained by Brown. It is evident that a flap may increase the dynamic lift which is proportional to its chord, span and deflection angle.

2.2. *Effect of flaps on resistance*

A flap may excite an added force and moment and hence change the boat's trim and center of gravity height. This in turn would alter the resistance. To investigate the effect of flaps on resistance, model 85 without and with fixed flaps (L_F = 0.125 · 2b, δ = 0° and 3°) was used to test.

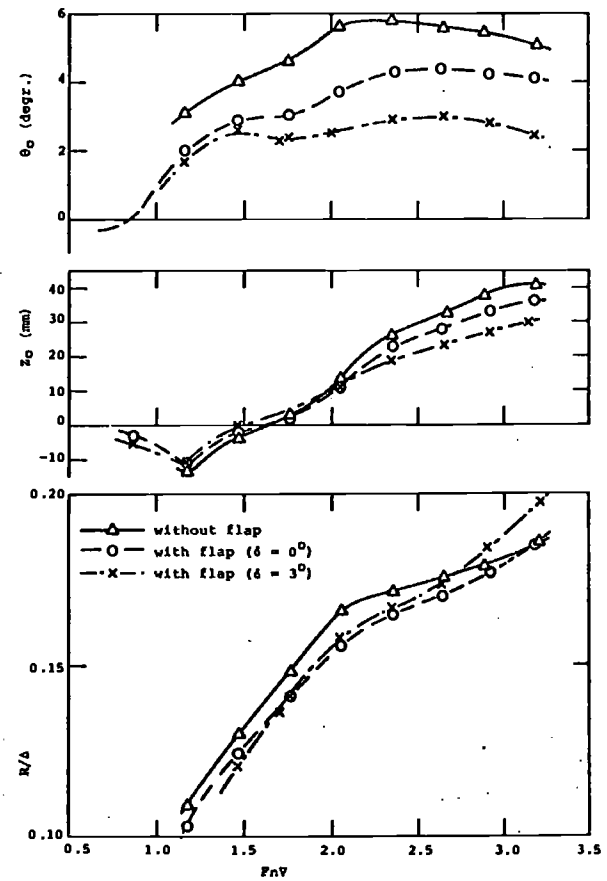

Figure 4. Model 85, center of gravity rise, angle of trim and resistance in calm water.

The experiments were carried out at the same model weight (27.34 kg) and the same center of gravity position (aft of A_p 8%) in still water. The variation of the resistance, trim angle and center of gravity height with Froude number were shown in figure 4 for the unflapped model and that with different deflection flaps. It is seen that:

1. Compared to the unflapped model, the model with flaps has lower running trim over the whole range of speeds.
2. The use of flaps may reduce the resistance over a range of speeds, but outside the range, it could increase the resistance.
3. The model resistance and the running trims vary with flap deflections.

In addition to the flap deflection, the flap length may also affect the resistance and running trim, as shown in figure 5, presented by Millward [7].

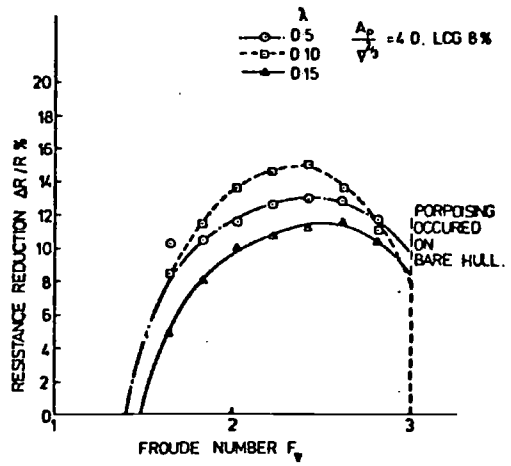

Figure 5. Effect of wedge length on resistance (model 4666)[7].

Though no attempt is going to be made for determination of the optimum parameters of flaps, depending on displacement, LCG position and speed, there is a flap to produce an optimum trim angle which would result in the minimum resistance. In other words a fixed flap can only be valuable at a certain speed and loading condition of a planing boat in still water. Once the operating condition changes, the planing boat with fixed flaps would lose its superiority to that without flaps.

Another experiment with the same model and flap was carried out at cruise speed (V = 4.5 m/s) for measurement of the resistance in waves. The results were presented in figure 6. It is found that in waves model 85 with fixed flaps has more resistance than that without flaps. But in still water the former has less resistance than the latter. With a controlled flap in waves the resistance is decreased.

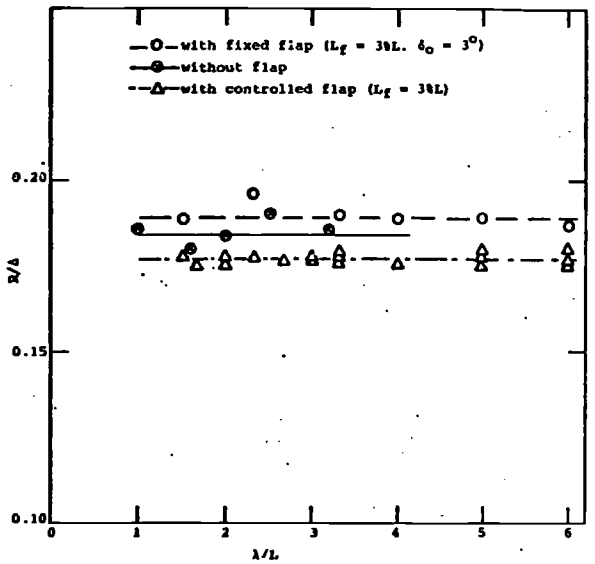

Figure 6. Model 85, resistance in waves at V = 4.5 m/s. Wave height H = 0.0555 b.

2.3 Vertical motions excited by oscillating flaps

As mentioned above, a fixed flap in planing boats can produce an added dynamic lift and moment proportional to its deflection angle. Therefore, if the flap deflection angle is changed in a sinusoidal manner:

$$\delta = \delta_a \sin \omega_o t$$

where:

δ_a = amplitude of the flap angle
ω_o = frequency of flap oscillation
t = time

a periodical force and moment would be generated, due to which the boat would be excited in still water into a simple harmonic motion in heave and pitch with the following forms:

$$z = z_a \sin(\omega_o t + \alpha_z)$$
$$\theta = \theta_a \sin(\omega_o t + \alpha_\theta)$$

where:

z_a, θ_a = amplitudes of the heave and pitch motion, respectively;
α_z, α_θ = phase angles by which the vertical motion lags the flap deflections.

To investigate the still water responses of a boat to a harmonic excitation by flaps, model 85 with an oscillating flap (σ = 1, λ_F = 12.5%) was used to test at given speed (V = 4.5 m/s) and different amplitudes and frequencies of the flap. The experimental results presented in figure 7 show that:

1. Oscillating flaps can excite a considerable motion in heave and pitch, especially when the flap oscillates at or near the natural frequency ω_o of 9.2 rad./sec.;
2. responses to small deflections of the flap are linear with amplitudes.

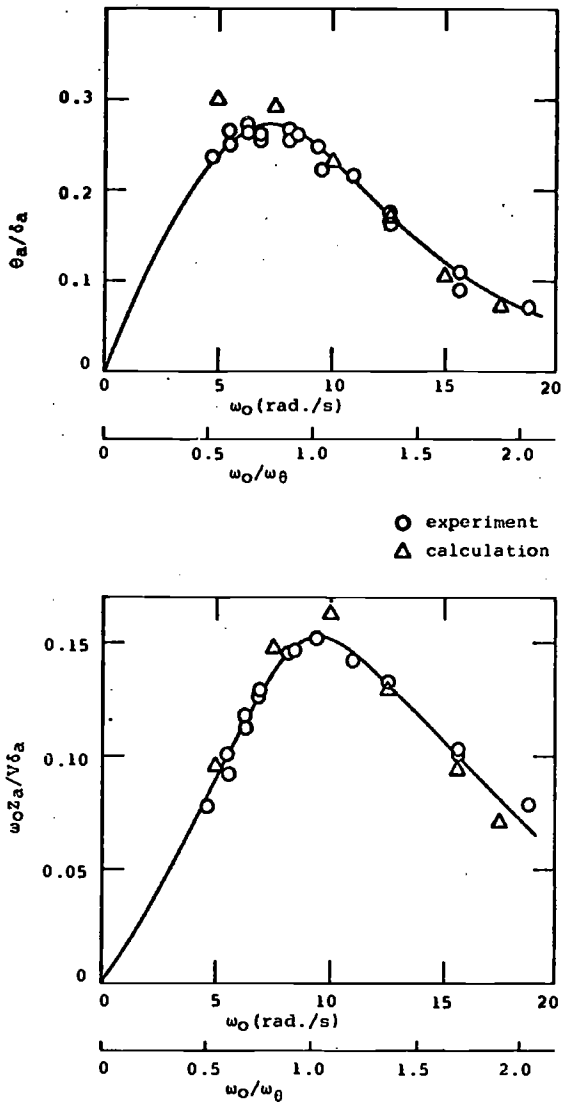

Figure 7. Still water vertical responses of model 85 to a harmonic excitation by flaps at V = 4.5 m/s. ω_o — the natural frequency.

Therefore, the linear equations of motion for planing boats may be used to solve this problem. A coordinate system is thought to be connected to the boat's center of gravity with the axes ox and oz respectively, along and at right angles to the direction of motion, as shown in figure 8. Considering the effect of flaps on the boat as a small perturbation, the motion of a planing boat with an oscillating flap in still water may be described by the following equations:

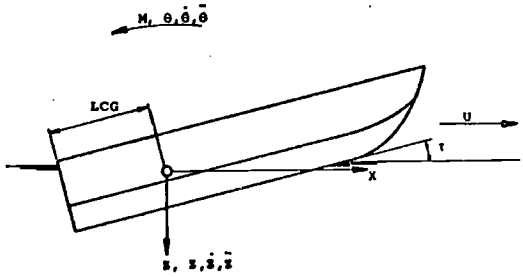

Figure 8. Coordinate system.

$$(z_{\ddot{z}} - M)\ddot{z} + z_{\dot{z}}\dot{z} + z_z z + z_{\ddot{\theta}}\ddot{\theta} + z_{\dot{\theta}}\dot{\theta} + z_\theta \theta = |\Delta F_o| e^{-i\omega_o t} \quad (1)$$

$$M_{\ddot{z}}\ddot{z} + M_{\dot{z}}\dot{z} + M_z z + (M_{\ddot{\theta}} - I_y)\ddot{\theta} + M_{\dot{\theta}}\dot{\theta} + M_\theta \theta = |\Delta M_o| e^{-i\omega_o t} \quad (2)$$

where:

$\ddot{z}, \dot{z}, z$ = heave acceleration, velocity and displacement, respectively.

$\ddot{\theta}, \dot{\theta}, \theta$ = pitch angular acceleration, velocity and displacement, respectively.

M = mass of boat.

I_y = pitch moment of inertia of boat.

$z_{\ddot{z}}, z_{\dot{z}}, z_z, z_{\ddot{\theta}}, z_{\dot{\theta}}, z_\theta$ = stability derivatives of boat (see reference 9).
$M_{\ddot{z}}, M_{\dot{z}}, M_z, M_{\ddot{\theta}}, M_{\dot{\theta}}, M_\theta$

$|\Delta F_o|, |\Delta M_o|$ = flap-excited force and moment amplitudes, respectively.

The steady-state solutions to the equations are:

for heave $z = z_a e^{-i\omega_o t}$ (3)

for pitch $\theta = \theta_a e^{-i\omega_o t}$ (4)

where the heave complex amplitude:

$$z_a = \frac{|\Delta F_o| B_2 - |\Delta M_o| A_2}{A_1 B_2 - A_2 B_1}$$

the pitch complex amplitude:

$$\theta_a = \frac{|\Delta M_o| A_1 - |\Delta F_o| B_1}{A_1 B_2 - A_2 B_1}$$

$$A_1 = (z_{\ddot{z}} - M)\omega_o^2 - z_z + i z_{\dot{z}}\omega_o$$

$$A_2 = z_{\ddot{\theta}}\omega_o^2 - z_\theta + i z_{\dot{\theta}}\omega_o$$

$$B_1 = M_{\ddot{z}}\omega_o^2 - M_z + i M_{\dot{z}}\omega_o$$

$$B_2 = (M_{\ddot{\theta}} - I_y)\omega_o^2 - M_\theta + i M_{\dot{\theta}}\omega_o$$

By taking the Laplace transform of both sides of equations (1) and (2) we obtain:

$$\begin{bmatrix} (z_{\ddot{z}} - M)s^2 + z_z s + z_z & z_{\ddot{\theta}} s^2 + z_{\dot{\theta}} s + z_\theta \\ M_{\ddot{z}} s^2 + M_{\dot{z}} s + M_z & (M_{\ddot{\theta}} - I_y)s^2 + M_{\dot{\theta}} s + M_\theta \end{bmatrix} \begin{bmatrix} z(s) \\ \theta(s) \end{bmatrix} = \begin{bmatrix} \Delta F(s) \\ \Delta M_o(s) \end{bmatrix}$$

where s indicates the Laplace operator. It is obvious that

$$\begin{bmatrix} (z_{\ddot{z}} - M)s^2 + z_z s + z_z & z_{\ddot{\theta}} s^2 + z_{\dot{\theta}} s + z_\theta \\ M_{\ddot{z}} s^2 + M_{\dot{z}} s + M_z & (M_{\ddot{\theta}} - I_y)s^2 + M_{\dot{\theta}} s + M_\theta \end{bmatrix} = 0$$

is the resulting characteristics equation. From the roots of the equation the dynamic characteristics of the boat may be obtained. In fact, a complex pair of roots $s = s_R \pm i s_I$ represents an oscillating mode and the magnitude of the imaginary part of the root s_I is the natural frequency of the boat motion.

Model 85 with an oscillating flap ($\sigma = 1, \lambda_F = 0.125$) is also used to calculate as an example for the application of the theory. The calculation was carried out under the same conditions as the experiments and its results also presented in figure 7, are in agreement with those of the experiments.

3. The mathematical model for the vertical motions

3.1. Dynamic responses of the system

The block diagram for the dynamic responses of a planing boat with flaps is indicated as figures 9 and 10.

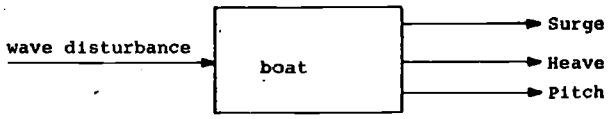

Figure 9. Block diagram for the open loop responses.

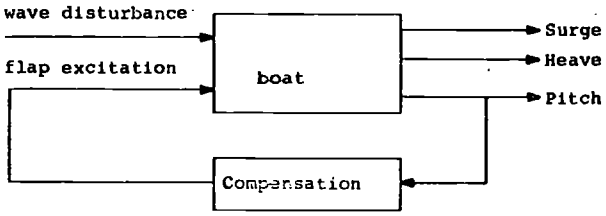

Figure 10. Block diagram for the closed loop responses.

For the open loop responses, the flap always lies in a certain position, because no feedback takes place in the system. Therefore, the boat motion only depends on the wave disturbances. While in the closed-loop responses, pitch motion, namely pitch velocity, is fed back to the flap, which would in turn be controlled to deflect up or down, therefore, an added excitation is generated and the responses of the boat to the external disturbances would be compensated. By means of an automatic control system, it is possible to establish a suitable phase relationship between wave disturbances and flap excitation for minimizing undesirable motion in pitch and heave.

3.2. Motion equations

There are two coordinate systems being used here, as shown in figure 11. The fixed one (x_o, z_o) consists

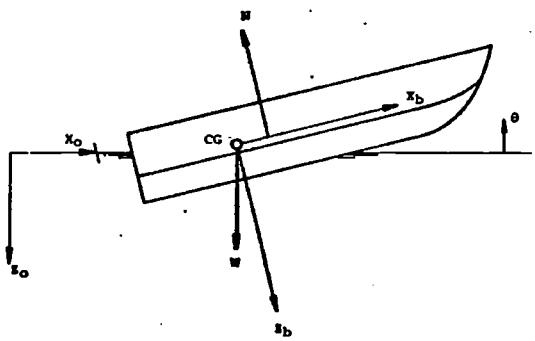

Figure 11. Coordinate system.

of x_o-axis in the direction of the forward speed, $x_o - y_o$ plane on the undisturbed free surface, and z_o-axis pointing downward; the body coordinate system (x_b, z_b) with axes x_b and z_b, respectively, along and at right angles to the baseline, is connected to the boat's center of gravity.

It is assumed that:

1. the effect of flaps is regarded as an external disturbance and because the flap deflection angle usually is small the normal force of the flap is taken as a vertical force exerted on the boat;
2. the boat is moving at a constant speed $\dot{x}_{CG}$;
3. the thrust and drag force are small in comparison to the hydrodynamic forces thought to pass through the center of gravity.

The vertical motions of a planing boat with controlled transom flaps in waves may be described by the following mathematical models:

$$\begin{aligned} M\ddot{x}_{CG} &= 0 \\ M\ddot{z}_{CG} &= -N\cos\theta + w + \Delta F(\delta) \\ I_y\ddot{\theta} &= Nx_c + \Delta M(\delta) \end{aligned} \tag{5}$$

where:

M = mass of boat
I_y = pitch moment of inertia of boat
N = total hydrodynamic force
x_c = distance from center of gravity (CG) to center of pressure for force N
$\Delta F(\delta)$ = exciting force by flap
$\Delta M(\delta)$ = exciting moment by flap

It is seen that the vertical motion of the planing boat depends on the total hydrodynamic force N and the flap disturbance.

3.3. Total hydrodynamic force

The normal force per unit length dN is assumed to consist of the following three parts:

1. the rate of change of momentum of the fluid

$$\frac{D}{Dt}(m_a V) = \dot{m}_a V + \dot{V} m_a - U\frac{\partial}{\partial x_b}(m_a V)$$

2. the drag due to the vertical velocity

$$\rho C_{D,C} b V^2$$

3. the hydrostatic force

$$a\rho g A_R$$

in which:

m_a = added mass
V = relative fluid velocity normal to baseline
U = relative fluid velocity parallel to baseline
ρ = density of water
$C_{D,C}$ = crossflow drag coefficient
b = half-beam of section
a = a correction factor of floating force
g = acceleration of gravity
A_R = cross-section area under water line

Using a modified low-aspect-ratio- or strip theory and connecting added mass m_a, relative fluid velocity V, U with the wave geometrical properties and orbital velocity at the surface and integrating the force and added mass per unit length, E. Zarnick [10] derived the following formulas:

– the hydrodynamic force in z-direction:

$$\begin{aligned} -N\cos\theta = \{ & -M_a\cos\theta\ddot{z}_{CG} + Q_a\ddot{\theta} + M_a\dot{\theta}(\dot{z}_{CG}\sin\theta - \dot{x}_{CG}\cos\theta) \\ & + \int_1 m_a\frac{dw_z}{dt}\cos\theta\, dx_b - \int_1 m_a w_z\dot{\theta}\sin\theta\, dx_b \\ & - \int_1 m_a V\frac{\partial w_z}{\partial x_b}\sin\theta\, dx_b + \int_1 m_a U\frac{\partial w_z}{\partial x_b}\cos\theta\, dx_b \\ & - UVm_a|_{\text{stern}} - \int_1 V\dot{m}_a dx_b - \rho\int_1 C_{D,C} b V^2 dx_b\}\cos\theta \\ & - \int_1 a\rho g A_R\, dx_b \end{aligned} \tag{6}$$

– the hydrodynamic moment in pitch:

$$\begin{aligned} Nx_c = & -I_a\ddot{\theta} + Q_a\cos\theta\ddot{z}_{CG} - Q_a\dot{\theta}(\dot{z}_{CG}\sin\theta - \dot{x}_{CG}\cos\theta) \\ & - \int_1 m_a\cos\theta\frac{dw_z}{dt}x_b dx_b + \int_1 m_a\dot{\theta}\sin\theta\, w_z x_b dx_b \\ & + \int_1 V\dot{m}_a x_b dx_b + \int_1 \rho C_{D,C} b V^2 x_b dx_b \\ & + m_a UVx_b|_{\text{stern}} + \int_1 m_a UV dx_b \\ & + \int_1 m_a V\frac{\partial w_z}{\partial x_b}\sin\theta\, x_b dx_b \\ & - \int_1 m_a U\frac{\partial w_z}{\partial x_b}\cos\theta\, x_b dx_b \\ & + \int_1 a\rho g A_R\cos\theta\, x_b dx_b \end{aligned} \tag{7}$$

where:

$$M_a = \int_1 m_a dx_b$$
$$Q_a = \int_1 m_a x_b dx_b$$
$$I_a = \int_1 m_a x_b^2 dx_b$$

w_z = vertical component of wave orbital velocity. The derivation of the terms m_a, w_z, v and u are shown in appendix 2.

3.4. Flap-exciting force

The flap-exciting force ΔF and moment ΔM, as mentioned above, are a function of flap areas and deflection angles at a certain speed. For the controllable flap whose chord and span are usually fixed, the excit-

ing force and moment due to it only depend on its deflection angle δ, that is

$$\Delta F = C\delta$$
$$\Delta M = l_a C\delta$$

in which:

$C = 0.042\ [\frac{1}{2}\rho(2b)^2 U^2]\lambda_F \sigma$, l_a is the arm of ΔF with respect to the center of gravity CG.

The flap deflection angle δ is controlled by both heave and pitch motions. In general, it may be expressed as

$$\delta = \delta_{\text{heave}}(z, \dot{z}, \ddot{z}) + \delta_{\text{pitch}}(\theta, \dot{\theta}, \ddot{\theta})$$

But usually the heave motion is not so sensitive to the flap exciting force, which is small in comparison to the hydrodynamic force. It seems to be reasonable to use the flap as a stabilizing fin for pitch motion. Therefore we have:

$$\delta = K_1\theta + K_2\dot{\theta} + K_3\ddot{\theta}$$

where K_i are system gain and sensitivities.

It is evident that pitch angle, velocity and acceleration feedback may be used to increase the pitch restoring moment, damping and inertia of the boat, respectively. Some experiments carried out later show that a pitch velocity feedback seems to be the best among all the feedback types. This was to be expected while the velocity may be considered to be the out of phase component with respect to the motion.

For simplification of the control system, it is introduced that:

$$\delta = K_2\dot{\theta}$$

With the control function of the pitch stabilizing system, the flap-exciting force and moment acting on the boat may be expressed in the following forms:

$$\Delta F = K_{CF}\tfrac{1}{2}\rho(2b)^3 U\dot{\theta}$$
$$\Delta M = K_{CM}\tfrac{1}{2}\rho(2b)^4 U\dot{\theta} \qquad (8)$$

where the coefficient K_{CM} is derived in appendix 3. K_{CF} depends on the flap geometrical properties and the behaviour of the control system. $K_{CF} = K_{CM} \cdot 2b/l_a$.

3.5. Solution of the motion equations

With the determination of the total hydrodynamic force and the flap-exciting force, equation of motions (5) could be solved. After substitution of equations (6) (7) and (8) into equation (5), the right hand side of equation (5) contains the terms of displacement (x_{CG}, z_{CG} and θ), velocity ($\dot{x}_{CG}$, $\dot{z}_{CG}$ and $\dot{\theta}$) and acceleration ($\ddot{x}_{CG}$, $\ddot{z}_{CG}$ and $\ddot{\theta}$). By moving the terms $\ddot{x}_{CG}$, $\ddot{z}_{CG}$ and $\ddot{\theta}$ to the left hand side of equation (5), an inertial matrix A and an acceleration vector ($\ddot{x}_{CG}$, $\ddot{z}_{CG}$, $\ddot{\theta}$) can be obtained. Therefore the right side of equation (5) only has the terms of velocity and displacement, which form a force vector $\vec{F}$:

$$A\begin{pmatrix}\ddot{x}_{CG}\\ \ddot{z}_{CG}\\ \ddot{\theta}\end{pmatrix} = \vec{F} \qquad (9)$$

By means of a state vector $\vec{x} = (\dot{x}_{CG}, \dot{z}_{CG}, \dot{\theta}, x_{CG}, z_{CG}, \theta)$, equation (9) can be changed into the following form:

$$A\vec{\dot{x}} = \vec{F}$$

so that:

$$\vec{\dot{x}} = A^{-1}\vec{F} \qquad (10)$$

where A^{-1} is inverse of the inertial matrix A.

The right hand side of equation (10) can be determined by using the hulliform data and initial conditions. In fact, $\dot{x}_{CG}$ is the forward speed of the boat, $\dot{z}_{CG}$, $\dot{\theta}$ and x_{CG} are taken as zero at initial time T_o. z_{CG} and θ are either from the calculation of steady-state equilibrium or from model test in still water. Selecting an adequate step size, $\vec{\dot{x}}$ may be integrated by using a numerical method, Therefore, the $\vec{x}$, the accelerations, the force and moment acting on the boat at time T can be obtained.

3.6 Computed results

1. Computer program.

A computer program [10] for the calculation of motions of a craft with a constant deadrise angle, planing in regular waves, was extended to the more conventional-type planing boat with controlled transom flaps. To make the program suitable for the variable situations, following improvements have been taken:

- real hull form data, which includes the section positions and the distribution of chine breadths and deadrise along the length and height of keel over the baseline, is put into the program in stead of a constant beam and deadrise of the prismatic hulls;
- the calculation of the added mass per section is corrected by a coefficient K_a, while the considered section deviates from circular form, so:

$$m_a = K_a \frac{\pi}{2}\rho b^2$$

K_a may be determined by a combination of theoretical and experimental relationships, for model 85, $K_a = 0.77$;

- the cross flow drag coefficient $C_{D,C}$ is determined according to the section shape from reference [9], here $C_{D,C} = 1.3$.

2. Computed model

The computation was carried out for model 85, a high speed planing boat, which was also used for con-

trol test in the towing tank. Its main particulars are given in appendix 1. The controlled flap is outboard, as shown in figure 1. The details of the flap are as follows:

span - beam ratio σ 1
chord - beam ratio λ_F 12.5%
distance from the flap trailing edge to CG 0.660 m
arm of the flap exciting force about CG, l_a 0.462 m
initial deflection angle δ_o 4 degr.

The flap exciting force acting on the model will be:

$$\Delta F = 0.042\,[\tfrac{1}{2}\rho(2b)^2U^2]\,\lambda_F\delta_o + K_{CM}\frac{2b}{l_a}[\tfrac{1}{2}\rho(2b)^3]\,U\dot{\theta}$$

The flap exciting moment about the center of gravity CG is:

$$\Delta M = l_a \cdot 0.042[\tfrac{1}{2}\rho(2b)^2U^2]\,\lambda_F\delta_o + K_{CM}\tfrac{1}{2}\rho(2b)^4\,U\dot{\theta}$$

3. Computed conditions and items

The computed model was towed through CG at constant speeds in regular head waves under the following conditions.

- the forward speed V = 4.5 m/sec. and 5.5 m/sec. corresponding to $Fn\nabla$ = 2.6 and 4.5;
- the wave lengths λ = 1.0, 1.5, 3.0, 4.0 and 6.0 L, and the wave heights $H = 0.222b$, which means that the wavelengths were long in comparison to the boat length and that the wave slopes were small.

The calculations were made with the control gain coefficients K_{CM} = 0, 0.5, 1.0, 1.5 and 2.0 for the following items:

- pitch amplitude θ_a
- heave amplitude z_a
- vertical acceleration at bow and center of gravity
- flap deflection response δ_a.

4. Computed results

The numerical results are given in figures 12 to 25 for two speeds in a non-dimensional form

$\theta_a/(2\pi r_o/\lambda)$	for pitch response
z_a/r_o	for heave response
$\delta_a/(2\pi r_o/\lambda)$	for flap deflection response
accelerations/g	for vertical accelerations

as a function of the modified non-dimensional wave number parameter

$$C_\lambda = \frac{L}{\lambda}[C_\Delta/(L/2b)^2]^{1/3}$$

where:

$C_\Delta = w/[\rho g(2b)^3]$
r_o = wave amplitude.

Open loop responses

The open loop responses of the model to waves correspond to the control gain coefficient K_{CM} = 0, which means a system without control. In that case, the flap is always on the initial position (δ_o = 4°). Therefore the open loop responses may be used as a base for the comparison. From the curves K_{CM} = 0, it is seen that:

- the vertical motions reach their maximum amplitude very close to the predicted resonant encounter frequency (ω_e = 9.2 rad/s at V = 4.5 m/s, ω_e = 10.4 rad/s at V = 5.5 m/s), corresponding to the value of C_λ = 0.097;
- the motion amplitudes are small at shorter waves, but relatively large at long waves, while the acceleration at the bow increase with the encounter frequency;
- the model responses are more sensitive at high speed than at lower speed.

Calculations were also carried out for model 85 without flap in an attempt to investigate the influence of flaps on the vertical motion. The results, presented in figures 12 to 15, show that adding a flap to model 85 without control would cause a little larger pitch motion in almost the whole range of wavelengts, while the effect of the flap on heave motion does not appear to be significant. In that case, it seems to be not ne-

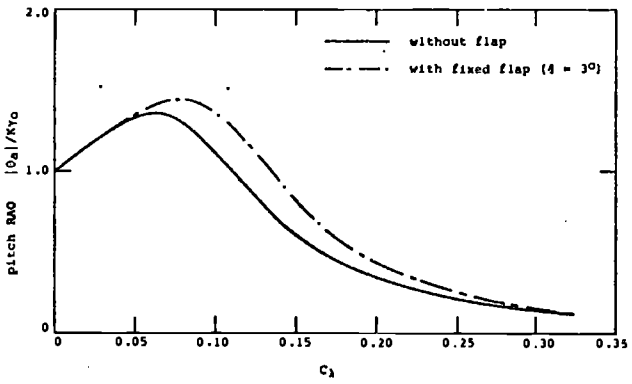

Figure 12. Pitch response for model 85 at V = 4.5 m/s.

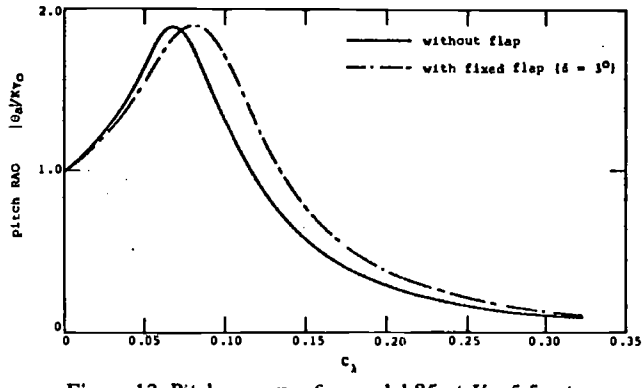

Figure 13. Pitch response for model 85 at V = 5.5 m/s.

cessary for the control system to introduce a heave motion feedback.

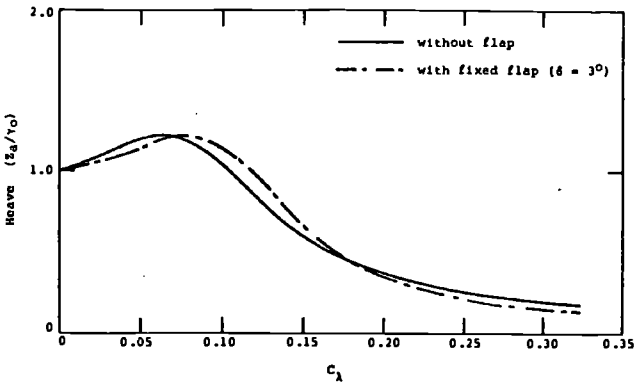

Figure 14. Heave response for model 85 at $V = 4.5$ m/s.

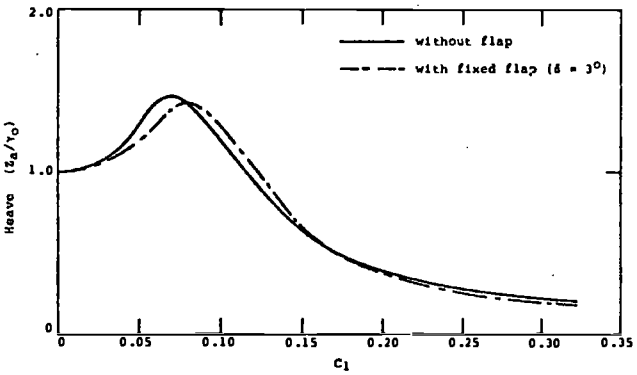

Figure 15. Heave response for model 85 at $V = 5.5$ m/s.

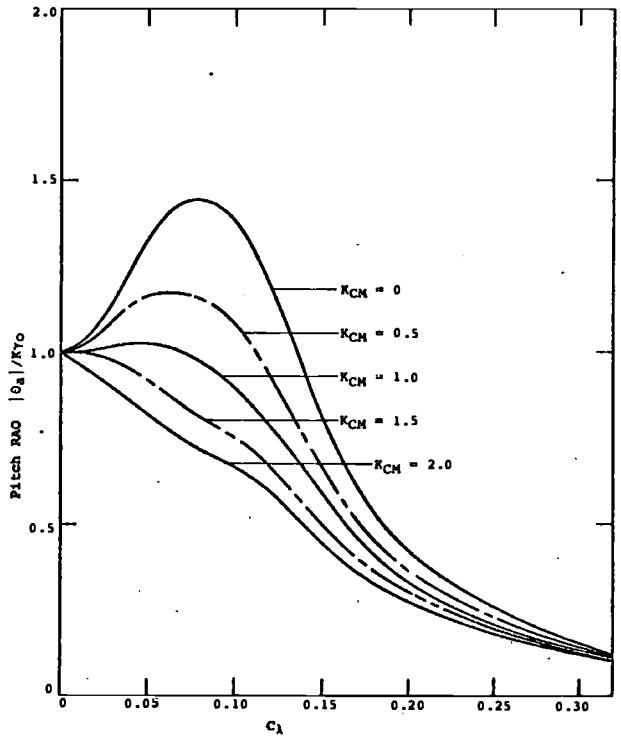

Figure 16. Pitch response for model 85 at $V = 4.5$ m/s.

Closed loop responses

Based on the open loop responses, comparisons have been made to the closed loop responses when pitch velocities were fed back to the flap with different control gain coefficients K_{CM}. As can be seen from figures 16 to 25, the pitch responses are improved in the whole range of the calculated wavelengths, and the greater the control gain coefficient, the more the pitch amplitude reduces. When K_{CM} reaches 2, the resonance has almost disappeared. The largest reduction in pitch amplitude happens when the encounter frequency is at or near the natural pitch frequency. It is also seen that with increase in the control gain coefficient the bow acceleration reduces more, and the largest reduction happens at shorter waves.

Though the heave motion does not feed back to the flap, fortunately the effect of the control flap on it is also good. Similar to the pitch responses, the heave amplitude and the acceleration of *CG* reduces with increase in control gain coefficient at most wave frequencies of interest. Only at higher frequencies, they were amplified a little. This depends on the phase angle difference between the heave motion and the flap swing.

The model speed is also an important factor which influences the flap control. Making a comparison between figure 16 and 17, it can be seen that the higher the speed, the more the motion reduces. It means that the use of flaps at high speed is more effective, which could be expected.

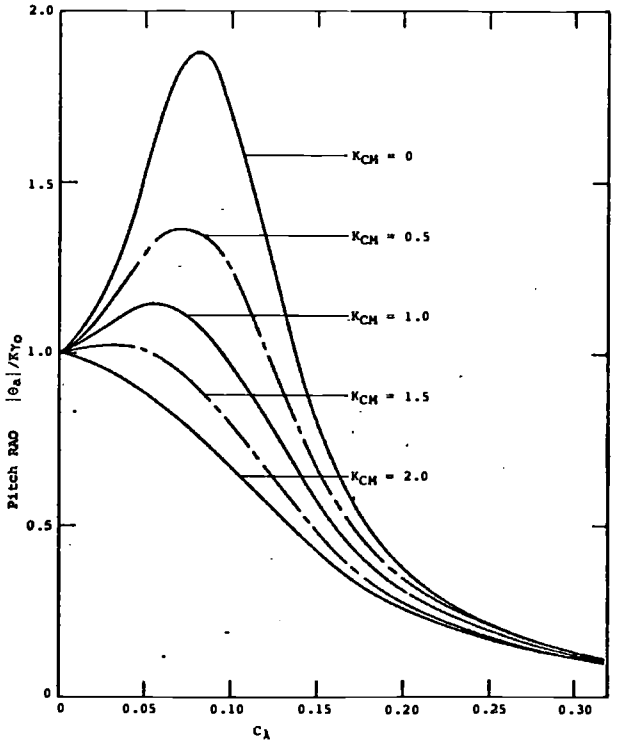

Figure 17. Pitch response for model 85 at $V = 5.5$ m/s.

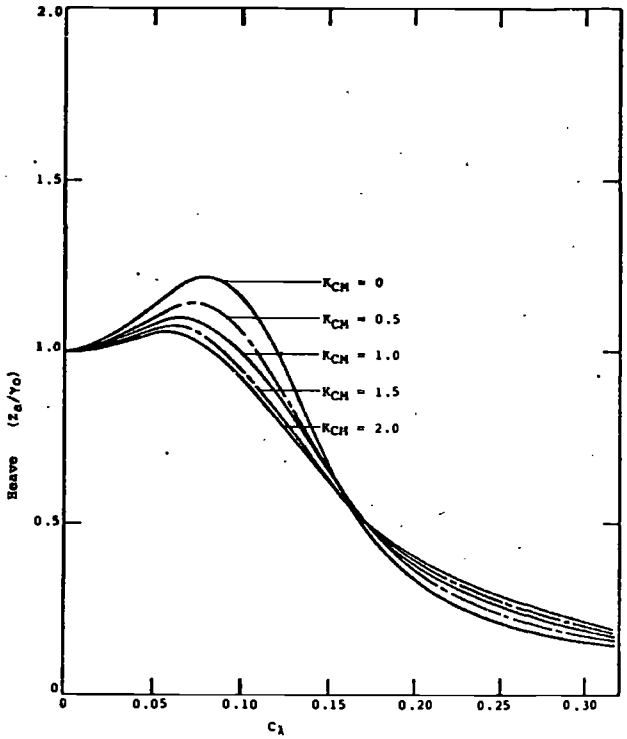

Figure 18. Heave response for model 85 at V = 4.5 m/s.

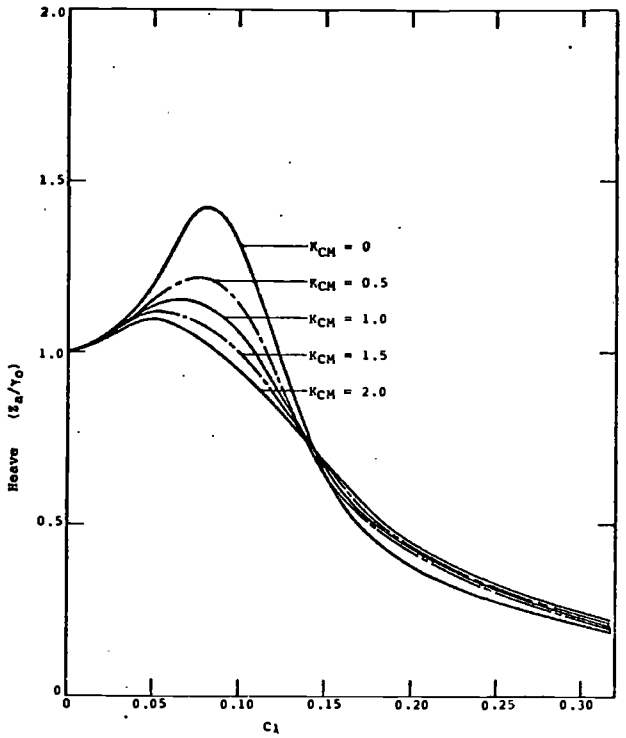

Figure 19. Heave response for model 85 at V = 5.5 m/s.

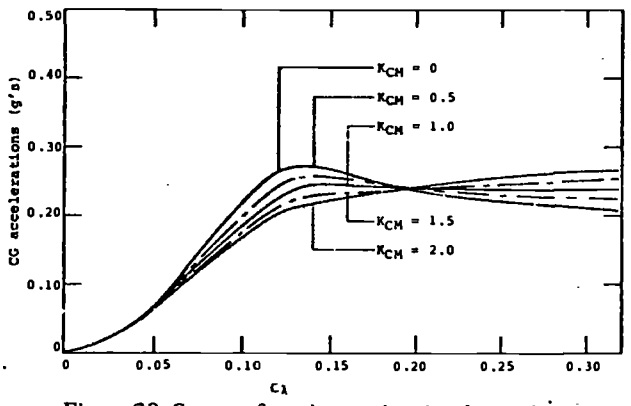

Figure 20. Center of gravity acceleration for model 85 at V = 4.5 m/s.

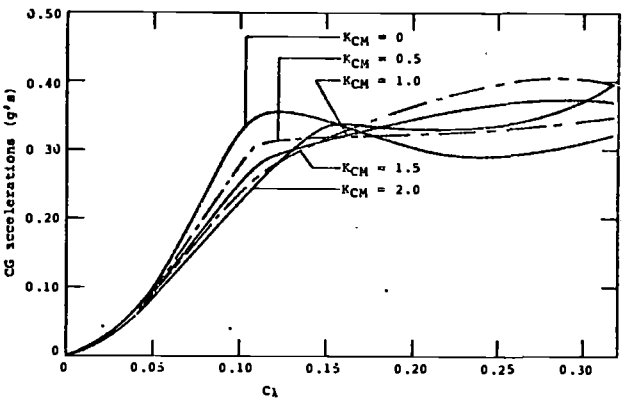

Figure 21. Center of gravity acceleration for model 85 at V = 5.5 m/s.

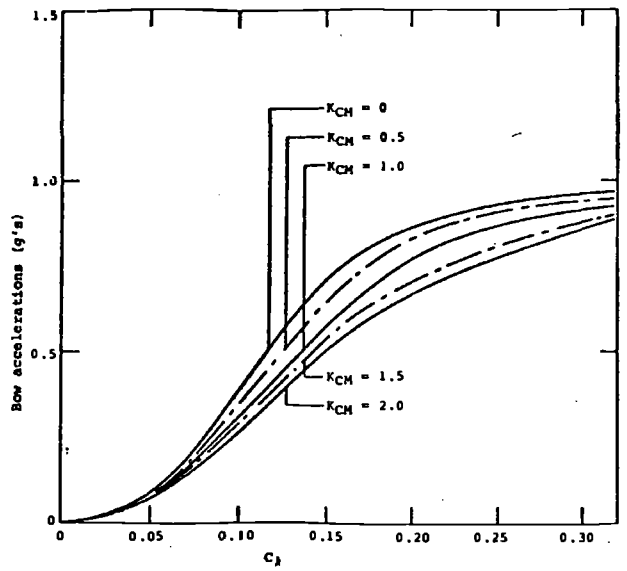

Figure 22. Bow acceleration for model 85 at V = 4.5 m/s.

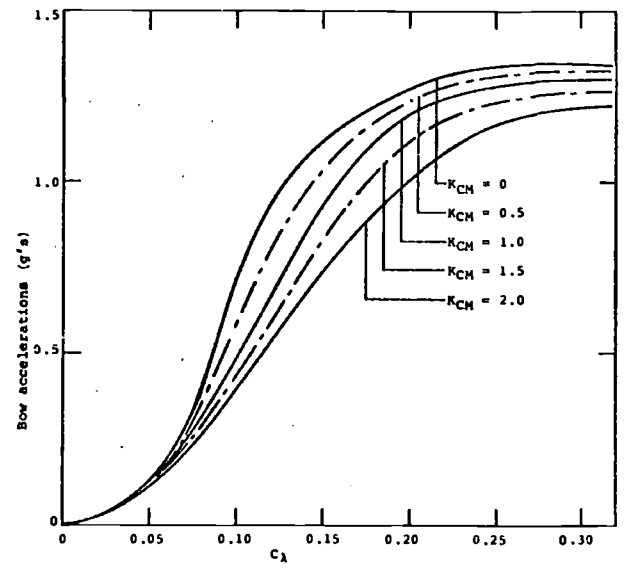

Figure 23. Bow acceleration for model 85 at V = 5.5 m/s.

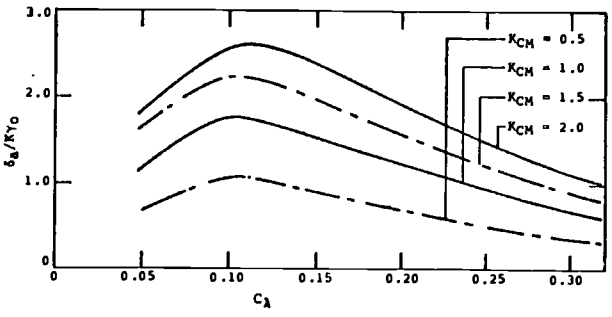

Figure 24. Flap deflection responses for model 85 at $V = 4.5$ m/s.

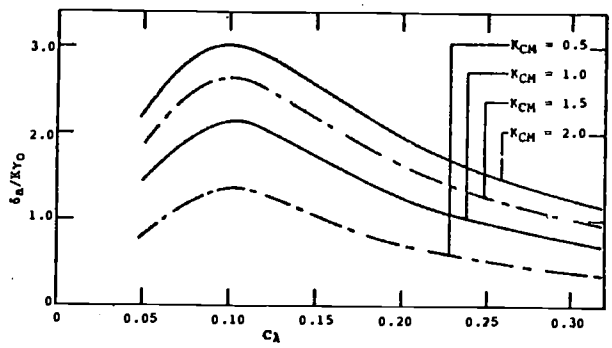

Figure 25. Flap deflection responses for model 85 at $V = 5.5$ m/s.

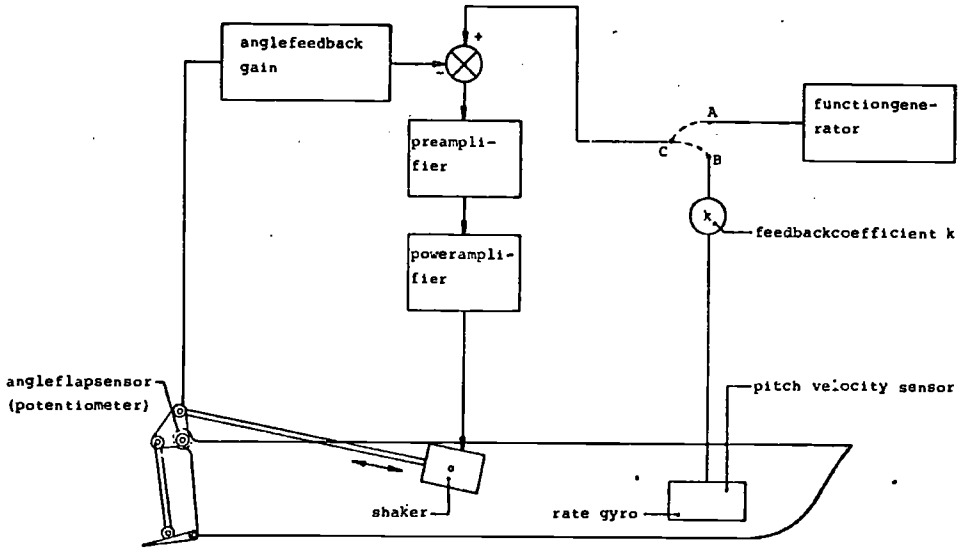

Figure 26.

The motion-reduction effect of flaps may be explained as that the pitch velocity feedback control increases the apparent damping coefficient of the model. The relatively large horizontal level of the flap exciting force makes the pitch motion controlled more effective than the heave.

Flap deflection responses were expressed in a non-dimensional form (flap angle to wave slope) in figures 24 and 25. From:

$$\delta = K_{\dot{\theta}}\,\dot{\theta}$$

it follows that the flap angle increases with the pitch velocity feedback and its sensitivity. The maximum flap deflection responses also occur at or near the natural pitch frequency of the model. In general, with the increase in the flap deflection responses, the motion responses improve more and more.

4. Model test

Model tests have also been carried out with a rate gyro as the feedback element. The flap servo was used as a pitch stabilizer. Figure 26 shows the flow diagram for the control system, and the instrumentation for the pitch reduction experiment is given in appendix 4.

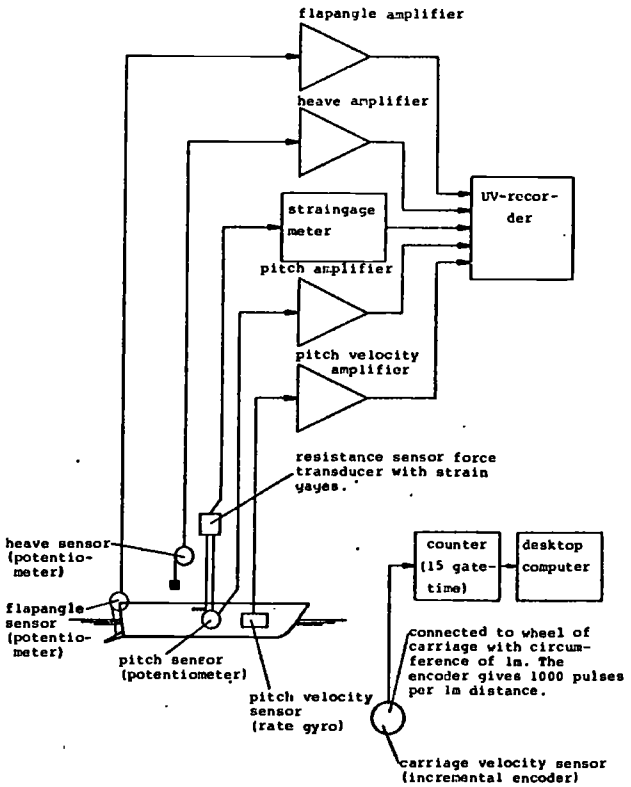

Figure 27.

The experiments were made in regular waves under the following conditions:

test model	Model 85
controlled flap	$\sigma = 1, \lambda_F = 12.5\%$
model speed	$V = 4.5$ m/s
wave height	$H = 0.111b$
wave lengths	$\lambda = 1.0, 1.5, 2.0, 3.0, 4.0$ and $6.0\,L$

The following items were measured for control gain coefficients $K_{CM} = 0$, 1.0, 2.0 and 4.0:

pitch amplitude	θ_a
pitch velocity	$\dot{\theta}$
heave amplitude	Z_a
flap deflection	δ_a
model resistance on waves	

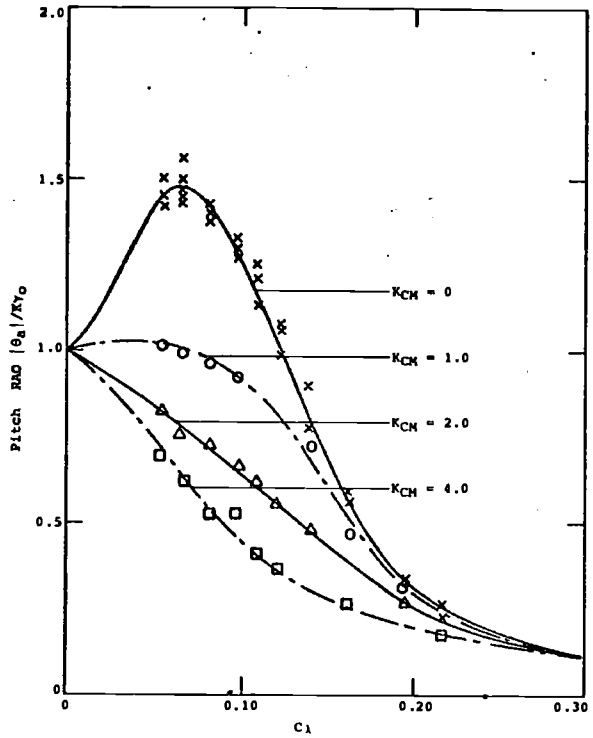

Figure 28. Pitch response fo. model 85 with controlled flaps at $V = 4.5$ m/s.

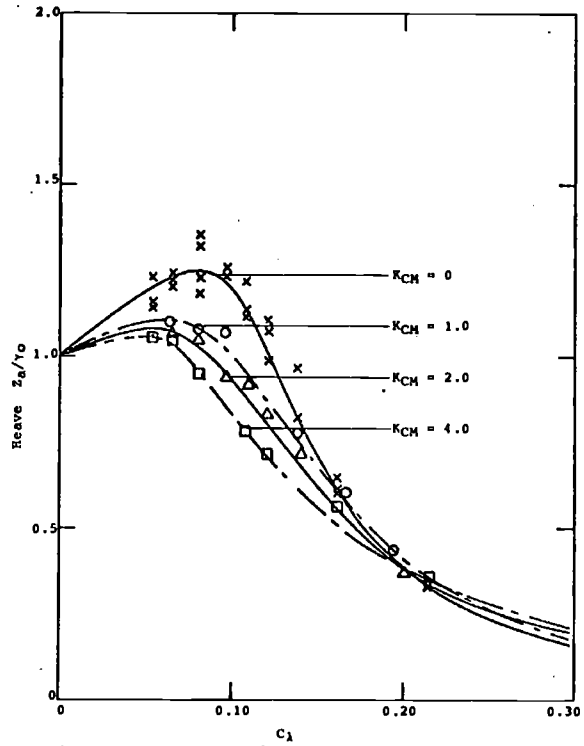

Figure 29. Heave response for model 85 with controlled flaps at $V = 4.5$ m/s.

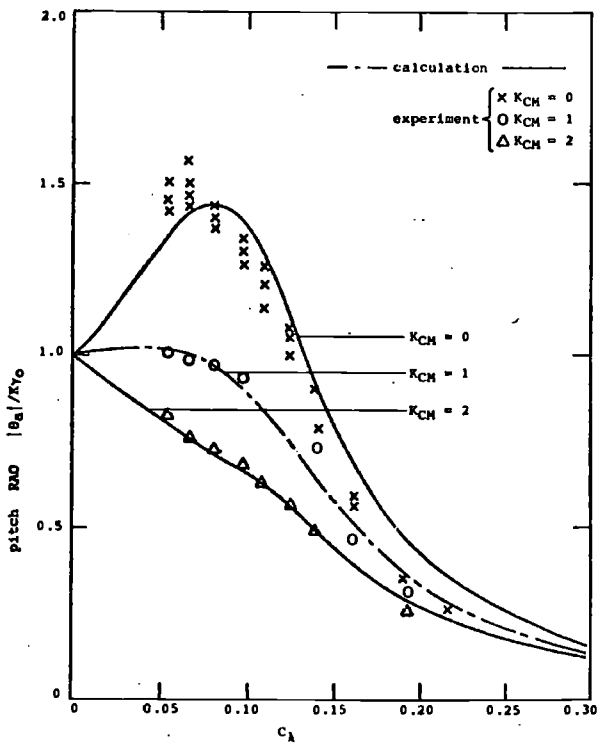

Figure 30. Comparison of the calculated and experimental pitch responses for model 85 at $V = 4.5$ m/s.

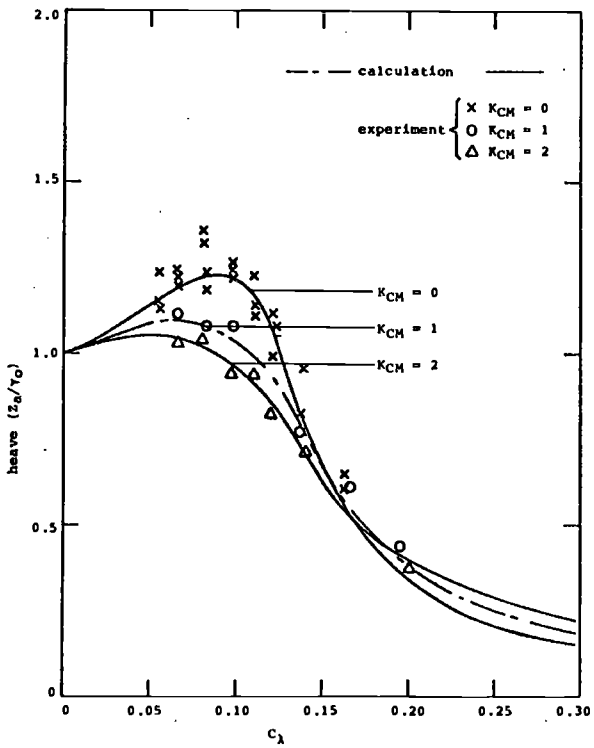

Figure 31. Comparison of the calculated and experimental heave responses for model 85 at $V = 4.5$ m/s.

The open loop responses were determined first. These are presented in figures 28 and 29 by $K_{CM} = 0$ where it can be seen that the pitch and heave responses show a peak at the natural frequency of the model. The curves have the same tendency as the calculations and their values are very close to the computed results, as shown in figures 30 and 31.

The open loop resistance of the model in waves was measured and plotted in figure 6.

In the closed loop response tests, various types of pitch feedback were tried. Using just a pitch angle feedback produced a satisfactory reduction in the peak pitch amplitude, but it worsened heave responses at low frequencies, while pitch velocity feedback successfully resulted in reduction, not only in the peak pitch amplitude, but also in the heave motion. The results shown in figures 28 and 29 indicated a maximum reduction in pitch amplitude of 70% at $K_{CM} = 4$, which is in concordance with the calculations in figures 16 through 19. The experiments also show that it is difficult to control the motion of the model due to external disturbances at high frequencies, but the use of a controllable flap in the situation could reduce the acceleration.

After feedback control, the model runs smoothly in waves and its resistance is lower than without control as can be seen in figure 6.

5. Conclusions

The theoretical study and model tests have shown the contribution of controllable transom flaps to improve the overall performance of a planing boat. Controllable flaps could be designed to make a planing boat run at or near optimum attitude in various environments, which results in a minimum resistance and avoids porpoising. Especially the vertical motion amplitude velocity and acceleration of the boat on waves may be reduced. The agreement between the calculated and experimental results demonstrated that the theoretical method proposed in this report seems to be reasonable for prediction of the response characteristics of planing boats with controllable flaps in waves, at least it may be used to estimate the effect of flaps on performance of a boat.

The model tests also proved that introducing a pitch velocity feedback to the flap in automatic control systems is very effective.

6. Acknowledgement

The author would like to express his deep gratitude to Prof.ir. J. Gerritsma and W. Beukelman, under whose supervision and guidance the present work was started and finished.

It is also pleased for the author to appreciate the assistance and co-operation from his colleagues at the Ship Hydromechanics Laboratory of the Delft University of Technology.

7. References

1. Bosch, J.J. van den, 'Tests with two planing boat models in waves', Report no. 266 of the Ship Hydromechanics Laboratory of the Delft University of Technology, February 1970.
2. Fridsma, G., 'A systematic study of rough-water performance of planing boats', Davidson Laboratory, Stevens Institute of Technology, Report R-1275, November 1969.
3. Fridsma, G., 'A systematic study of rough-water performance of planing boats', Davidson Laboratory, Stevens Institute of Technology, Report R-1495, March 1971.
4. Day, J.P. and Haag, R.J., 'Planing boat porpoising', Thesis submitted to Webb Institute of Naval Architecture, Glen Cove, N.Y., May 1952.
5. Savitsky, D., 'Hydrodynamic design of planing hulls', Marine Technology, vol. 1, No. 1, October 1964.
6. Brown, P.W., 'An experimental and theoretical study of planing surfaces with trim flaps' Stevens Institute of Technology, Davidson Laboratory, Report SIT-DL-71-1463, 1971.
7. Millward, A., 'Effect of wedges on the performance characteristics of two planing hulls', Journal of Ship Research, Vol. 20, No. 4, December 1976.
8. Savitsky, D. and Brown, P.W., 'Procedures for hydrodynamic evaluation of planing hulls in smooth and rough water', Marine Technology, Vol. 13, No. 4, October 1976.
9. Martin, M., 'Theoretical prediction of motions of high-speed planing boats in waves', Journal of Ship Research, vol. 23, No. 3, September 1978.
10. Zarnick, E.E., 'A non-linear mathematical model of motions of a planing boat in regular waves', DTNSRDC-78/032, March 1978.
11. Shuford, C.L.D., 'A theoretical and experimental study of planing surfaces including effects of cross section and plan form', NACA Report 1355, 1957.
12. Clement, E.P. and Blount, D., 'Resistance tests of systematic series of planing hull forms', Trans. SNAME, Vol. 71, 1963.

8. Appendix 1
Model data

The model used to test, denoted as model 85, was derived from the 'Clement' form of the Series-62 [12] by doubling the angle of deadrise, keeping all other dimensions as equal as possible.

The form of model 85 is shown in figure 32.

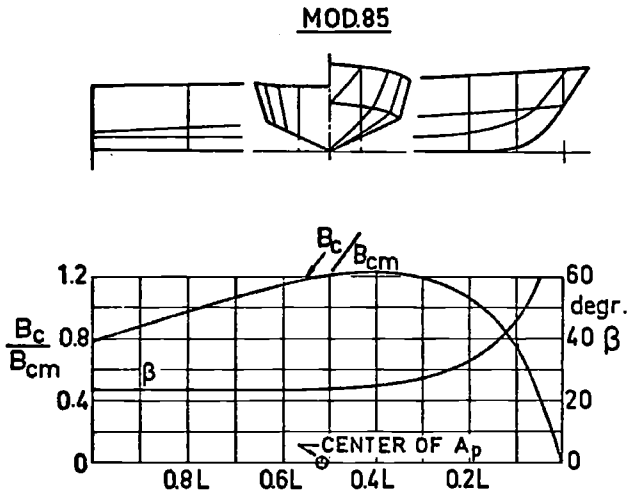

Figure 32. Form characteristics of model 85.

The main particulars are given in the following table.

A_p	projected area of chines and transom	0.555 m^2
L	length of projected area A_p	1.500 m
B_c	breadth over chines at any cross section	
B_{cmax}	maximum breadth over chines	0.450 m
B_{CM}	mean breadth of area A_p	0.370 m
∇	volume of displacement at rest	0.0273 m^3
x_p	center of the projected area A_p (forward of transom)	0.729 m
G	center of gravity (forward of transom)	0.615 m
β	deadrise angle	24°
I_y	pitch moment of inertia	0.42 kgm sec^2

The transom flaps used in this investigation are as follows:

	Chord λ_F	Span σ	Angle δ (degrees)
Fixed flaps	8.3%	full	0, 3, 6, 9
	16.7%	full	0, 3, 6, 9
Controlled flap	12.5%	full	

The model with transom flaps is shown in figure 6.

Appendix 2
Hydrodynamic force and moment

The hydrodynamic force in the z-direction as derived in [10] is:

$$F_z = -\int_1 \left[m_a \dot{V} + \dot{m}_a V - U\left(\frac{\partial m_a}{\partial x_b} V + \frac{\partial V}{\partial x_b} m_a\right) + C_{D,C}\rho b V^2 \right] \cos\theta \, dx_b - \int_1 a\rho \, g A_R \, dx_b$$

the moment for F_z about CG:

$$M_\theta = \int_1 \left[m_a \dot{V} + \dot{m}_a V - U\left(\frac{\partial m_a}{\partial x_b} V + \frac{\partial V}{\partial x_b} m_a\right) + C_{ox}\rho b V^2 + a\rho g A_R \cos\theta \right] x_b \, dx_b$$

where:

$$U = \dot{x}_{CG}\cos\theta - (\dot{z} - w_z)\sin\theta$$

$$V = \dot{x}_{CG}\sin\theta + (\dot{z} - w_z)\cos\theta - \dot{\theta} x_b$$

Because:

$$\dot{V} = \ddot{x}_{CG}\sin\theta - \ddot{\theta} x_b + \ddot{z}_{CG}\cos\theta - \dot{w}_z\cos\theta + \dot{\theta}(\dot{x}_{CG}\cos\theta - \dot{z}_{CG}\sin\theta) + w_z\dot{\theta}\sin\theta$$

$$\frac{\partial V}{\partial x_b} = -\dot{\theta} - \frac{\partial w_z}{\partial x_b}\cos\theta$$

$$\frac{\partial U}{\partial x_b} = \frac{\partial w_z}{\partial x_b}\sin\theta$$

$$\frac{dw_z}{dt} = \dot{w}_z - U\frac{\partial w_z}{\partial x_b}$$

$$\int_1 UV\frac{\partial m_a}{\partial x_b} dx_b = -UVm_a|_{\text{stern}} - \int_1 m_a \frac{\partial UV}{\partial x_b} dx_b$$

and-

$$\int_1 m_a dx_b = M_a$$

$$\int_1 m_a x_b dx_b = Q_a$$

$$\int_1 m_a x_b^2 dx_b = I_a$$

therefore the force and moment become:

$$F_z = -\{M_a\cos\theta\,\ddot{z}_{CG} - M_a\sin\theta\,\ddot{x}_{CG} + Q_a\ddot{\theta} + M_a\dot{\theta}(\dot{z}_{CG}\sin\theta - \dot{x}_{CG}\cos\theta) + \int_1 m_a\frac{dw_z}{dt}\cos\theta\,dx_b - \int_1 m_a w_z\dot{\theta}\sin\theta\,dx_b - \int_1 m_a V\frac{\partial w_z}{\partial x_b}\sin\theta\,dx_b + \int_1 m_a U\frac{\partial w_z}{\partial x_b}\cos\theta\,dx_b - UVm_a|_{\text{stern}} - \int_1 \dot{m}_a dx_b - \rho\int_1 C_{D,C} b V^2 dx_b\}\cos\theta - \int_1 a\rho g A_R dx_b$$

$$M_\theta = -I_a\ddot{\theta} + Q_a\cos\theta\,\ddot{z}_{CG} - Q_a\dot{\theta}(\dot{z}_{CG}\sin\theta - \dot{x}_{CG}\cos\theta)$$
$$-\int_1 m_a\cos\theta\frac{dw_z}{dt}x_b\,dx_b + \int_1 m_a\dot{\theta}\sin\theta\, w_z x_b\,dx_b$$
$$+\int_1 V\dot{m}_a x_b\,dx_b + \int_1 \rho C_{D,C}\,bV^2 x_b\,dx_b$$
$$+ m_a UVx_b|_{\text{stern}} + \int_1 m_a UV\,dx_b$$
$$+\int_1 m_a V\frac{\partial w_z}{\partial x_b}\sin\theta\, x_b\,dx_b$$
$$-\int_1 m_a U\frac{\partial w_z}{\partial x_b}\cos\theta\, x_b\,dx_b$$
$$+\int_1 a\rho g A_R\cos\theta\, x_b\,dx_b$$

where the added mass of a section is expressed as:

$$m_a = K_a\pi/2\rho b^2$$
$$\dot{m}_a = K_a\pi\rho b\dot{b}$$

b depends on the effective depth of the keel d_e, that is

$$b = d_e\cot\beta = \frac{\pi}{2}d\cot\beta$$

When wavelengths are long in comparison to the draft and wave slopes ν are small, the immersion of a section d is approximately:

$$d \cong \frac{z-\nu}{\cos\theta - \nu\sin\theta}$$
$$\dot{d} \cong \frac{\dot{z}-\dot{\nu}}{\cos\theta - \nu\sin\theta}$$

in which

$$\nu = -r_o K\sin[K(x_{CG} + x_b\cos\theta + z_b\sin\theta) + \omega t]$$

Therefore

$$\dot{m}_a = K_a\pi\rho b\,(\frac{\pi}{2}\cot\beta)\frac{\dot{z}-\dot{\nu}}{\cos\theta - \nu\sin\theta}$$

Appendix 3
Determination of the feedback gain

The purpose of this appendix is to determine the feedback gain in the closed loop system. As described in (2.3), the dynamic equations can be written as:

$$\begin{aligned}(z_{\ddot{z}} - M)\ddot{z} + z_{\dot{z}}\dot{z} + z_z z + z_{\ddot{\theta}}\ddot{\theta} + z_{\dot{\theta}}\dot{\theta} + z_\theta\theta = F(t)\\ (M_{\ddot{\theta}} - I_y)\ddot{\theta} + M_{\dot{\theta}}\dot{\theta} + M_\theta\theta + M_{\ddot{z}}\ddot{z} + M_{\dot{z}}\dot{z} + M_z z = M(t)\end{aligned} \tag{3.1}$$

By taking the Laplace transformation on both sides of (3.1), the set of differential equations may be changed into a set of algebraic equations as a matrix form:

$$\begin{bmatrix}(z_{\ddot{z}} - M)s^2 + z_{\dot{z}}s + z_z & z_{\ddot{\theta}}s^2 + z_{\dot{\theta}}s + z_\theta\\ M_{\ddot{z}}s^2 + M_{\dot{z}}s + M_z & (M_{\ddot{\theta}} - I_y)s^2 + M_{\dot{\theta}}s + M_\theta\end{bmatrix}\begin{bmatrix}z(s)\\ \theta(s)\end{bmatrix} = \begin{bmatrix}F(s)\\ M(s)\end{bmatrix} \tag{3.2}$$

where s indicates the Laplace operator.

Using the inverse of the matrix, the pitch angle θ may be obtained from (3.2), that is:

$$\theta(s) = \frac{[(z_{\ddot{z}} - M)s^2 + z_{\dot{z}}s + z_z]M(s) - [M_{\ddot{z}}s^2 + M_{\dot{z}}s + M_z]F(s)}{[(M_{\ddot{\theta}} - I_y)s^2 + M_{\dot{\theta}}s + M_\theta][(z_{\ddot{z}} - M)s^2 + z_{\dot{z}}s + z_z] - [M_{\ddot{z}}s^2 + M_{\dot{z}}s + M_z][z_{\ddot{\theta}}s^2 + z_{\dot{\theta}}s + z_\theta]} \tag{3.3}$$

Assuming that the external force $F(t)$ is zero, (3.3) may be simplified as:

$$\theta(s) = \frac{[(z_{\ddot{z}} - M)s^2 + z_{\dot{z}}s + z_z]M(s)}{[(M_{\ddot{\theta}} - I_y)s^2 + M_{\dot{\theta}}s + M_\theta][(z_{\ddot{z}} - M)s^2 + z_{\dot{z}}s + z_z] - [M_{\ddot{z}}s^2 + M_{\dot{z}}s + M_z][z_{\ddot{\theta}}s^2 + z_{\dot{\theta}}s + z_\theta]} \tag{3.4}$$

The transform function from $M(s)$ to $\theta(s)$ is:

$$\begin{aligned}W(s) &= \frac{(z_{\ddot{z}} - M)s^2 + z_{\dot{z}}s + z_z}{[(M_{\ddot{\theta}} - I_y)s^2 + M_{\dot{\theta}}s + M_\theta][(z_{\ddot{z}} - M)s^2 + z_{\dot{z}}s + z_z] - [M_{\ddot{z}}s^2 + M_{\dot{z}}s + M_z][z_{\ddot{\theta}}s^2 + z_{\dot{\theta}}s + z_\theta]}\\ &= \frac{(z_{\ddot{z}} - M)s^2 + z_{\dot{z}}s + z_z}{A_4s^4 + A_3s^3 + A_2s^2 + A_1s + A_o}\end{aligned} \tag{3.5}$$

where:

$$A_o = M_\theta z_z - M_z z_\theta$$
$$A_1 = (M_{\dot{\theta}}z_z + M_\theta z_{\dot{z}}) - (M_{\dot{z}}z_\theta + M_z z_{\dot{\theta}})$$

$$A_2 = [(M_{\ddot{\theta}} - I_y)z_{\dot{z}} + M_{\dot{\theta}} z_{\dot{z}} + M_{\theta}(z_{\dot{z}} - M)] - [M_{\dot{z}} z_{\theta} + M_{\dot{z}} z_{\dot{\theta}} + M_z z_{\ddot{\theta}}]$$

$$A_3 = [(M_{\ddot{\theta}} - I_y)z_{\bar{z}} + M_{\dot{\theta}}(z_{\bar{z}} - M)] - [M_{\dot{z}} z_{\dot{\theta}} + M_{\dot{z}} z_{\bar{\theta}}]$$

$$A_4 = (M_{\ddot{\theta}} - I_y)(z_{\bar{z}} - M) - M_{\dot{z}} z_{\ddot{\theta}}$$

In this report the pitch angular rate is as an attitude measurement for the stabilization of the system, therefore, it may be fed back to reduce the amplitude of pitch angle. The block diagram of the closed loop system follows:

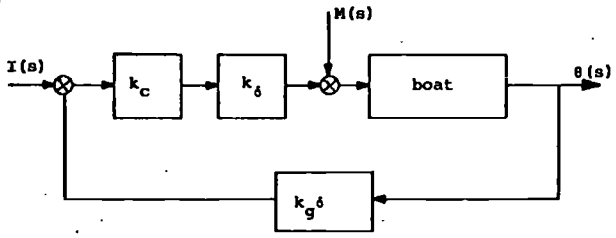

where K_c is a control gain to be determined, K_δ is the coefficient between control torgue and control electric signal, and K_g is the coefficient of the rate gyro. The open loop transform function should be:

$$w_o(s) = \frac{K_c K_\delta K_g s[(z_{\bar{z}} - M)s^2 + z_{\dot{z}} s + z_z]}{A_4 s^4 + A_3 s^3 + A_2 s^2 + A_1 s + A_o} \tag{3.6}$$

and frequency characteristics may be obtained from (3.6) by changing the Laplace operator s into $j\omega$, that is:

$$w_o(j\omega) = \frac{K_c K_s K_g (j\omega)[(z_{\bar{z}} - M)(j\omega)^2 + z_{\dot{z}}(j\omega) + z_z]}{A_4(j\omega)^4 + A_3(j\omega)^3 + A_2(j\omega)^2 + A_1(j\omega) + A_o} \tag{3.7}$$

To determine the control gain K_c, two conditions for the critical stabilization may be used, they are:

$$|w_o(j\omega)| = 1 \tag{3.8}$$

and

$$\underline{/w_o(j\omega)} = -180° \tag{3.9}$$

From (3.7), (3.8) and (3.9) and assuming $K_\delta = K_g = 1$ the module condition is the form:

$$|w_o(j\omega)| = \frac{\sqrt{(K_c z_{\dot{z}} \omega^2)^2 + [K_c \omega (z_z - (z_{\bar{z}} - M)\omega^2)]^2}}{\sqrt{(A_4\omega^4 - A_2\omega^2 + A_o)^2 + (A_3\omega^3 - A_1\omega)^2}} = 1 \tag{3.10}$$

and phase condition is the form:

$$\underline{/w_o(j\omega)} = 180° - \tan^{-1}\frac{K_c\omega[z_z - (z_{\bar{z}} - M)\omega^2]}{K_c z_{\dot{z}}\omega^2} + \tan^{-1}\frac{A_3\omega^3 - A_1\omega}{A_4\omega^4 - A_2\omega^2 + A_o} = -180° \tag{3.11}$$

which can be rewritten as:

$$A_4(z_{\bar{z}} - M)\omega^6 + [A_3 z_{\dot{z}} - A_4 z_z - A_2(z_{\bar{z}} - M)]\omega^4 + [A_2 z_z + A_o(z_{\dot{z}} - M) - A_1 z_{\dot{z}}\omega]^2 - A_o z_z = 0 \tag{3.12}$$

Taking the positive real root of equation (3.12), and substituting it into (3.10), the control gain under the condition of critical stabilization is:

$$K_c = \frac{\sqrt{(A_4\omega_c^4 - A_2\omega_c^2 + A_o)^2 + (A_3\omega_c^3 - A_1\omega_c)^2}}{\sqrt{(z_{\dot{z}}\omega_c)^2 + \omega_c^2[z_z - (z_{\bar{z}} - M)\omega_c^2]^2}} \tag{3.13}$$

where ω_c is the positive real root of equation (3.12). If the system is asymptotically stable, the control gain should satisfy the following condition:

$$0 < K_c < \frac{\sqrt{(A_4\omega_c^4 - A_2\omega_c^2 + A_o)^2 + (A_3\omega_c^3 - A_1\omega_c)^2}}{\sqrt{(z_{\dot{z}}\omega_c)^2 + \omega_c^2[z_z - (z_{\bar{z}} - M)\omega_c^2]^2}}$$

Appendix 4
Instrumentation for the pitch reduction experiments

The instrumentation and equipment used during the experiments can be divided into two groups. One group contains instrumentation that measured resistance and processed the required signals, whereas the second group is formed by the control system that controlled the flaps.

Our description of the equipment used will also adhere to this division into two groups.

In figure 26 the set-up of the instrumentation of group one is shown.

The figure shows what kind of sensor was used to measure the parameters mentioned in this report. All signals from the sensors were fed to an amplifier to amplify them to a suitable level and then recorded on paper by means of a UV-recorder. The carriage speed was measured using an optical encoder and the results fed to the computer which calculated an average speed for the run.

From the paper recordings the parameters like trim angle, heave, phases between signals (when planing in waves) etc. could be obtained. To assure the highest possible accuracy the calibrations were controlled daily.

The flap control system which comprises group two will be taken into consideration now. Its block diagram is pictured in figure 27. It is a conventional feedback system. The shakers used to drive the flaps are types normally used when testing vibration modes of structures having a large bandwidth. However, the maximum force and stroke they can deliver, was rather low for our experiments. Another problem was the friction of the bearings of the system. Proper attention has to be paid to this problem during experiments.

With a strap between the points A and C or B and C, a selection could be made between a function generator or the pitch signal as the driving signal for the flaps. The function generator was used when excitating the model in still water with the flaps. The pitch velocity signal was used as a feedback signal, when the boat was planing in waves and the pitch motion has to be reduced using the flaps.

9. Nomenclature

A	Mass matrix
A_R	Section area
a	Correction factor for buoyancy force
b	Half-beam of boat
b_F	Flap span
$C_{D,C}$	Crossflow drag coefficient
C_Δ	Load coefficient $\Delta/[\rho g(2b)^3]$
C_λ	Wavelength coefficient $L/\lambda\,[C_\Delta/(L/2b)^2]^{1.5}$
g	Acceleration of gravity
H	Wave height
I_a	Added pitch moment inertia
I_y	Pitch moment of inertia
K	Wave number
K_a	Two-dimensional added-mass coefficient
K_{CM}	Feedback control coefficient
L	Boat length
l_a	Arm of ΔF with respect to CG
LCG	Longitudinal center of gravity
L_F	Flap chord
M	Mass of boat
M_a	Added mass of boat
m_a	Section added mass
$M_{\ddot{z}}, M_{\dot{z}}, M_z, M_{\ddot{\theta}}, M_{\dot{\theta}}, M_\theta$	Stability derivatives of boat
N	Hydrodynamic force normal to baseline
r	Wave elevation $r = r_o \cdot \cos(kx + \omega t)$
r_o	Wave amplitude
U	Relative fluid velocity parallel to baseline
V	Relative fluid velocity normal to baseline
w	Weight of boat
w_z	Vertical component of wave orbital velocity
$\dot{w}_z$	Vertical component of wave orbital acceleration
x_o	Fixed horizontal coordinate
$\vec{x}$	Vector of state variables
x_c	Distance from CG to center of pressure for N
x_b	Body coordinate parallel to baseline
$x_{CG}, \dot{x}_{CG}, \ddot{x}_{CG}$	Surge displacement, velocity and acceleration
z_o	Fixed vertical coordinate
z_a	Heave amplitude
z_b	Body coordinate normal to baseline
$z_{CG}, \dot{z}_{CG}, \ddot{z}_{CG}$	Heave displacement, velocity and acceleration
$z_{\ddot{z}}, z_{\dot{z}}, z_z, z_{\ddot{\theta}}, z_{\dot{\theta}}, z_\theta$	Stability derivatives of boat
β	Deadrise angle
Δ	Boat displacement
$\Delta C_{L_{\text{Flap}}}$	Flap lift increment coefficient
$\Delta C_{M_{\text{Flap}}}$	Flap moment increment coefficient
ΔF	Flap lift increment
ΔM	Flap moment increment
λ	Wavelength
λ_F	Flap chord-beam ratio
$\theta, \dot{\theta}, \ddot{\theta}$	Pitch angle, velocity and acceleration
θ_a	Pitch amplitude
ρ	Density of water
σ	Flap span-beam ratio
δ	Flap deflection angle
δ_a	Amplitude of flap angle
ω_o	Flap oscillation frequency
ω	Wave frequency

TECHNISCHE HOGESCHOOL DELFT
AFDELING DER MARITIEME TECHNIEK
LABORATORIUM VOOR SCHEEPSHYDROMECHANICA

PITCH AND HEAVE CHARACTERISTICS OF HIGH-SPEED PLANING BOATS

Wang Long-Wen

September 1983 Reportnr.597

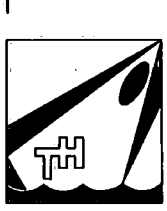

Delft University of Technology
Ship Hydromechanics Laboratory
Mekelweg 2
2628 CD DELFT
The Netherlands
Phone 015 -786882

Contents.

Summary.

The dynamic coefficients of the pitch and heave equations have been determined in an experimental way by means of forced oscillation technique for two models of conventional-type planing hulls and a planing wedge in the Ship Hydromechanics Laboratory of the Delft University of Technology.
Corresponding calculations have been carried out using a linear strip theory developed by M. Martin.
Comparison of the experiment and the results of the calculations shows that to a certain extent, the motion is linear in the planing condition; it seems possible to extend the use of the motion coefficients valid for prismatic planing hulls to more conventional-types.

1. Introduction.

As known the pitch and heave motions of high-speed planing hulls at constant speeds may be described by a set of coupled linear equations as follows:
heaving:

$$(a_{zz}+\rho\nabla)\ddot{z} + b_{zz}\dot{z} + c_{zz}z - a_{z\theta}\ddot{\theta} - b_{z\theta}\dot{\theta} - c_{z\theta}\theta = F \quad (1)$$

pitching:

$$(a_{\theta\theta}+k_y^2\rho\nabla)\ddot{\theta} + b_{\theta\theta}\dot{\theta} + c_{\theta\theta}z - a_{\theta z}\ddot{z} - b_{\theta z}\dot{z} - c_{\theta z}z = M \quad (2)$$

For estimating dynamic characteristics, it is required to know the two-dimensional damping and added mass of the boat's sections. By emplying the Schwarz-Christoffel transformation Hwang [1] investigated cylinders with typical straight frames in vertical oscillation at high frequencies and presented calculated values of added mass coefficient K. Martin [2] derived the coefficients of the motion variables in the linear equations on the assumption that the boat could be treated as a slender body with an empirical three-dimensional correction.
The coefficients of these motion equations are a function of the geometric and operational characteristics of the boats.
By giving the model of a boat a forced oscillation in still water and measuring the forces and moments required to maintain a steady state harmonic motion, it is possible to determine the coefficients of the left hand side of these motion equations experimentally.
For the first time, a planing wedge was tested by using this oscillator technique in the Ship Hydromechanics Laboratory of the Delft University of Technology to ivestigate its dynamic characteristics [3].
However all above mentioned work including solutions of the motion equations was meant only for prismatic planing hull forms. It seems to be attractive to extend the application to more conventional-type planing hulls such as

the "Clement" form of the Series-62 [4] and the "Delft" form [5] .
Therefore two models 84 and 85 with conventional-type planing hull forms were tested for further investigation of the problem in the laboratory.
Moreover some calculations were carried out by means of Martin's linear theory for comparison with experimental results.
In addition to the first harmonics of the dynamic forces and moments, the second harmonics of them were also measured in the oscillation tests and subsequent analysis of the results were made in an attempt to verify whether the motion is linear or quasi-linear.

2. Experiments.

Test models.
Two models of which only the deadrise angles differed, were used in the experiment. The first one, denoted a model 84, was quite similar to the "Clement" form of Series-62 [4], the other, model 85, was derived from the first one by doubling the angle of deadrise and keeping all other dimensions as equal as possible [5] .
The form of both models is shown in figure 1.
The main particulars are given in the following Table.

A_p	projected area of chines and transom	0.5550 m^2
L	length of projected area A_p	1.500 m
B_c	breadth over chines, at any cross section	
B_{cmax}	maximum breadth over chines	0.450 m
B_{cm}	mean breadth of area A_p	0.370 m
∇	volume of displacement at rest	0.02734 m^3
X_p	center of the projected area A_p (forward of transom	0.729 m
G	center of gravity (forward of transom)	0.665 m
$\nabla^{1/3}$		0.301 m
$L/\nabla^{1/3}$		4.98
$A_p/\nabla^{2/3}$		6.11
L/B_{cm}		4.05
L/B_{cmax}		3.33

The deadrise angle of the prismatic part of the planing bottom of model 84 was 12 degrees, that of model 85 was 24 degrees.

Experimental technique.

Figure 2 shows a schematic view of the oscillator used in the present study. The model is forced to oscillated in the vertical direction by means of a Scotch-Yoke mechanism. The forces were measured by two straingauge dynamometers, which connected the model to two oscillator struts, fore and aft. The dynamometers are sensitive for forces perpendicular to the baseline of the model only.

The vertical forces acting on the model are separated into the components in phase with the displacement and into the quadrature components by an electronic analoge system which, in principle, is described in reference [6] as follows in a short way: the measured signal is multiplied with sin ($n\omega t$) and cos ($n\omega t$) by means of a sine-consine synchro resolver connected to the main shaft of the mechanical oscillator, where ω is the circular frequency, and n = 1, 2, or 3. After integration the first, second, or third harmonics of the in-phase and quadrature components can be found.

Forced oscillation - Heave.

From the equations of motion for pitch and heave we know that to evaluate the coefficient experimentally it is necessary to perform two linearily independent experiments at each frequency to measure the exciting force and moment. Therefore the two experiments can be designed so that only one mode of motion is present in each experiment. Forced oscillation test were conducted to determine the damping and the hydrodynamic inertia forces for heaving motions in still water as a function of forward speed and frequency. The range of the frequencies for the test was between: ω = 5 and 30 rad/sec and two speeds of advance were considered, namely $V/\sqrt{L}$ = 3.67 and 4.49 corresponding to the conditions that the flow separates from the chine. The oscillation amplitudes for heave were 0.003 m, 0.006 m and 0.009 m. When the model performs a forced harmonic oscillation in the vertical direction with an amplitude z_a and a

circular frequency ω without pitching, it is assumed that

$$z = z_a \cos\omega t \tag{3}$$

if only the first harmonics of the measured forces are taken into account, the linear equeations of motion will be:

$$\begin{aligned} (a_{zz}+\rho\nabla)\ddot{z} + b_{zz}\dot{z} + c_{zz}z &= F_{za}\cos(\omega t+\varepsilon_{zf}) \\ -a_{\theta z}\ddot{z} - b_{\theta z}\dot{z} - c_{\theta z}z &= m_{za}\cos(\omega t+\varepsilon_{zm}) \end{aligned} \tag{4}$$

where:

a_{zz} = added mass
b_{zz} = damping coefficient
c_{zz} = restoring force coefficient
$a_{\theta z}, b_{\theta z}, c_{\theta z}$ = cross coupling coefficients
F_{za} = amplitude of the first harmonic of exciting force
$\varepsilon_{zf}, \varepsilon_{zm}$ = phase angles
m_{za} = amplitude of the first harmonic of exciting moment

After substitution of (3) in (4), the hydrodynamic coefficients could be soluted with the following results:

$$\begin{aligned} a_{zz} &= \frac{c_{zz}z_a - F_{za}\cos\varepsilon_{zf}}{z_a\omega^2} - \rho\nabla \\ b_{zz} &= \frac{F_{za}\sin\varepsilon_{zf}}{z_a\omega} \\ a_{\theta z} &= \frac{c_{\theta z}z_a + m_{za}\cos\varepsilon_{zm}}{z_a\omega^2} \\ b_{\theta z} &= \frac{m_{za}\sin\varepsilon_{zm}}{z_a\omega} \end{aligned} \tag{5}$$

in which:

$$F_{za}\cos\varepsilon_{zf} = F_{zAa}\cos\varepsilon_{zA} + F_{zva}\cos\varepsilon_{zv}$$

$$F_{za}\sin\varepsilon_{zf} = F_{zAa}\sin\varepsilon_{zA} + F_{zva}\sin\varepsilon_{zv}$$

$$M_{za}\cos\varepsilon_{zm} = (F_{zAa}\cos\varepsilon_{zA} - F_{zva}\cos\varepsilon_{zv})\tfrac{1}{2}l$$

$$M_{za}\sin\varepsilon_{zm} = (F_{zAa}\sin\varepsilon_{zA} - F_{zva}\sin\varepsilon_{zv})\tfrac{1}{2}l$$

where:

F_{zAa} = force amplitude on the aft strut with phase angle ε_{zA}

F_{zva} = force amplitude on the fore strut with phase angle ε_{zv}

l = distance between the struts; in this case two struts are at equal distance from the centre of gravity of the model

c_{zz} and $c_{\theta z}$, which are a function of the forward speed of the model may be obtained from:

$$c_{zz} = F_{za}/Z_a \quad \text{and} \quad c_{\theta z} = -m_{za}/Z_a$$

From the measured values of $F_{zAa}\cos\varepsilon_{zA}$, $F_{zAa}\sin\varepsilon_{zA}$, $F_{zva}\cos\varepsilon_{zv}$, and $F_{zva}\sin\varepsilon_{zv}$, the hydrodynamic coefficients for heave were calculated and their results are given in the Fig. 3 through 14 on a base of frequency for two speeds of advance.

Forced oscillation - pitch.

In the case of a pure pitching motion the model was restrained for heave, but it was free to perform pitching oscillations. The frequency range and forward speeds of the model were the same as described for heave while the oscillation amplitude was different and varied from $\theta_a = 0.00875$ to 0.02625 rad. When the model performs a forced harmonic oscillation for pitch with an amplitude θ_a and a circular frequency ω it is assumed that:

$$\theta = \theta_a \cos\omega t \tag{6}$$

and if only the first harmonics of the measured forces and moments are taken into account, the linear equations of motion will be:

$$-a_{z\theta}\ddot{\theta} - b_{z\theta}\dot{\theta} - c_{z\theta}\theta = F_{\theta a}\cos(\omega t + \varepsilon_{\theta f})$$

$$(a_{\theta\theta} + K_y^2\rho\nabla)\ddot{\theta} + b_{\theta\theta}\dot{\theta} + c_{\theta\theta}\theta = m_{\theta a}\cos(\omega t + \varepsilon_{\theta m}) \tag{7}$$

where:

$a_{\theta\theta}$ = added mass moment of inertia

$b_{\theta\theta}$ = damping moment coefficient

$c_{\theta\theta}$ = restoring moment coefficient

$a_{z\theta}, b_{z\theta}, c_{z\theta}$ = cross coupling coefficients

$F_{\theta a}$, $m_{\theta a}$ = amplitude of the first harmonic of exciting force and moment respectively

$\varepsilon_{\theta f}$, $\varepsilon_{\theta m}$ = phase angels

Substituting (6) into (7), delivers the following results:

$$a_{\theta\theta} = \frac{c_{\theta\theta}\theta_a - m_{\theta a}\cos\varepsilon_{\theta m}}{\theta_a \omega^2} - K_y^2 \rho \nabla$$

$$b_{\theta\theta} = \frac{m_{\theta a}\sin\varepsilon_{\theta m}}{\theta_a \omega}$$

$$a_{z\theta} = \frac{c_{z\theta}\theta_a + F_{\theta a}\cos\varepsilon_{\theta f}}{\theta_a \omega}$$

$$b_{z\theta} = \frac{F_{\theta a}\sin\varepsilon_{\theta f}}{\theta_a \omega}$$

$$c_{\theta\theta} = m_{\theta a}/\theta_a \quad \text{and} \quad c_{z\theta} = -F_{\theta a}/\theta_a \qquad (8)$$

in which:

$$m_{\theta a}\cos\varepsilon_{\theta m} = (F_{\theta Aa}\cos\varepsilon_{\theta A} - F_{\theta va}\cos\varepsilon_{\theta v})\ \tfrac{1}{2}1$$

$$m_{\theta a}\sin\varepsilon_{\theta m} = (F_{\theta Aa}\sin\varepsilon_{\theta A} - F_{\theta va}\sin\varepsilon_{\theta v})\ \tfrac{1}{2}1$$

$$F_{\theta a}\cos\varepsilon_{\theta f} = F_{\theta Aa}\cos\varepsilon_{\theta A} + F_{\theta va}\cos\varepsilon_{\theta v}$$

$$F_{\theta a}\sin\varepsilon_{\theta f} = F_{\theta Aa}\sin\varepsilon_{\theta A} + F_{\theta va}\sin\varepsilon_{\theta v}$$

while:

$F_{\theta Aa}$ = force amplitude on the aft strut with phase angle $\varepsilon_{\theta A}$

$F_{\theta Va}$ = force amplitdue on the fore strut with phase angle $\varepsilon_{\theta v}$.

The hydrodynamic coefficients for pitch are given in the Fig.14 through 26 on a base of frequency for two speeds of advance.

3. Calculations.

At first the hydrodynamic coefficients of the motion equations have been determined experimentally. Now they also may be calculated theoretically by treating the boat as a slender body with an empirical three-dimensional correction. Recently M. Martin developed a theoretical method for prediction motions of high-speed planing boats in waves [7], and gave the dynamic coefficients in the motion equations as follows [2] :

$$Z_{\ddot{z}} = -\phi(\lambda)\cos^2\tau \int u'\,ds'$$

$$Z_{\dot{z}} = -z\phi(\lambda)\mu'_s \cos^3\tau$$

$$Z_z = \frac{\partial Z'_s}{\partial \lambda} \frac{\partial \lambda}{\partial Z'}$$

$$Z_{\ddot{\theta}} = \phi(\lambda)\cos\tau \int \mu'(a'-s')\,ds'$$

$$Z_{\dot{\theta}} = -2\phi(\lambda)\mu'_s \lambda_g \cos^2\tau$$

$$Z_\theta = \frac{\partial Z_{s'}}{\partial \tau} + \frac{\partial Z_{s'}}{\partial \lambda} \frac{\partial \lambda}{\partial \tau}$$

$$M_{\ddot{z}} = \phi(\lambda)\cos\tau \int \mu'(a'-s')\,ds'$$

$$M_{\dot{z}} = 2\phi(\lambda)\cos^2\tau \left(\int \mu' ds' - \lambda_g \mu'_s \right)$$

$$M_z = \frac{\partial M_{s'}}{\partial \lambda} \frac{\partial \lambda}{\partial Z'}$$

$$M_{\ddot{\theta}} = -\phi(\lambda) \int \mu'(a'-s')^2\,ds'$$

$$M_{\dot{\theta}} = -2\phi(\lambda)\cos\tau \left(\mu_{s'}\lambda_g^2 + \int \mu'(a'-s')\,ds' \right)$$

$$M_\theta = \frac{\partial M_{s'}}{\partial \tau} + \frac{\partial M_{s'}}{\partial \lambda} \frac{\partial \lambda}{\partial \tau}$$

in which:

τ = equilibrium trim angle
λ = mean wetted length-to-beam ratio
$\phi(\lambda)$ = three-dimensional correction factor

μ' = non-dimensional sectional added mass
μ_s' = non-dimensional added mass at transom
λ_g = non-dimensional distance from transom to center of gravity
s' = non-dimensional distance from foremost wetted point on Keel to any boat section
a' = value of s' at boat center of gravity
z_s' = non-dimensional steady-state force
M_s' = non-dimensional steady-state moment

Now we amploy these formulas to calculate the hydrodynamic coefficients for the tested models and for a planing wedge form [3] for comparison with experimental results. Because the hydrodynamic coefficients derived by Martin are only for prismatic hull forms with constant deadrise angle, it is necessary for calculating the equilibrium trim angle τ and mean wetted length-to-beam λ to take an average beam and deadrise angle of conventional-type planing hulls as prismatic one to insert into following equations:

$$\frac{\lambda}{1+\lambda}\ \frac{\pi}{2}\sin\tau\cos^2\tau(1-\sin\beta) + C_{D,C}\lambda\sin^2\tau\cos^3\tau\cos\beta$$

$$+ \frac{0.624}{C_v^2}\lambda^2\sin\tau\cos\tau - \lambda c_f\sin\tau/\cos\beta - w' = 0$$

$$\frac{\pi}{4}\ \frac{\sin 2\tau(1-\sin\beta)\lambda}{1+\lambda}\ (\lambda + h(\tau) - \lambda_g) + C_{D,C}(\sin 2\tau)^2\cos\beta$$

$$(\frac{\lambda}{2} - \lambda_g)\ \frac{\lambda}{4}$$

$$+ \frac{0.624\sin\tau}{C_v^2}\lambda^2(\frac{\lambda}{3} - \lambda_g) - \frac{C_f}{\cos\beta}\lambda\ (\lambda_v - \frac{\tan\beta}{4}) = 0$$

where:

β = deadrise angle
C_v = $U/\sqrt{gb}$, speed coefficient
C_f = skin friction coefficient
λ_v = non-dimensional value of normal distance of center of gravity from keel
w' = non-dimensional boat weight

The calculation was carried out for three models under the following conditions:

V = 3.66. 4.48, and 5.66 m/sec for planing wedge
V = 4.5 m/sec for model 84
V = 4.5 and 5.5 m/sec for model 85
corresponding to the tested conditions.
In the computation of the planing wedge two equilibrium trim angles and mean wetted lengths were tried: one from the solution of the equation (9), the other from the tested measurement. The measured and calculated trim angles were shown in figure 35.
The results of the calculations were shown in the figures together with the experimental results.

4. Discussion.

The oscillator experiments were carried out for three amplitudes of motion, which were 0.003, 0.006 and 0.009 m for heave and 0.00825, 0.0175 and 0.07625 rad for pitch. For each amplitude the first and the second harmonic exciting force and moment were measured. The results from measurements and subsequent calculation showed that in comparison with the first harmonic force and moment, the second one is small-less than 5%, and the hydrodynamic coefficients, obtained from different amplitudes were very close. Consequently, to a certain extent the motion was linear under the tested conditions. However, it was also shown that with the increase of speed and oscillator amplitudes, the motion could be more sensitive for non-linear effects. It was also found that under the conditions of lower frequencies, the obtained dynamic coefficients were not so stable because of small amplitude of exciting force.
In the figures 27 through 34, a comparison was made between experimental results and computed values for the planing wedge and in the figures 3 through 26 for models 84 and 85. It is evident that the computed dynamic coefficient values agree better with the experimental results for the planing wedge than with that for models 84 and 85, because the theory had been developed mainly for prismatic planing boats. The planing wedge is more similar to a prismatic hull form. Although models 84 and 85 have constanct aft deadrise angles matching to prismatic body, they differ from it in

the fore body section and in the distribution of the beam. In the computation they are considered as a prismatic body by taking an average beam and deadrise angle. As a result, in every case the agreement of experimental results with calculated values for the added mass and damping is satisfactory, but for the added mass moment of inertia and damping moment the deviation of the experiments from calculations is rather large, as shown in the figures.
The accuracy of the calculation of the equilibrium trim angle and wetted length has an important effect on the determination of the dynamic coefficients. It was found that the calculated trim angles were lower than measured values, especially at higher speeds, which led to increase in theoretical added mass and damping. If the measured trim angle was used instead of the computed values to estimate dynamic characteristics, the results would be closer to the experimental values, as shown in figures 27 through 34.

5. Conclusions.

For the first time, oscillator technique was used to determine the dynamic characteristics of high-speed planing boats. The agreement between experimental and calculated motion (dynamic coefficents) of the planing wedge demonstrated, to a certain extent the linearity under the planing condition untill $V/\sqrt{L} = 4.5$.
Comparison of the experimental data and calculated results of the planing wedge provided a possibility to estimate deviations from the theory, and an approximative method for computation of more conventional-type planing hulls might be obtained by accounting for the detailed geometric characteristics of boats, especially the distribution of deadrise angles and beams.

6. Acknowledgement.

The author is greatly indebted to prof.ir. J. Gerritsma and W. Beukelman for their continuing encouragement and patient guidance due to which all experiments and calculations could be finished smoothly. The author's appreciation is also ex-

tended to Mr. J.A. Keuning and R. Onnink for their valuable assistance in carrying out all the experiments, and to Mr. P.W. de Heer and Mrs. J.F.M. Bergfeld for producing figures and typing the manuscript.

Nomenclature.

a_{zz}, b_{zz}, c_{zz}, $a_{z\theta}$, $b_{z\theta}$, $c_{z\theta}$	coefficients of the equations of motion for heave and pitch
$a_{\theta\theta}$, $b_{\theta\theta}$, $c_{\theta\theta}$, $a_{\theta z}$, $b_{\theta z}$, $c_{\theta z}$	
$Z_{\ddot{z}}$, $Z_{\dot{z}}$, Z_z, $M_{\ddot{z}}$, $M_{\dot{z}}$, M_z	non-dimensional coefficients of the equations of motion for heave and pitch
$M_{\ddot{\theta}}$, $M_{\dot{\theta}}$, M_θ, $Z_{\ddot{\theta}}$, $Z_{\dot{\theta}}$, Z_θ	
F, M	total exciting force and moment
F_{za}, M_{za}	force and moment amplitude for heave oscillation
F_{zAa}, M_{zAa}	force and moment amplitude on the aft strut for heave oscillation
F_{zVa}, M_{zVa}	force and moment amplitude on the aft strut for heave oscillation
$F_{\theta a}$, $M_{\theta a}$	force and moment amplitude on the fore strut for heave oscillation
$F_{\theta a}$, $M_{\theta a}$	force and moment amplitude for pitch oscillation
$F_{\theta Aa}$, $M_{\theta Aa}$	force and moment amplitude on the aft strut for pitch oscillation
$F_{\theta Va}$, $M_{\theta Va}$	force and moment amplitude on the fore strut for pitch oscillation
a'	value of s' at boat center of gravity
b	mean beam of chines
$C_{D,C}$	cross flow drag coefficient
C_v	speed coefficient $V / \sqrt{gb}$
C_f	skin friction coefficient
Fn_∇	Froude number based on volume of water displaced at rest
g	acceleration of gravity
K_y	radius of inertia of model
$M_{s'}$	non-dimensional steady-state moment
l	distance between the struts
s'	non-dimensional distance from foremost wetted point on keel to any boat section
t	time

V	forward speed of model
w'	non-dimensional boat weight
Z_a	heave amplitude
$Z_{s'}$	non-dimensional steady-state force
β	deadrise angle
ε	phase angle between the motions (forces, moments) and the oscillator
θ_a	pitch amplitude
λ	mean wetted length-to-beam ratio
λ_g	non-dimensional distance from transom to center of gravity
λ_v	non-dimensional value of normal distance of center of gravity from keel
μ'	non-dimensional sectional added mass
$\mu_{s'}$	non-dimensional added mass at transom
ρ	mass density of water
τ	equilibrium trim angle
$\phi(\lambda)$	three-dimensional correction factor
∇	volume of water displaced at rest
ω	circular frequency

References.

[1] Hwang, J.H.,
"Added Mass of Two-Dimensional Cylinders with the Sections of Straight Frames Oscillating Vertically in a Free Surface", the Journal of the Society of Naval Architects of Korea, Vol. 5, No. 2, November 1968.

[2] Martin, M.,
"Theoretical Determination of Porpoising Instability of High-Speed Planing Boats", Journal of Ship Research, Vol. 22, No. 1, March 1978.

[3] Zwaan, A.P. de,
"Oscillatieproeven met een planerende wig",
Delft Shipbuilding Laboratory, Report no. 376-M, 1973.

[4] Clement, E.P. and D. Blount,
"Resistance Tests of Systematic Series of Planing Hull Forms", Trans. SNAME, Vol. 71, 1963.

[5] Keuning, J.A. and J. Gerritsma,
"Resistance Tests of A Series of Planing Hull Forms with 25 Degrees Deadrise Angle",
ISP, Vol. 29, No. 337, September 1982.

[6] Zunderdorp, H.J. and M. Buitenhek,
"Oscillator-Techniques at the Shipbuilding Laboratory",
Delft Shipbuilding Laboratory, Report no. 111, 1963.

[7] Martin, M.,
"Theoretical Prediction of Motions of High-Speed Planing Boats in Waves", Journal of Ship Research, Vol. 22, No. 3, September 1978.

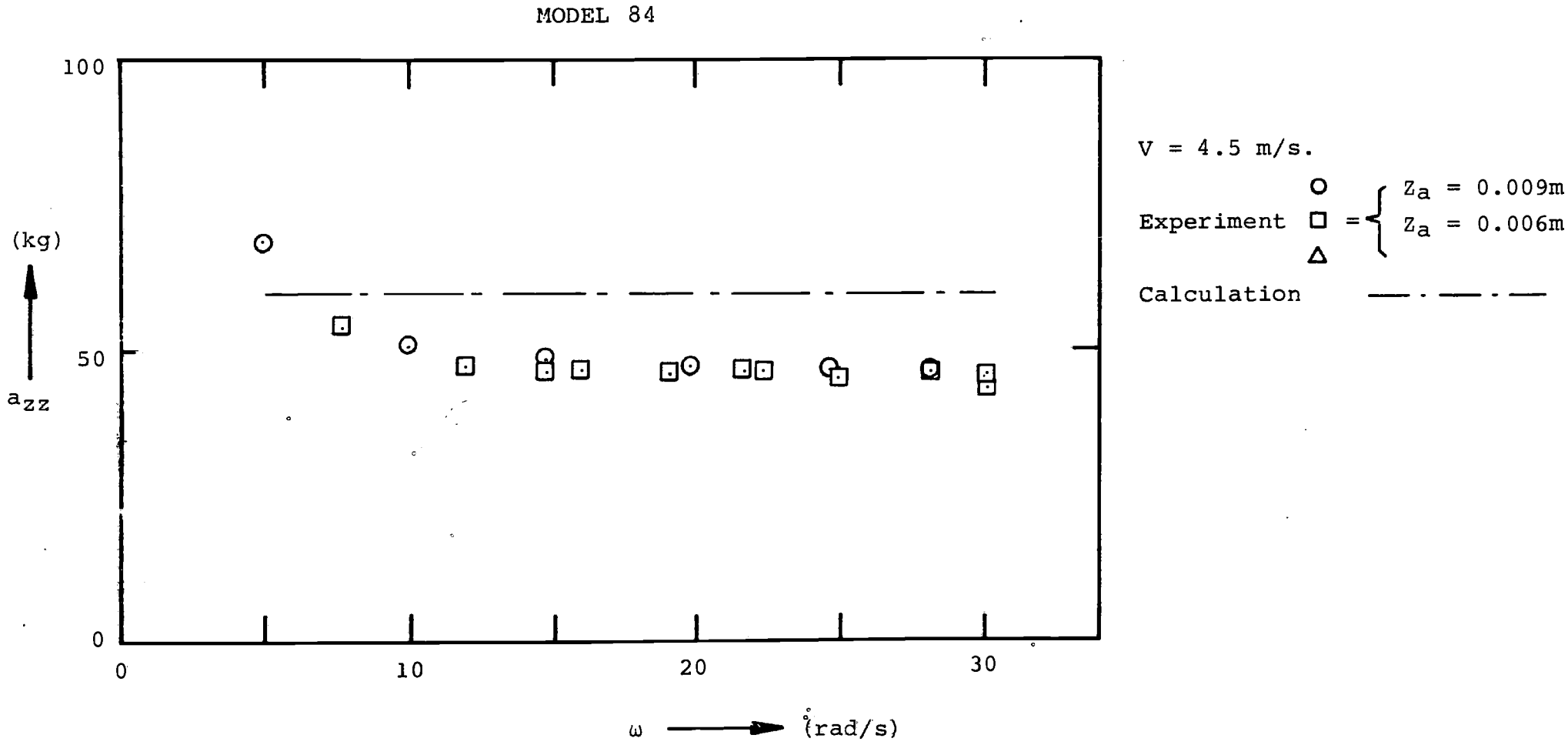

Figure 3. Comparison of the experimental and calculated added mass coëfficiënt a_{zz}.

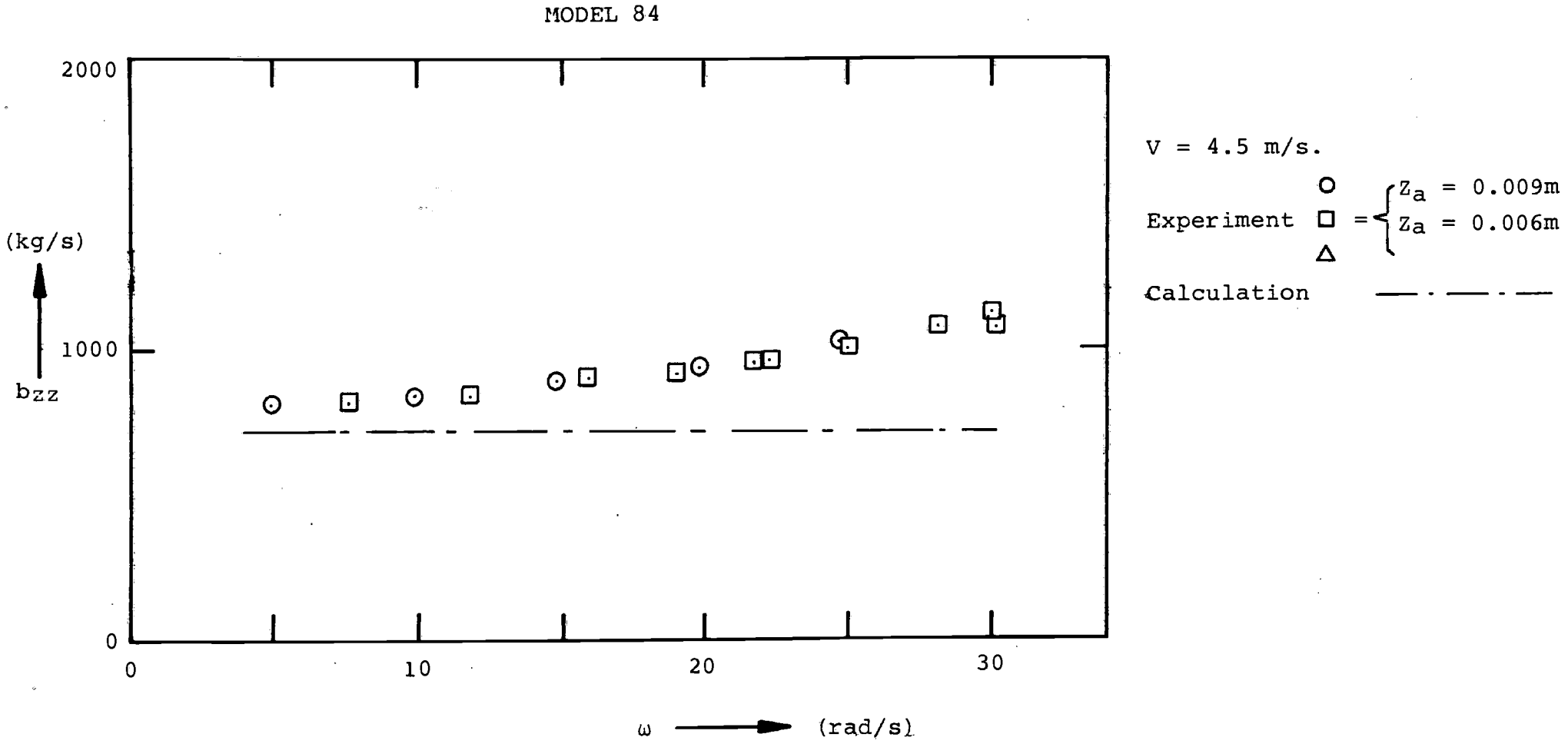

Figure 4. Comparison of the experimental and calculated damping coëfficiënt b_{zz}.

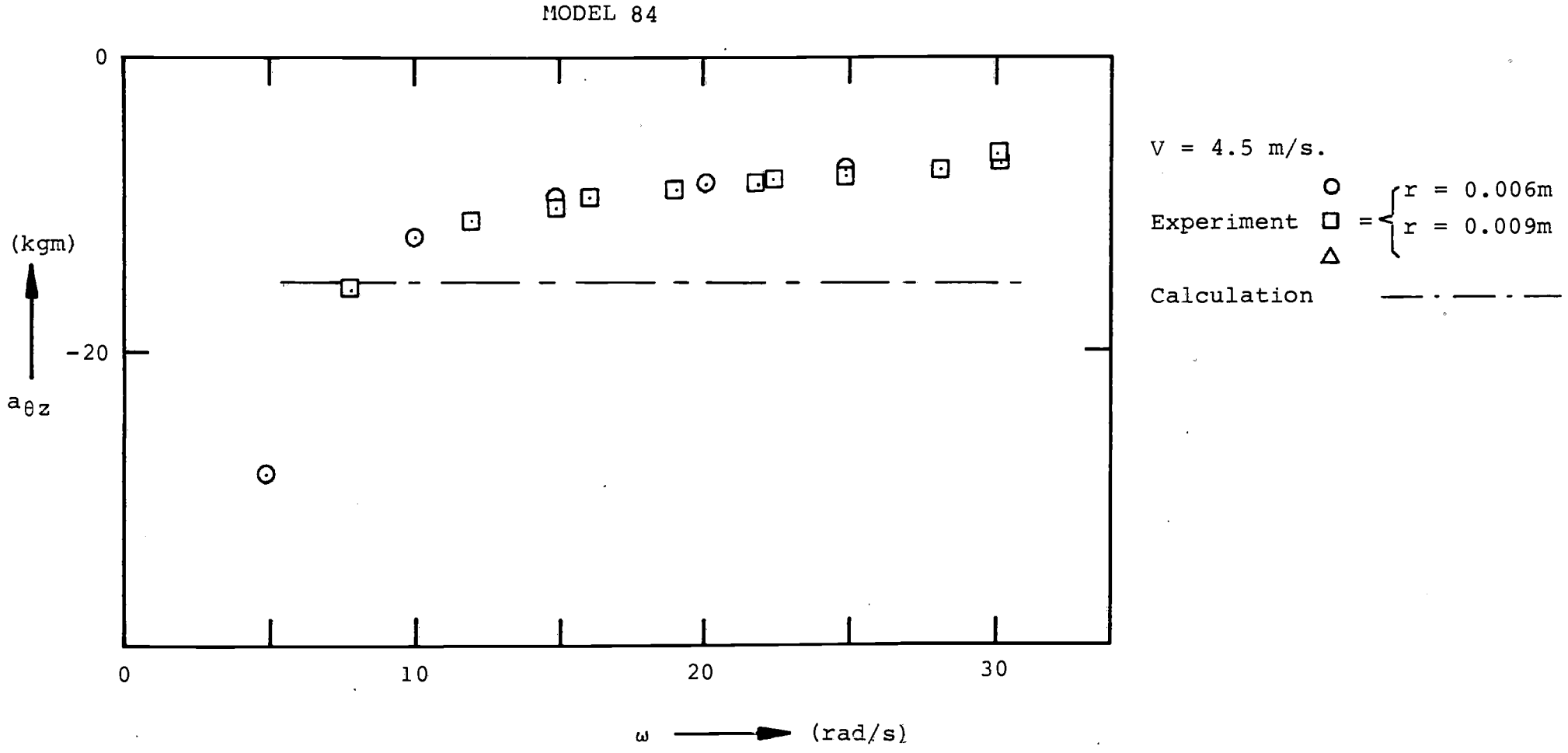

Figure 5. Comparison of the experimental and calculated mass coupling coëfficiënt $a_{\theta z}$.

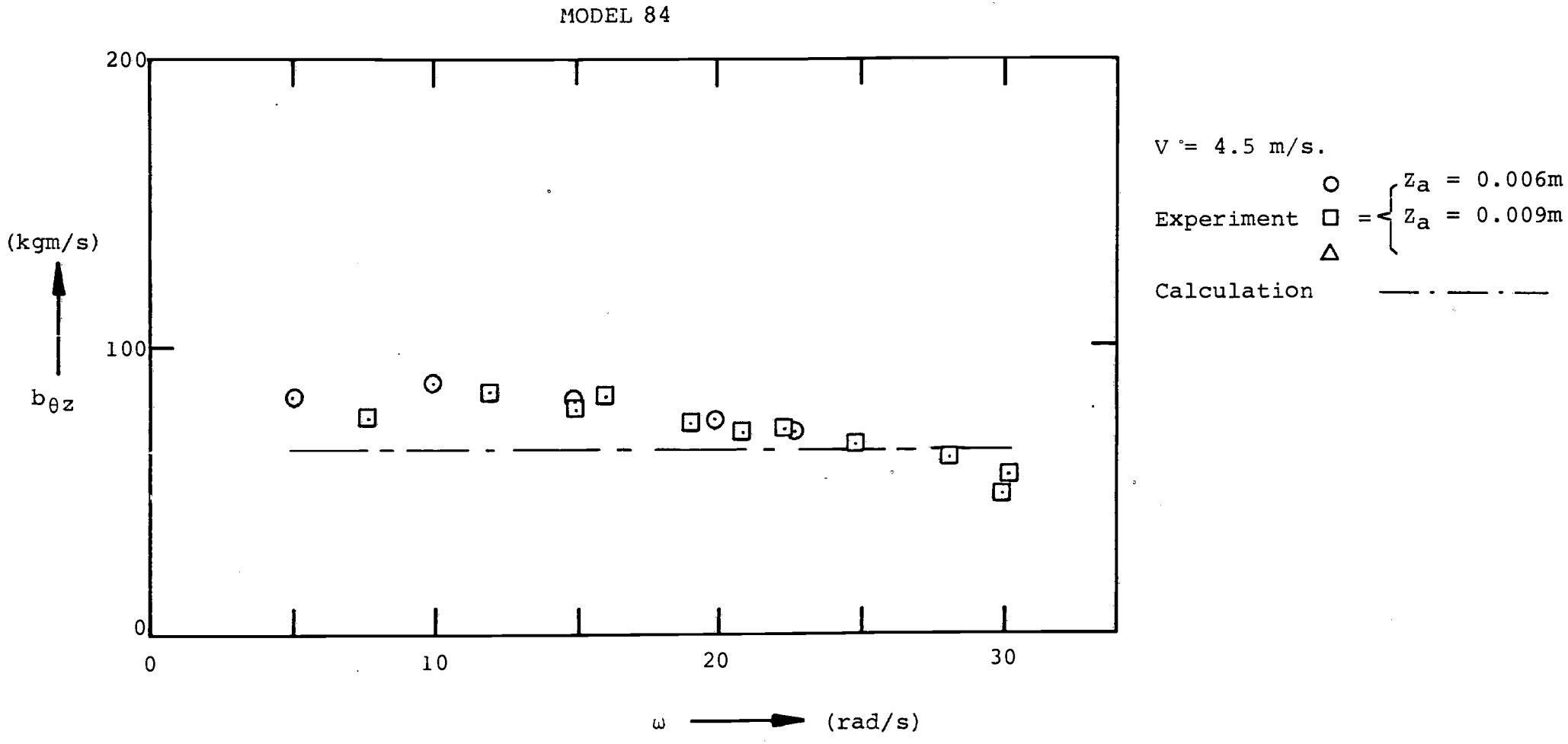

Figure 6. Comparison of the experimental and calculated coupling coëfficiënt for damping $b_{\theta z}$.

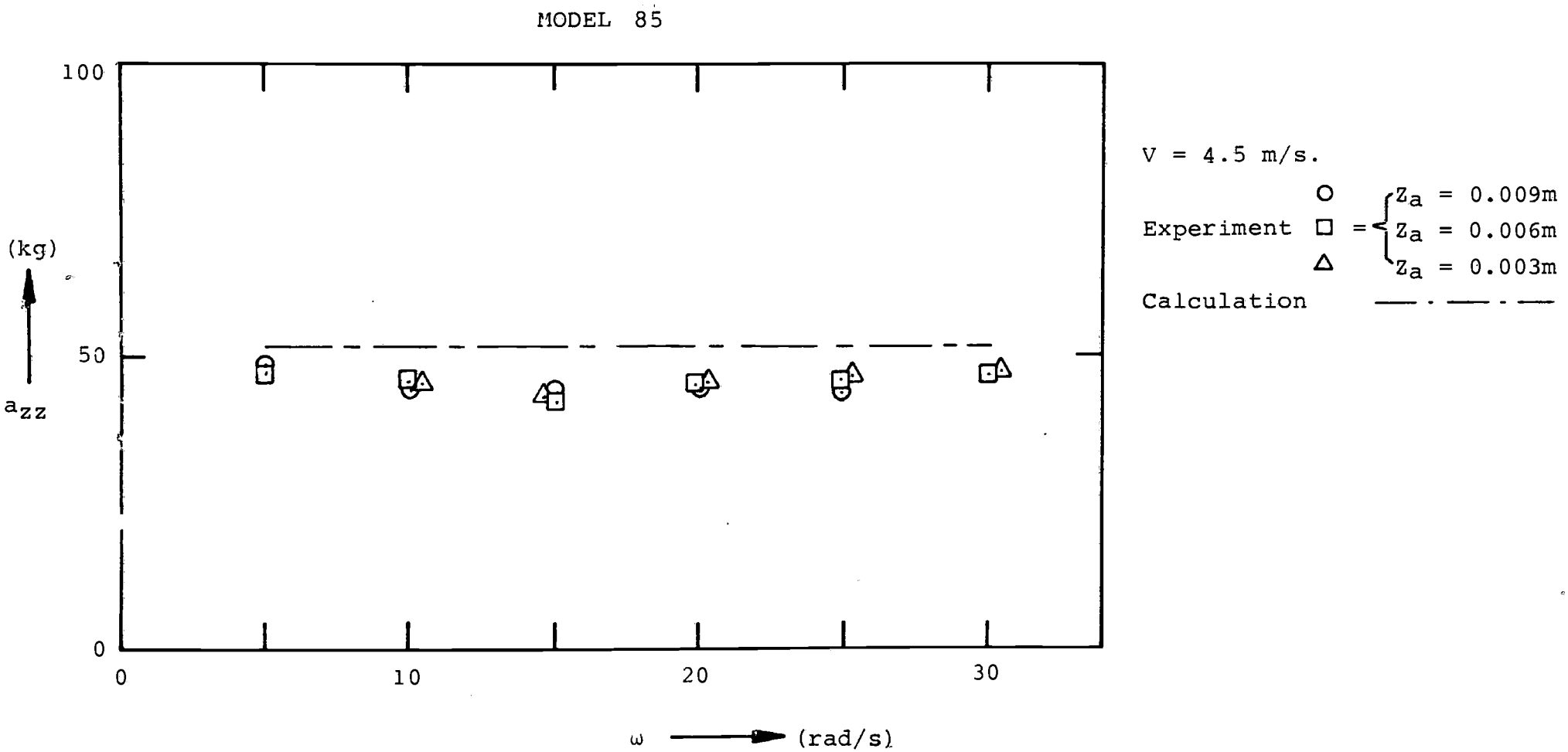

Figure 7. Comparison of the experimental and calculated added mass coëfficiënt a_{zz}.

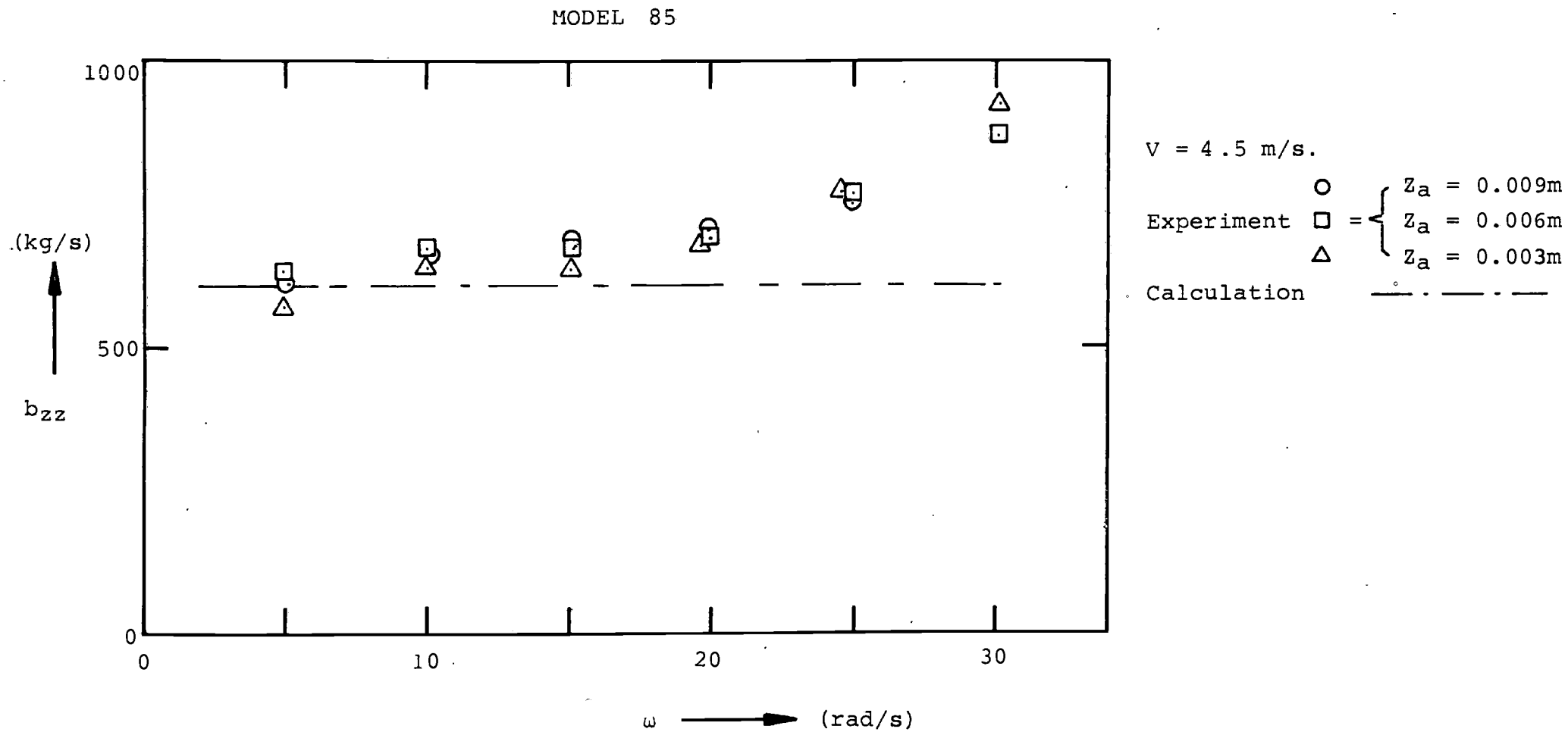

Figure 8. Comparison of the experimental and calculated damping coëfficiënt b_{zz}.

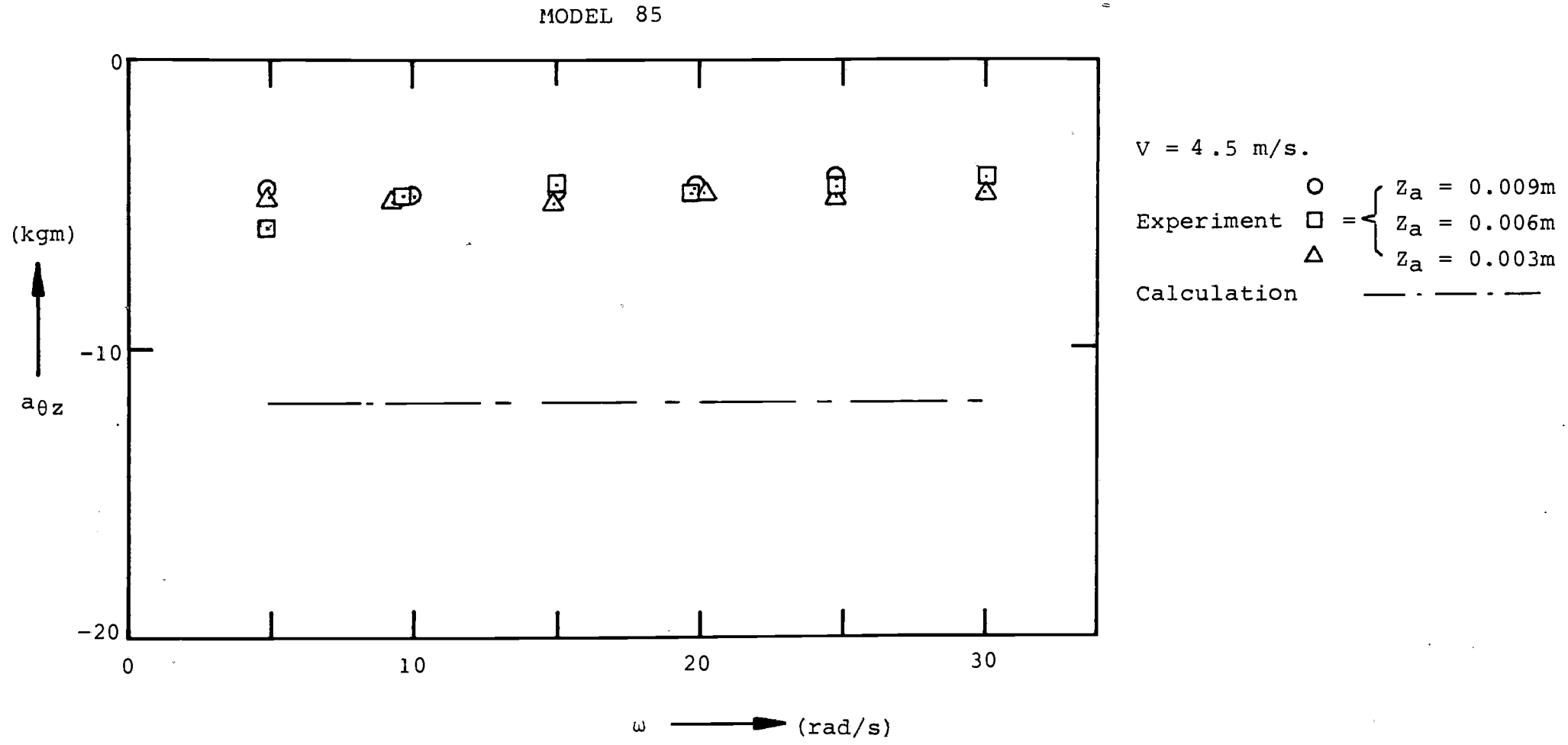

Figure 9. Comparison of the experimental and calculated mass coupling coëfficiënt $a_{\theta z}$.

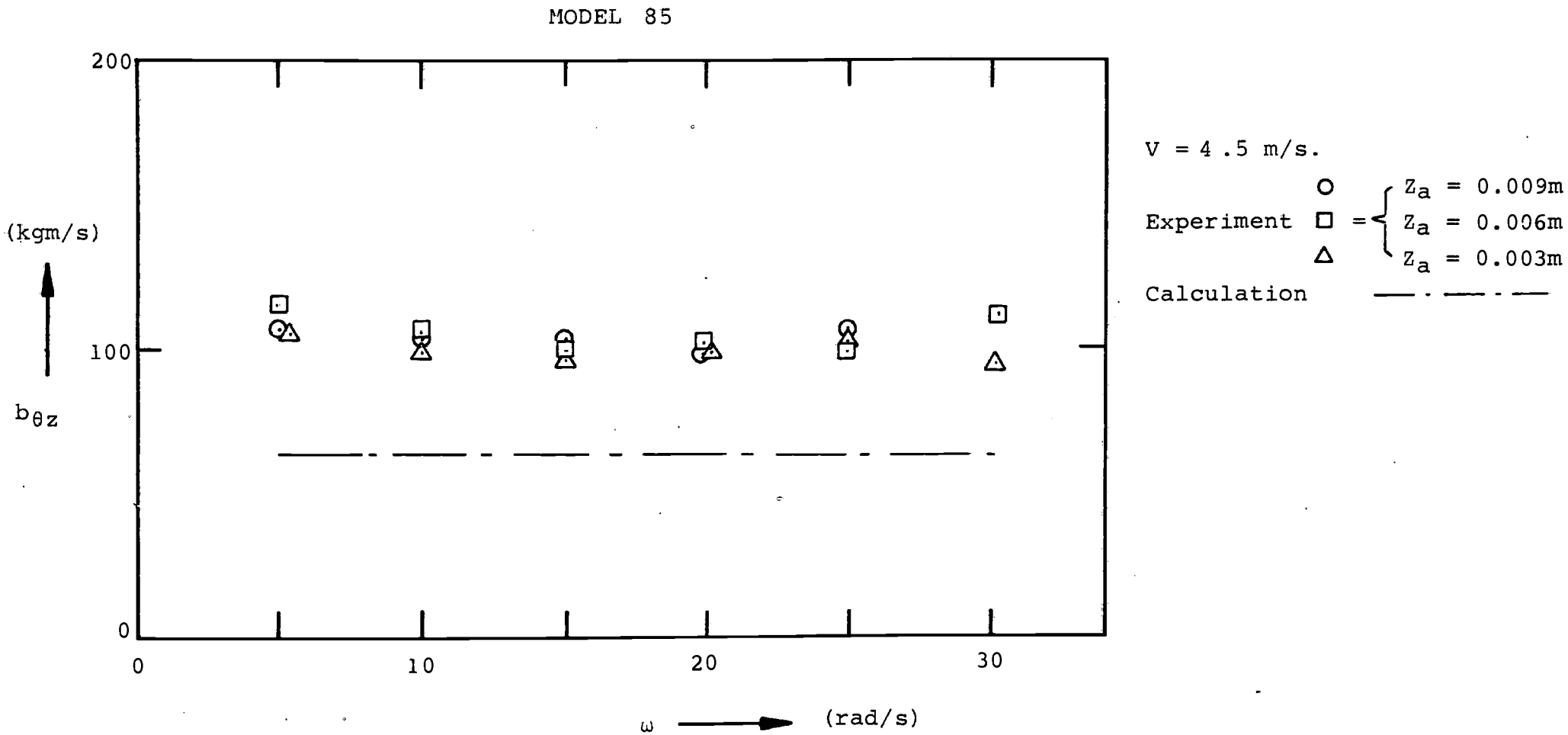

Figure 10. Comparison of the experimental and calculated coupling coëfficiënt for damping $b_{\theta z}$.

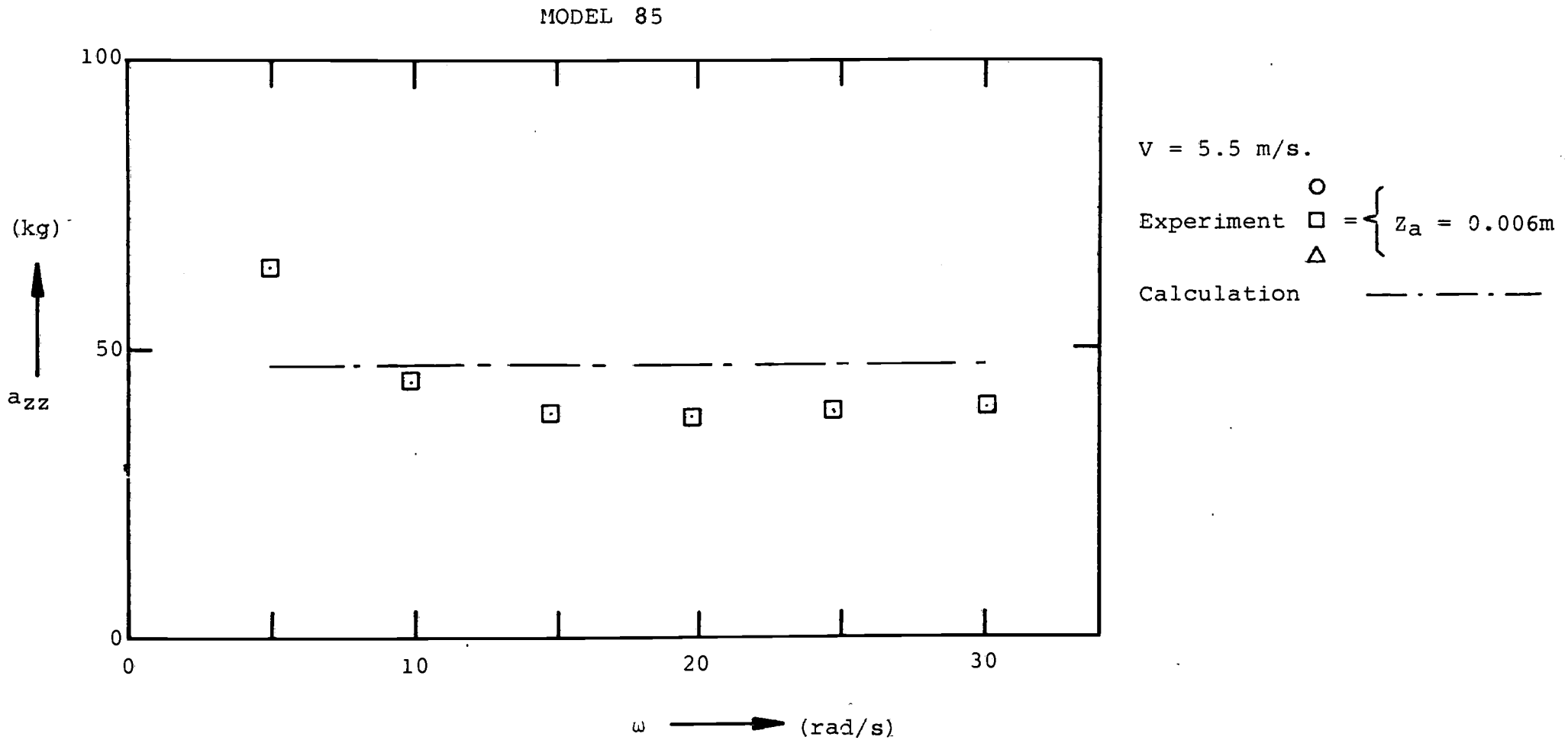

Figure 11. Comparison of the experimental and calculated added mass coëfficiënt a_{zz}.

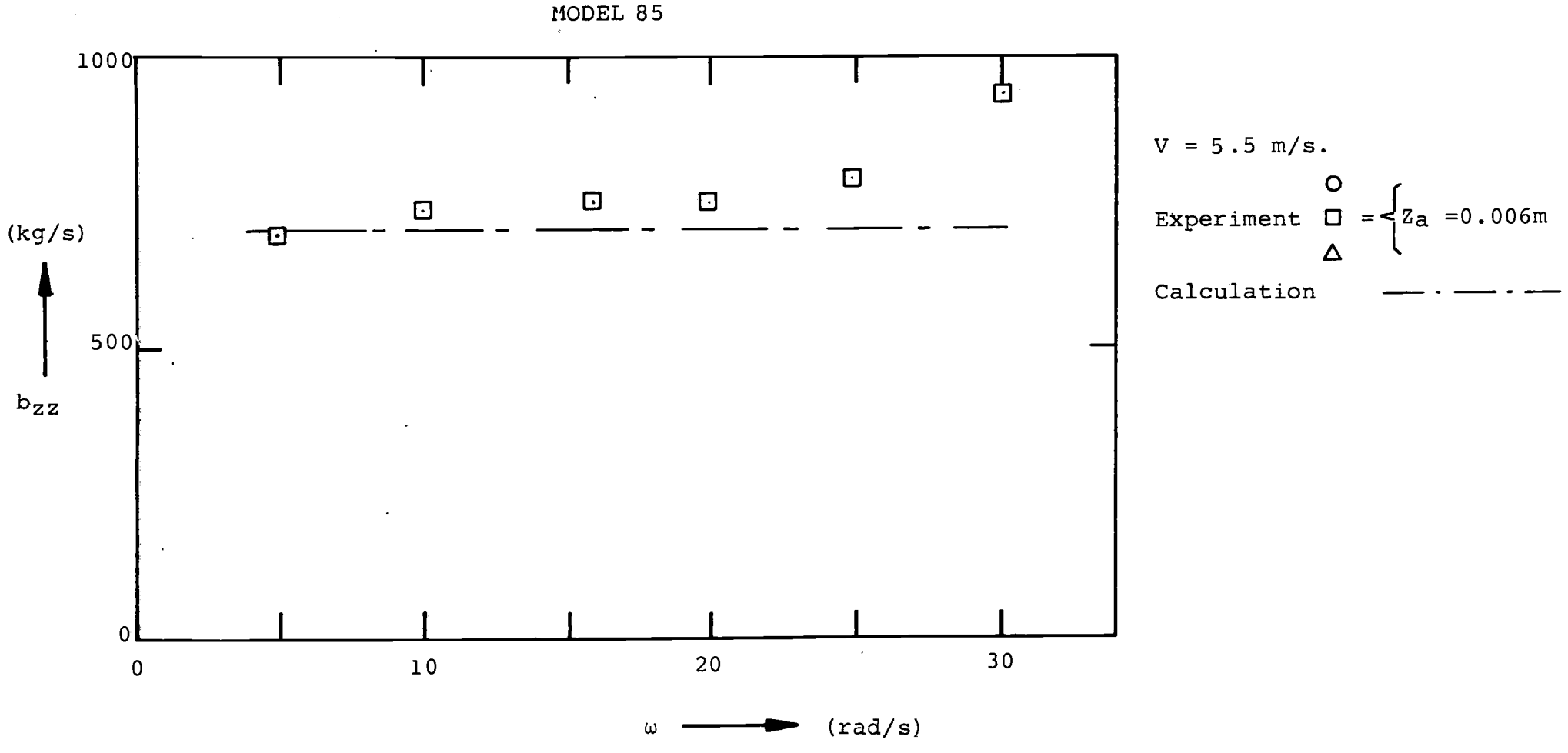

Figure 12. Comparison of the experimental and calculated damping coëfficiënt b_{zz}.

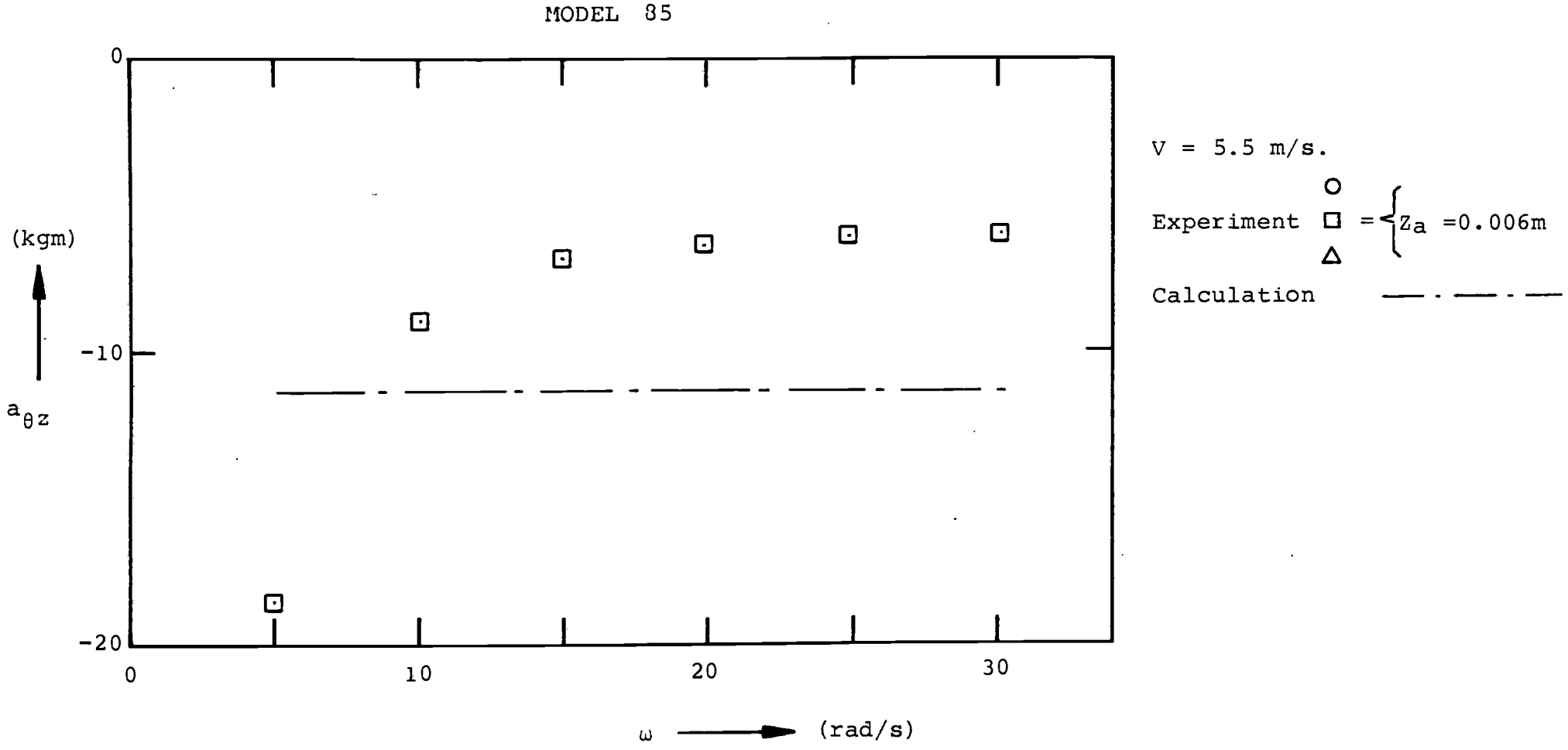

Figure 13. Comparison of the experimental and calculated mass coupling coëfficiënt $a_{\theta z}$.

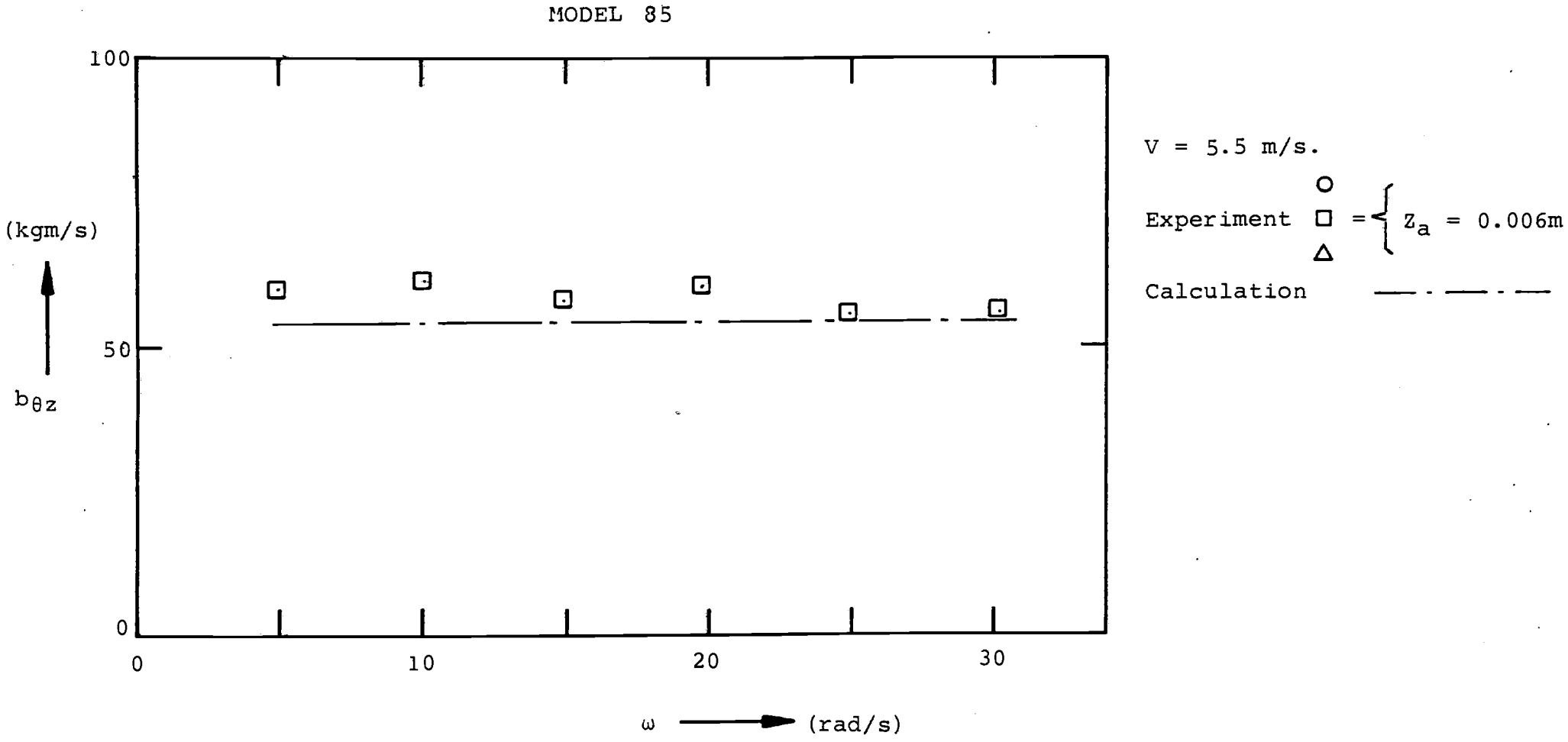

Figure 14. Comparison of the experimental and calculated coupling coëfficiënt for damping $b_{\theta z}$.

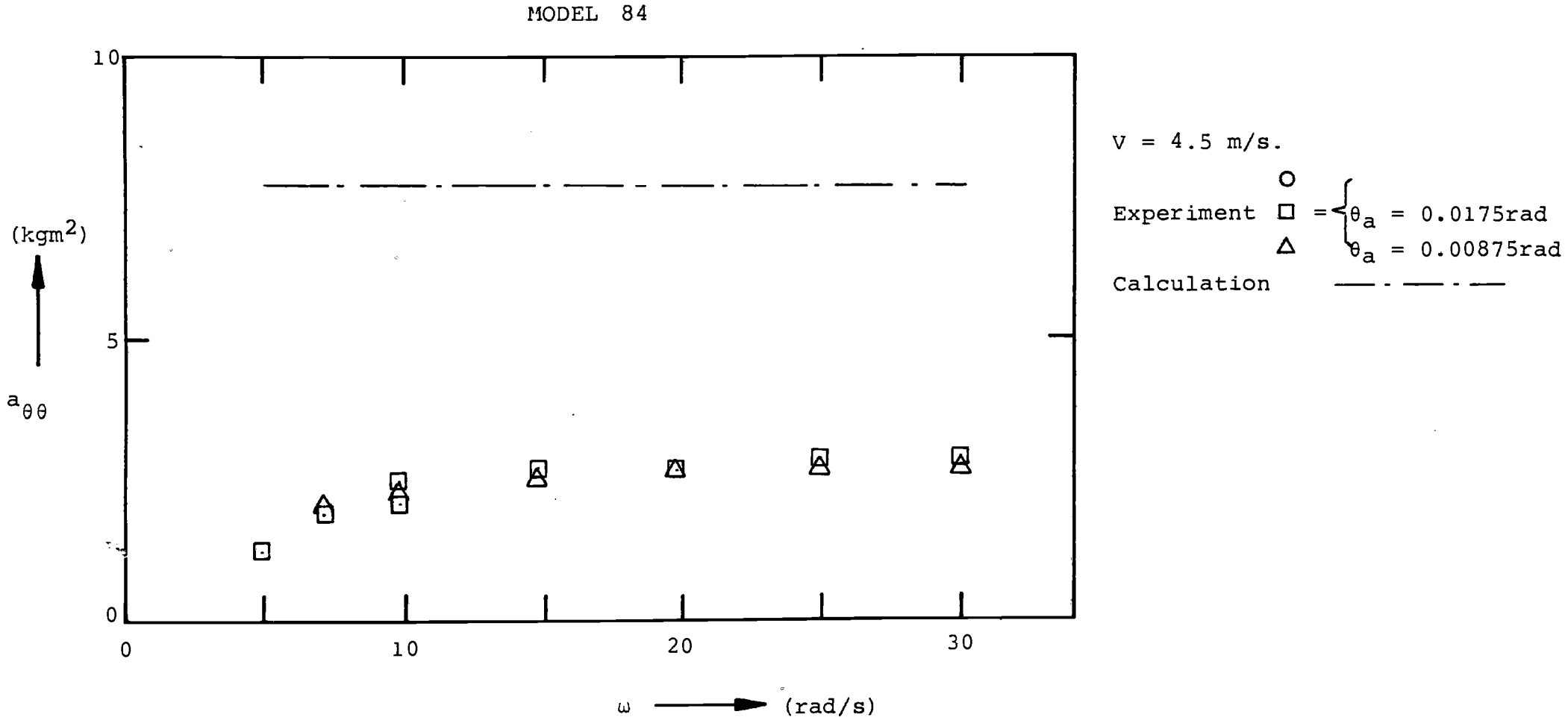

Figure 15. Comparison of the experimental and calculated coëfficiënt of added mass moment of inertia $a_{\theta\theta}$.

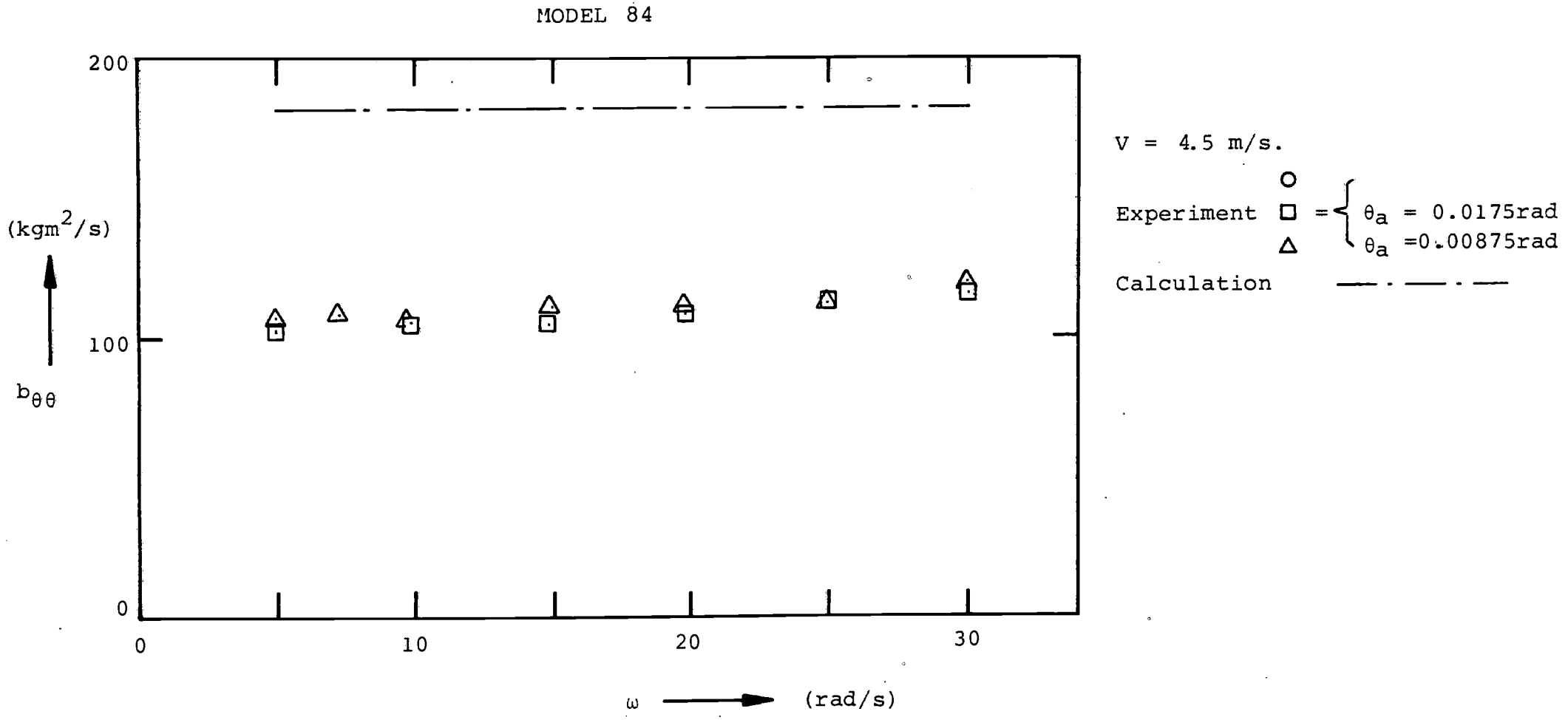

Figure 16. Comparison of the experimental and calculated damping moment coëfficiënt $b_{\theta\theta}$.

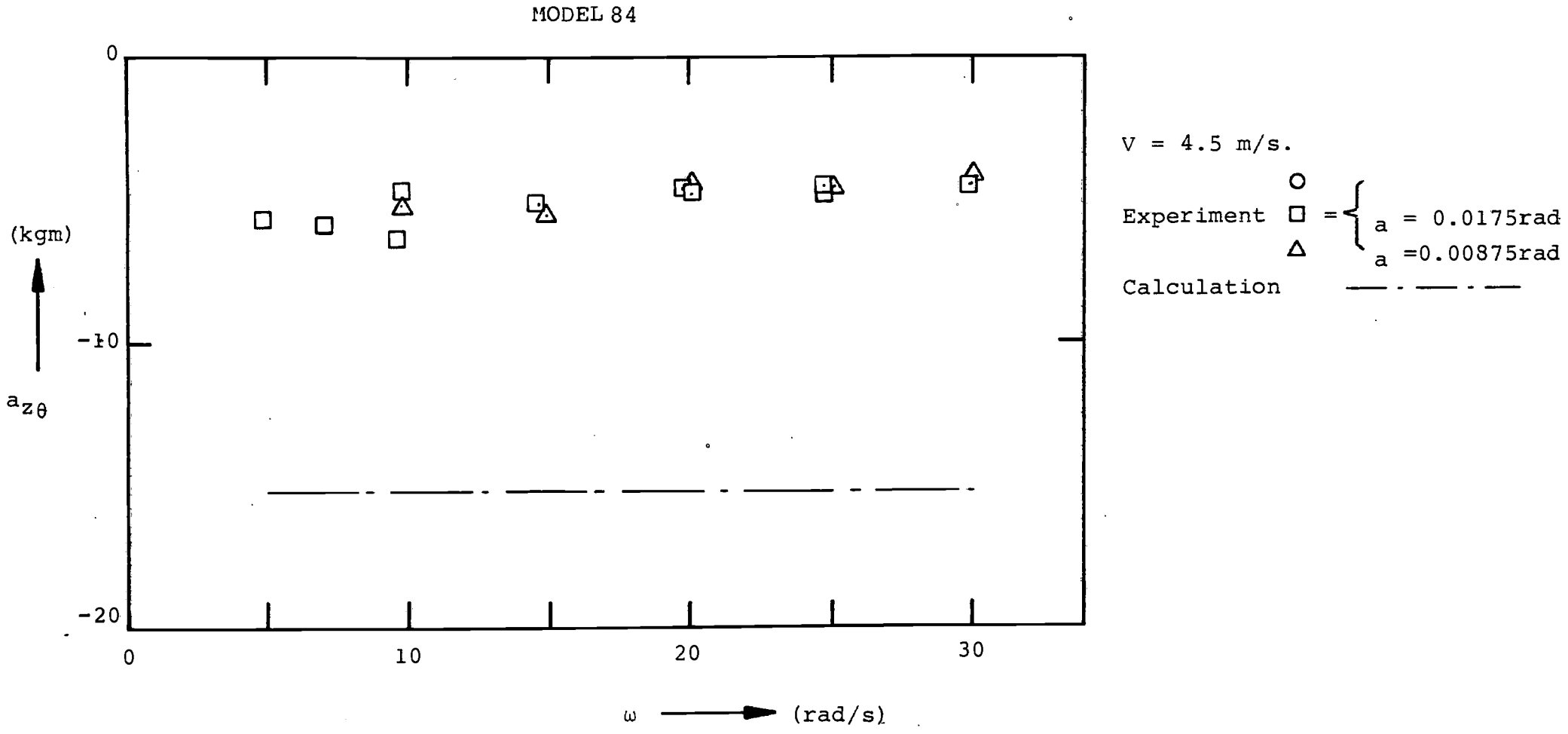

Figure 17. Comparison of the experimental and calculated mass coupling coëfficiënt $a_{z\theta}$.

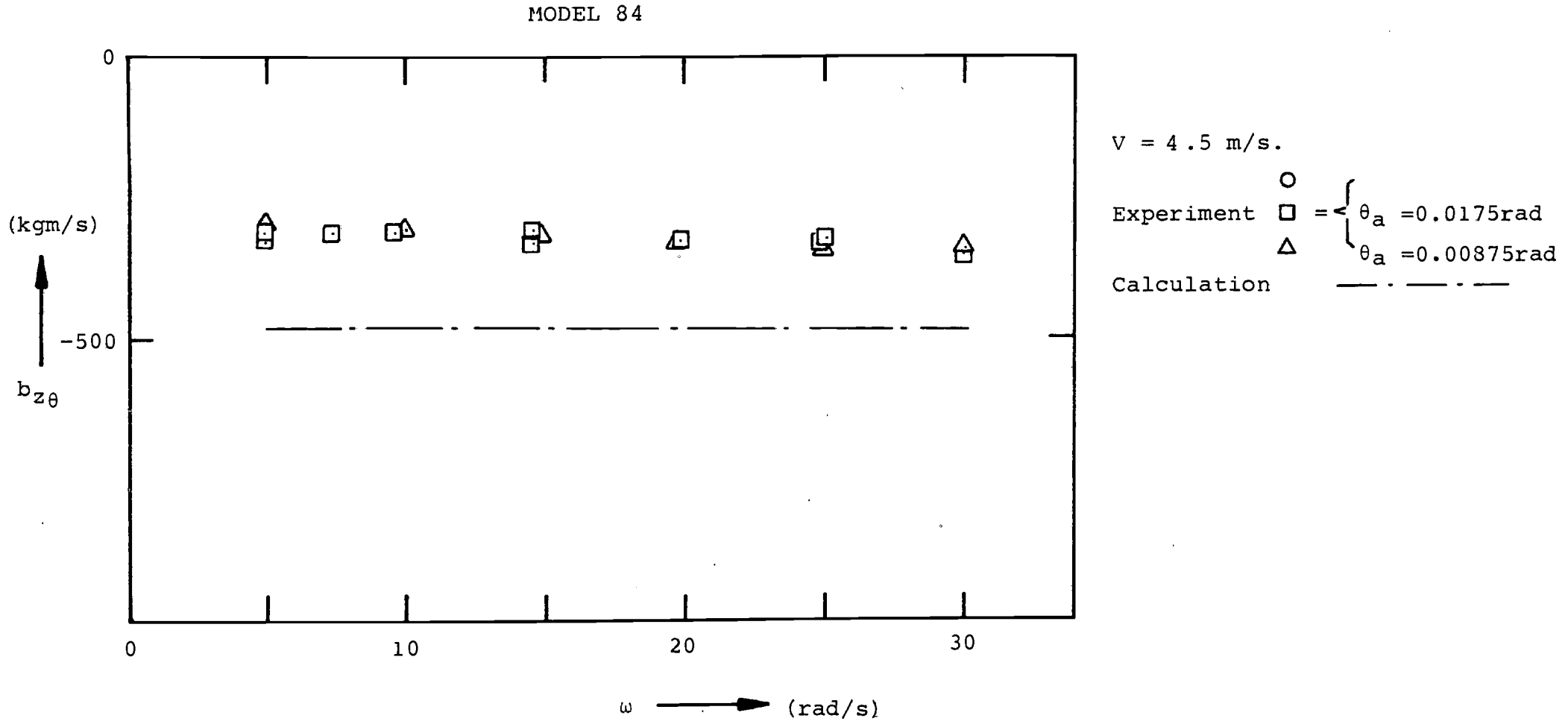

Figure 18. Comparison of the experimental and calculated coupling coëfficiënt for damping $b_{z\theta}$.

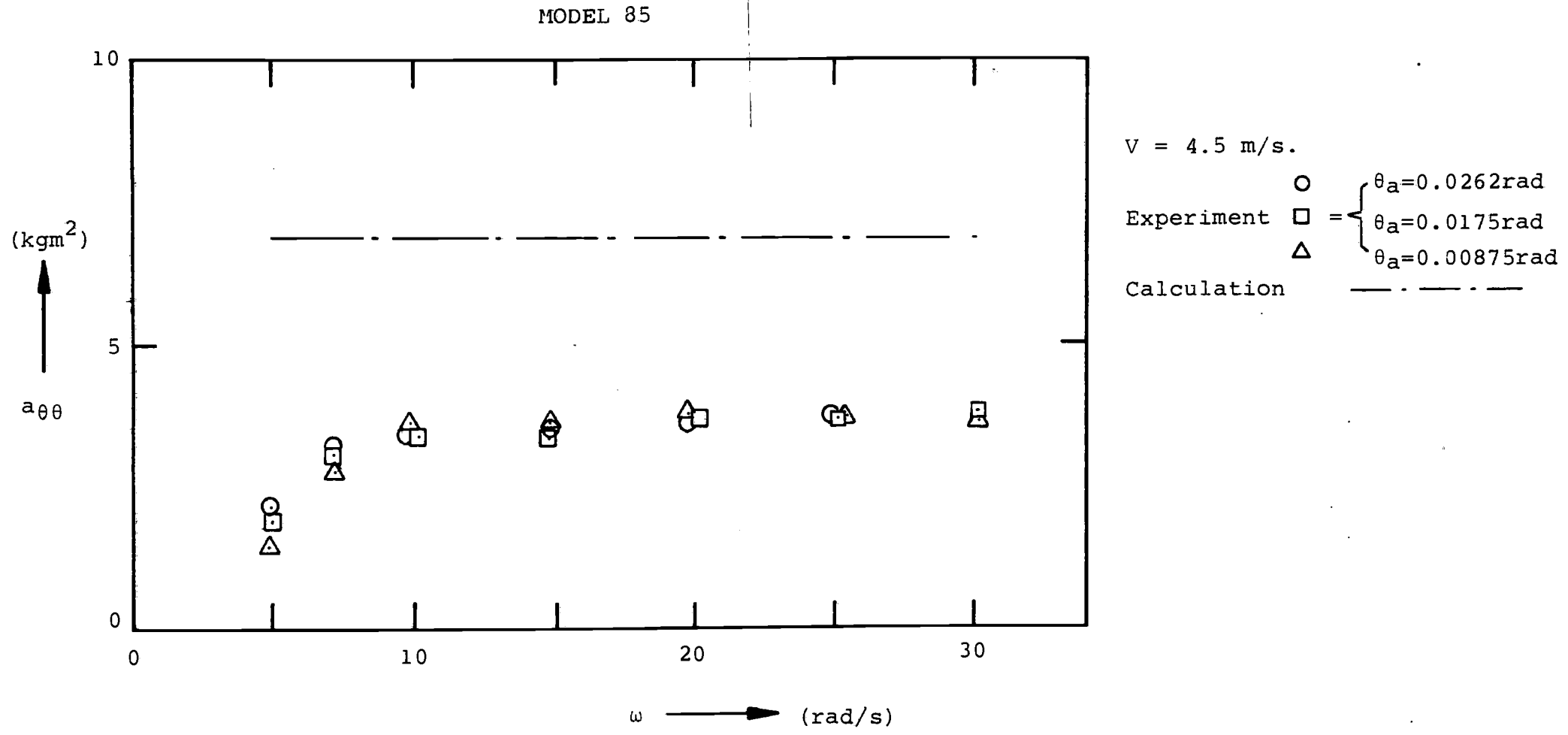

Figure 19. Comparison of teh experimental and calculated coëfficiënt of added mass moment of inertia $a_{\theta\theta}$.

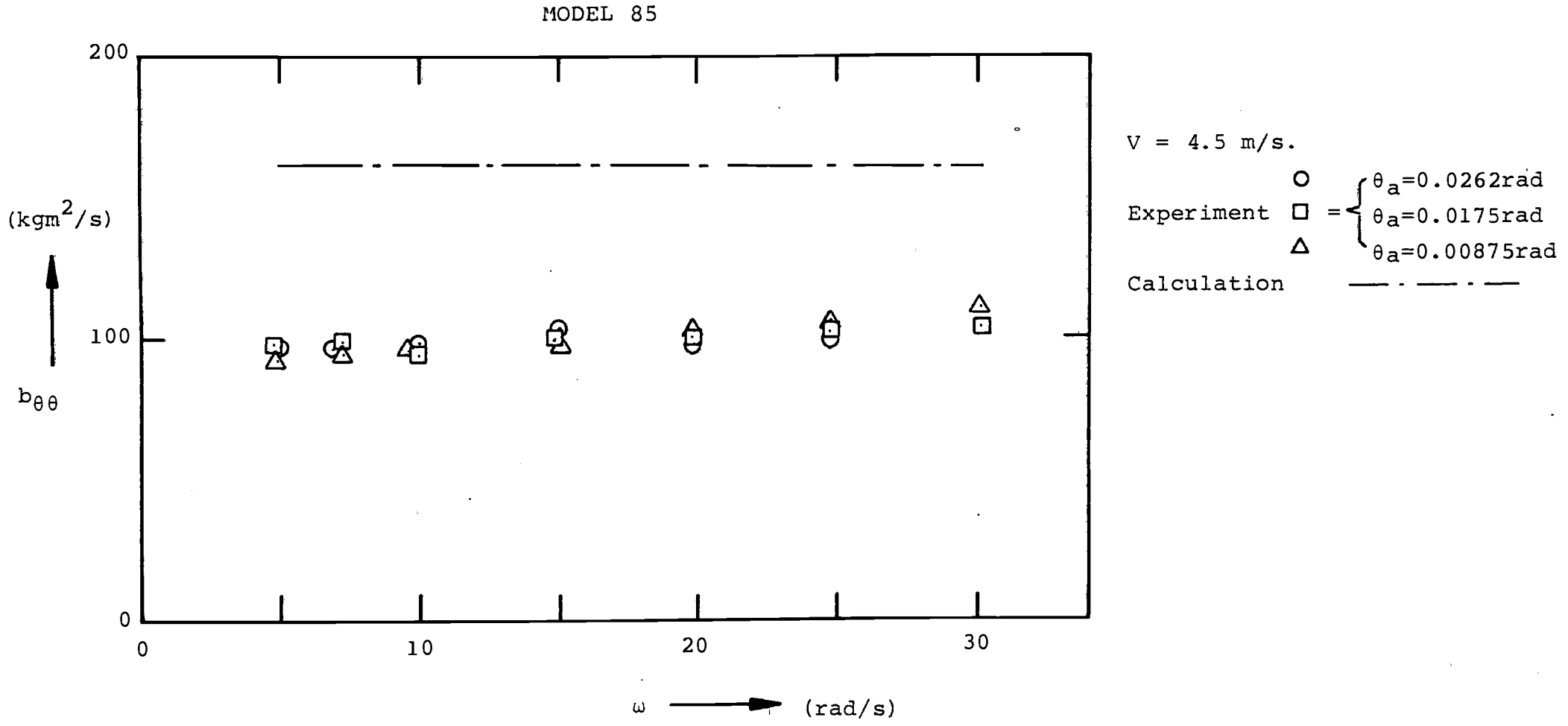

Figure 20. Comparison of the experimental and calculated damping moment coëfficiënt $b_{\theta\theta}$.

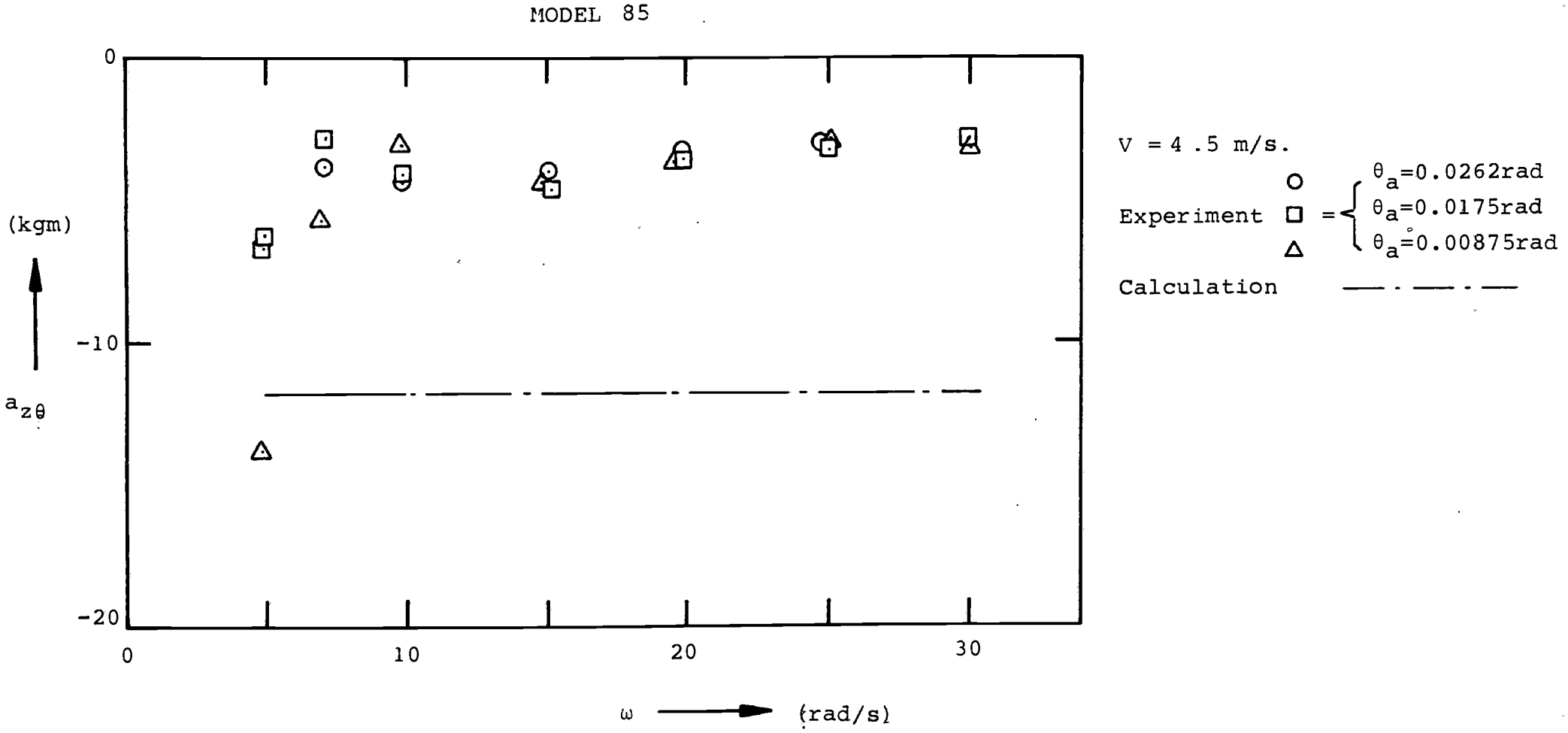

Figure 21. Comparison of the experimental and calculated mass coupling coëfficiënt $a_{z\theta}$.

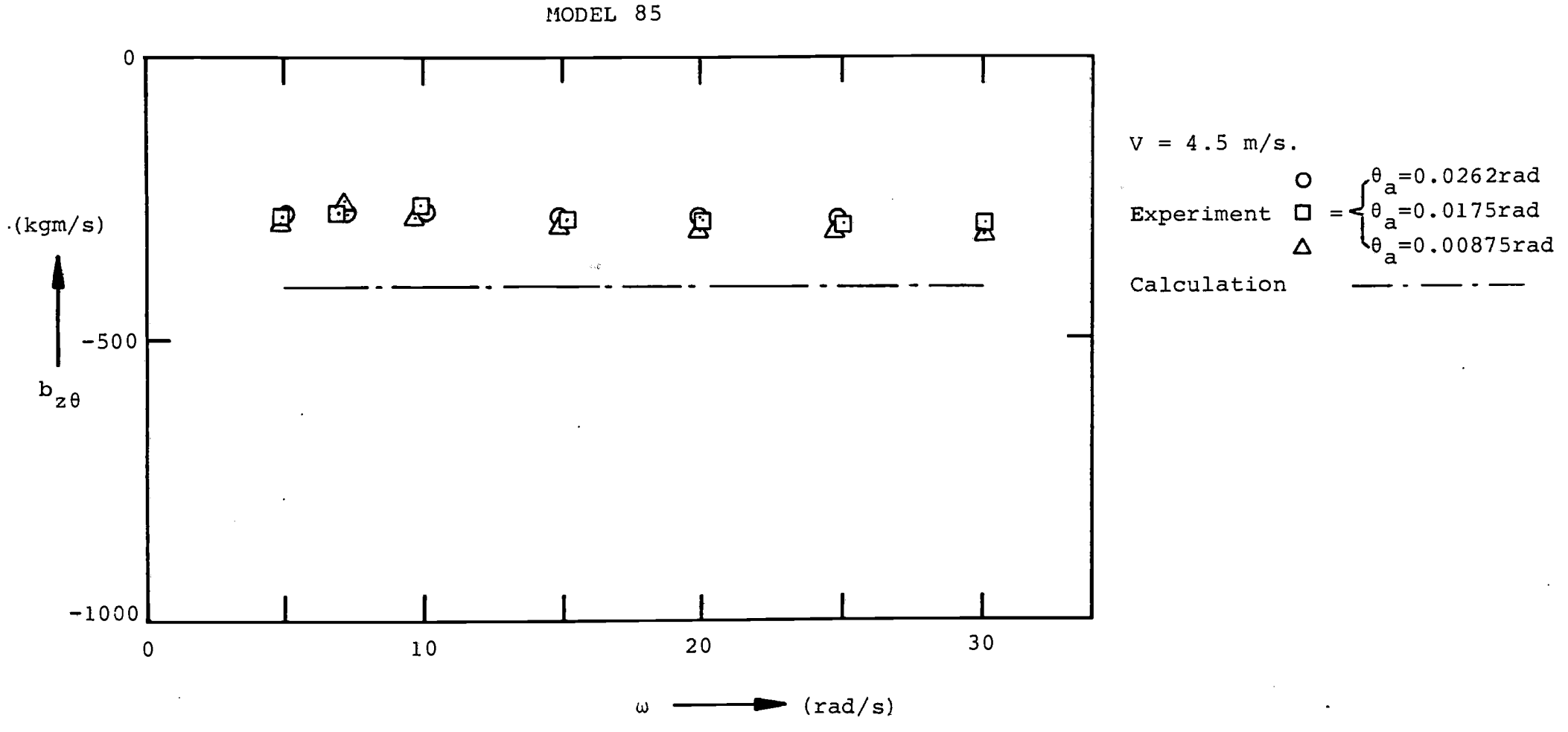

Figure 22. Comparison of the experimental and calculated coupling coëfficiënt for damping $b_{z\theta}$.

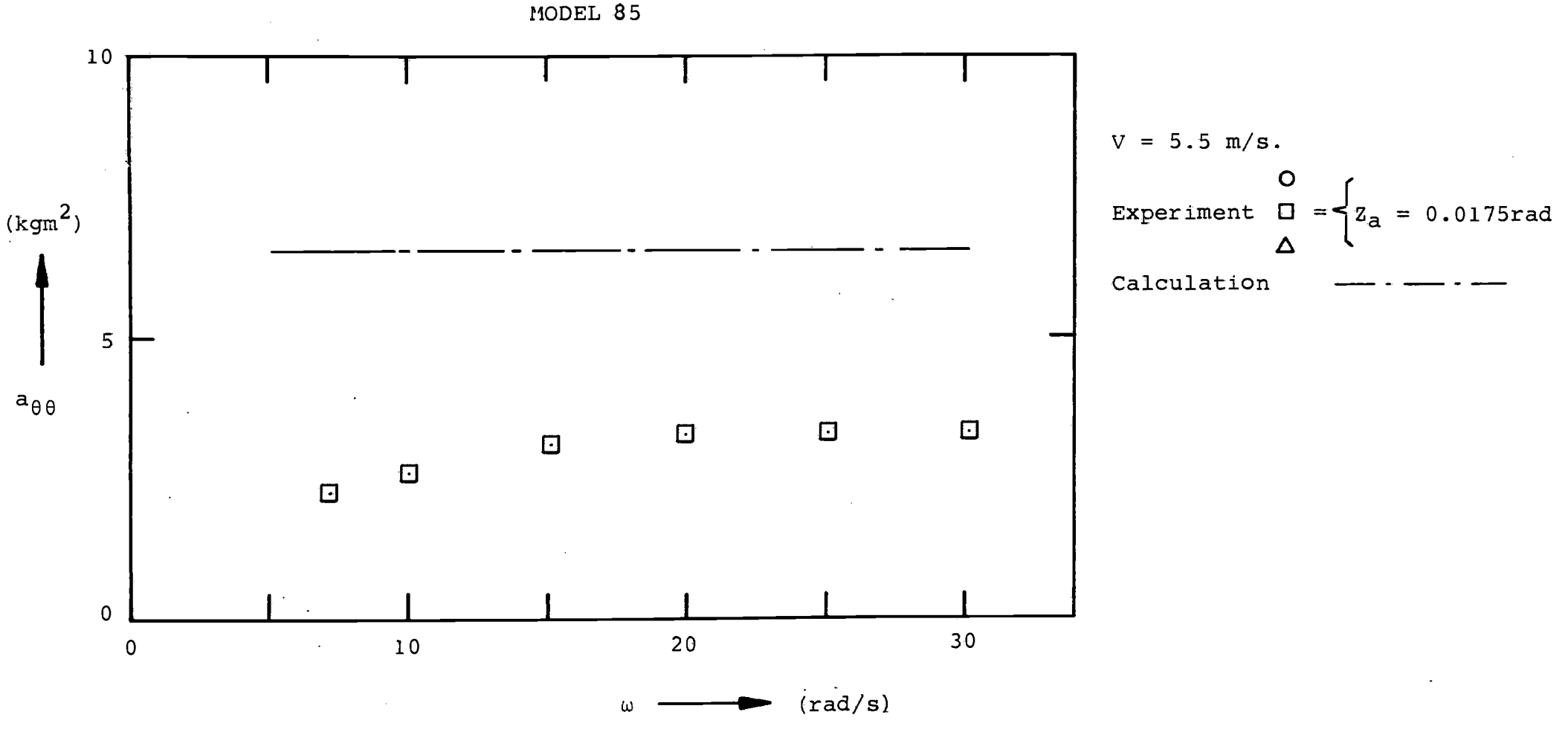

Figure 23. Comparison of the experimental and calculated coëfficiënt of added mass moment of inertia $a_{\theta\theta}$.

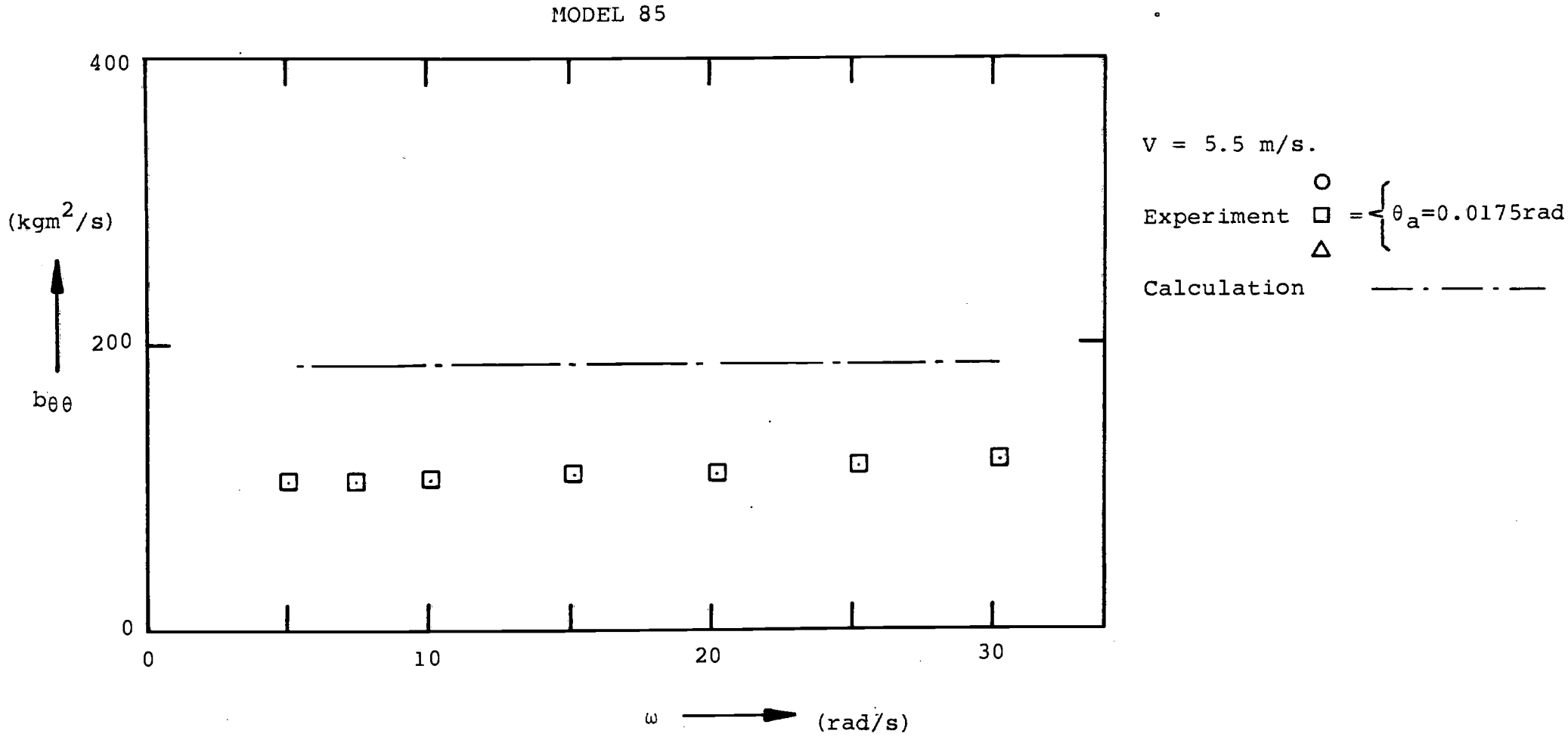

Figure 24. Comparison of the experimental and calculated damping moment coëfficiënt $b_{\theta\theta}$.

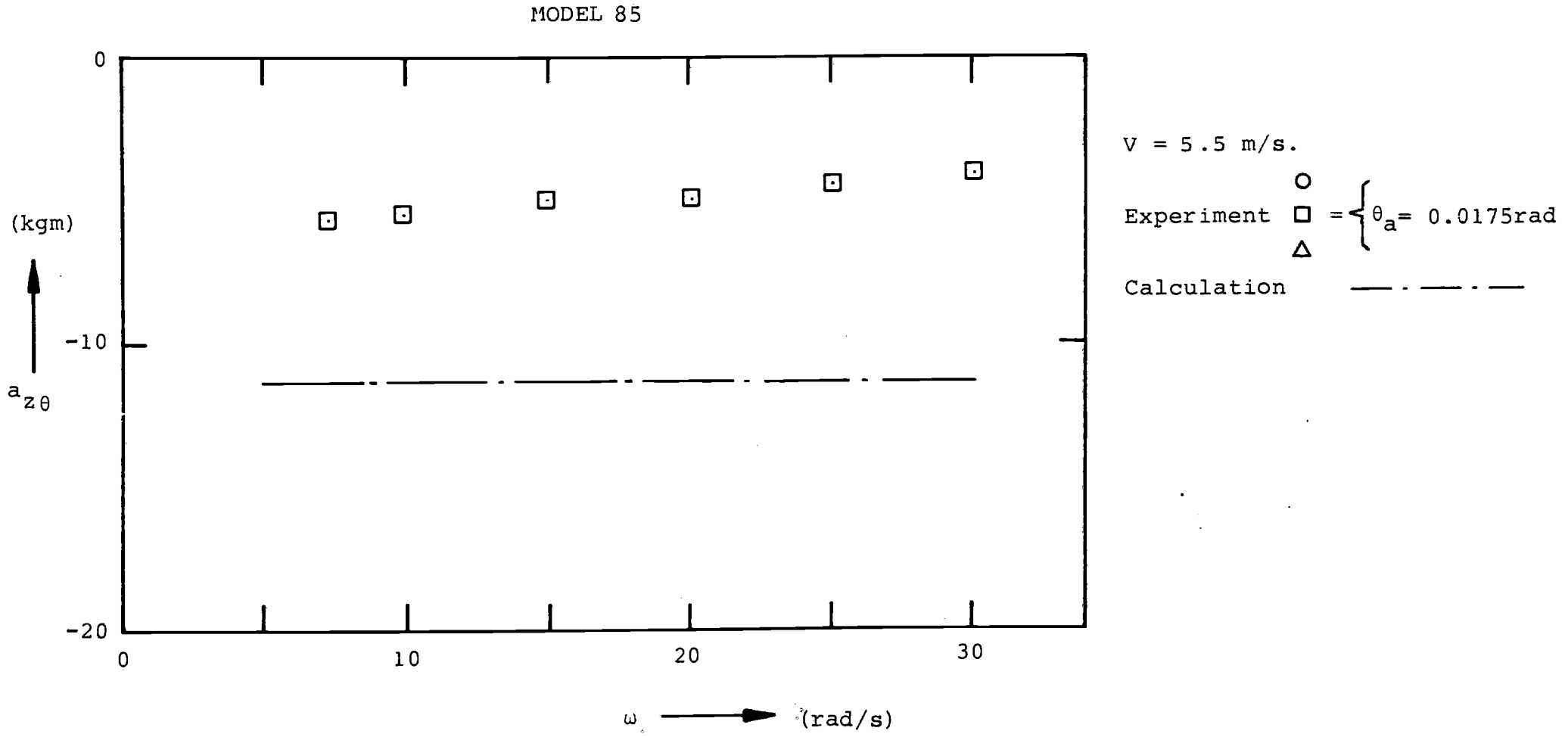

Figure 25. Comparison of the experimental and calculated mass coupling coëfficiënt $a_{z\theta}$.

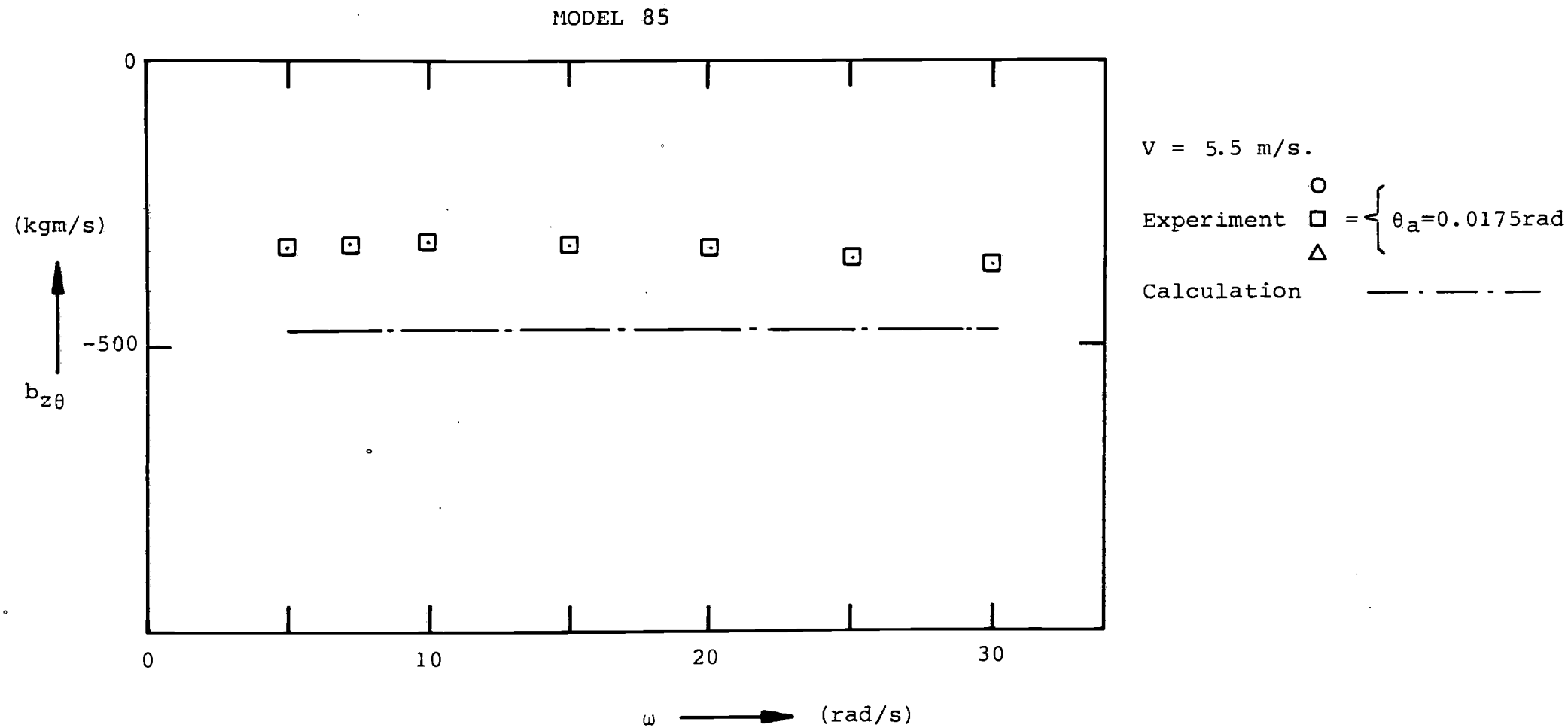

Figure 26. Comparison of the experimental and calculated coupling coëfficiënt for damping $b_{z\theta}$.

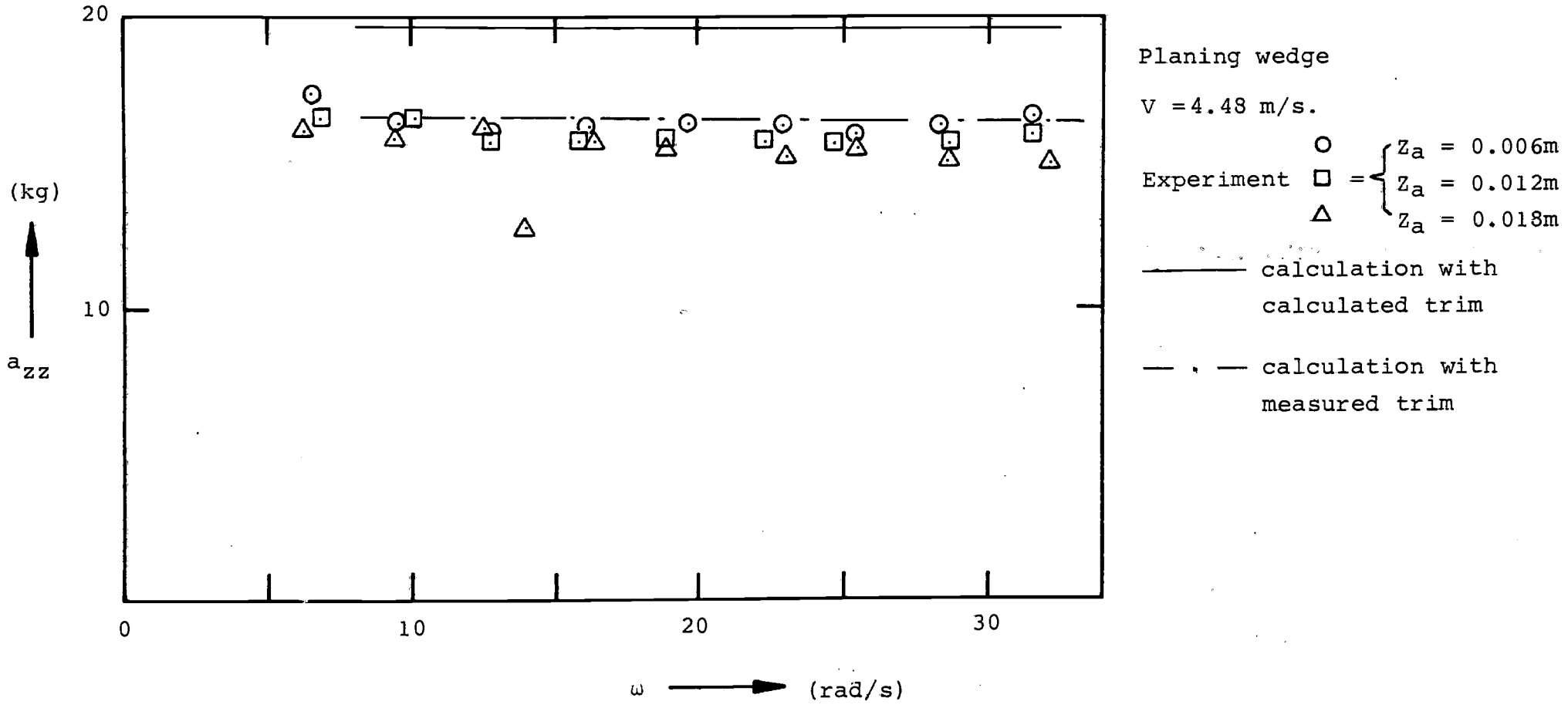

Figure 27. Added mass coëfficiënt a_{zz}.

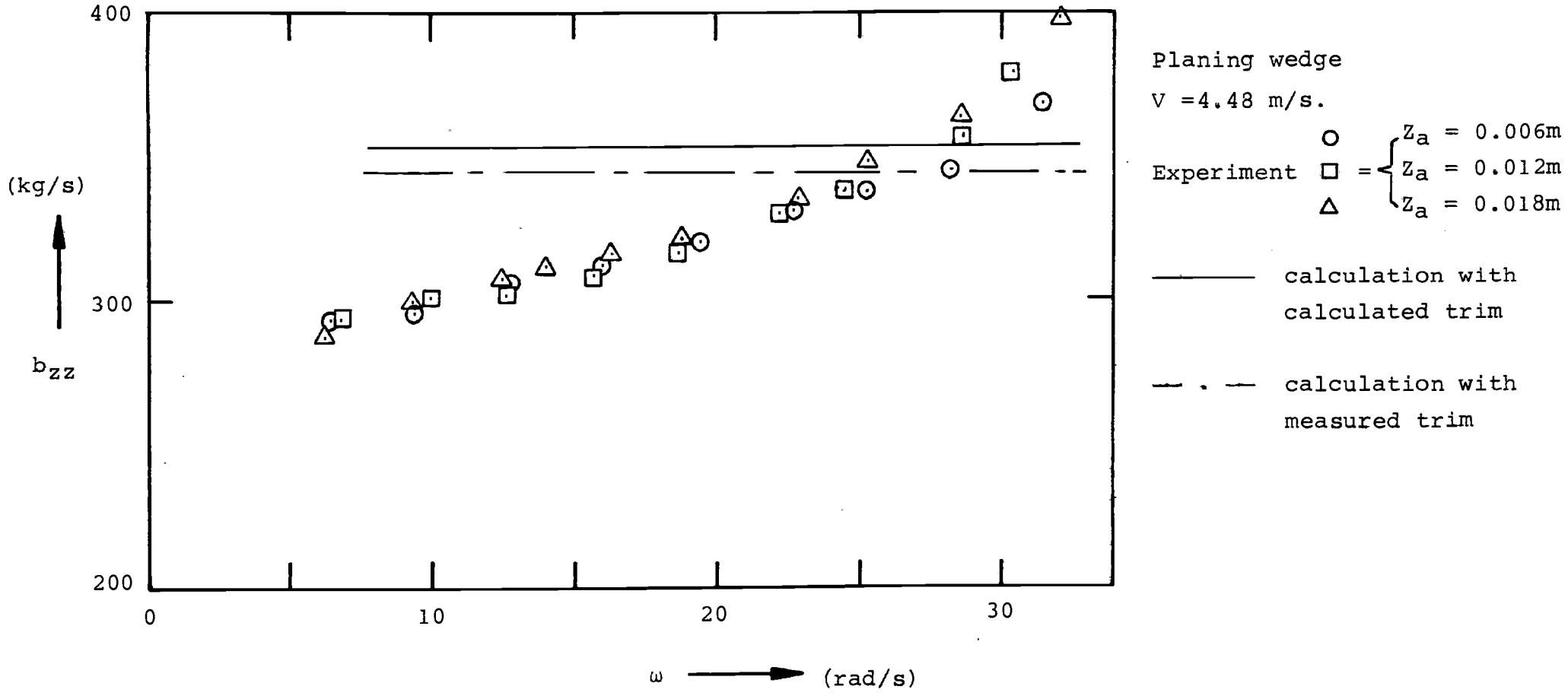

Figure 28. Damping coëfficiënt b_{zz}.

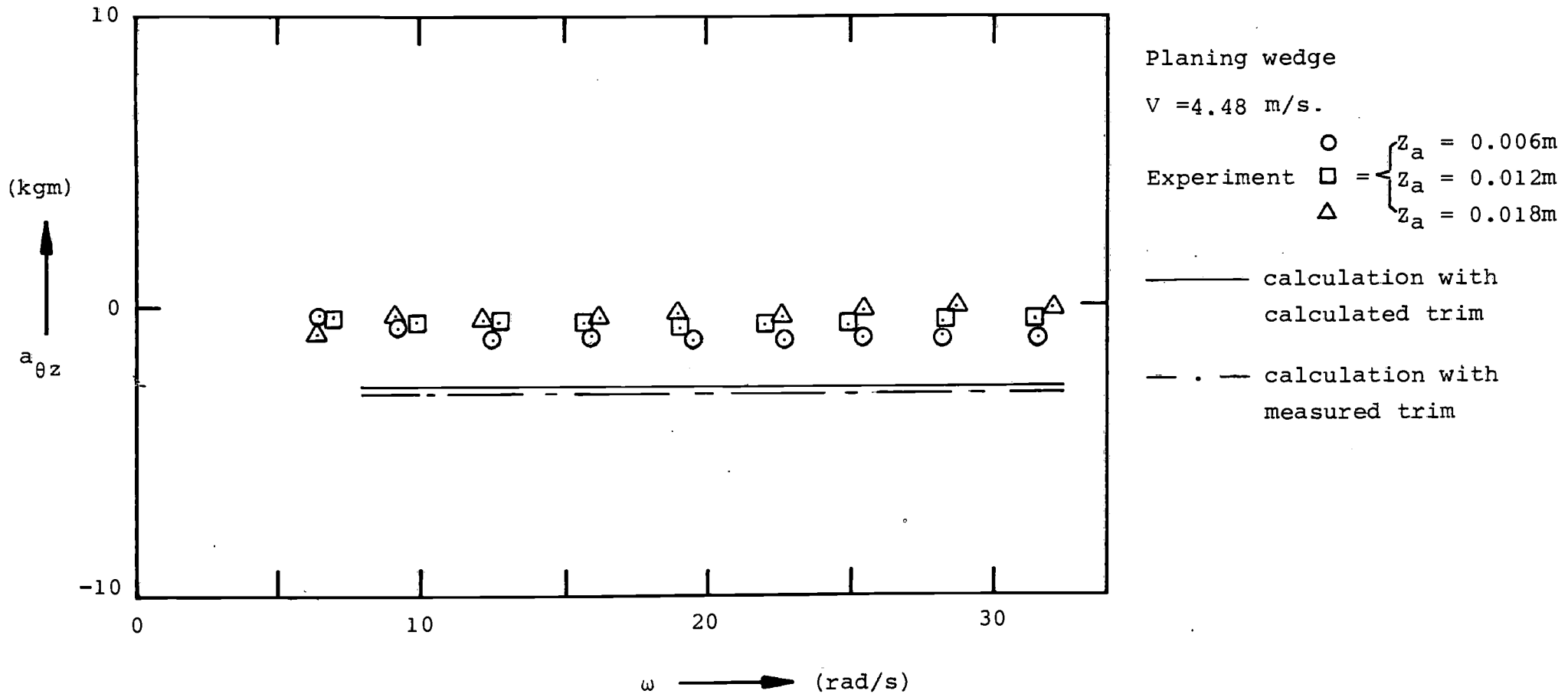

Figure 29. Mass coupling coëfficiënt $a_{\theta z}$.

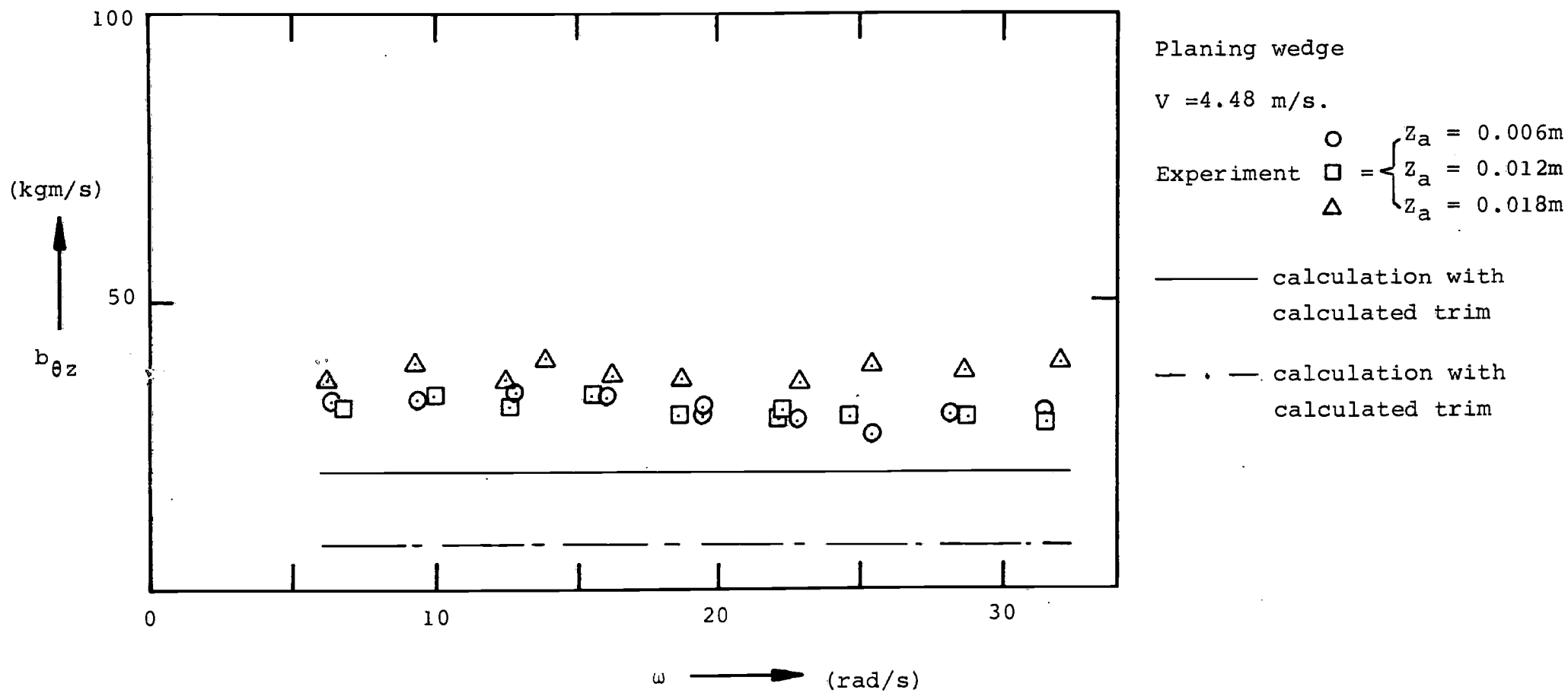

Figure 30. Damping coupling coëfficiënt $b_{\theta z}$.

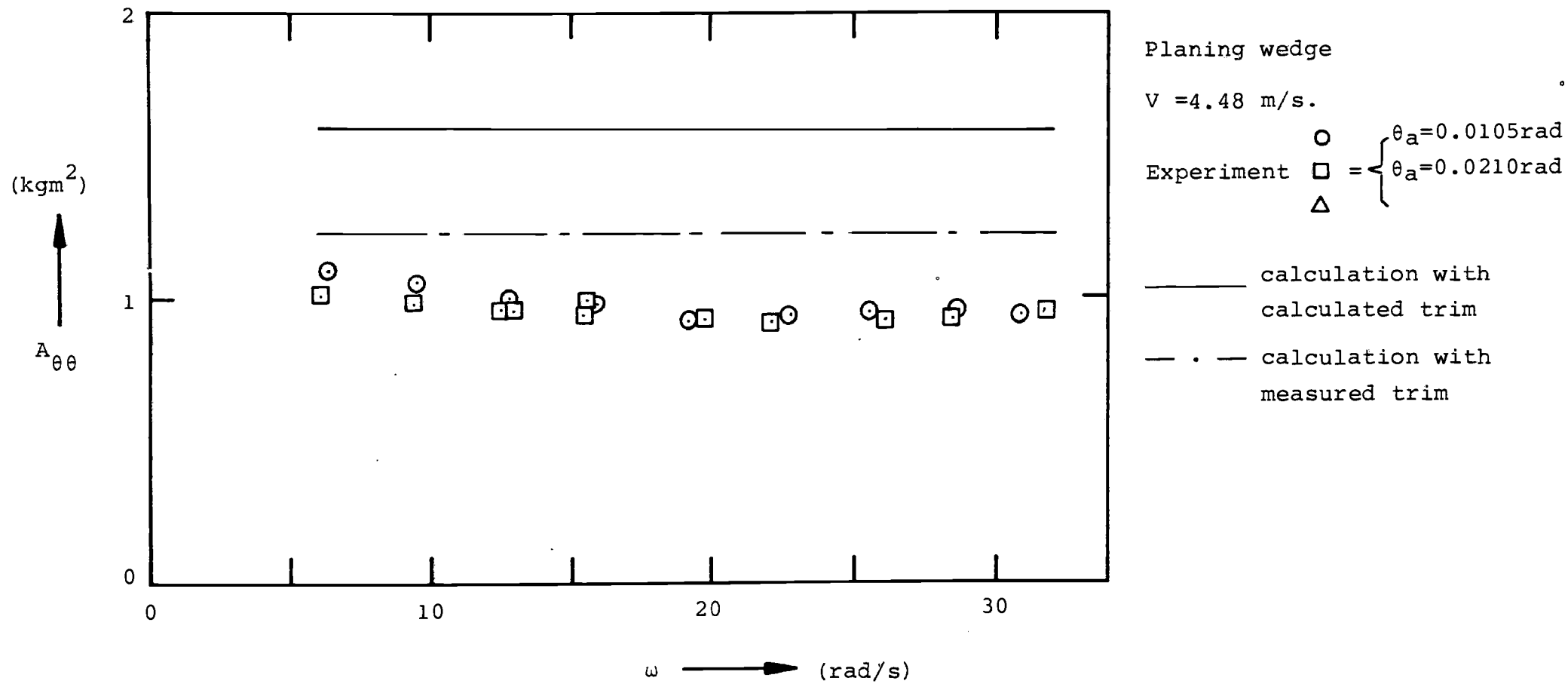

Figure 31. Coëfficiënt of added mass moment of inertia $A_{\theta\theta}$.

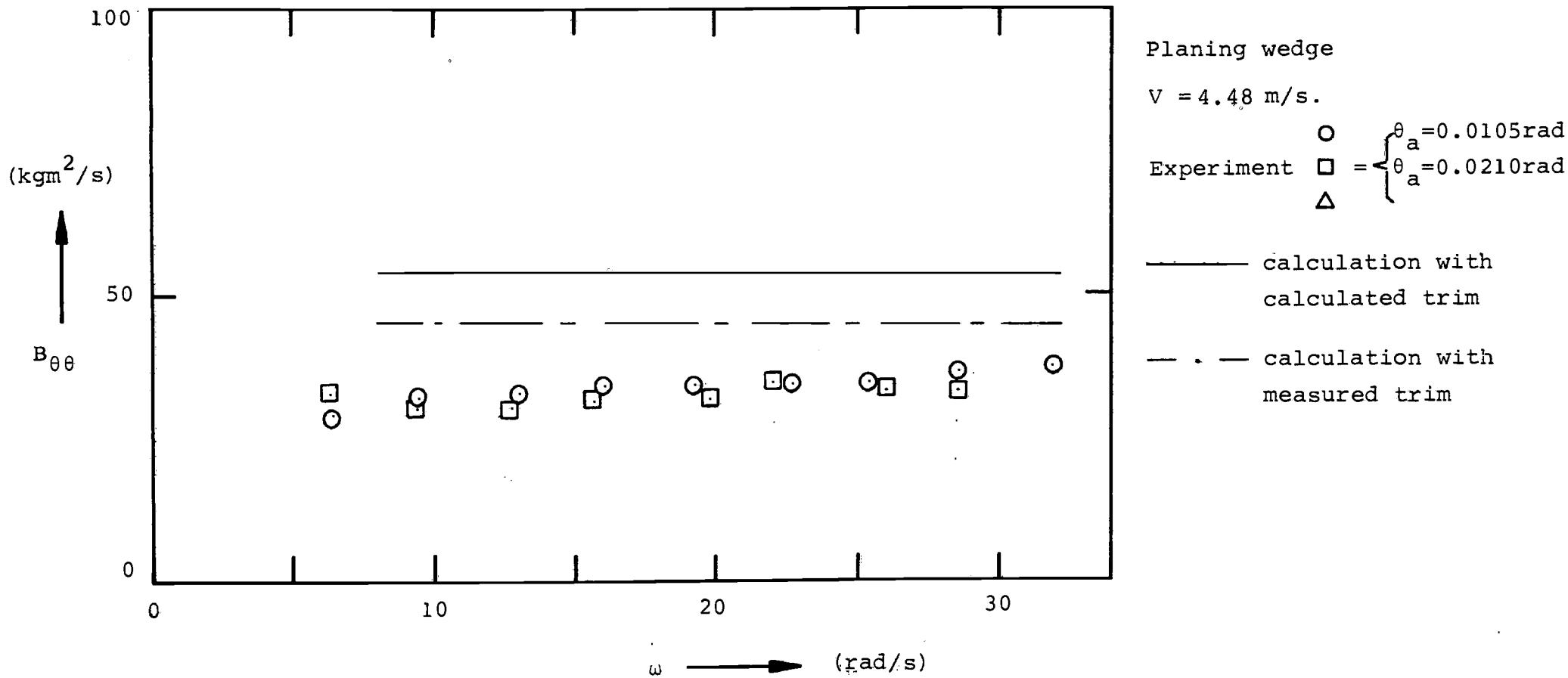

Figure 32. Damping moment coëfficiënt $B_{\theta\theta}$.

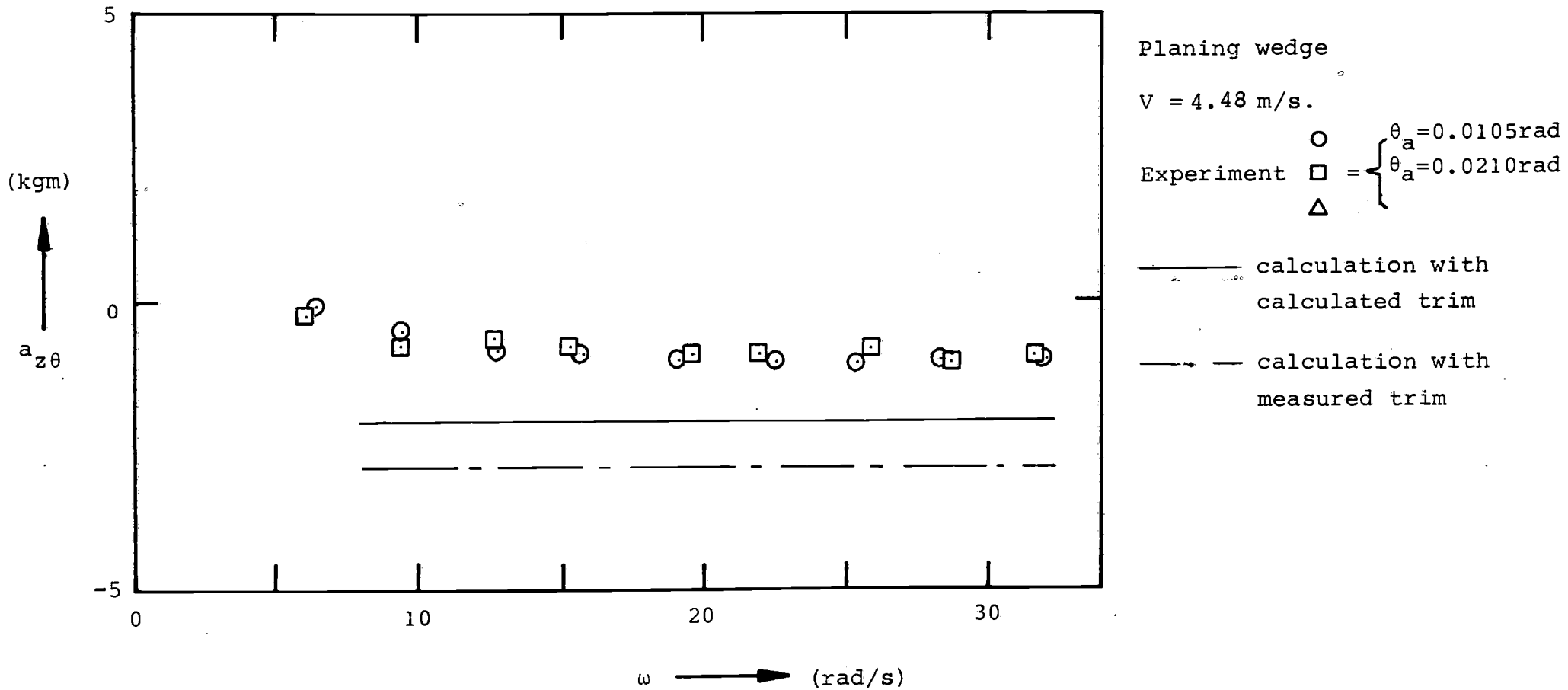

Figure 33. Mass coupling coëfficiënt $a_{z\theta}$.

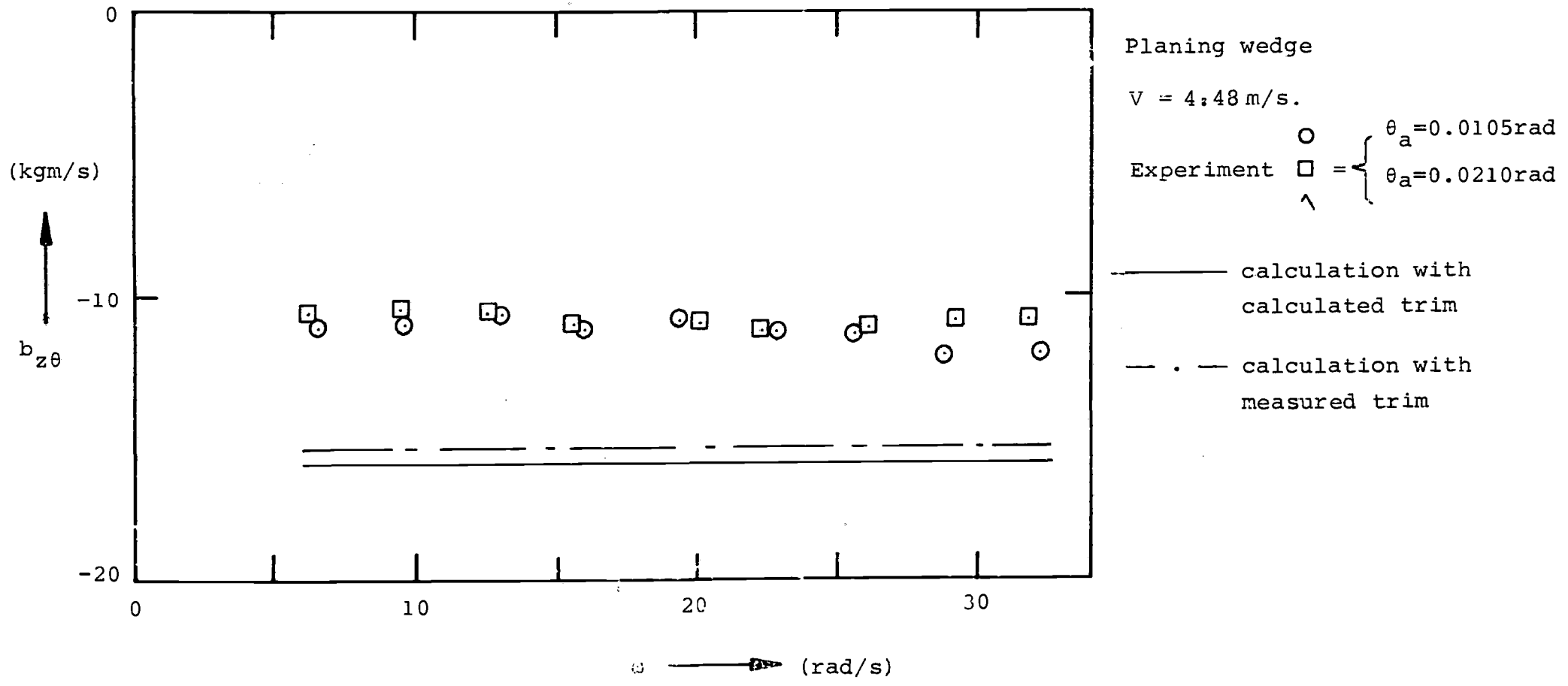

Figure 34. Damping coupling coëfficiënt $b_{z\theta}$.

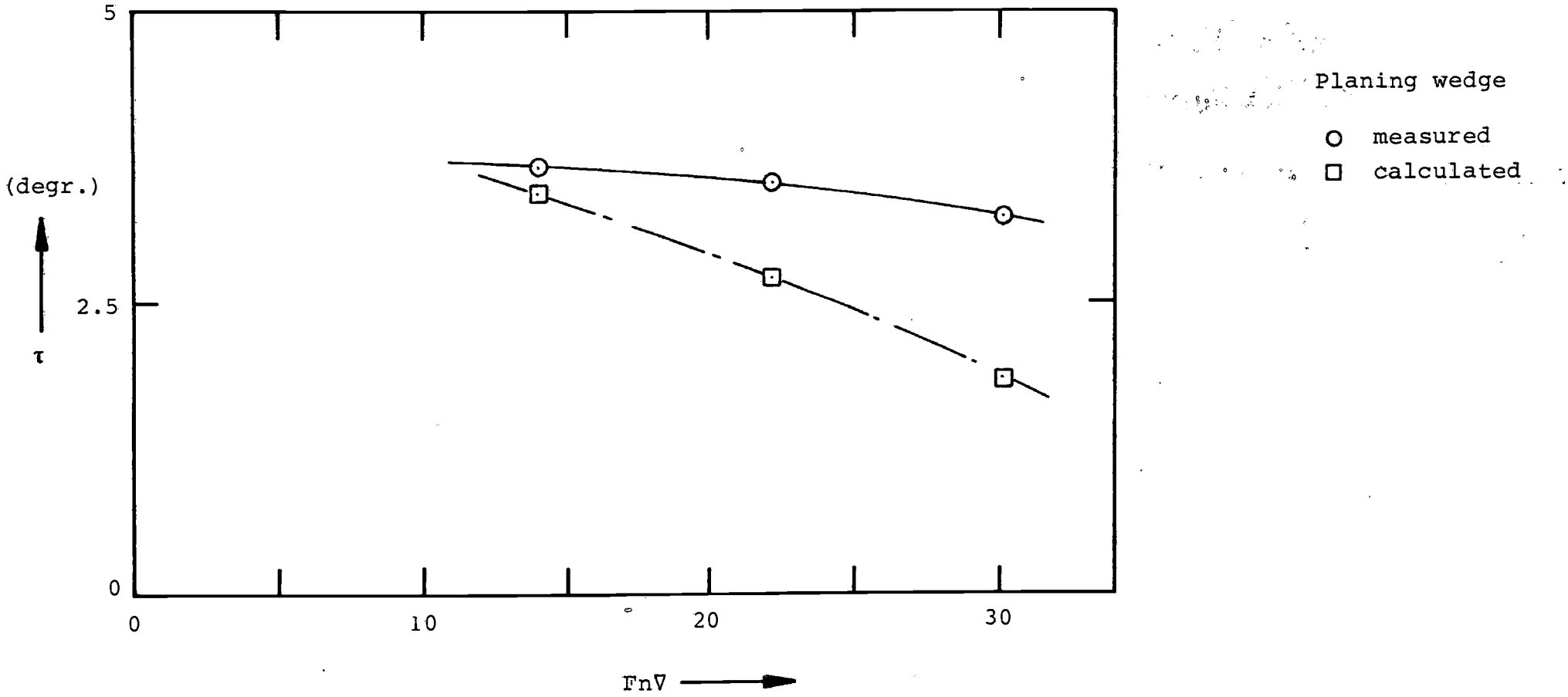

Figure 35. Comparison of the measured and calculated trim angles.